Ricardo Alexandre Ventura das Chagas

Mestre em Viticultura e Enologia

Protein haze formation in white wines: from mechanism to resolution

Dissertação para obtenção do Grau de Doutor em
Química Sustentável

Orientador: Professor Ricardo Boavida Ferreira, professor catedrático, ISA - ULisboa
Co-orientador: Professora Luísa Maria Ferreira, professora auxiliar, FCT - UNL

Protein haze formation in white wine: from mechanism to resolution.

Acknowledgements

Durante os últimos quatro anos tive a oportunidade de realizar um grande objectivo pessoal, tirar o Doutoramento. Tive a sorte de estar rodeado por pessoas que me apoiaram muito, me motivaram, me fizeram querer aprender mais e principalmente crescer. Foram quatro anos que mudaram a minha vida; conheci muitas pessoas de ramos completamente diferentes, trabalhei em três universidades, aprendi um grande conjunto de técnicas e consegui consolidar bastantes conhecimentos.

Sou engenheiro alimentar de base, mas de momento, sinto-me parte engenheiro, parte químico, parte enólogo, parte bioquímico. Atribuo a "culpa" disto não só a mim, à minha maneira de pensar e de abraçar os problemas, mas também às pessoas que me acompanharam nesta aventura e que tanto contribuíram para ser o que sou. Apesar de ter a tese escrita em inglês, os agradecimentos serão feitos em português (aos portugueses) para que não se perca informação com eventuais traduções.

Em primeiro lugar, um agradecimento especial às duas pessoas que me acompanharam desde o início neste trabalho, os meus orientadores. Ao Professor Ricardo Boavida Ferreira pelo apoio, disponibilidade, pelas longas conversas sobre proteínas, vinho, entre outros variados temas. Deu-me oportunidade de continuar um trabalho que vinha a ser desenvolvido no nosso laboratório há já vários anos e também a possibilidade de mudar o rumo desse mesmo trabalho. Um agradecimento muito especial à Professora Luísa Ferreira por todo o apoio, amizade e paciência ao longo destes anos. Receber alguém de uma área totalmente diferente, com outra linguagem e forma de trabalhar, já é de si difícil. Ajudou-me, acompanhou-me, abriu-me os horizontes e empurrou-me para fora de pé em inúmeras situações. Isso foi algo que mudou por completo a minha maneira de estar e de trabalhar. Muito obrigado por tudo.

À Professora Ana Lourenço, por todo o carinho, disponibilidade e vontade de ajudar em tudo o que fosse preciso. Muito obrigado.

Ao Professor César Laia, que começou a trabalhar comigo para me ajudar num ensaio de DLS e acabou a trabalhar comigo praticamente até ao final do trabalho. Aprendi muito com ele, mesmo que por vezes estivéssemos na mesma conversa a falar duas linguagens diferentes. Muito obrigado pelo apoio e amizade.

À Bacalhoa Vinhos por ceder as amostras de vinho que usei durante o meu Mestrado e início do Doutoramento. Ao José Caninhas e ao Filipe Cardoso da Quinta do Piloto por cederem as uvas para a produção dos vinhos usados na última parte da minha tese. Ao David Ferreira pela amizade e por todas as "discussões enológicas" à volta do tema.

À Doutora Paula Pinto pela oportunidade de trabalhar no RAIZ e ao José Carlos por toda a ajuda na produção das folhas.

À Professora Paula Branco, Professora Manuela Pereira, Professora Sara Monteiro, Professor Manuel Malfeito Ferreira, Professora Catarina Prista, Professora Jorge Ricardo da Silva, Professora Isabel Coelhoso, muito obrigado pela ajuda, motivação e amizade.

Aos meus colegas de enologia que estão a fazer os vinhos que alegram muitos almoços, jantares e fins de tarde por todo o mundo.

Dado que o meu tempo foi partilhado entre o Laboratório 202 e 205 do DQ (FCT) e o Laboratório de Fisiologia Vegetal (ISA), muitas pessoas influenciaram o meu trabalho e vida pessoal. À Catarina Fonseca, Luís Batista (que me ajudou muito no início do meu trabalho, ainda antes de começar o meu mestrado), Regina Freitas, Isabel Silva, Ana Cristina, Diana, Carla, Sara Santos, Ana Lima, João Fernandes, Maria João, João Graça, Senhor António e todo o resto da equipa. Obrigado pela ajuda e principalmente pela amizade. Do lado dos "químicos", obrigado ao Diogo, Fausto, Carlos, Sequeira, Catarina, Luís, Sara, Daniela, Edgar, Marina, Cátia, Rita Otrelo e a todos os outros (que foram muitos) que me acompanharam. Ao pessoal do laboratório de análises, Nuno, Carla (obrigado pelas análises "para ontem"), Luz, Elisabete (obrigado pelas noitadas a olhar para o CD), Ana Teresa e Cecília.

Um obrigado muito especial a duas pessoas que me ajudaram com muitas dúvidas de química, muitas dúvidas existenciais, mas principalmente pela amizade e companhia ao longo desta aventura. Luísa Carvalho e Patrícia Máximo.

Um obrigado gigante a um grupo de amigos que me acompanham no meu dia a dia, aos quais agradeço não só a amizade, os bons concelhos (e maus), paciência (!) mas também a capacidade que têm e tiveram de me ajudar a relativizar vários problemas. Ao Alex, Bento, João, Rita e Carla. Muito, muito obrigado por tudo.

To Professor Thomas Heinze for his availability to welcome me in his laboratory and for the chance to work with him. It was an awesome experience not only because I had the opportunity to learn with some of the experts in the area but also the experience of living in a new country.

To Martin and Andreas for all the help and friendship during my stay in the group. Thank you!

To Marcus, Konrad, Lars, Robert and Peter for the help in the lab and for the friendship during my stay in the group.

Quero agradecer aos responsáveis por estar aqui hoje, aos meus pais. Por acreditarem em mim, por estarem sempre do meu lado e por todo o amor que me dão diariamente. Quaisquer palavras não chegam para agradecer o vosso apoio e tudo o que fizeram por mim.

Por fim, à pessoa que me atura todos os dias, que me apoia em tudo, que me motiva, me impulsiona a seguir os meus sonhos e me ama, à Maura. Sem ti, tudo isto tinha sido muito mais difícil. Obrigado por acreditares em mim, por seres um exemplo e por me apoiares sempre nas minhas maluqueiras. Amo-te.

Funding

This work was supported by the Associate Laboratory for Green Chemistry LAQV which is financed by national funds from FCT/MEC (UID/QUI/50006/2013) and co-financed by the ERDF under the PT2020 Partnership Agreement (POCI-01-0145-FEDER - 007265). This work was also supported by Fundação para a Ciência e a Tecnologia (FCT) under the PhD grant SFRH/BD/84749/2012 and by the National NMR Facility supported by Fundação para a Ciência e a Tecnologia (RECI/BBB-BQB/0230/2012).

I have not failed 700 times. I have not failed once.
I have succeeded in proving that those 700 ways will not work.
Thomas Edison

Wine is grape-juice. Every drop of liquid filling so many bottles has been drawn out of the ground by the root of a vine. All these different drinks have at one time been sap in a stick. It is the first of many strange and some – despite modern research – mysterious circumstances which go to make wine not only the most delicious, but the most fascinating drink in the world.

Hugh Johnson

Abstract

Wine clarity is an important oenological feature affected by the presence of undissolved matter in the wine. One of the reasons for a wine to turn turbid relies on the insolubilization and aggregation of residual proteins that remain in wine after the fermentation process by a phenomenon commonly known as protein haze. This phenomenon usually occurs after exposure to heat stress during inappropriate shipping and storage conditions

Despite the extensive research performed during the last decades, the multifactorial mechanism responsible for white wine protein haze formation is not fully characterized. After testing different metabolites and model wine solutions containing different protein fractions, a new model is proposed based on the experimental identification of sulfur dioxide as the non-proteinaceous factor that induces white wine protein haze formation upon heating. Unlike other reducing agents, addition of sulfur dioxide to must/wine upon heating cleaves intraprotein disulfide bonds, hinders thiol-disulfide exchange during protein interactions and leads to formation of novel interprotein disulfide bonds. The formation of these new bonds together with hydrophobic interactions between unstable proteins are ultimately responsible for wine protein aggregation following a nucleation-growth kinetic model. The model was tested in wine model solution and validated under real wine conditions.

To avoid protein haze formation in white wine, winemakers remove these unstable proteins from solution with bentonite, a negatively charged clay than adsorbs positive proteins from wine by ion exchange. Though effective, the addition of this product presents many drawbacks like negative impact on the organoleptic characteristics of wine or high lees formation leading on wine loss and waste formation. With the aim of producing a bentonite alternative, we synthesized and characterized a new crosslinked polymer that can remove wine proteins in an in-line manner using it as a processing aid (filter) or as an additive (powder). The produced polymer was tested using model proteins and some preliminary tests validated that this material can be used to remove proteins from wine at laboratory scale.

Keywords

wine; protein haze; sulfur dioxide; protein aggregation; protein stabilization

Resumo

A limpidez é uma característica enológica de grande importância para a aceitação de um vinho por parte do consumidor a qual é particularmente afectada pela presença de matéria em suspensão. Uma das razões para um vinho ficar turvo está relacionada com a agregação e precipitação de proteínas que permanecem no vinho após a fermentação. Este fenómeno é designado por turvação proteica e é causado após exposição do vinho a temperaturas elevadas durante o seu transporte ou armazenamento.

Apesar da extensa pesquisa realizada durante as últimas décadas, o mecanismo multifactorial responsável pela formação de turvação proteica em vinho branco não está totalmente caracterizado. Após testar diferentes metabolitos e soluções modelo contendo diferentes fracções de proteína, é proposto um novo modelo com base na identificação experimental do dióxido de enxofre como factor indutor de turvação proteica após exposição ao calor. Ao contrário de outros agentes redutores, a adição de dióxido de enxofre ao mosto/vinho (e posterior aquecimento) provoca a redução de ligações dissulfureto intra-proteína, dificulta a troca tiol-dissulfureto durante interacções proteicas e leva à formação de novas ligações dissulfureto inter-proteína na fase de arrefecimento. A formação destas novas ligações, juntamente com interacções hidrofóbicas entre as proteínas instáveis são, em última instância, responsáveis pela agregação das proteínas no vinho. Este novo modelo de turvação envolvendo SO_2 foi testado em solução modelo e validado em condições reais com vinho.

Para evitar a formação de turvação proteica em vinhos brancos, é prática comum, os enólogos removerem do meio as proteínas potencialmente instáveis recorrendo à adição de bentonite, uma argila com carga negativa ao pH do vinho que adsorve proteínas de carga positiva por permuta iónica. Embora seja bastante eficaz, a adição desta argila apresenta muitas desvantagens como o impacto negativo nas características organolépticas do vinho, a perda de vinho e a produção de resíduos devido à formação de borras após a sua adição. Com o objectivo de desenvolver uma alternativa à bentonite, sintetizámos um novo polímero reticulado que tem a capacidade de adsorver as proteínas do vinho ao ser usado como um auxiliar de processamento (como filtro ou pó). Este novo polímero foi testado com proteínas modelo e, testes preliminares usando vinho da casta Moscatel, validaram a sua capacidade para remover proteínas de vinho à escala laboratorial.

Palavras-chave

vinho; turvação proteica; dióxido de enxofre; agregação proteica; estabilização proteica

Contents

LIST OF FIGURES ..... **XVII**

LIST OF TABLES ..... **XXIII**

1. MOTIVATION **1**

1.1 BACKGROUND 1

1.2 QUESTIONS AND GOALS 3

2. INTRODUCTION **5**

2.1 PROTEIN INSTABILITY 5

2.2 PURIFICATION AND CHARACTERIZATION OF HAZE-FORMING PROTEINS IN WINES 7

2.3 OTHER NON-PROTEINACEOUS FACTORS THAT MODULATE PROTEIN HAZE FORMATION IN WINES 9

2.4 REVIEW ON THE MECHANISM OF PROTEIN HAZE FORMATION 13

2.5 WINE PROTEIN STABILIZATION 14

3. PROTEIN HAZE FORMATION MECHANISM IN WHITE WINES. **19**

3.1 ISOLATION AND IDENTIFICATION OF THE COMPOUNDS PRESENT IN WHITE WINE PROTEIN AGGREGATES AFTER ALKALINE HYDROLYSIS. 21

3.1.1 Background *23*

3.1.2 Objective *24*

3.1.3 Results and discussion *24*

3.1.3.1 Protein haze sediment 24

3.1.3.2 Qualitative analysis of the compounds present in the white wine sediment 24

3.1.3.3 Isolation and identification of the compounds present in the ethyl acetate soluble fraction of the alkaline hydrolysed white wine sediment. 25

3.1.3.4 Quantification of caffeic acid in the untreated wine 27

3.1.3.5 Does the presence of caffeic acid (1) in the heat-induced wine sediment warrant its identification as a modulating factor in protein haze formation? 28

3.1.4 Conclusion *31*

3.2 MOTIVATION TO CHANGE THE WINE MODEL SOLUTION 33

3.3 THE CHALLENGING SO_2-MEDIATED CHEMICAL BUILD-UP OF PROTEIN AGGREGATES IN WINES. 37

3.3.1 Background *39*

3.3.2 Objective *40*

3.3.3 Results and discussion *40*

3.3.3.1 Interaction of SO_2 with wine total proteins 40

3.3.3.2 Interaction of SO_2 with protein fractions differing in hydrophobicity 42

3.3.3.3 Effect of protein reduction on wine total protein aggregation 47

3.3.3.4 Study of the impact of SO_2 on the aggregation of wine thaumatins. 51

3.3.3.5 Structural studies on iTLP aggregates 63
3.3.3.6 Effect of SO_2 addition on protein haze formation under real wine conditions 70
3.3.3.7 Updated mechanism for wine protein haze formation 74
3.3.4 Conclusions 75

4. FINDING A BENTONITE ALTERNATIVE – DEVELOPMENT OF A NEW POLYMER TO REMOVE UNSTABLE PROTEINS FROM WHITE WINES 79

4.1 SYNTHESIS AND STRUCTURAL CHARACTERIZATION OF DICARBOXYMETHYLCELLULOSE 81
4.1.1 Introduction 83
4.1.1.1 Synthesis of cellulose derivatives 85
4.1.1.2 Cellulose ethers 86
4.1.1.3 Applications in Food Products 88
4.1.1.4 Cellulose derivatives as ion exchangers 89
4.1.1.5 Cellulose based ion exchangers in the wine industry 90
4.1.2 Objective 92
4.1.3 Results and discussion 92
4.1.3.1 Synthesis of dicarboxymethyl cellulose 92
4.1.3.2 Structure elucidation of DCMC 97
4.1.3.3 Acetylation of DCMC 104
4.1.3.4 Infrared analysis of DCMC 107
4.1.3.5 X-ray analysis of DCMC and Avicel 108
4.1.3.6 DCMC degree of substitution (DS) 110
4.1.3.7 DCMC degree of polymerization (DP) and intrinsic viscosity 114
4.1.3.7.1 Size exclusion chromatography (SEC) 114
4.1.3.7.2 Viscosity measurements 115
4.1.4 Conclusions 117
4.2 PRODUCTION OF A WATER-INSOLUBLE FORM OF DCMC FOR THE ADSORPTION AND REMOVAL OF POSITIVE PROTEINS FROM A SOLUTION 119
4.2.1 Introduction 121
4.2.2 Objective 122
4.2.3 Results and discussion 122
4.2.3.1 First approach in the synthesis and production of DCMC films 122
4.2.3.1.1 Polymer preparation 122
4.2.3.1.2 Crosslinked sodium DCMC films preparation 124
4.2.3.1.3 Protein adsorption on the crosslinked NaDCMC films 124
4.2.3.2 Second approach in the synthesis and production of DCMC films 126
4.2.3.2.1 Polymer preparation 126
4.2.3.2.2 Films preparation 127
4.2.3.2.3 Cytochrome *c* (cytc) adsorption on the crosslinked NaDCMC 130
4.2.3.2.4 Isolated wine protein adsorption on crosslinked NaDCMC 133
4.2.3.2.5 Removal of soluble proteins from wine with DCMC11 powder 135

4.2.3.2.6 Synthesis cost analysis 136
4.2.4 Conclusion *137*
4.3 PRODUCTION OF A CELLULOSE MEMBRANE FILTER CONTAINING DCMC POLYMER FOR IN-LINE FILTRATION AND REMOVAL OF SOLUBLE PROTEINS. 139
4.3.1 Objective *141*
4.3.2 Results and discussion *141*
4.3.2.1 Polymer synthesis 141
4.3.2.2 Production of cellulose sheets with added DCMC 145
4.3.2.3 Evaluation of the ion exchange capacity of the filter sheets containing DCMC 146
4.3.2.4 Removal of soluble proteins from wine with cellulose/DCMC membrane 150
4.3.3 Conclusions *151*
5. GENERAL CONCLUSIONS 153
6. EXPERIMENTAL 157
6.1 REAGENTS AND STANDARDS 157
6.2 EQUIPMENT 157
6.3 BIOLOGICAL MATERIALS 158
6.4 DYNAMIC LIGHT SCATTERING (DLS) 159
6.5 SULFUR DIOXIDE QUANTIFICATION 159
6.6 PROTEIN INSTABILITY TEST 159
6.7 PROTEIN HAZE SEDIMENT ISOLATION 160
6.8 ALKALINE HYDROLYSIS OF WINE PROTEIN SEDIMENTS 160
6.9 RP-HPLC-DAD INSTRUMENTATION 160
6.10 SEPARATION OF ISOLATED WINE PROTEINS BY HYDROPHOBIC INTERACTION CHROMATOGRAPHY (HIC) 161
6.11 SIZE EXCLUSION CHROMATOGRAPHY (SEC) 161
6.12 SYNTHETIC ROUTE FOR CAFTARIC ACID (6) 162
6.13 ANALYSIS OF THE PROTEIN SECONDARY STRUCTURE BY CIRCULAR DICHROISM (CD) 163
6.14 FLUORESCENCE SPECTROSCOPY 163
6.15 STATISTICAL ANALYSIS 163
6.16 DTNB ASSAY 163
6.16.1 DTBN assay of protein without heat stress *164*
6.16.2 DTNB assay of heat stressed protein *164*
6.17 SYNTHESIS OF 2-BROMOMALONIC ACID (BMA) AND SODIUM 2-BROMOMALONATE (11) 166
6.18 SYNTHESIS OF DICARBOXYMETHYLCELLULOSE IN ISOPROPANOL/AQUEOUS NAOH 166
6.19 ACETYLATION OF DCMC 168
6.20 FORMYLATION OF DCMC 169
6.21 SODIUM CONTENT DETERMINATION BY ICP-AES 169
6.22 INTRINSIC VISCOSITY 169

6.23 SIZE EXCLUSION CHROMATOGRAPHY (SEC) OF DCMC 170
6.24 ANION EXCHANGE CHROMATOGRAPHY (AE-HPLC) 170
6.25 X-RAY DIFFRACTION (XRD) 170
6.26 DCMC FILM PREPARATION 170
6.27 DCMC FILM CROSSLINKING 171

7. REFERENCES 172

8. APPENDIX A 198

List of figures

Figure 1- Schematic representation of what wrong storage or shipping, by exposure of wine to high temperatures, may induce to wine unstable protein. Left) white wine prior to heat; Right) the same wine after heat stress. 1

Figure 2 - Temperature profile of a wine shipment from California to Illinois during summer. Measured [4]. Unprotected – Temperature floctuations registered on top of the pallets above the thermal blanket. Protected – Temperature fluctuations registered below the insulation (thermal blanket). 6

Figure 3 - Detail of the differences in loop regions of Domain I between protein I/4L5H chain A (purple) and protein F2/4JRU (in blue) [24]. 9

Figure 4 - Revised unfolding and aggregation mechanism of heat-unstable proteins in wine [5]. 13

Figure 5 - Chromatogram of the ethyl acetate soluble fraction obtained by liquid-liquid extraction of the hydrolyzed wine protein precipitate monitored at 320 nm. The collected peaks are identified as 1 and 2. 25

Figure 6 - ^{1}H NMR spectrum in CD_3OD of caffeic acid isolated from fraction #2. 26

Figure 7 - Synthetic route adopted for the synthesis of caftaric acid (**6**). 28

Figure 8 - ^{1}H NMR spectrum in CD_3OD of caftaric acid (**6**) after isolation by RP-HPLC. 29

Figure 9 - The interaction of SO_2 with hydrogen peroxide and quinones following catechol oxidation, so preventing oxidation of ethanol by the Fenton reaction [144]. 34

Figure 10 - (A) Cation exchange chromatogram of Moscatel of Alexandria wine sample on a Resource S (5 mL) column (6 mL/min flow rate). Loading and washing steps were omitted for clarity. Approximately 1 L of wine was loaded onto the column (ca. 100 mg protein). The total wine protein fractions were pooled (T1 fraction) based on the elution profile monitored at 280 nm. (B) Effect of increasing total SO_2 concentration (added as $NaHSO_3$) in the wine model solution on the haze produced after the heat stability test. The wine model solution consisted of 100 mg/L total wine protein (T1 fraction), 12% (v/v) ethanol, 5 g/L tartaric acid, pH 3.2 41

Figure 11 - (A) HIC chromatogram of the total wine protein previously isolated by cation exchange chromatography (Figure8). Abbreviated names were assigned to HIC individual protein fractions and correspond to the numbered peaks eluted from the HIC column preceded by an 'H'. HIC was performed on a Phenyl Superose HR 5/5 column. Lyophilized protein was dissolved in 25 mM K_2HPO_4 containing 1.25 mM $(NH_4)_2SO_4$, pH 7.0, prior to loading. (B) Protein content (mg) and the proportion it represents relative to total protein in the chromatogram (%) for each fraction (H1–H7) obtained after HIC (A). 42

Figure 12 - (A) Haze development after heat stability test of the isolated HIC fractions (adjusted to 100 mg/L protein) in two model wine solutions. Control: no added SO_2. SO_2: model wine solution containing 120 mg/L total SO_2 (added as $NaHSO_3$). H3–H6 indicate protein fractions obtained by HIC separation as shown in Figure 11A. Means not sharing the same letter are significantly different (OneWay-ANOVA, Fisher LSD, $P < 0.05$). (B) Visualization of the haze produced after heat stability test of HIC fractions H3–

H6 in model wine solutions with and without added SO_2. Cuvettes represented in the picture correspond to the ones used in the experiment described in (A). 44

Figure 13 - A) Cation exchange chromatogram of Moscatel of Alexandria (2014) wine sample on a Resource S (6 mL) column (6 mL/min flow rate). Loading and washing steps were omitted for clarity. Approximately 0.5 L of wine was loaded onto the column. The total wine protein fractions were pooled (F1 fraction) based on the elution profile monitored at 280 nm. B) HIC chromatogram of the total wine protein previously isolated by cation exchange chromatography (Figure 13A). Abbreviated names were assigned to HIC individual protein fractions and correspond to the numbered peaks eluted from the HIC column preceded by an 'H'. HIC was performed on a Phenyl Superose HR 5/5 column. Lyophilized protein was dissolved in 30 mM sodium citrate containing 1.25 M ammonium sulfate, pH 3.0, prior to loading. 45

Figure 14 – A) Autocorrelation curve acquired by DLS nanoanalysis of the protein fraction H4 (native state) in wine model solution at 25 °C. B) Size distribution frequency acquired by DLS nanoanalysis (represented as the protein diameter in nm) of the iTLP (native state) in wine model solution before heat stress. 47

Figure 15 - Effect of TCEP or $NaHSO_3$ on the haze produced after heat stability test in a wine model solution. Final concentrations are indicated in the X-axis labels. The model solution consisted of 100 mg/L total wine protein (F1 fraction, Figure 13A), 12% (v/v) ethanol, 5 g/L tartaric acid and pH 3.2. 49

Figure 16 - Dependence of particle diameter on time and temperature for the aggregation of iTLP (at 500 mg L^{-1}) in model wine solution containing SO_2 (at 600 mg L^{-1}). The count rate is represented by (o) and the measured diameter by (x). The time required to decrease the temperature from 70 to 15 °C (i.e. 8 min) is represented by the vertical dashed lines. 52

Figure 17 - A) Dependence of hydrodynamic diameter on time for aggregation of protein iTLP (solid line). Also represented are the peaks of the size distributions of B) including: (■) first, (□) second, (●) third aggregated forms. Horizontal lines correspond to the average particle size of these forms. B) Distribution of particle size registered at different times of iTLP at 15 °C after heat stress. 53

Figure 18 - Dependence of light scattering intensity on time for aggregation of iTLP with Boltzmann curve fitting. 55

Figure 19 – Absorption spectra of iTLP during CD analysis. A) iTLP in model wine solution (absence of SO_2). B) iTLP in model wine solution in the presence of SO_2. Temperatures of 20 °C (prior to heat stress), 70 °C (after 120 min at 70 °C) and 15 °C (after 60 min at 15 °C following heat stress at 70 °C) are highlighted in blue, orange and green respectively. The remaining spectra gathered during the trial are represented as solid grey lines. 57

Figure 20 – A) CD spectra of iTLP (at 500 mg L^{-1}) in model wine solution (absence of SO_2). B) CD spectra of iTLP in model wine solution in the presence of SO_2 (at 600 mg L^{-1}). Spectra corresponding to temperatures of 20 °C, 70 °C and 15 °C are represented in blue, orange and green, respectively. The different spectra gathered during the time window of the trial are represented as solid grey lines. 58

Figure 21 – Changes in molar ellipticity of iTLP at 222 nm. The temperature gradient consisted of 10 °C increments in the temperature range between 20 and 70 °C. Within parenthesis is represented the time at which the protein was at that temperature. 60

Figure 22 - Tryptophan emission intensity of A) and B) iTLP (100 mg L^{-1} in model wine solution in the absence of SO_2) and C) and D) iTLP (100 mg L^{-1} in model wine solution) in the presence of SO_2 (120 mg/L total SO_2). A) and C), heating: blue 25 °C, green 40 °C, black 60 °C and red 70 °C; B) and D), cooling (following heat stress represented in A) and C): red 70 °C, black 50 °C, green 25 °C and blue 15 °C). Black arrows represent the shift of the curves with time and temperature. 62

Figure 23 - A) Autocorrelation curve acquired by DLS nanoanalysis of the iTLP in wine model solution after heat stress. B) Size distribution frequency acquired by DLS nanoanalysis (represented as the protein diameter in nm) of the iTLP after heat stress dissolved in buffer A. 64

Figure 24 - Size-exclusion chromatogram of non-reduced (A) and reduced (B) iTLP dissolved in MWS (–), iTLP after heat stability test (absence of SO_2) (–), pellet (–) and supernatant (–) of iTLP after heat stability test (presence of SO_2) in buffer A. First peak at 7.9 min corresponds to blue dextran used as internal standard (IS)..... 65

Figure 25 - A) Experimental data and corresponding fitting of the chromatographic profile of the heat stressed iTLP in the presence of SO_2 (baseline corrected). Multi-peak Gaussian analysis of the chromatogram is represented by the different Fit Peaks represented in the figure: iTLP after heat stability test (presence of SO_2) (–), fit peak 1 (–), fit peak 2 (–), fit peak 3 (–) and cumulative fit peak (–). B) The table describes the different protein species and discriminates their relative amounts based on the peaks integrals. 67

Figure 26 - Size-exclusion chromatogram of non-reduced iTLP dissolved in WMS (100 mg/L) (–), iTLP after heat stability test without SO_2 addition (–), pellet of iTLP after heat stability test with SO_2 (120 mg/L) dissolved in buffer A (–), pellet of iTLP after heat stability test with SO_2 (200 mg/L) dissolved in buffer A (–) and pellet of iTLP after heat stability test with SO_2 (600 mg/L) dissolved in buffer A (–)..... 69

Figure 27 - Reaction of iTLP with DTNB reagent in buffer E containing 200 mM Tris-HCl, 8 M urea, pH 8.0. Control corresponds to the assay performed in the absence of protein. Mean values not sharing the same letter are significantly different (OneWay-ANOVA, Tukey HSD, $P < 0.05$). 70

Figure 28 - A) Total and free SO_2 content of the sample wine (W), of the <3 kDa fraction (<3 kDa) and of the <3 kDa fraction after lyophilisation (<3 kDa AL). B) Haze development after heat stability test of sample wine (W; 80 mg/L protein), of the <3 kDa fraction added of total wine protein (<3 kDa; 80 mg/L protein), of the <3 kDa fraction after lyophilization added of total wine protein (<3 kDa AL; 80 mg/L protein), and of the <3 kDa fraction added of 120 mg/L total SO_2 without protein addition (<3 kDa + SO_2). 71

Figure 29 - Proposal of new mechanism for wine protein haze formation. 74

Figure 30 - Structural hierarchy of the cellulose fiber components from plant fiber to the glucose molecule [177]..... 84

Figure 31 - Global use of wood for cellulose derivatives production in 2003 [179] 85

Figure 32 - Examples of commercial cellulose ethers (adapted) [176]. 87

Figure 33 – Conversion of neutral cellulose into a polyelectrolyte by pH change: schematic representation of the ionization of the hydroxyls of cellulose in strong alkali medium (extremely high pH) [186]. 88

Figure 34 – Representation of diethylaminoethyl cellulose (7), carboxymethyl cellulose (8), quaternary aminoethyl cellulose (9) and sulphopropyl cellulose (10). In the figure cellulose is represented by an anhydroglucose unit. 89

Figure 35 - Schematic representation of the reaction between the sodium bromomalonate (11) and the anhydroglucose unit of cellulose. In the figure, we can see a representation of a DS = 1 molecule substituted in the primary alcohol in C6. 93

Figure 36 - ^{1}H NMR spectrum of sample DCMC3 in D_2O (water soluble fraction of the product). 94

Figure 37 - ^{13}C NMR spectrum of sample DCMC3 in D_2O (water soluble fraction of the product). 95

Figure 38 – Reaction by-products and starting materials possibly present in the crude of the cellulose derivatization. 95

Figure 39 - Stacked ^{1}H NMR spectra of sample DCMC2 to DCMC5 in D_2O (water soluble fraction of the product). 98

Figure 40 - Stacked ^{13}C NMR spectra of sample DCMC2 to DCMC5 in D_2O (water soluble fraction of the products). 99

Figure 41 - COSY spectra of sample DCMC4 in D_2O. 100

Figure 42 - HSQC spectra of sample DCMC4 in D_2O. Horizontal axis corresponds to the ^{1}H spectra, vertical axis corresponds to ^{13}C 101

Figure 43 – Summary of the signals assignment of dicarboxymethylcellulose. A) schematic representation of the anhydroglucose unit and the substituent B) ^{1}H NMR spectra of DCMC4 C) ^{13}C NMR spectra of DCMC4. 102

Figure 44 - HMBC spectra of sample DCMC4 in D_2O. 103

Figure 45 - ^{1}H NMR spectra of acetylated DCMC4 in DMSO. 105

Figure 46 - ^{13}C NMR spectra of acetylated DCMC4 in DMSO. 106

Figure 47 - ^{1}H NMR spectra of malonyl cellulose sample DCMC4 after hydrolytic chain degradation by D_2SO_4 during 5 hours at 90 °C. O represents the oxygen atom at position i (i=2,3 and 6), H-1 the proton at the anomeric carbon atom, α and β the configuration of glucose, s is used for substituted and u for unsubstituted positions. 107

Figure 48 - A) Infrared spectra of the different synthesized samples B) expansion of the 2000 – 400 nm region in samples DCMC4 and underivatized cellulose (Avicel MN 400). 108

Figure 49 – Avicel and DCMC diffractograms 109

Figure 50 - Representative chromatograms of samples DCMC2 to DCMC5 hydrolytically depolymerized. 113

Figure 51 - Molecular weight distributions of samples DCMC2 to DCMC5 analyzed by size exclusion chromatography. 114

Figure 52 - A) Concentration dependence of reduced viscosity of samples DCMC2 to DCMC5 at 20 °C (samples were dissolved in 6% NaOH) B) Intrinsic viscosity of samples DCMC2 to DCMC5. 116

Figure 53 - Regioselective oxidation of C6 primary hydroxyls of cellulose to C6 carboxylate groups by TEMPO/NaBr/NaClO oxidation in water at pH 10–11 [248]. 121

Figure 54 - DCMC6 film (150 mg of polymer) before crosslinking reaction. 124

Figure 55 - A) Experimental adsorption isotherm for cytochrome *c* on a DCMC6 film in 25 mM citrate buffer, pH 3.2. B) Linear fitting of the experimental values presented in A based on the Langmuir isotherm model. 125

Figure 56 – Visualization of the increasing quantity of DCMC6 (from left to right) on the protein adsorption capacity. This image was gathered after 24 hours of contact between the polymer and the solution at 25 °C. 125

Figure 57 -Polymer (DCMC11) after dialysis and freeze drying. 127

Figure 58 - Film of DCMC12 after drying and detaching from the Teflon casting. 128

Figure 59 - Representation of the heat crosslinking reaction of DCMC. 129

Figure 60 - A) Experimental adsorption isotherm for cytc (1mg/mL) on a NaDCMC11 powder in 25 mM citrate buffer, pH 3.2, for 30 minutes. In red is represented the nonlinear fitting using the Langmuir model equation B) Linear fitting of the experimental values presented in A based in the Langmuir model (R2 = 0.998) 132

Figure 61 - Polymer DCMC11 crosslinked (powder form) added to a solution of Cytc (at 1 mg/mL). This image was taken after 1 minute contact between the polymer and protein solution. Vials were centrifuged prior to the photo to emphasize the difference between pellet and supernatant. 133

Figure 62 - A) Experimental adsorption isotherm for isolated wine protein (IWP) at 1 mg/mL, for 30 minutes, on NaDCMC6 in model wine solution (5 g/L tartaric acid, 12% ethanol, pH 3.2). B) Linear fitting of the experimental values presented in A based on the Langmuir model (R^2 = 0.982). 133

Figure 63 - Diagram showing mechanism of the Krapcho reaction. 137

Figure 64 - Apparatus used to generate HCl gas. The dry cellulose samples were exposed to HCl gas for 30 minutes to guarantee their protonation. 143

Figure 65 - FTIR-ATR spectra of Kraft pulp (-), dialyzed DCMC 13 (-), crosslinked protonated DCMC 13 (-) and crosslinked deprotonated (sodium salt) DCMC 13 (-). 145

Figure 66 - Paper sheet with DCMC added at a concentration of 18% (w/w). The spots scattered along the sheet correspond to the added DCMC. 146

Figure 67 - Filtration apparatus used to test the DCMC sheets. 146

Figure 68 - Representation of the DCMC membranes after filtration of Cytc solution and washing with deionized water..... 148

Figure 69 - DCMC acetylation reaction scheme. 168

List of tables

Table 1 - Retention times (t_R), spectral bands (λmax in bold) and detection wavelength ($\lambda_{detection}$) of the compounds selected in Figure 1. 25

Table 2 - Concentration of caffeic acid (1) in the untreated wine under analysis, isolated by SPE followed by RP-HPLC-DAD. The calibration curve was prepared using 99% pure caffeic acid. 27

Table 3 - Changes in turbidity of wine and wine model solutions after heat stability test measured at 540 nm. IWP + <3 kDa: <3 kDa wine fraction supplemented with 190 mg/L of isolated wine protein; IWP + WMS: isolated wine protein (190 mg/L) in wine model solution; 1: caffeic acid (1.1 or 5 mg/L) added to IWP in wine model solution; 6: caftaric acid (1.1 or 5 mg/L) added to IWP in wine model solution. The pH of all samples was adjusted to 3.2. Different letters represent distinct homogeneous subsets for p = 0.05 (ANOVA, Tukey HSD). 30

Table 4 - Different model wine solutions described in the literature used to study wine protein interactions/aggregation. 33

Table 5 - Summary table of the LC-MS/MS of the H4 protein fraction isolated by HIC. 46

Table 6 - Secondary structure analysis of iTLP (with and without added SO_2) by the deconvolution of CD spectra with the algorithms SELCON3, CONTIN and CDSSTR. The values presented in this table correspond to the averages of the results acquired by the different algorithms per each point represented as percentage. The dataset used in these analyses were the SP175 available in the Dichroweb portal. The individual values per each algorithm are available in Appendix A. 58

Table 7 - Molecular weight of the different molecular species present in the protein peaks depicted in Figure 24, calculated after their fractionation by non-reducing size exclusion chromatography. 66

Table 8 - Summary analysis of two varietal wines, each one produced with and without added SO_2. Means not sharing the same letter are significantly different (OneWay-ANOVA, Tukey HSD, P < 0.05). 73

Table 9 - Summary of reaction conditions for DCMC1 to DCMC5. 93

Table 10 – Water soluble percentages and elemental analysis results for samples DCMC1 to DCMC5. .. 97

Table 11 - Integrals of the different protons in samples DCMC2 to DCMC5. As reference, the area between 4.05 and 3.1 was adjusted to 6 protons. 98

Table 12 - Literature where acetylation of CMC was performed and corresponding protocol. 104

Table 13 – Sodium quantification by ICP-AES of deprotonated samples DCMC 2 to 5 (sodium salt form). The samples were hydrolyzed in nitric acid prior to ICP-AES analysis to protonate the samples. 111

Table 14 - Areas and area percentage of the different substituted AGU units in samples DCMC2 to DCMC5 113

Table 15 - Degree of polymerization of the different samples after treatment of the SEC results. The DS used to calculate the DP was calculated based on ICP-AES results. 115

Table 16 - Conditions used for the derivatization of cellulose with different quantities of sodium 2-bromomalonate (**11**). 123

Table 17 -Degree of substitution calculated from the sodium content measured by ICP-AES and water solubility of the different samples. 123

Table 18 - Conditions used for the synthesis of DCMC11. 126

Table 19 - Sodium quantification using ICP-AES and calculated degree of substitution (DS) of samples DCMC11 and DCMC11 crosslinked. 130

Table 20 - DCMC production cost analysis (1.02 g of polymer DCMC11). The prices described in the table are based on commercially available reagents except for 2-bromomalonic acid. 136

Table 21 - Natural composition of pine and birch wood and corresponding kraft pulps derived from them (adapted from [263]) 141

Table 22 - Conditions used for the derivatization of cellulose with sodium 2-bromomalonate (**11**). 142

Table 23 - A summary of the weight loss (starting from 2 g of each sample) during the purification and crosslinking steps of DCMC polymers 12 to 15. 143

Table 24 - Sodium quantification using ICP-AES and calculated degree of substitution (DS) of samples DCMC 12 to 15. 144

Table 25 – Protein adsorption capacity calculations for polymers DCMC 12CL, 13CL and 15CL. Each membrane was tested in duplicate. 149

Table 26 – Protein adsorption capacity calculation of polymer DCMC15CL (incorporated in cellulose sheets) after filtering 10 mL of Moscatel of Alexandria wine. In this trial, two sheets of 2.6 cm of diameter were used. Both starting and final protein concentration were measured directly in the wine prior and after filtration by the Bradford method. 150

Table 27 - Detailed description of the DTNB method used for the quantification of the free thiol groups in the different protein species. 165

Table 28 - Results from the different algorithms used in the analysis of the circular dichroism results. . 198

Abbreviations and Symbols

AGU	anhydroglucose unit
AU	absorbance units
BMA	bromomalonic acid
BSA	bovine serum albumin
c	protein concentration in the buffer (mg/mL)
CD	circular dichroism
CD_3OD	deuterated chloroform
CMC	carboxymethylcellulose
CPLL	combinatorial peptide ligand libraries
Cys	cysteine
cytc	cytochrome *c*
D_2O	deuterium oxide
DCMC	dicarboxymethyl cellulose
DEAE	diethylaminoethyl cellulose
DEPT	distortionless enhancement by polarization transfer
DLS	dynamic light scattering
DMSO	dimethyl sulfoxide
DP	degree of polymerization
DS	degree of substitution
DSC	differential scanning calorimetry
DTNB	5,5′-dithiobis(2-nitrobenzoic acid)
DTT	dithiotreitol
EC	ethylcellulose
EtOH	ethanol

FPLC	fast protein liquid chromatography
HEC	hydroxyethylcellulose
HIC	hydrophobic interaction chromatography
hL	hectolitres
HMBC	heteronuclear multiple bond correlation
HPC	hydroxypropylcellulose
HPLC	high pressure liquid chromatography
HSQC	heteronuclear single quantum coherence
ICP-AES	inductively coupled plasma - atomic emission spectrometry
IgG	Immunoglobulin G
iTLP	isolated thaumatin-like protein
IWP	isolated wine protein
kDa	kilodaltons
MC	methylcellulose
MCC	microcrystalline cellulose
MPEE	mannoproteins extracted by enzymes
MWS	model wine solution
NMR	nuclear magnetic resonance
OIV	International Organization of Vine and Wine
PC	phosphate cellulose
PGMA-g-Cell-SO3H	poly(glycidylmethacrylate)-grafted-cellulose sulfonate functional groups
Phe	phenylalanine
ppm	parts per million

PR-proteins	pathogen related
PVPP	poly(vinylpolipirrolidone)
Q_{max}	polymer maximum adsorption capacity (mg/g)
RDV	rotary vacuum drying system
RP-HPLC-DAD	reversed phase high performance liquid chromatography with diode array detector
SCX	strong cation exchange
SDS-PAGE	sodium dodecyl sulfate polyacrylamide gel electrophoresis
SEC	size-exclusion chromatography
SPE	solid phase extraction
TBAF	tetra-n-butylammonium fluoride
TBDMS-Cl	*tert*-butyldimethylsilyl chloride
TCA	trichloroacetic acid
TCEP	tris(2-carboxyethyl) phosphine
TEMPO	2,2,6,6-tetramethylpiperidine-1-oxyl
TFA	trifluoroacetic acid
TLP	thaumatin-like proteins
T_m	melting temperature value
t_R	retention time
Trp	tryptophan
Tyr	tyrosine
UV-visible	ultraviolet-visible

1. Motivation

1.1 Background

Wine clarity is one of the characteristics most easily affected by inappropriate shipping and storage conditions (Figure 1). One of the reasons for a white wine to turn turbid during storage resides on the insolubilization and aggregation of residual proteins that remain in wine after the fermentation process, a phenomenon commonly known as protein haze. Formation of these unattractive precipitates in bottled wine is a common defect of commercial wines, making them unacceptable for sale. For this reason, ensuring wine stability prior to bottling is an essential step of the winemaking process and presents a significant challenge for winemakers.

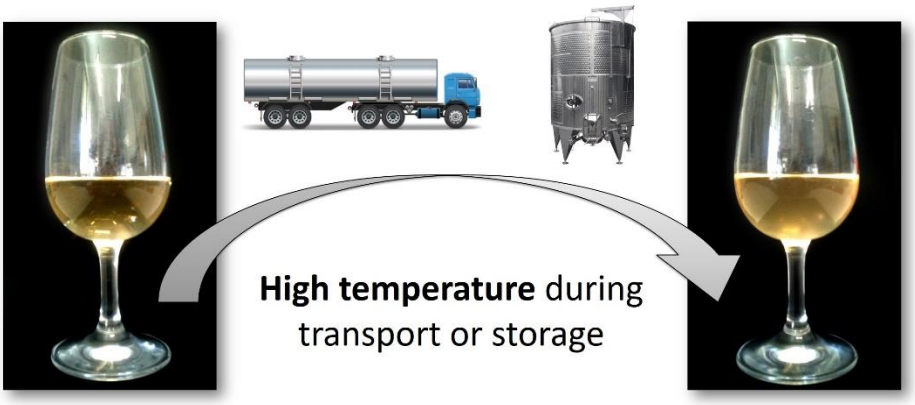

Figure 1- Schematic representation of what wrong storage or shipping, by exposure of wine to high temperatures, may induce to wine unstable protein. Left) white wine prior to heat; Right) the same wine after heat stress.

While being just an aesthetic issue, protein haze formation in wines has been described and studied for more than 30 years with incidence not only on the characterization of unstable wine proteins but also on the mechanism(s) by which protein haze formation in white wine occurs. Based on the literature, several variables that contribute to wine protein instability are known: protein concentration, pH, temperature and other wine components that modulate the susceptibility of the proteins to aggregate. To understand which "other wine components" modulate wine protein haze formation, an extensive collection of compounds has already been tested including esters, phenolic compounds, organic acids and salts, among others. However, up to the present work, besides proteins, there is no precise answer about what other compounds trigger white wine protein haze formation.

To tackle the problem of white wine protein haze formation, winemakers remove the soluble proteins from unstable wines avoiding its precipitation once bottled. This is routinely done by cation exchange, i.e. fining the wine with bentonite. Bentonite is a negatively charged clay that is very effective in removing proteins from wines, though it has negative impact not only on cost, but also on the wine aroma and mouthfeels and in production of undesirable by-products (higher lees production, sediments difficult to treat in water treatment stations). Because winemakers do not know the identity of the compounds (besides proteins) which trigger this process, many wines are unnecessarily fined with bentonite since commercially available stability tests often give results based only in the wine protein content.

Increased growing-season temperatures are an actual problem in wine producing countries. Wines from these regions will present higher protein content which consequently will need higher doses of bentonite to become stable. Thereby, there is the need to develop new technologies, alternative to bentonite, that allow winemakers to stabilize white wines without such impact not only on the wine but also on the environment.

1.2 Questions and goals

Concerning the problems raised above, some questions become scientifically significant:

- Besides proteins, which wine compounds (from the grape, yeast or artificially added) trigger protein aggregation upon heat stress?
- How do these compounds interact with wine proteins upon heat stress?
- Are we able to remove these compounds from the wine, thus avoiding the use of bentonite to remove the proteins?
- If we cannot remove the compounds that interact with wine proteins, can we remove the proteins using a lower impact alternative method?

To address these questions, the following research strategy was applied:

- Study the wine protein aggregation mechanism.
- Isolate and identify which compounds are present in the protein haze sediment.
- Test if these isolated compounds, together with other reactive compounds present in wine, induce the aggregation of wine proteins in a model wine solution.
- If aggregation occurs, study how do these compounds induce protein aggregation.
- Development of a bentonite alternative.
- Development of a new design polymer, from a renewable source, which binds wine proteins and removes them from solution.

2. Introduction

In 2015 there were 7.5 x 10^{10} m^2 hectares of cultivated grape vines where Spain, China, France, Italy and Turkey represent 50% of the world planted vineyard [1]. Altogether, grapes were considered by FAO the fruit crop with the highest area harvested in 2014 [2]. Around 48% of the produced grapes are wine grapes, which rendered an estimated wine production of 2.59 x 10^8 hL in 2016. The contribution of the wine sector to the world economy in 2013 reached a value of US$277.5 billion, with a large proportion of the wine exported [3]. Thus, a substantial volume of wine is subject to potentially damaging conditions during transportation and storage, such as inappropriate temperature or humidity, that can cause deleterious modifications of the organoleptic features of the wine [4,5].

Wine clarity, especially that of white wines, is important to most consumers and is also one of the characteristics that is most easily affected by inappropriate shipping and storage conditions. This aspect will not only be a key element in the visual satisfaction of the consumer but also will enhance the impression of quality on the palate. For this reason, securing wine stability prior to bottling is an essential step of the winemaking process and presents a significant challenge for winemakers [5,6]. A stable white wine is one that is clear and free from precipitates at the time of bottling, through transport and storage, to the time of consumption. The presence of precipitates or the appearance of haze after storage are some of the most commonly defects in wines. These can be caused by several factors including residual sediments from the vinification process, microbial growth, oxidation, tartrate precipitation, colouring matter (in the case of rosé and red wines), metallic casse (including ferric and copper casses) or heat unstable proteins [6].

2.1 Protein instability

Protein aggregation is a common phenomenon and a major obstacle to handling proteins *in vitro* [7]. Most proteins are physically and chemically unstable. Factors that influence the stability of a protein were divided into two categories [8]: (1) intrinsic factors, derived from the inherent physicochemical properties of the protein, and (2) the extrinsic factors, derived from the environment of the protein such as pH, temperature, ionic strength and excipients. These factors can impact on disulfide (S-S) bonds. Location of S-S bond reshuffling has been proposed to have a high impact on protein aggregation. Intramolecular disulfide bonds may alter protein conformation, whereas intermolecular bonds change particle molecular weight [9]. Protein aggregation poses concerns when the proteins are for use as pharmaceutical products, as aggregates can stimulate the immune system, but also in agriculture and food industry. One of the food industries affected by this type of problem is the wine industry. Heat unstable proteins will

precipitate in commercial wines mainly due to the exposure of wine to elevated temperatures during storage or transport.

Proteins play a significant role in the colloidal stability and clarity of white wines [10]. The isolation and characterization of white wine proteins in grape juice, wine and protein precipitate is thoroughly described in the literature [11–15]. Some of these proteins are known has haze-forming proteins. These proteins can self-aggregate under elevated temperatures into light-dispersing particles causing the so-called protein haze or protein casse [16]. [4] presented relevant data about the fluctuation of temperatures a wine can be exposed during transportation by truck and railroad (Figure 2).

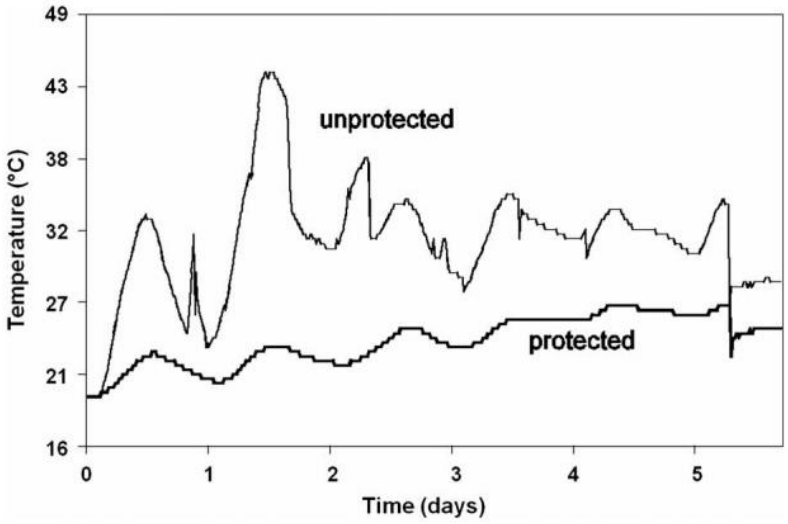

Figure 2 - Temperature profile of a wine shipment from California to Illinois during summer. Measured [4]. Unprotected – Temperature floctuations registered on top of the pallets above the thermal blanket. Protected – Temperature fluctuations registered below the insulation (thermal blanket).

The authors placed test packages inside shipping containers on top of the pallets above the thermal blanket (unprotected) and in the nose or tail of the container in pallets below the insulation (protected). The temperature changes within 1 day in the unprotected wine went up to 21 ˚C, which can have a negative impact in the wine. The authors emphasised that the extreme temperature fluctuations were observed only in the top packages and therefore not in the commercial wines that were shipped. However, wines that are shipped without any additional protection (such as blankets as described in this study) will be prone to extreme heat exposure, as well as major bottle variation even within cases from one single shipment. These heat fluctuations followed by refrigeration can trigger protein haze formation in unstable commercial wines. Formation of these unattractive precipitates in bottled wine is a common defect of commercial wines, making them unacceptable for sale [17]. A survey on the distribution of the most recent

research about this problem (between 2005 and 2013) showed that the published works focused almost equally among the elucidation of protein haze-forming mechanisms (36.6%), the methods for protein purification, quantification, identification and predicting wine haze potential (26.8%), and finding alternative strategies for wine stabilization (36.6%) [5].

2.2 Purification and characterization of haze-forming proteins in wines

The most abundant classes of haze-forming proteins that occur both in must and white wine are thaumatin-like proteins (TLP) and chitinases. These proteins are pathogen-related proteins (PR-proteins) that are normally found in white wines together with other minor occurring PR-proteins (e.g. osmotins, invertases, β-1,3-glucanases, lipid transfer proteins) [18,19]. These are the major proteins synthesized during all maturation stages of the grape following veraison and act as a defence mechanism for the plant against pathogen agents, though they can reach high concentrations regardless of the pathogen exposure [20–22]. The expression and accumulation of these protein families are mainly determined by the environmental and pathological conditions at which the grapes are exposed during the maturation period [23]. TLP and chitinases are compact and small proteins (< 35 kDa), have globular structure, are positively charged at the normal wine pH, are resistant to proteolytic attack and are tolerant to low pH in both grape juice and wine [19,24]. Protein content of wines is usually lower than protein content present in musts. This difference is related to the proteolytic activity manifested during the vinification process (which degrades the vast majority of the housekeeping proteins) and to precipitation due to polyphenols and to unfavorable wine conditions, such as low pH and alcohol content [10]. However, the major proteins remaining in wines are PR proteins thanks to their stability at low pH and high resistance to proteolysis [25]. During the vinification process, vacuolar acids and hydrolytic enzymes are released to the must precipitating and/or degrading many proteins present in grapes, thus favouring the predominance of PR proteins [13]. The combination of all these factors ensures that only the resistant proteins, in this case PR proteins, resist the vinification process, making them the principal precursors for protein haze formation in white wines [13,26].

Purification, quantification and characterization of wine total soluble proteins are actual investigation areas. Initially, denaturing electrophoresis was used to separate the proteins by their molecular weight. Four distinct bands were initially observed indicating four different protein groups, varying in concentration according to the environmental conditions prevailing and different varieties studied [27,28]. Newer techniques enabled a better characterization of proteins, like ion-exchange chromatography using FPLC [16,29,30]; chromatofocusing [31]; size exclusion chromatography [32]; affinity chromatography [30,32,33]; RP-HPLC [34,35]; and isoelectric focusing [12].

Purification, separation and characterization of proteins present in musts and wines is complex, due to their low concentrations and their interactions with non-protein wine compounds like phenolics. More recently, it was possible to achieve an even higher resolution on the purification and characterization of wine proteins using cation exchange chromatography (SCX) followed by hydrophobic interaction chromatography (HIC) and combinatorial peptide ligand libraries (CPLL) [14,36–38]. Isolating the different classes of haze-forming proteins allowed to not only to sequence them but also to study their individual aggregation behaviour.

In wines, different classes of haze-forming proteins display different thermal stabilities, as demonstrated by differential scanning calorimetry (DSC). Chitinases showed to be generally less stable than TLPs and can denature within minutes at temperatures >40 °C, compared to weeks for TLPs under the same conditions. Though chitinases showed the lowest melting temperature value (T_m), ranking them as the least stable of the grape proteins, thaumatin-like proteins were the next most likely candidate for haze formation showing, a T_m value marginally higher than that of chitinase. The most notorious difference between both protein groups was that TLPs could reverse the heat-induced unfold process, thus indicating that these specific proteins do not readily form irreversible aggregates under the tested conditions. Oppositely, chitinases did not refold after heating, resulting in denaturation of the proteins and consequently their precipitation under the tested conditions [39]. Another study, using dynamic light scattering (DLS), also indicated that TLPs do not contribute to the formation of visible aggregates in wine model system, though when analysing wine submitted to a heat stress (70 ^{o}C), both chitinases and TLPs were heat precipitated [40]. These findings emphasize the necessity to confirm the types of phenomena under real conditions since model systems may not mimic what happens in real wine conditions.

Recently, [24] determined the crystal structure and some physico-chemical parameters of three grape TLP isoforms using crystallography. The three isoforms had a high degree of structural similarity but showed not only different unfolding temperatures but also differences in the conformation of a single loop. From the superposition of the different isoforms, it was noticeable differences in two regions of the proteins. The biggest difference was characterized by a longer loop in the Domain I of protein F2/4JRU, attributed to the presence of five extra amino acids residues in its sequence.

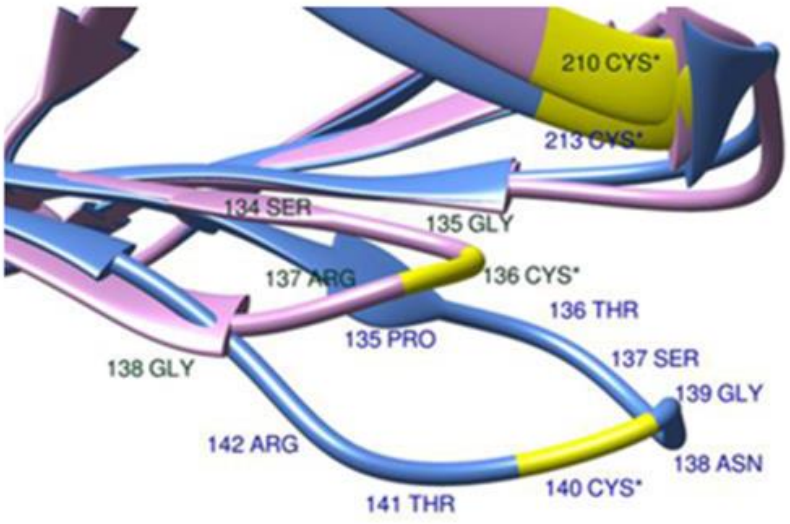

Figure 3 - Detail of the differences in loop regions of Domain I between protein I/4L5H chain A (purple) and protein F2/4JRU (in blue) [24].

Other observed differences were related to the unfolding behaviour upon heating of the three isoforms. Protein F2/4JRU showed a significantly lower unfolding temperature (56 ˚C) than the two remaining isoforms (with a melting temperature of 62 ˚C). The aggregation upon heat (in model wine solution) was also evaluated for the three proteins and revealed that aggregation was taking place only for protein F2/4JRU. This result was particularly relevant for the characterization of the haze forming properties of this protein, although these trials was performed using a wine model solution containing 1 g/L of K_2SO_4 which does not mimic real wine conditions. The three isoforms also presented different electrophoretic mobility depending on the presence or absence of a reducing agent. Comparing to the other two, protein F2/4JRU showed to be more compact and migrated to a lower level in the non-reducing SDS-PAGE analysis. This change shows that the small differences in the loops between the other isoforms can be significant enough to result in a change of the mobility and compactness of protein F2/4JRU. The authors hypothesised that the presence of the disulphide bridge in that different loop is probably the key for the unfolding/refolding behaviour of that area which could lead to the destabilization of the protein and subsequent aggregation, hence resulting in haze formation in wines.

2.3 Other non-proteinaceous factors that modulate protein haze formation in wines

Although PR proteins are the major compounds of the precipitate when haze occurs, it has been generally accepted that one or more non-proteinaceous compounds are required to trigger this process, whereas several nonprotein compounds and conditions seem to modulate/influence either positively or negatively the wine protein haze mechanism. These observations are strongly

supported by the results obtained by several authors [27,28] who demonstrated that the total protein content, by itself, failed to correlate with wine heat instability. Protein haze formation in wines is described as a multi-factorial process in which some modulating elements have already been recognized (protein content, pH, ionic strength, organic acids commonly encountered in wines and sulfate), whereas others remain to be identified such as the essential non-proteinaceous component(s) generally termed X-factor [41–43]. Two of these factors are pre-requisites for protein haze formation under the conditions prevailing in wines: the proteins themselves and the X-factor. The remaining elements act as positive or negative modulators in protein insolubilization and aggregation.

In an attempt to decipher which compounds interact with wine proteins to form haze, [43] proposed that sulfate could be the missing non-proteinaceous essential factor for protein haze formation. The modulating effect of sulfate was attributed to the possible promotion of hydrophobic interaction-driven aggregation through kosmotropic affect as well as the suppression of electrostatic repulsion between proteins by the increment of the ionic strength of the medium [40]. It is important to note that in this study, the effective sulfate concentration required to induce wine protein haze formation is in the range of 1 to 4 g/L, thus exceeding the legal sulfate limit for most wines. Even though wines with added sulfate produced higher haze, other factors like the reduction of the medium, tested by the addition of dithiothreitol (DTT), improved the aptitude of wine TLPs to form haze in the presence of wine tannins [36].

Of all non-proteinaceous factors that may be involved in wine protein haze, phenolic compounds have been the most extensively studied and substantial evidence exists to propose that their interactions with proteins are significant [44]. Koch [45] was among the first investigators to determine that isolated grape proteins were associated with tannins. It was shown that protein haze formation in beer and apple juice could decreased using poly(vinylpolypyrrolidone) (PVPP, a fining agent used to remove polyphenols) to remove haze-active polyphenols [46]. PVPP was added to white wines [43] and it was observed that the removal of phenolic compounds from the wine turned it more stable when submitted to heat stability test, confirming previous tests performed by other authors [47,48]. In fact, wines fined with PVPP presented lower haze formation after heat stability test, when compared to unfined wines [43]. High doses of isolated white wine tannins were tested with isolated must proteins, showing that protein-polyphenol interaction can cause haze formation [47]. The same authors also found that the monomeric phenolic fraction did not interfere in the haze formation. Despite these results, the tannin content used in the tests does not reflect the normal content of tannins present in white wines. Other authors showed that haze formation in wines seems to be related to hydrophobic interactions occurring between proteins and tannins [36]. These interactions should occur on hydrophobic tannin-binding sites, whose exposition on the proteins can depend

on both protein heating and reduction. They also hypothesized that, during the time after bottling, the decrease of the wine redox potential together with temperature fluctuations during storage, could cause the exposition of hydrophobic binding sites on wine proteins available for tannin complexation, resulting in haze formation during storage of white wines, an hypothesis confirmed by structural studies on TPLs [24].

Polysaccharides were also studied for their action on inducing and inhibiting protein haze formation in wines. Fifteen different polysaccharides of different origins, were tested and they either did not affect or increased haze during heat test [32]. Other authors showed that a wine fraction containing polysaccharides as major compounds increased the protein instability in wine at a range of temperatures between 40 and 50 °C [49]. A multifactorial study revealed a particular kind of polysaccharide, pectin, to be important in haze formation [50]. Pectin represents from 0.02 to 0.6% of the fresh grape weight but, due to the recurrent use of commercial enzymes, many these polymers are hydrolysed during the vinification process. These enzymes, with grape origin or those added by the winemaker, are mainly pectinases, polygalacturonases, cellulases and hemicellulases, which main action is on the colloidal structure of the juice, facilitating natural settling. Despite its importance in the haze of musts, pectin also is active as a protective colloid, inhibiting the growth of nuclei and crystallization of potassium bitartrate [6].

Yeast-derived mannoproteins are considered non-haze-forming proteins that inhibit protein haze formation. Mannoproteins were described as a haze protective factor due to their ability to reduce the particle size of the suspended haze [30]. This was corroborated by other authors who showed that wines produced with three transgenic wine yeast strains, deleted for genes involved in cell-wall biogenesis causing them to release increased amounts of mannoproteins, required 20 to 40% less bentonite to assure protein stabilization than those made with their wild-type counterparts [51]. Other non-haze-forming proteins present in wines are grape invertases and grape cell wall glycoproteins and arabinogalactan-proteins [52,53]. The presence of these proteins can increase wine protein stability and influence the foaming properties of sparkling wines [54–56]. Other authors presented that some polysaccharides can increase protein instability under moderately high temperatures (from 40 to 50 °C) [49]. These disparities can be linked to differences in protein/polysaccharide ratios or to the type of protein used in the analysis [57].

The role of metal ions in protein haze formation is poorly understood, particularly in what concerns copper and iron. The concentration of copper in wine decreased after heat treatment and protein haze removal, suggesting that copper is part of the protein precipitate or interacted somehow with the proteins [58]. In view of the involvement of a protein support in the colloid flocculation occurring in copper casse in white wines, bentonite may be used to treat this problem.

Apparently, ferric casse has no proteins involved so bentonite is ineffective to treat this problem [6].

The effect of pH on protein haze formation is incompletely studied and the existing published work focuses mainly in other beverages like beer. The effect of pH on the formation of protein-polyphenol complexes in wine was described, but the use of white wines non-characteristic proteins and polyphenols (i.e. gelatin and catechin respectively), turned out questionable the significance of these results to the wine industry [59]. Using wine samples instead of wine model solutions, other authors showed that white wine became increasingly heat stable as the pH rose from 2.5 to 7.5 [49]. However, it indicated the existence of at least two different mechanisms responsible for the heat-induced precipitation of the white wine proteins: one occurring at higher wine pH values, that appears to result mainly from the isoelectric precipitation of the wine proteins, and the other, at lower wine pH values (but possibly operating also at other pH values), that depends on the presence of a non-proteinaceous factor, known as the X-factor [41]. Protein type also showed to be a factor when studying pH impact on aggregation. Variations in wine pH ranging from 2.5 to 4.0 were sufficient to disrupt the native state of some isolated chitinases at room temperature, resulting in the exposure of hydrophobic binding sites of these proteins. Oppositely, TLPs were stable under the same conditions [60].

Organic acids constitute another factor with great interest in what concerns protein instability not only due to their effect on pH but also in total acidity and ionic strength. Five different organic acids were tested (L-(+)-tartaric, L-(-)-malic, citric, succinic and gluconic acids) and their effect on wine protein haze potential analysed [41]. The results indicate that these acids induce a stabilizing effect upon the haze potential of wine proteins at all pH values tested from 2.8 to 3.8. The same work raised the hypothesis that organic acids, carrying a net negative electric charge at wine pH, interact electrostatically with the wine proteins, positively charged at the wine pH, from pH 2.8 through to pH 3.8, preventing the interaction of the X-factor with the wine protein. Tartaric acid is also capable of interacting with the X-factor, either in the presence or absence of protein, partially removing it from solution together with tartrate crystals precipitation, thus inducing a partial stabilizing effect of the wine.

The alcohol content of white wines can present a significant variability. This is an important factor since, due to climate change, the alcohol levels in wines from regions like Alsace, Australia or Napa are increasing [61]. The interaction between alcohol content and protein haze formation, tested by the addition of extra alcohol to white wine samples (0.5, 1.0 and 2.0% v/v), showed no relevant influence [49]. These results corroborate previously published data [62] which showed, in the case of beer, that alcohol concentration had little influence in haze formation at the normal pH of the beverage.

More recently the interaction of ethyl esters with wine proteins was also evaluated. Results from fluorescence and circular dichroism (CD) spectroscopy revealed that purified wine thaumatin-like (VVTL1) protein can bind to ethyl esters of different chain lengths. In the presence of C12, C10 and C6 ethyl esters, the CD signal of the non-native conformation of VVTL1 decreased in the order: C10 < C12 < C6, showing the negative contribution of ethyl hexanoate to protein stability. Oppositely, the addition of C8 ester increased the reversibility of the thermal denaturation of the protein. Though it was possible to quantify the interaction of these compounds with VVTL1 protein, the main conclusions of that work focused more on the removal of aroma compounds (ethyl esters) by the addition of bentonite than about protein stability itself [63].

2.4 Review on the mechanism of protein haze formation

Protein haze formation in white wines is caused by the unfolding and aggregation of wine proteins that can lead to precipitation. Different heat stress tests showed that wine proteins unfold has the wine is heated but it only turns hazy when the solution is cooled after the heat stress. So there are two different steps comprising the unfold of the protein due to temperature increase and its aggregation after cooling, as confirmed by DLS [64]. A revised mechanism of the aggregation mechanism was recently presented [5] and its scheme is represented in Figure 4.

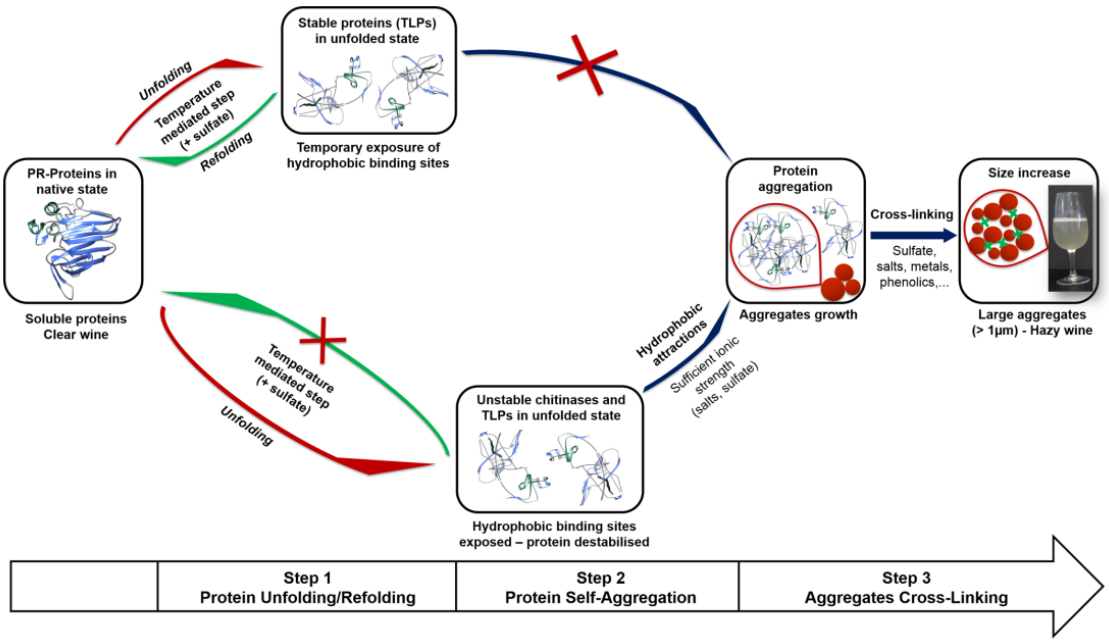

Figure 4 - Revised unfolding and aggregation mechanism of heat-unstable proteins in wine [5].

Following winemaking, the wine is clear and its proteins are stable and in their native state. After exposure to high temperatures, the proteins will unfold exposing their hydrophobic binding sites that are generally buried in their core. Also, some TLPs isoforms have an exposed loop stabilized

by a disulphide bridge that when destabilized by heat can expose other protein regions. In the case of the TLP 4JRU, protein regions that can be exposed by reduction of this disulphide bridge are hydrophobic. In a second stage, unstable proteins will start to self-aggregate via hydrophobic interactions. Other factor like salts and sulfate (the latter only in concentrations not normally found in commercial wines) content can modulate this step further promoting protein aggregation [36]. In a third stage, protein aggregation would start due to the action of sulphates and polyphenols. The presence of sulfate and salts would neutralize protein net charges and reduce the electrostatic repulsion between similarly charged proteins, whereas polyphenols would more likely cross-link protein aggregates via hydrophobic interactions. With this, the authors hypothesised that sulfate participates in all different steps by modifying the melting point of the proteins, neutralize protein net charges after unfolding and mediating the aggregation of small protein aggregates through a possible cross-linking action after protein self-aggregation. Though sulfate showed to modulate protein haze formation, the tested doses (1 to 4 g/L applied as K_2SO_4) do not normally mimic real wine conditions. Previous results show that white wines contain on average between 100 and 400 mg/L of sulphates (expressed in K_2SO_4), except for heavily sulphured sweet wines or wines with repeated sulphuring (and oxidation of the SO_2) during aging, which can result in sulfate concentrations of around 2 g/L [6,65]. By the OIV, the maximum acceptable limit of sulfates in wines is of 1 g/L (or up to 2.5 g/L in specific types of wines) [66].

The most commonly employed test for assessing the haze potential of a white wine is commonly known as the "heat test". [5] reported that this test may overestimate the risk that a wine will haze by denaturing both haze-forming and non-haze forming proteins. This test was considered to be the most appropriate stability test since it is the one that gave the most similar results to the natural wine precipitate in terms of chemical composition [11]. Other commercially available tests include the Immuno Test π (Sofralab, 2008), the Proteotest (Vason, 2009), the Proteostab (Martin Vialatte OEnologie) and the Bentotest [67] .

2.5 Wine protein stabilization

Bentonite fining is an essential operation performed on unstable wines, with an estimated annual cost between U.S. $300 million and $1 billion to the world wine industry [68,69]. Bentonite is composed of montemorillonite and is negatively charged due to some of the Al^{3+} ions present in the octahedral positions being displaced by Mg^{2+}, Fe^{2+} and Fe^{3+}, leading to charge imbalances [70]. This clay interacts electrostatically with positively charged wine molecules (e.g. proteins) because of its negative net charge at the wine pH, which produces flocculation [12]. Due to its non-selectiveness for proteins, fining with bentonite interferes negatively with the organoleptic characteristics of the wine since it adsorbs electrostatically other molecules with positive net

charge [71,72]. Besides its effectiveness to remove protein from wine, it has been demonstrated that bentonite treatment negatively affects flavour by the removal of aroma compounds [73–75] and texture [76] of wine. However, recent studies indicate that the effect of bentonite treatments on aroma substances in white wine depends on the chemical nature and initial concentration of the volatile compounds and on the abundance and nature of proteins in the wine [74]. Other problems resulting from bentonite fining include dilution of the wine by the bentonite slurry, handling and disposal problems associated with used bentonite, and quality loss of the wine recovered from lees [39]. Between 5 and 20% of the wine may stay occluded in the lees after a fining treatment [77,78] and, after a possible rotary vacuum drying system (RDV) filtration, this occluded wine may be downgraded in quality when compared to the fined wine mainly due to oxidation phenomena. The handling and disposal of used bentonite continues to be a great problem due to high labour input, associated costs, safety issues and ambient impact given the high content of ethanol and phenolic compounds present in the lees [44,79]. Although alternative strategies exist to tackle wine haze protein formation, removal of unstable proteins by bentonite fining remains the most efficient protein-stabilizing wine operation, unlike many other, commonly used fining agents [80]. The search for an efficient alternative stabilization technique, and consequently an alternative to bentonite, is a relevant topic among research groups.

Several attempts using continuous processes to stabilize white wine were reported in the literature. Studies using immobilized tannic acid were effective in removing proteins and tannins without affecting the level of peptides and the acidity of the wine. On the other hand, the high cost of this methodology would most probably make it non-viable [81]. Other options for continuous process stabilization are packed columns and percolated beds [82]. Packed columns with cation-exchange resins [83] showed that the levels of polyphenols and proteins decreased, but the colour and aroma of the wines were negatively affected. Metal-oxides [84,85] and zirconia [86] were tested as well with model wine solutions. After analysis, neither treatment significantly affected the physicochemical properties of the final product. This technology was also used in wines by enclosing zirconia pellets in a metallic cage and submerging it in different wines. This proved to be a plausible product for the wine industry though to be effective it requires not only agitation but also high doses of zirconia (up to 25 g zirconia/L of wine) [87]. To suppress the agitation problem, zirconia pellets were applied during fermentation of different musts resulting in fully heat stable wines with no loss of wine as lees, since the cage with the pellets can be simply removed from the tanks [88]. Although this technique may be a viable alternative to bentonite, the status of zirconia as an allowed winemaking additive remains to be established.

The addition of proteases to wines and musts is another alternative under study. Commercial enzymatic preparations, mainly pectinases, can be added to the must during the clarification

operation. The objective is to reduce the content in pectic substances of the must that difficult the settling of the suspended solids. These pectic substances are complex heteropolysaccharides with origin in the plant cell walls [89], and represent from 0.02 to 0.60% (w/w) of fresh grape weight [6]. These substances are present in colloidal form, protecting the must proteins and affecting their removal. In general, pectic substances increase the haziness and viscosity of the must [90], causing clarification and stabilization problems [91]. The commercial pectolytic enzyme preparations may contain some proteases in their composition, but they are not the majority, their action is not selective, and they do not use wine proteins as subtract. The musts treated with this type of commercial enzymes show greater clarity [92] and in some barrel fermented wines the addition of these enzymes lead to the production of superior wines with higher levels of alcohol, esters and terpenic compounds [93]. Regarding the eventual degradation of wine proteins that participate in the protein haze formation by these commercial enzymes, no positive effects have been reported in the literature. A heat treatment (90 °C for 1 min) combined with the addition of proteases can reduce the incidence of haze formation but, because of the low specificity to degrade wine proteins which participate in protein haze formation of the commercially available proteases, the possibilities offered by this method are heavily compromised [94].

Protease activity occurs in all living cells. In what wine protein stabilization is concerned, this activity has been reported in grape berries [95], wine yeast [96,97] and in the malolactic transformation bacteria *Oenococcus oeni* [98], but they exhibit low (if any) activity towards haze-forming proteins. Numerous different proteolytic enzymes are produced by yeasts [99,100]. Some studies revealed the presence of extracellular acid protease production among various species of *Saccharomyces* [101–105], but the main part of the yeast proteases, in particular of *S. cerevisiae*, are intracellular and located in various compartments (cytosol, vacuole, mitochondria, endoplasmic reticulum, and Golgi complex) and cellular membranes of the cell [99,100]. After cell lysis and death, these proteases can be released to the surrounding medium where they may retain activity. Of the many cellular proteases present in yeasts, the vacuolar acid protease (endoproteinase A) has been widely studied since it has been considered to play a significant role in enology [105,106]. This vacuolar acid protease appears to be very active in degrading grape proteins once released from the cells and its activity is detected for long periods of time during aging on the yeast lees [107]. However, PR proteins, the principal precursors for protein haze formation in white wines [13,15,26] have high resistance to proteolysis [15,25,94], remaining in the wine even after the vinification process. Other proteases that are being tested about their effectiveness in degrading heat-unstable proteins from white wines are bromelain from pineapple and papain from papaya [108–110]. Particularly, bromelain proved to be effective in the degradation of wine proteins (both in model solution and wine) when immobilized in chitosan beads and used in a bench-scale packed-bed reactor [111,112]. The most promising protease for the stabilization of white wine is Proctase. Proctase is the commercial name of the proteases

Aspergillopepsin I and II from *Aspergillus niger* and is commercialized by the Australian Wine and Research Institute. The action of these proteins was evaluated in different musts resulting in the removal of around 90% of total protein when combined with juice heating (70 – 75 °C for 1 min) [18]. Though this technology was approved for use in Australian wines and is being used in wineries such as Yalumba and De Bortoli Wines, it was not yet approved for the use in the European market.

Several studies allowed the identification of some components in the wine colloidal fraction described to be haze protective factors. As presented above, some polysaccharides apparently protect the wine proteins against heat-induced haze formation [113]. Mannoproteins are a haze-protective factor, and represent the majority (ca. 80%) of all polysaccharides released by yeast during fermentation and aging on the lees, containing 90% of mannose and 10% of protein. However, the purified heat-stabilizing product is a 31.8 kDa mannoprotein (known as MP32), consisting of 37% protein and 62% mannose [6]. This glycoprotein was isolated from a wine prepared from grapes of the variety Moscatel and showed protective effect on wine proteins, even if the wine suffers heat test [26]. Another mannoprotein, analogue to the Moscatel isolated one, was purified from wine of the variety Carignan Noir and is referred to as Hpf1p. A third haze protective mannoprotein (Hpf2p) has also been isolated by ethanol precipitation of a chemically defined grape juice medium fermented by the winemaking strain of *S. cerevisiae*, Maurivin PDM [114]. The haze-protective effect of mannoproteins was independently confirmed by other authors but the exact mechanism by which mannoproteins afford haze protection remains unclear [44]. Nevertheless, it was described that these compounds do not inhibit proteins from precipitate but decrease the size of the suspended particles, making them invisible (or hard to detect) to the naked eye [30]. [115] showed that the extraction methods for mannoproteins from *S. cerevisiae* are not very efficient and estimated that to decrease 20% of the haze, 500 mg of mannoproteins need to be applied to one litre of wine. However, [116] after applying 250 mg/L of mannoproteins extracted by enzymes (MPEE) from yeast cell walls (purified by ultrafiltration and dried), demonstrated that they can halve the dose of bentonite required for protein stabilization of extremely heat-sensitive wines. Since most the haze-protective factor was in the supernatant, it was suggested that these factors act by competing with other wine proteins for other non-proteinaceous wine components, required for the formation of large insoluble aggregations of protein.

One other alternative for the stabilization of heat-unstable proteins are polysaccharides. One of the most studied polysaccharides capable of stabilizing heat-unstable proteins from wine is carrageenan [117,118]. Carrageenan applications made before or during fermentation originated stable wines comparable to bentonite finning. However, post-fermentation additions of this polysaccharide resulted in wines that failed heat stability tests. Other technical difficulties

resulting from the use of carrageenan are the possibility of excess frothing (for the additions made before or during fermentation) and increased difficulty in the filtration of the wine, since carrageenan may clog the filtration membranes, particularly when the addition is made after fermentation [118].

The most recent technologies under development are reticulated biopolymers [119] and acrylic acid-coated magnetic nanoparticles [120] for the removal of PR-proteins from wines. The new reticulated biopolymers consist of β-cyclodextrins and cyclic nigerosyl-1,6-nigerose, among other polysaccharides, cross-linked with citric acid. After testing the synthesized polymers with wines from three different varieties, the authors identified that 2 polymers could remove proteins from wine with a performance similar to bentonite. These polymers consisted of a β-cyclodextrin cross-linked with citric acid and other consisted of a linecaps derivative, which consists on a type of amylose. These were developed during the FP7 funded project 'Stabiwine', though there are not much available data about the synthesis and characterization of these polymers. The magnetic nanoparticles [120] can perform cation exchange in the wine due to carboxylic acid groups available in the modified surface. Although effective in removing most of the soluble proteins in the tested wines, these particles had to be added to a concentration of 1.66% (v/v), which corresponds to 13.3 g/L. This result can be related with the pKa of the carboxylic group available on the surface of the nanoparticles, which can be very similar to the wine pH causing it to be partially protonated and therefore incapable to perform cation exchange with the positively charged wine proteins. A similar phenomenon happens with the addition of carboxymethylcellulose (CMC) to protein unstable wines [121] since it also has one carboxylic acid group per substituted position on the anhydroglucose unit. Since CMC has an average pKa value of 3.65 [255], it will be partially deprotonated at the wine pH and will interact with wine proteins turning the wine hazy. That is the reason why the addition of CMC to avoid tartaric acid precipitation must be performed only in protein stable wines.

To display a lower impact not only on the wine but also to human health and environment, the next generation polymers for the adsorption of wine proteins must pass through the production of polymers made from renewable resources but presenting a lower pKa than the normal pH of the wine.

3. Protein haze formation mechanism in white wines.

3.1 Isolation and identification of the compounds present in white wine protein aggregates after alkaline hydrolysis.

This chapter gave origin to the following paper:

Chagas R., Lourenço A. M., Monteiro S., Ferreira R. B., Ferreira L. P. (2017) "Is caffeic acid, as the major metabolite present in Moscatel wine protein haze hydrolysate, involved in protein haze formation?", Food Research International, 98, 103-109.

(http://dx.doi.org/10.1016/j.foodres.2016.09.007)

3.1.1 Background

The occurrence of protein precipitates, induced by temperature fluctuations during storage or intentional heat treatments, has also been reported for other beverages like fruit juice and beer. For these, as well as for the wine precipitates, the presence of phenolic compounds, presumably interacting directly with the proteins, is often observed. In the sediments gathered from Evergreen blackberry juice and Muscadine grape juice and wine, ellagic acid was identified as one of the major compounds present [123][124]. Haze and sediment formation in blackberry juices was attributed to the possible hydrolysis of ellagitannins, which comprise the less water-soluble ellagic acid [124]. For Muscadine wine sediments, the authors reported the necessity to identify the remaining compounds in the precipitate for further elucidation on the sediment formation process [123]. In both cases, acid hydrolysis was performed to facilitate extraction of the compounds present in the sediments. Using a similar approach, [11] studying phenolic compounds present in natural protein precipitates from white wines, identified vanillic acid, *trans-p*-coumaric and ethyl-coumaric acid ester by direct analysis of the dissolved precipitate, whereas following Bate-Smith hydrolysis, vanillic acid, cyanidin and quercetin were identified. The authors concluded that phenolic compounds are present in the protein precipitate and suggested, as already hypothesised by [43] and [41], that those compounds are probably involved in the mechanism of haze formation in white wines. However, to date, no direct correlation between the identified phenolic compounds and the haze induction potential was demonstrated.

Though acid hydrolysis may prove useful in the purification of some of the compounds present in wine sediments, it can degrade other metabolites such as flavonols [125] and/or camouflage the presence of potentially relevant compounds. As an alternative, alkaline hydrolysis is described as more effective in releasing phenolic compounds from mixtures, since unlike mild acid hydrolysis, it cleaves ester bonds. Alkaline hydrolysis is commonly used to extract bound phenolic acids and other related compounds from cereal grains [126] and exhibits higher extraction yields for metabolites like ferulic acid when compared to acid hydrolysis [127].

3.1.2 Objective

Since the methodologies described in the literature proved to be insufficient in the identification of the main compounds present in wine protein haze, the aim of this study was to isolate and identify the compounds present in induced wine protein haze precipitate after alkaline hydrolysis and to assess their potential contribution to wine protein haze formation using a wine model solution.

3.1.3 Results and discussion

3.1.3.1 Protein haze sediment

Protein haze sediment was obtained from a sample wine prone to protein haze formation after heat treatment. The wine used in these trials was regarded as protein unstable because it presented a difference in absorbance between heated and unheated control of 0.233 ± 0.023 AU at 540 nm [87]. The sediment was isolated from 5 L of wine and then subjected to alkaline hydrolysis as described in the Experimental chapter.

3.1.3.2 Qualitative analysis of the compounds present in the white wine sediment

The alkaline hydrolysed sample was subjected to liquid-liquid extraction and evaporated to dryness. The resulting ethyl acetate-soluble extract (35.5 mg) corresponds to 8.47% (w/w) of the total dried sediment. During the liquid-liquid extraction with ethyl acetate, we observed that part of the sediment containing the yellowish compounds remained in the aqueous phase. This coloured material is likely to consist of low molecular mass compounds insoluble in the organic phase and residual protein fragments. Similar phenomena were reported by some authors in the literature while trying to isolate compounds present in blackberry juice sediment [124].

The ethyl acetate extract was dissolved in 1 mL acetonitrile/water (1:1), filtered and analysed by RP-HPLC-DAD. The chromatogram of the total ethyl acetate soluble fraction is represented in Figure 5.

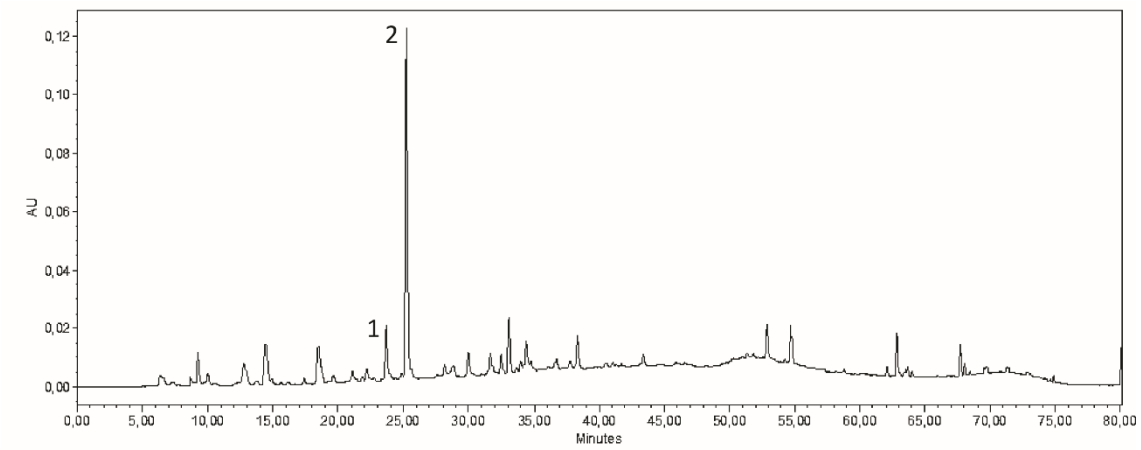

Figure 5 - Chromatogram of the ethyl acetate soluble fraction obtained by liquid-liquid extraction of the hydrolyzed wine protein precipitate monitored at 320 nm. The collected peaks are identified as 1 and 2.

The UV-vis spectra of the two major compounds present in the extract, identified in Figure 1, were subsequently obtained. The information gathered by RP-HPLC-DAD of the compounds is described in Table 1.

Table 1 - Retention times (t_R), spectral bands (λmax in bold) and detection wavelength ($\lambda_{detection}$) of the compounds selected in Figure 1.

#	t_R (min)	UV bands (nm)	$\lambda_{detection}$ (nm)
1	26.69	240, 308	320
2	27.75	217, 240, 319	320

3.1.3.3 Isolation and identification of the compounds present in the ethyl acetate soluble fraction of the alkaline hydrolysed white wine sediment.

After qualitative evaluation of the compounds present in the ethyl acetate soluble fraction of the alkaline hydrolysed white wine sediment, they were fractionated using a semi-preparative PFP column as described in the materials and methods section. Gradient optimization was performed in the analytical column and later adapted to the semi-preparative scale to achieve the best possible separation.

The peaks marked in Figure 2 were collected and dried in a rotary evaporator. After drying, the vials containing the different fractions were connected to a vacuum pump to eliminate traces of organic solvent and water.

Fractions #1 and #2 (corresponding to peaks 1 and 2 in Figure 5, respectively) were dissolved in methanol-d4 prior to ^{1}H NMR analysis. Analysis of the ^{1}H spectrum of fraction #2 showed the presence of caffeic acid (1) as the major compound present with the following chemical shifts: 7.53 (1 H, d, J = 15.9 Hz), 7.07 (1 H, d, J = 2.0 Hz), 6.95 (1 H, d, J = 8.2), 6.81 (1 H, d, J = 8.2), 6.24 (1 H, d, J = 15.9 Hz) (Figure 6). This spectrum is in accordance with previously published data of caffeic acid isolated from a natural source [128]. The ^{1}H spectrum of fraction #1 from Figure 5 (data not shown) revealed 1 as the major compound, similarly to fraction #2.

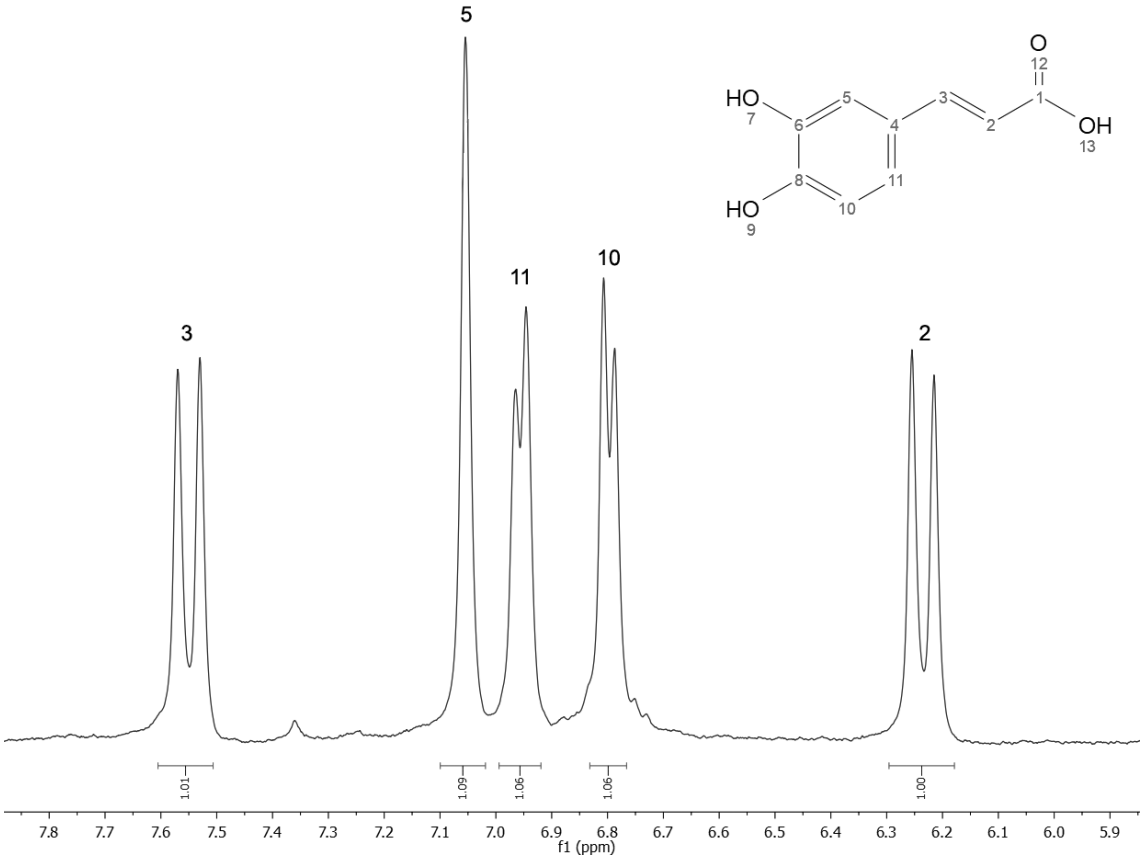

Figure 6 - ^{1}H NMR spectrum in CD_3OD of caffeic acid isolated from fraction #2.

Caffeic acid (1) was the major compound present in both fractions #1 and #2 isolated by RP-HPLC-DAD (1 mg and 1.9 mg total caffeic acid, respectively). Analysing both UV-vis spectra of fractions #1 and #2 and comparing with the information available in the literature [129] suggests that the major compound present in fraction #1 corresponds to caffeate (with reported absorption peaks at wavelengths 240, 283 and 309 nm) and the one in fraction #2 corresponds to caffeic acid (1) (with described absorption peaks at wavelengths 216, 235 and 321 nm). ^{1}H NMR analysis of both compounds returned equal spectra which corroborates that they are, in fact, the two different protonation forms off the same compound (Figure 2). The cause for this phenomenon is related

to the pH of the extract prior to HPLC injection. Since the most common pH range in wines lies between 3.0 and 3.6, the most abundant form of this compound in haze recovered will be as 1.

3.1.3.4 Quantification of caffeic acid in the untreated wine

Caffeic acid (1) is one of the major cinnamic acids in wine together with *p*-coumaric, ferulic and sinapic acids [6]. This acid has already been described to bind several types of proteins, causing different changes in their functionality or modifications inducing enhanced heat stability [130], increased tensile strength [131] or decreased isoelectric point [132]. As an *o*-diphenol, caffeic acid oxidises to *o*-quinone under alkaline conditions, which then reacts with the nucleophilic functional groups of proteins resulting in covalent binding of 1 to the protein [133]. In reason of wine pH the wine proteins should be spared to this event.

A quantification step was conducted to determine the content of caffeic acid in the original wine sample (without protein haze induction). To increase caffeic acid extraction yield, thus improving quantification accuracy, the solid phase extraction (SPE) method described by [134] was applied. The separation of hydroxycinnamic acids from wine was carried using an Oasis HLB column, which has an *N*-vinylpyrrolidone-divinylbenzene copolymer as sorbent. Following sample loading and elution with ethyl acetate, the sample was dried in a rotary evaporator and dissolved in acetonitrile/water containing 0.1% (w/v) TFA (20:80). Subsequent RP-HPLC-DAD analysis allowed the quantification of caffeic acid in the untreated wine sample with a concentration of 1.1 mg/L ± 0.1 mg/L (Table 2).

Table 2 - Concentration of caffeic acid (1) in the untreated wine under analysis, isolated by SPE followed by RP-HPLC-DAD. The calibration curve was prepared using 99% pure caffeic acid.

Compound	Concentration (mg/L)	$\lambda_{detection}$ (nm)	m	b	R^2
Caffeic acid (**1**)	1.1 ± 0.1	320	5^6	-585256	0,9998

3.1.3.5 Does the presence of caffeic acid (1) in the heat-induced wine sediment warrant its identification as a modulating factor in protein haze formation?

Caffeic acid (1) was isolated from an extract previously subjected to alkaline hydrolysis. The amount of caffeic acid present in both fractions #1 and #2 (Figure 2) gives a total of 2.9 mg, providing an estimate of the total (free + bound) caffeic acid present in the original wine sediment of 5 L of wine. This hydroxycinnamic acid occurs in wines in free form, as a glycoside or bound to other compounds, such as in caftaric acid [135]. Thus, hydrolysis of these compounds (if present in the sediment) can release large quantities of caffeic acid. To understand the impact of both caffeic acid and its ester caftaric acid, we have synthesised the second one instead of isolating from the wine. The synthesis of caftaric acid (**6**) is schematized in Figure 7.

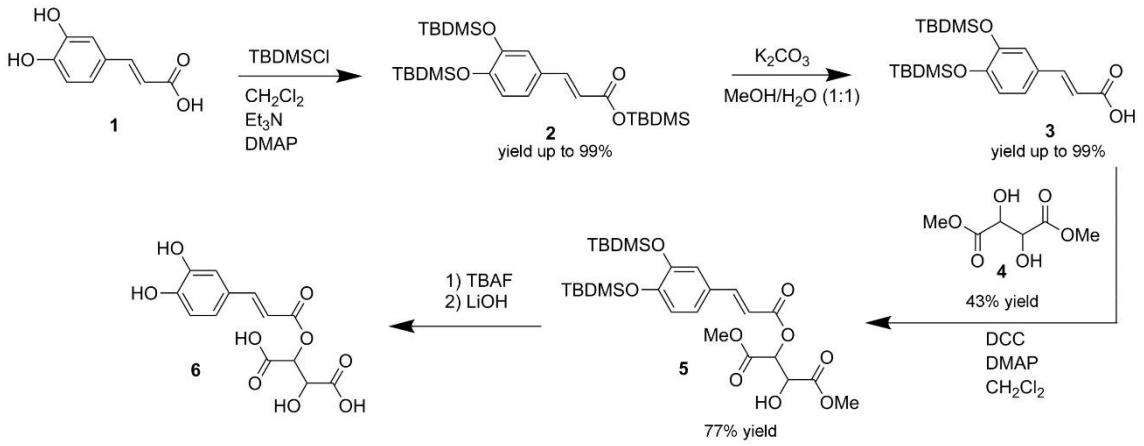

Figure 7 - Synthetic route adopted for the synthesis of caftaric acid (**6**).

Comparing our synthesis with the one described [136] there are some differences. TBDMS-Cl was used instead of TBDMS triflate with no significant difference in the yields obtained. Compound **5** was prepared with dimethyl L-tartrate instead of diethyl L-tartrate with equivalent yield compared to the reaction using diethyl L-tartrate. Dimethyl L-tartrate (**4**) was synthesised reacting L-tartaric acid with dry methanol and sulfuric acid giving a yield of 43%.

In the last synthesis step, we opted to deprotect **5** with tetra-n-butylammonium fluoride (TBAF) followed by LiOH though with pour results. At the end of these reactions we had a mixture of **5**, **6**, partially deprotected intermediates and TBAF. To isolate **6**, we separated the crude by RP-HPLC. At the end, we managed to isolate 2 mg of **6** which amounts to a yield of 1.7 %. The deprotection of an intermediate similar to **5** (with diethyl instead of the dimethyl L-tartrate) with

acetic acid followed by LiOH gave the final product with a yield of 67 % [136]. The ^{1}H spectrum of **6** is represented in Figure 8.

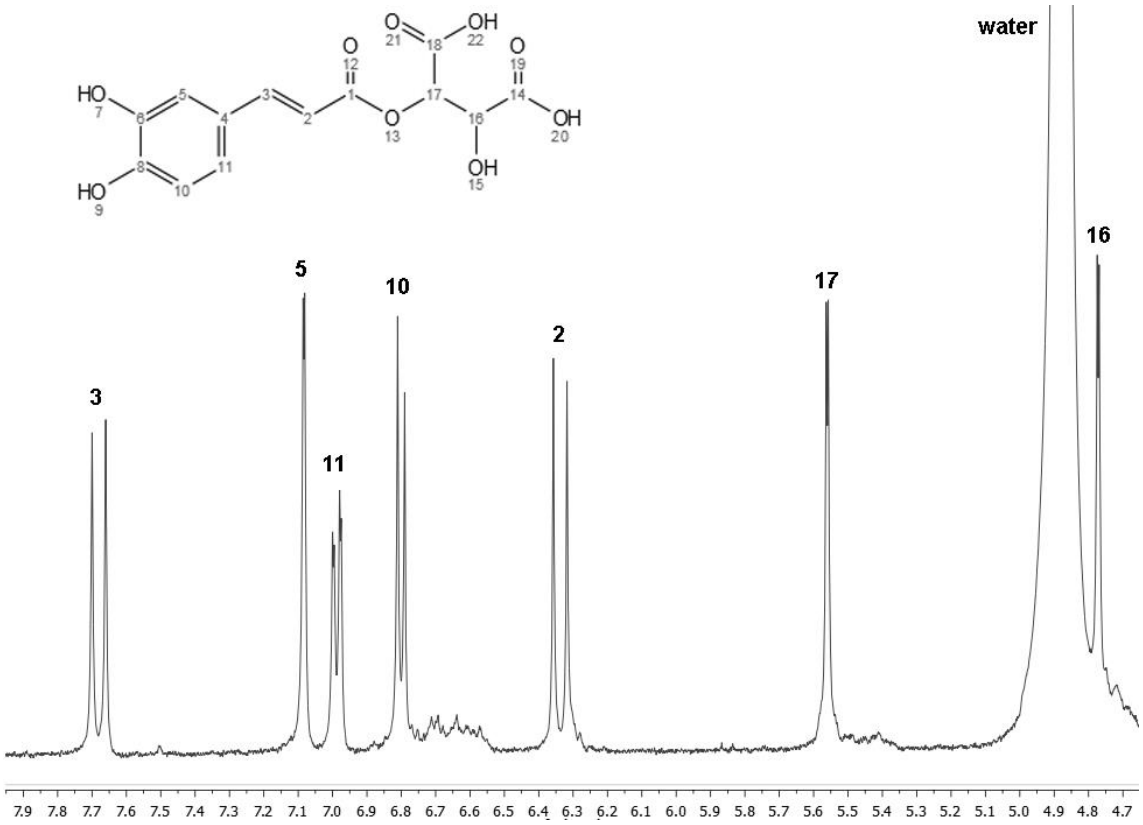

Figure 8 - ^{1}H NMR spectrum in CD_3OD of caftaric acid (**6**) after isolation by RP-HPLC.

Based on our results, the protocol previously described [136] is much more sound for the production of *trans*-caftaric acid since a yield of 1.7% is not viable. Nevertheless, synthesised caftaric acid (**6**) was used in the following protein interaction assays.

Commercial caffeic acid and synthesised caftaric acid were added to a model wine solution containing isolated wine protein to test its possible modulatory effect on protein haze formation. Following complete solubilisation of both compounds, the model solutions were subjected to a heat stability test as described in the experimental section. For the heat stability test, two different concentrations of the hydroxycinnamic acids, 1.1 and 5 mg/L respectively, were selected. The first concentration corresponds to the caffeic acid quantified in the test wine (Table 2) and the second to the maximum concentration found in white wines [137].

As expected, the isolated wine protein (IWP) in model solution revealed significant differences in the formed haze when compared with the control wine (Table 3), which confirms previously published data [41]. The same authors also demonstrated that protein haze formation in white wine

exhibits an absolute requirement for one or more low molecular mass (<3 kDa) wine components which became known as the X-factor.

Table 3 - Changes in turbidity of wine and wine model solutions after heat stability test measured at 540 nm. IWP + <3 kDa: <3 kDa wine fraction supplemented with 190 mg/L of isolated wine protein; IWP + WMS: isolated wine protein (190 mg/L) in wine model solution; 1: caffeic acid (1.1 or 5 mg/L) added to IWP in wine model solution; 6: caftaric acid (1.1 or 5 mg/L) added to IWP in wine model solution. The pH of all samples was adjusted to 3.2. Different letters represent distinct homogeneous subsets for p = 0.05 (ANOVA, Tukey HSD).

Sample	Absorbance at 540 nm
Control wine	0.233 ± 0.023^{a}
IWP + <3 kDa	0.182 ± 0.004^{b}
IWP + WMS	0.004 ± 0.001^{d}
1.1 mg/L (1)	0.005 ± 0.001^{d}
5 mg/L (1)	0.012 ± 0.003^{d}
1.1 mg/L (6)	0.013 ± 0.001^{d}
5 mg/L (6)	0.013 ± 0.001^{d}

Simultaneously to the test using caffeic and caftaric acids, we included a sample containing <3 kDa fraction of the same wine supplemented with isolated wine protein in wine model solution. The haze induced by the <3 kDa fraction is significantly different from all the remaining samples, and corresponds to approximately 77% of the control wine haze (Table 3). There is no significant difference between the samples containing caffeic or caftaric acids, nor with the sample containing isolated wine protein in wine model solution.

These results indicate that neither 1 nor its ester 6 are main modulators in wine protein haze formation. Since these trials were performed in wine model solution, we cannot account for potential synergistic interactions which may occur between caffeic (of caftaric) acid and other minor compounds present in the wine matrix on triggering wine protein haze formation. Considering that this compound occurs bound to the proteins in the precipitate, it interacted with the unstable proteins somewhere during the aggregation reaction. We can hypothesise that due to the exposure of protein hydrophobic surfaces through heating, caffeic acid can be more reactive to bind to these specific zones, though we do not have yet any proof about this reaction mechanism. It would be of great interest to understand when and at which conditions caffeic acid binds to these proteins.

Caffeic acid was previously identified in the composition of natural protein precipitate of white wines [11]. These authors reported that 0.052% (w/w) of the natural precipitate was caffeic acid among other compounds like tyrosol, vanillic acid or *trans-p*-coumaric acid. After acid hydrolysis

by Bate-Smith reaction, they did not register any trace of caffeic acid in the extract. Despite the common detection of caffeic acid as one of the major compounds contained in the wine sediment, the type of protein precipitates obtained may present different compositions since the authors used natural protein precipitate in the analysis whereas in our study protein haze was induced by heat treatment.

Several wine compounds were tested, either individually or in combination, with isolated wine protein to understand their impact on wine protein haze formation [43]. Caffeic acid was also tested, revealing no relationship with protein haze modulation within the range of concentrations from 20 to 100 mg/L. Albeit using much larger caffeic acid concentrations, this experiment resembles the one described in our study. Still, the authors used pure wine thaumatin-like protein at a concentration of 500 mg/L, in contrast to our trial where the protein was a mixture of the proteins presents in wine and concentration was adjusted to mimic the control wine protein concentration (190 mg total wine protein /L).

3.1.4 Conclusion

After analysing the composition of a heat-treated wine sediment, the major non-protein compound found was caffeic acid (1). This hydroxycinnamic acid was isolated using HPLC-DAD and its structure validated by ^{1}H NMR. This observation could be interpreted to suggest that caffeic acid could play a role in wine protein haze formation. Using total wine proteins, we tested different concentrations of caffeic acid and its ester caftaric acid (6) in a wine model solution. Our results show that neither caffeic acid nor caftaric acid are modulators of wine protein haze formation.

3.2 Motivation to change the wine model solution

At the end of the previous work, there was one question: if these trials do not work, is it the compounds that do not react with the protein or is it the conditions where the compound is added to the protein that do not reflect what happens in real conditions?

That said, one of the variables that has such importance as the compounds in test, is the wine model solution where every interaction trial is performed. Until now, there was little to no modification of the wine model solutions used in heat stability tests by different research groups, as represented in Table 4.

Table 4 - Different model wine solutions described in the literature used to study wine protein interactions/aggregation.

Reference	Model wine solution used
[43]	500 mg/L thaumatin, 12% ethanol, 4 g/L tartaric acid, pH 3.2
[138]	12% ethanol, 10 g/L tartaric acid, pH 3.6
[36]	75 mg/L total wine protein, 12% ethanol, 5 g/L tartaric acid, pH 3.2
[41]	280 mg/L total wine protein, 12% ethanol with different organic acids (L-(+)-tartaric, L-(-)-malic, citric, succinic and gluconic acid), pH from 2.8 to 3.8
[139]	100 mg/L protein (different wine protein fractions), 12% ethanol, 4 g/L tartaric acid, pH 3.0
[24]	50 mg/L protein (different fractions), 12% ethanol, 2 g/L malic acid, 1 g/L K_2SO_4, pH 3.2
[140]	30 mM tartaric acid/ sodium tartrate, 12% ethanol, pH 3.2

The average model wine solution consists of an ethanol solution containing tartaric acid with the pH adjusted to around 3.2, with some differences depending on the trial. Although these solutions showed to be useful in some studies, it is very limitative when trying to compare the results with real wines.

The hydroxycinnamic acids discovered in the protein precipitate can affect the protein on a molecular level through the formation of adducts. These are mainly caused by the formation of covalent and non-covalent bonds between the hydroxycinnamic acids and the proteins. Covalent bonds are formed in the reactions of enzymatic and non-enzymatic browning. In the enzymatic browning reactions, the presence of catechol group with two aromatic hydroxyl groups in the ortho position determines the formation of *o*-quinones with electrophilic properties, which can participate in the nucleophilic addition reaction with proteins [141,142]. Such chemical structure is found for example in caffeic acid and chlorogenic acid. Initiation of this reaction can occur through the mechanism of spontaneous reaction of oxygen from the environment with reactive hydrogen from the hydroxyl group in the aromatic ring, reaction that can be exacerbated by heat. The reaction depends on temperature, pH, oxygen availability, the concentration of polyphenols, and the number and position of hydroxyl groups. Quinone and semi-quinone radicals are electrophilic molecules and are subject to nucleophilic additions with the reactive side chains of proteins. They bind to highly nucleophilic thiol and amine groups and a hydrophobic aromatic group of proteins [143]. A reaction of quinones with proteins and protein cross-linking occurs mainly through the side chains of lysine, cysteine, methionine, and tryptophan [142]. Though, in wines, these redox reactions are modulated by the action of sulfur dioxide. A schematic representation of the reaction between bisulfite, quinones and hydrogen peroxide is represented in Figure 9.

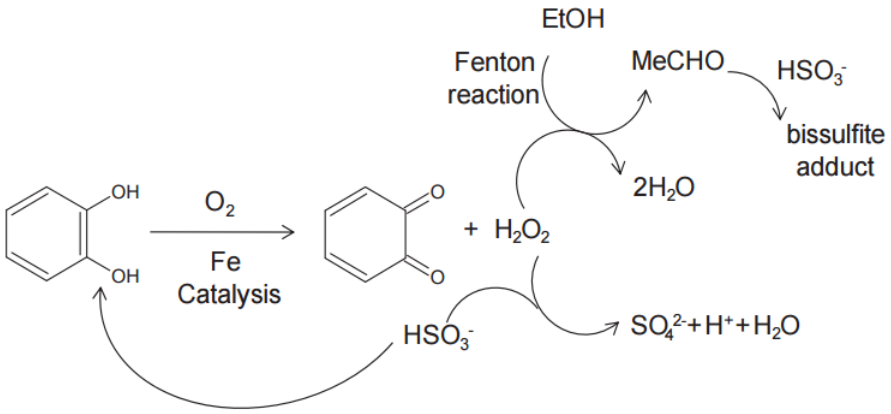

Figure 9 - The interaction of SO_2 with hydrogen peroxide and quinones following catechol oxidation, so preventing oxidation of ethanol by the Fenton reaction [144].

The addition of a reducing agent like SO_2 can also affect the protein itself, apart from the remaining compounds in solution. The reaction between sulfite and the cystine from the protein can yield cysteine and *S*-sulfo derivatives which can change not only the protein activity but also its solubility or its isoelectric point [145]. Since the addition of sulfur dioxide is almost ubiquitous in winemaking (oppositely to the addition of ascorbic acid, another reducing agent only used in

specific cases), we opted to include it in our model wine solution to modulate the redox potential, mimicking what happens in real wine condition.

It was also presented that the addition of dithiothreitol (DTT) improved the amplitude of wine thaumatins to form haze in the presence of wine tannins, opening the discussion of the redox potential in wine protein haze formation [36]. Though being an effective reducing agent, DTT as well as other thiols is very ineffective at low pH. Nevertheless, this result emphasizes the evident importance of the redox potential of the wine model solution when studying the interaction of different compounds with isolated wine proteins.

Preliminary studies using sulphur dioxide confirmed its possible involvement in wine protein haze formation, opening a new path to the study of sulfur dioxide mediated protein aggregation mechanism in white wines.

3.3 The challenging SO_2-mediated chemical build-up of protein aggregates in wines.

This sub-chapter gave origin to the following papers:

Chagas R., Laia C. A. T., Ferreira R. B., Ferreira L. P. (2017) "Sulfur dioxide induced aggregation of thaumatin-like proteins: role of disulfide bonds.", submitted to Food Chemistry

Chagas R., Ferreira L. P., Laia C. A. T., Monteiro S., Ferreira R. B. (2016) "The challenging SO_2-mediated chemical build-up of protein aggregates in wines.", Food Chemistry 192, 460-469. (http://dx.doi.org/10.1016/j.foodchem.2015.07.052)

3.3.1 Background

In an attempt to decipher which compounds interact with wine proteins to form haze, [43] proposed that sulfate anion could be the missing non-proteinaceous essential factor for protein haze formation. In these studies, the sulfate concentration effective in wine protein haze formation increased in the range of 1 to 4 g/L, thus exceeding those generally encountered in wines. In fact, in a recent work focused on the characterization of some haze-forming wine thaumatin-like proteins, potassium hydrogen sulfate anion was used as haze modulating factor [24]. The modulating effect of sulfate anion was attributed to the possible promotion of hydrophobic interaction-driven aggregation through kosmotropic affect as well as the suppression of electrostatic repulsion between proteins by the increment of the ionic strength of the medium [40]. More recently, [5] revised the mechanism of protein haze formation where sulfate was said to participate in all different steps by modifying the melting point of the proteins, screening the exposed protein charges after unfolding and mediating the aggregation of small protein aggregates through a possible cross-linking action after protein self-aggregation.

Even though wines with added sulfate produced higher haze, other factors like the reduction of the medium, tested by the addition of DTT, improved the aptitude of wine TLPs to form haze in the presence of wine tannins. These findings may suggest sulfur dioxide, the most important additive in winemaking, as a relevant factor in white wine protein haze formation mechanism. In this respect, it was hypothesized [24] that SO_2 added to wines to prevent faults due to oxidation, could exacerbate haze formation via cleavage of a specific disulfide bridge (that established between Cys 140 and Cys 213) in a TLP isoform, thus allowing hydrophobic aggregation to take place.

Sulfur dioxide, often abbreviated to sulphite, the anionic counterpart of the hydrated form of this gas, is the most important chemical compound widely used by the wine industry due to its antiseptic and antioxidant properties [146]. Concerning its mode of action, particularly its antioxidant properties, it is now accepted that the main function of sulfite in wines is to quench the hydrogen peroxide resultant from the reduction of O_2, thus inhibiting aldehyde formation and preventing the oxidation of other easily oxidizable compounds [147]. The reaction is known to occur at the typical wine pH values and most likely proceeds by nucleophilic attack of the bisulfite ion (HSO_3^-) by H_2O_2 to form a peroxymonosulfuric acid intermediate, which is subsequently rearranged to afford sulfuric acid by the following equations (adapted [148]):

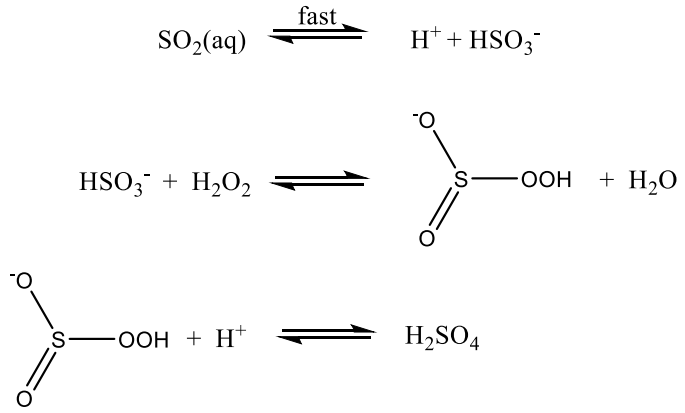

The reaction does not involve free radicals and is an effective mean of disabling the oxidation potential of H_2O_2 in wine [147,148].

Bisulfite (in the form of $NaHSO_3$) added to proteins acts as a reducing agent, cleaving disulfide bonds, and affecting protein properties like viscosity, solubility and hydrophobicity [149,150]. To our knowledge, limited information exists concerning the interaction of SO_2 with wine proteins and the possible link between the supposed protein reduction and protein haze formation.

3.3.2 Objective

The purpose of this study was to investigate, for the first time, the effect of SO_2 addition on the modulation of wine protein haze formation. SO_2-induced protein haze was also evaluated using two different wines, both of which were analysed with and without SO_2 addition.

3.3.3 Results and discussion

3.3.3.1 Interaction of SO_2 with wine total proteins

Total Moscatel of Alexandria wine proteins were isolated by strong cation exchange chromatography (Figure 10A) and collected in a single fraction (T1) as previously described [36]. To evaluate the SO_2 haze inducing effect on these proteins, heat stability tests were performed in the presence of increasing SO_2 concentrations (0, 25, 90 and 200 mg/L) using a wine model solution (12% v/v ethanol, 5 g/L tartaric acid, pH 3.2) supplemented with 100 mg/L of T1 fraction protein (Figure 10B). The SO_2 concentration range used in the experiments was selected based on the limits established by the International Code of Oenological Practices (OIV, 2014).

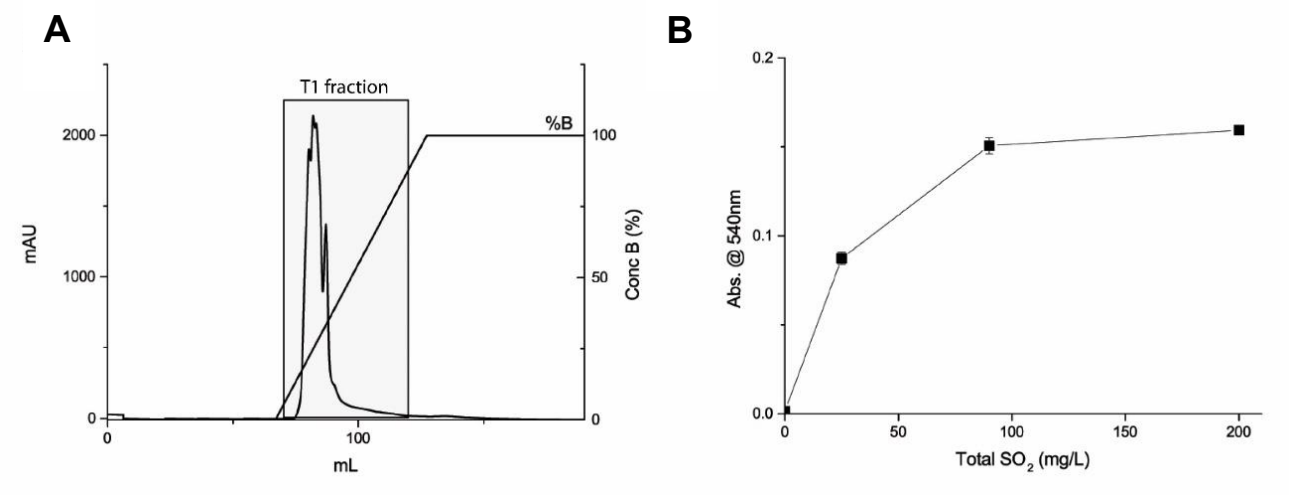

Figure 10 - (A) Cation exchange chromatogram of Moscatel of Alexandria wine sample on a Resource S (5 mL) column (6 mL/min flow rate). Loading and washing steps were omitted for clarity. Approximately 1 L of wine was loaded onto the column (ca. 100 mg protein). The total wine protein fractions were pooled (T1 fraction) based on the elution profile monitored at 280 nm. (B) Effect of increasing total SO_2 concentration (added as $NaHSO_3$) in the wine model solution on the haze produced after the heat stability test. The wine model solution consisted of 100 mg/L total wine protein (T1 fraction), 12% (v/v) ethanol, 5 g/L tartaric acid, pH 3.2.

As shown in Figure 10B, apart from the 0 mg/L SO_2 value, all samples produced haze visible to the naked eye after the heat stability test as evidenced by the increase in absorbance at 540 nm. Also, for increasing SO_2 concentrations at constant protein, a higher turbidity was observed, reaching a maximum at the highest SO_2 concentration tested (200 mg/L). Considering the turbidity behaviour along the various concentrations of SO_2, a hyperbolic-type curve is generated to a horizontal line that crosses the turbidity axis at an unknown, but potentially important technological value. For the protein concentration used, a steeper precipitation effect is observed between 0 and 100 mg/L of added SO_2. Within this range, turbidity may correlate directly with SO_2 concentration (first order kinetics). Further increases in SO_2 lead to successively lower increments in protein turbidity until a saturation point is reached, above which turbidity level is no longer dependent on SO_2 concentration (zero order kinetics). Thus, the turbidity increase observed between 100 and 200 mg/L seems to be associated with the total protein quantity in the sample which, above a certain SO_2 concentration, becomes maximally aggregated. The displayed turbidity dependence on SO_2 concentration suggests a potential direct involvement of this additive in in the mechanism of white wine protein precipitation.

3.3.3.2 Interaction of SO_2 with protein fractions differing in hydrophobicity

To assess whether a relation exists between the SO_2 induced haze formation potential and protein hydrophobicity, T1 fraction proteins were fractionated by hydrophobic interaction chromatography (HIC). The resulting HIC chromatogram (Figure 11B) is similar to the chromatograms published elsewhere for similar protein fractions [39], with slight differences in protein quantity ratios, most likely derived from the use of different biological samples. Fractions H1 to H7, referring to peaks 1 to 7 in Figure 11B, were obtained by the combination of five consecutive injections (5 mg of protein per injection) in the HIC column. For each fraction, protein content and the proportion it represents relative to total protein in the chromatogram were determined (Figure 11). The apparent bias in proportionality between size of peaks (Figure 11A) and their protein content (Figure 11B) is probably due to differences in the number of aromatic amino acids present in the various proteins.

A

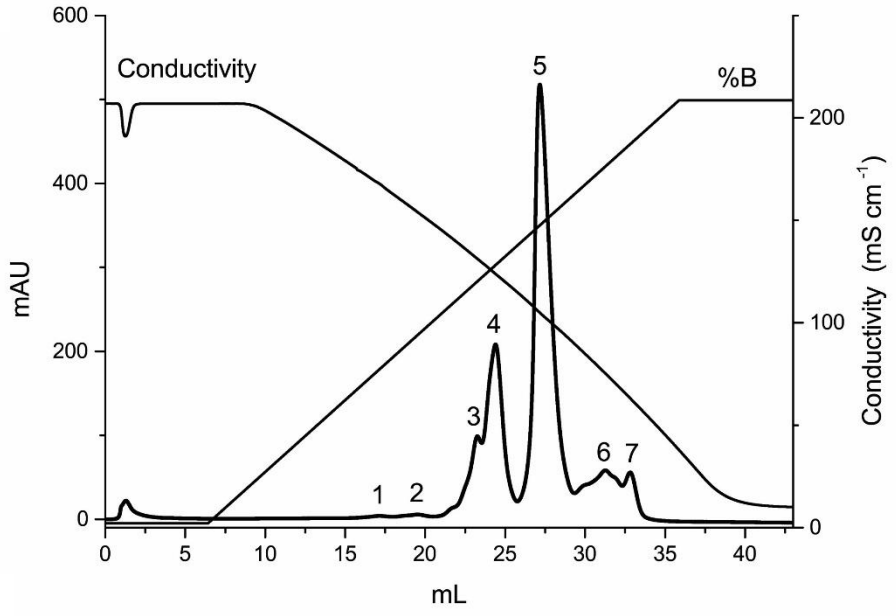

B

Fraction	H1	H2	H3	H4	H5	H6	H7
Mass (mg)	0.19	0.72	3.35	4.63	11	2.9	0.82
%	0.8	3.0	14.2	19.6	46.6	12.3	3.5

Figure 11 - (A) HIC chromatogram of the total wine protein previously isolated by cation exchange chromatography (Figure8). Abbreviated names were assigned to HIC individual protein fractions and correspond to the numbered peaks eluted from the HIC column preceded by an 'H'. HIC was performed on a Phenyl Superose HR 5/5 column. Lyophilized protein was dissolved in 25 mM K_2HPO_4 containing 1.25 mM $(NH_4)_2SO_4$, pH 7.0, prior to loading. (B) Protein content (mg) and the proportion it represents relative to total protein in the chromatogram (%) for each fraction (H1–H7) obtained after HIC (A).

The protein present in each of fractions H3 to H6, which account for 92.7% of the total protein, was dissolved in two wine model solutions, one containing 120 mg/L total SO_2 (added as $NaHSO_3$), the other without SO_2, and all adjusted to 100 mg/L protein before being subjected to a heat stability test. The results are illustrated by Figure 12A.

The data displayed in Figure 11A reveal that fraction H5, which is the most abundant protein fraction in the wine (corresponding to 46.6% of its total protein), was the one reacting the most with SO_2. Although the individual proteins present in each fraction were not identified, an analogy can be established with published data where the major HIC peak of wine samples was identified as containing mainly thaumatin-like TPLs [37]. In addition, these authors reported that this HIC fraction did not lead to relevant haze after heat stability test, even after addition of tannins. We have observed a similar behaviour with the control of H5, showing no visible haze after heat test. However, the addition of SO_2 to the wine model, shifted this fraction from stable to highly unstable, capable of originating the highest haze formation (Figure 12).

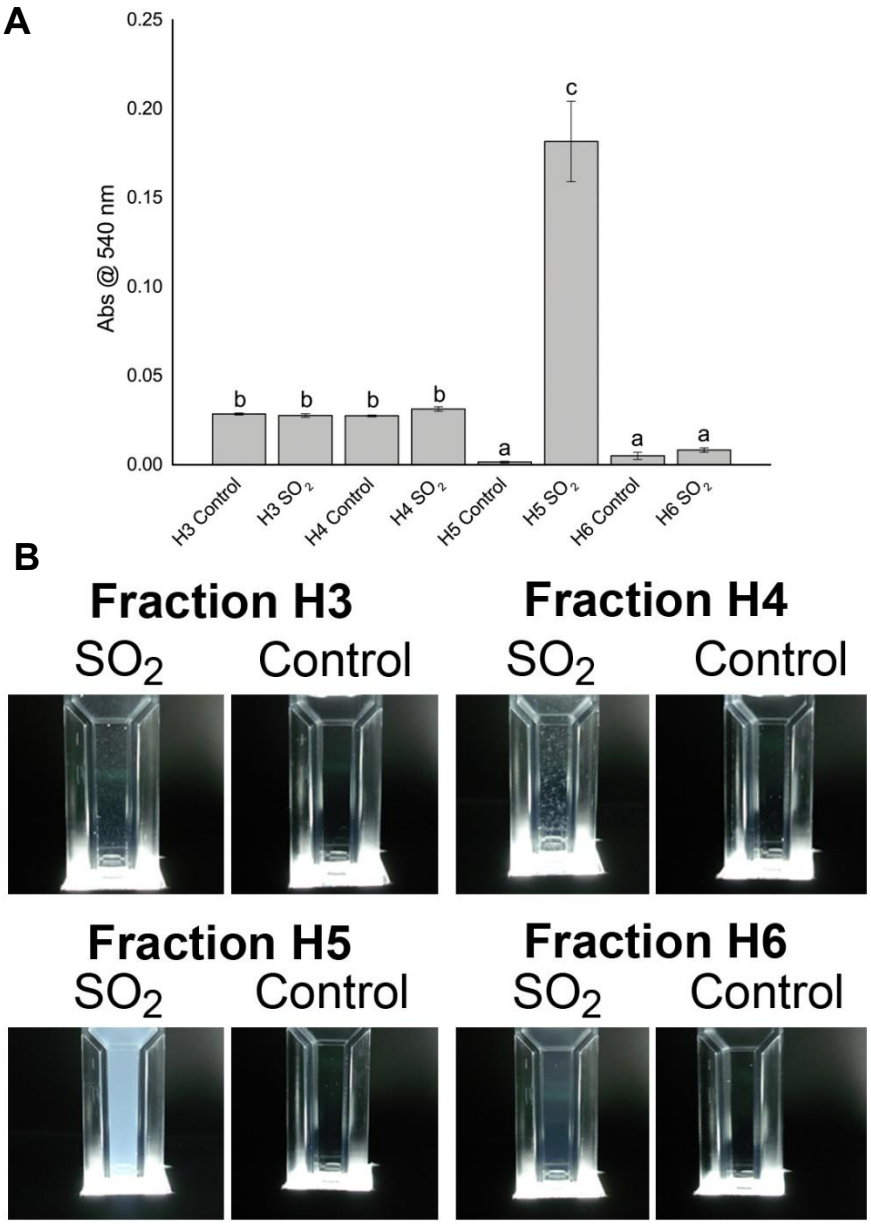

Figure 12 - (A) Haze development after heat stability test of the isolated HIC fractions (adjusted to 100 mg/L protein) in two model wine solutions. Control: no added SO_2. SO_2: model wine solution containing 120 mg/L total SO_2 (added as $NaHSO_3$). H3–H6 indicate protein fractions obtained by HIC separation as shown in Figure 11A. Means not sharing the same letter are significantly different (OneWay-ANOVA, Fisher LSD, $P < 0.05$). (B) Visualization of the haze produced after heat stability test of HIC fractions H3–H6 in model wine solutions with and without added SO_2. Cuvettes represented in the picture correspond to the ones used in the experiment described in (A).

Interestingly, although the heat stability tests have shown that SO_2 exerts a positive but negligible effect on the induction of haze formation for H3 and H4 fractions, visual inspection of these samples evidenced the presence of protein aggregates (Figure 12B). It was reported in the literature two distinct mechanisms underlying heat-induced wine protein haze formation: one dependent on the X-factor, the other resulting from isoelectric precipitation of the proteins, the

latter depending on the protein pI and the wine pH [36]. The types of haze observed in Figure 12 (large and flocculated versus small and homogeneous dispersion) suggest that different protein fractions react differently to the presence of SO_2. Although possible, protein precipitation due to the proximity of pI can be negligible given the pH of the MWS.

According to the turbidity values obtained for all the fractions, no apparent relation seems to exist between protein surface hydrophobicity and interaction with SO_2. Although protein precipitation may be somehow linked to protein hydrophobicity in fraction H5, it is most likely related to the type of proteins and other features of their structure.

In a second trial, more protein from a Moscatel of Alexandria wine (2014 vintage) was isolated to better characterize the proteins that participate in the SO_2 mediated aggregation. Similarly, to the first trial, proteins were isolated by strong cation exchange chromatography (Figure 13A) and collected in a single fraction (F1).

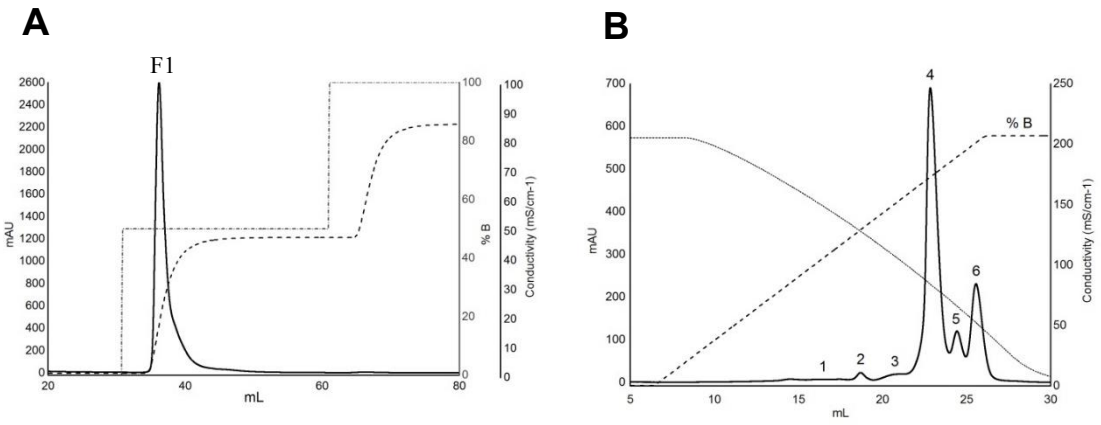

Figure 13 - A) Cation exchange chromatogram of Moscatel of Alexandria (2014) wine sample on a Resource S (6 mL) column (6 mL/min flow rate). Loading and washing steps were omitted for clarity. Approximately 0.5 L of wine was loaded onto the column. The total wine protein fractions were pooled (F1 fraction) based on the elution profile monitored at 280 nm. B) HIC chromatogram of the total wine protein previously isolated by cation exchange chromatography (Figure 13A). Abbreviated names were assigned to HIC individual protein fractions and correspond to the numbered peaks eluted from the HIC column preceded by an 'H'. HIC was performed on a Phenyl Superose HR 5/5 column. Lyophilized protein was dissolved in 30 mM sodium citrate containing 1.25 M ammonium sulfate, pH 3.0, prior to loading.

The F1 fraction proteins were further fractionated by their hydrophobicity using hydrophobic interaction chromatography (HIC). The resulting HIC chromatogram (Figure 13B) is similar to the chromatograms previously showed in Figure 10 and with others previously published, with slight differences in protein quantity ratios since a different biological sample was used. Fractions H1 to H6, referring to peaks 1 to 6 in Figure 13B, were obtained by the combination of three

consecutive injections in the HIC column accounting a total of 14 mg of total separated protein. All fractions were once more subjected to heat stability test in wine model solution containing $NaHSO_3$. After heat stability test, we have confirmed that the fraction that produced higher haze was the major fraction H4 (a fraction equivalent to previously presented H5, Figure 11). The proteins present in fraction H4 were further analysed by LC-MS/MS (Table 5).

Table 5 - Summary table of the LC-MS/MS of the H4 protein fraction isolated by HIC.

Protein fraction	Identification	Top annotated BlastP result	Identity	Peptides matched	Theoretical MW[a]	Theoretical pI[b]
H4	H4.1	gi|33329390|gb|AAQ10092.1| thaumatin-like protein [Vitis vinifera]	97%	11	23881.69	4.67
	H4.2	gi|2213852|gb|AAB61590.1| VVTL1 [Vitis vinifera]	82%	8	23968.95	5.09

[a] The identified peptides were compared to the non-redundant protein sequences database using BlastP (http://blast.ncbi.nlm.nih.gov/). Identities refer to the number of matching amino acids of the LC-MS/MS to the number of amino acids in the sequence associated with the BlastP result.

[b] Theoretical average MW and pI were calculated with the Expasy-Compute pI/MW tool (http://web.expasy.org/compute_pi/)

The peptides matched by LC-MS/MS were subjected to multiple alignment using Cluster Omega prior to BLAST analysis (http://www.ebi.ac.uk/Tools/msa/clustalo/). This operation allowed to remove redundant amino acids from the identified peptides to increase the precision of the analysis.

The sequences given by the analysis using BlastP represent similar proteins and not the actual sequences of the purified proteins since LC-MS/MS data do not provide complete coverage of any sequence. Nevertheless, both proteins present putative conserved domains from the GH64-TLP-SF superfamily which indicate that they are both from the thaumatin protein family. This data is in accordance with other authors [37] who presented a high content of thaumatin-like proteins in the major protein fraction of Semmilon wine protein fractionated by HIC.

Both fractions H4 and H5 correspond to the same proteins, though they result from two different isolation protocols. From this point on, we will refer to H4 and H5 protein fractions has isolated thaumatin-like protein (iTLP) since they were identified has thaumatins (Table 5).

The apparent diameter of these proteins was also evaluated by DLS. To increase the signal to noise ratio the concentration of iTLP fraction used in this study was adjusted to 500 mg/L in wine model solution. The size of the native iTLP was measured by nanoparticle sizing using dinamyc light scattering as represented in Figure 12. Using a nanoanalysis method we could detect an average diameter of 4.9 nm ± 0.88 nm (Figure 14B).

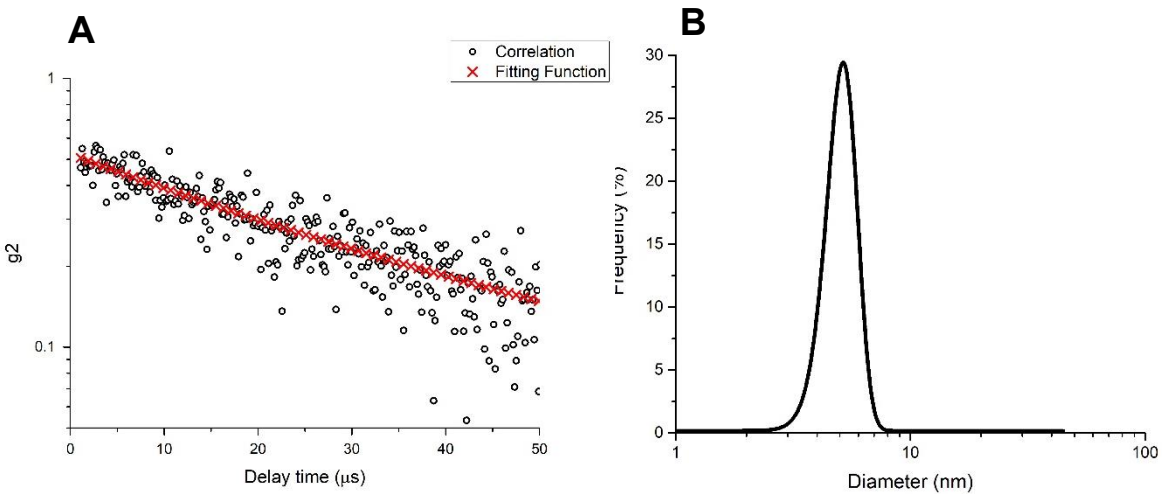

Figure 14 – A) Autocorrelation curve acquired by DLS nanoanalysis of the protein fraction H4 (native state) in wine model solution at 25 °C. B) Size distribution frequency acquired by DLS nanoanalysis (represented as the protein diameter in nm) of the iTLP (native state) in wine model solution before heat stress.

From the formula previously described [151] for the calculation of the minimal radius of a sphere (the simplest shape for our protein) that could contain a given mass of protein:

$$R_{min} = (3\,V/4\pi)^{1/3}$$

$$= 0.066\,M^{1/3}\ (M \text{ is given in Dalton, } R_{min} \text{ in nm})$$

The minimal radius for H4 protein using an average of 23.8 kDa (based on the data from the LC-MS/MS analysis) is 1.89 nm, which corresponds to a minimal diameter of 3.78 nm. Since proteins in general present an irregular shape (even globular proteins) their average radius will be larger than the minimum. That said it is plausible to assume that 4.9 nm can be the average diameter of iTLP in a wine model solution when present in its native form.

3.3.3.3 Effect of protein reduction on wine total protein aggregation

It was suggested that a reducing environment in the bottled wine could result in the exposure of additional hydrophobic sites on the proteins and consequently increase the accessibility of these

sites to tannins [36]. These processes are stalled by the presence of intramolecular disulfide bonds, but may be enhanced using reducing agents capable of cleaving such covalent bonds. To reduce the samples, the authors used dithiothreitol (DTT) which participates in disulfide exchange reactions, reducing the protein disulfide bonds. The same authors showed that the addition of DTT up to 420 mM to the wine model solution improved the aptitude of TLPs to form haze in the presence of wine tannins. However, DTT as well as other thiols, is very ineffective at low pH and totally inactive at pH 1.5 [1521](Han & Han, 1994)(Han & Han, 1994). Since DTT has a high pKa value (average for thiol compounds is 9.2), at pH 7.0 or lower only a small fraction of its thiol groups are present in the thiolate reactive form [153] and its action will be slow to none at acidic pH. Under these conditions, the predominant species will be the protonated non-reactive thiol. This may explain the high DTT concentration employed by Marangon and collaborators. Tris (2-carboxyethyl) phosphine (TCEP) can be used as an effective and selective reducing agent for disulfides, even in the presence of 100 mM HCl (pH 1.5). Unlike DTT, TCEP is a trialkylphosphine reducing agent (with no thiol groups) which makes it a useful reductant over a much wider pH range (1.5 to 8.5) [154].

To evaluate if SO_2 haze induction can be directly related to the medium reduction, a new assay was performed using TCEP as positive control. TCEP was added in two different concentrations to wine proteins in a wine model solution (Figure 15). There was no significant haze formation after heat stability test for both 5 and 25 mM TCEP. This result clearly indicates that heating the wine model solution in the presence of a reducing agent (i.e. TCEP) does not lead to the expected, significant haze formation. Indeed, although the sample treated with TCEP displayed an absorbance near or above the established instability threshold (0.02 AU, [40]) the corresponding turbidity is negligible when compared to the one induced by $NaHSO_3$. For the addition of $NaHSO_3$ (added to 1.8 mM - 120 mg/L of total SO_2), the results are in accordance with the data presented in Figure 10B.

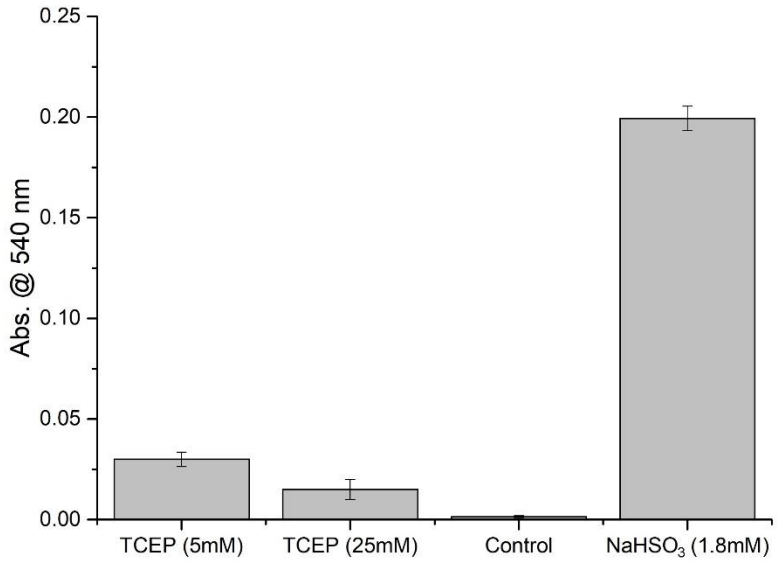

Figure 15 - Effect of TCEP or $NaHSO_3$ on the haze produced after heat stability test in a wine model solution. Final concentrations are indicated in the X-axis labels. The model solution consisted of 100 mg/L total wine protein (F1 fraction, Figure 13A), 12% (v/v) ethanol, 5 g/L tartaric acid and pH 3.2.

The mechanism by which $NaHSO_3$ reduces the medium and consequently cleaves protein disulfide bonds differs from the mode of action of TCEP or DTT since different Cys derivatives may be formed. One of the modifications that can occur following addition of $NaHSO_3$ to the solution is protein thiosulfonation or *S*-sulfonation. This reaction is also known as sulfitolysis [145]. Indeed, $NaHSO_3$ is not only a reducing agent but also a sulfhydryl-blocking reagent, hindering thiol-disulfide exchange during protein interaction [150]. In this reaction, some sulfhydryls resulting from reduction by $NaHSO_3$ are blocked as a sulfonate group as represented in the following reaction:

$$\text{Cys-S-S'-Cys'} + HSO_3^- \rightleftharpoons \text{Cys - SH} + \text{Cys'-S'-}SO_3^-$$

$$\text{Cys'-S'-}SO_3^- + \text{Cys - SH} \rightleftharpoons \text{Cys-S-S'-Cys'} + HSO_3^- \text{ (regenerated)}$$

Cleavage of disulfide bonds induced by $NaHSO_3$ modification can lead to structural conformation changes resulting in the exposure of some nonpolar groups previously buried inside the protein interior, especially if the proteins are simultaneously subjected to high temperature conditions. It was previously presented that modification of soy glycinin by $NaHSO_3$ increased the surface charge of the protein and shifted its minimum solubility range to lower pH [150]. However, unlike our case study, intermolecular disulfide exchange played a limited role in glycinin aggregation after $NaHSO_3$ treatment.

TLPs, along with chitinases, are the best characterized group of proteins found in wines [19,1552-3](Monteiro, Picarra-Pereira, Mesquita, Loureiro, Teixeira, & Ferreira, 2001; Waters, Hayasaka, Tattersall, Adams, & Williams, 1998)(Monteiro, Picarra-Pereira, Mesquita, Loureiro, Teixeira, & Ferreira, 2001; Waters, Hayasaka, Tattersall, Adams, & Williams, 1998) and were always studied side by side for their possible involvement in wine protein haze formation [394](Falconer, Marangon, Van Sluyter, Neilson, Chan, & Waters, 2010)(Falconer, Marangon, Van Sluyter, Neilson, Chan, & Waters, 2010). Differential scanning calorimetry (DSC) analysis of these proteins did not provide strong evidence that wine TLPs contribute to the haze formation process, whereas chitinases were described as the causative agent for heat-induced haze formation, even at temperatures as low as 30 °C. This evidence was not in accordance with analysis of wine protein precipitates, where VVTL1 protein was, among others, a major protein present [11]. More recently, the development of a methodology using strong cation exchange (SCX) followed by HIC enabled the isolation of large quantities of high purity proteins [14], facilitating the study of the role of different individual proteins in the mechanism of protein haze formation [24,36,42,60].

The structural elucidation of the three grape juice TLP isoforms F2/4JRU, I/4L5H and H2/4MBT allowed the detection of eight disulfide bonds in each of these proteins [24]. These authors suggested the involvement of the Cys140 - Cys 213 disulfide bridge in haze formation. They hypothesized that the use of SO_2 in vinification could exacerbate haze formation caused by protein F2/4JRU, assuming that S-S bond would be cleaved, thus allowing hydrophobic aggregation to take place. Although testing all protein fractions in wine and not individual ones, our work extends beyond this hypothesis since the aggregation of the major protein fraction was shown to be induced by the addition of sulfur dioxide at concentrations normally found in wines. In fact, pathogenesis-related proteins are typically encoded by multigene families. If on top of this we consider the range of possibilities offered by alternative splicing, post-translational modifications and the myriad of chemical modifications grape proteins undergo during the complex process that separates pulp from wine, we end up with a couple of sequence-related proteins in wines (e.g. chitinases, TLPs and osmotins), each of which exhibits a very high degree of microheterogeneity (possibly in the hundreds; [19]).

Hence, the hypothesis formulated in this manuscript, based on both our results and on those published in the literature, of a chemical mechanism based on cleavage of disulfide bonds by $NaHSO_3$ is proposed. After addition of HSO_3^- to must or wine (by the application of SO_2, $NaHSO_3$, $K_2S_2O_5$ or $KHSO_3$), the consequent medium reduction induces cleavage of wine intraprotein disulfide bonds. This reaction is exacerbated by high temperature-induced unfold of the proteins. After disulfide bond cleavage, the free sulfhydryl groups will be transiently blocked by HSO_3^-, which will delay thiol-disulfide exchange during protein interaction. This phenomenon allows the

interaction of each thiol-disulfide group with other sulfhydryl groups present in the same or in a different protein molecule, leading to formation of new intra- and interprotein disulfide bonds. Formation of disulfide bonds through thiol-disulfide interchange has been shown to be involved in the cross-linking of protein molecules to form aggregates, supporting the mechanism proposed above for wines [150,156].

It was proposed that the addition of sulfate (as HSO_4^-) to a model wine containing isolated thaumatin induced haze formation upon heat stress [43]. In addition, the same authors showed that 400 mg/L of sulfate were required to induce precipitation of a mixture of wine proteins, an observation which led them to suggest that sulfate is required for protein haze formation in white wines. By adding SO_2 to our samples, SO_4^{2-} formation would be expected to occur due to the oxidation of the first form. However, sulfur dioxide does not react directly with oxygen but only with its reduced form, hydrogen peroxide. When bisulfite reacts with H_2O_2, a product of the oxidation of catechol-containing polyphenols, it forms $SO_4^{2-} + H^+ + H_2O$ increasing the sulfate content of the wine [144]. However, since there is no catechol available in our wine model this pathway is not expected to occur.

3.3.3.4 Study of the impact of SO_2 on the aggregation of wine thaumatins.

The incidence of SO_2 addition on the different HIC protein fractions was investigated by heat stability test as reported in Figure 12A. As stated above, the fraction which produced higher haze when combined with SO_2 was H5 which corresponds to H4 in Figure 13B.

The data shown in Figure 10B and Figure 12A are expressed as absorbance units at 540 nm obtained after a heat test and do not provide any information about size or distribution of the protein aggregates formed. To address this issue, the aggregation of iTLP (in wine model solution) upon addition of SO_2 was followed by DLS.

As described in the methods section, after sample preparation a temperature cycle was performed in the DLS equipment consisting of 25 °C for 30 min, 70 °C for 120 min, and 15 °C for 120 min. In Figure 16, the dependence of particle diameter *vs.* time / temperature for the aggregation of iTLP in the presence of SO_2 is presented. During the first 120 min at 70 °C particles presented a size ≥ 10 μm, with light scattering intensity remaining constant within experimental error. When the protein is at 70 °C, there is a higher exposure of its hydrophobic side chains to the buffer. This will cause a decrease in the refractive index of the bulk protein/water network which explains the low light scattering intensity detected.

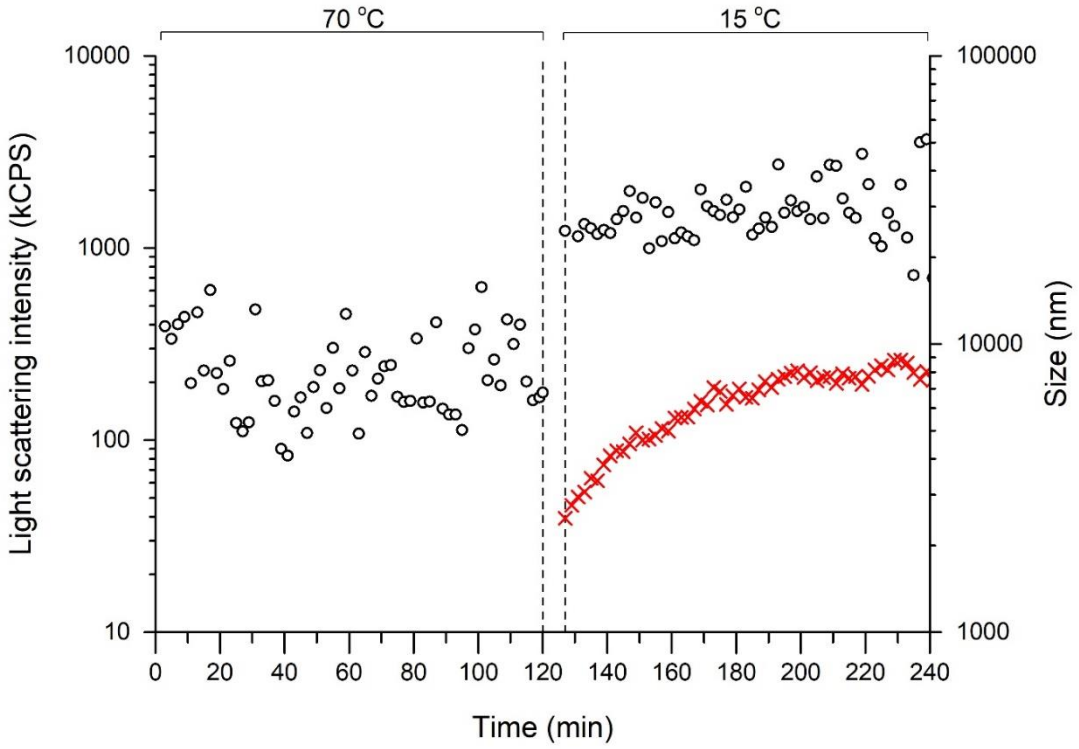

Figure 16 - Dependence of particle diameter on time and temperature for the aggregation of iTLP (at 500 mg L^{-1}) in model wine solution containing SO_2 (at 600 mg L^{-1}). The count rate is represented by (o) and the measured diameter by (x). The time required to decrease the temperature from 70 to 15 °C (i.e. 8 min) is represented by the vertical dashed lines.

After decreasing the temperature to 15 °C, light scattering intensity increased by two orders of magnitude and the measured particle size reached over 2 µm within the first 3 min. When the protein refolds, there is a lower exposure of the hydrophobic side chains to the buffer, causing an increase in the refractive index of the protein. This may explain the rapid increment of the light scattering intensity, immediately after decreasing the system temperature to 15 °C. At later times of the trial (between t = 220 and 240 min), the measured particle size was around 8 µm.

In a similar trial using iTLP at a concentration of 100 mg/L (mimicking wine protein concentration), we accompanied the increase of the hydrodynamic diameter at 15 °C after heat stress and analysed the size of the formed aggregates (Figure 17).

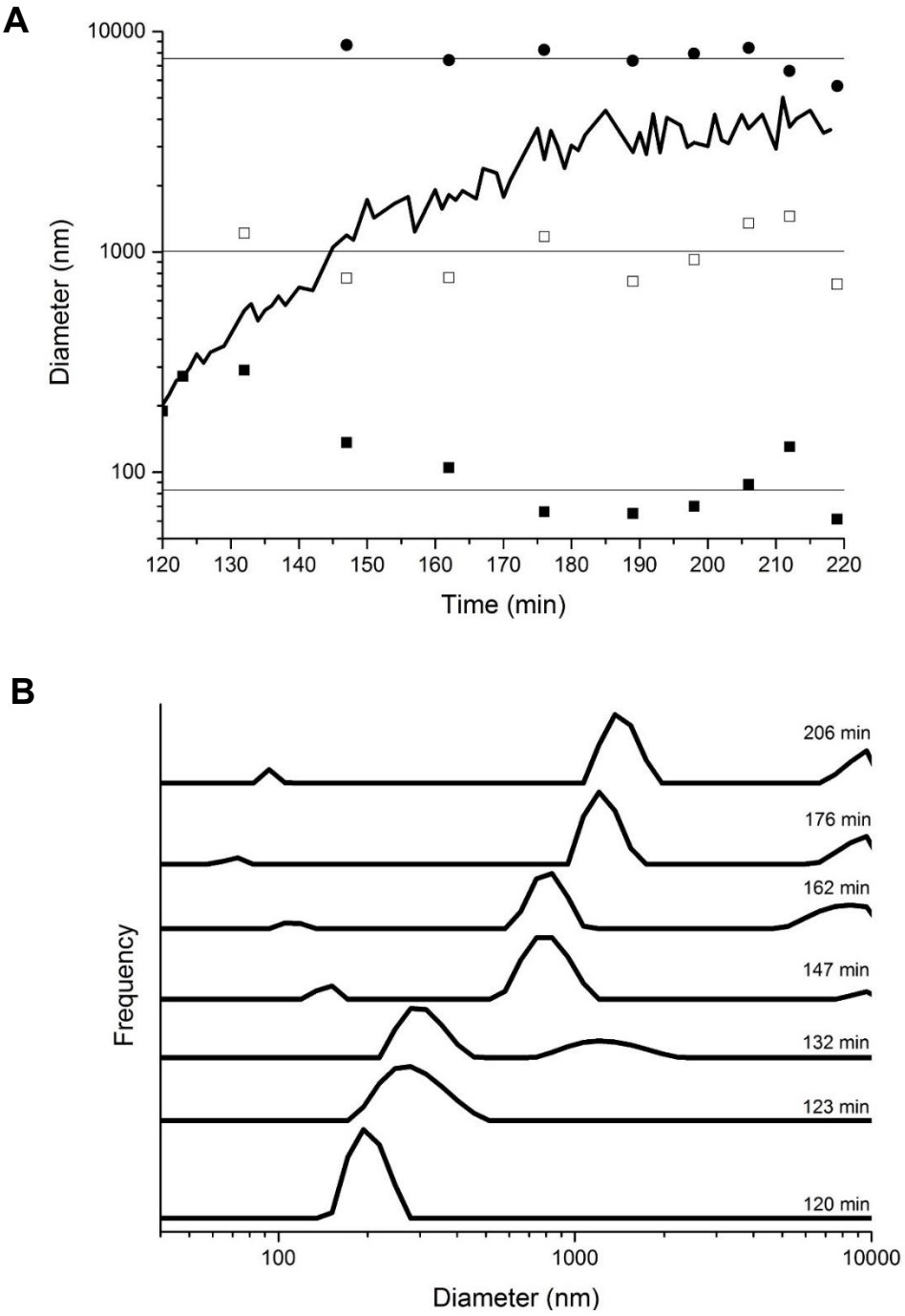

Figure 17 - A) Dependence of hydrodynamic diameter on time for aggregation of protein iTLP (solid line). Also represented are the peaks of the size distributions of B) including: (■) first, (□) second, (●) third aggregated forms. Horizontal lines correspond to the average particle size of these forms. B) Distribution of particle size registered at different times of iTLP at 15 °C after heat stress.

The average hydrodynamic diameter clearly increases after heat stress, indicating a gradual aggregation process. For short incubation times (120 to 130 min) the distribution function contains a single peak corresponding to the first aggregates that formed after heat stress (Figure 17B, t = 120 min). The average value of the hydrodynamic diameter for this peak was found to

be 84 nm ± 23 nm. However, Figure 17B shows that the DLS relaxation becomes multi-exponential afterwards, corresponding to two or three size distribution peaks obtained from the analysis of the experimental autocorrelation curves. On average and within experimental error, each of these size distribution peaks maintained a similar dimension throughout the experiment. During aggregation, a peak corresponding to a second aggregated form of iTLP formed, increasing gradually with time and exhibiting an average diameter of 1008 nm ± 288 nm (Figure 17B, t = 132 to 206 min). A third peak corresponding to the third aggregated form of iTLP and with an average size of 7540 nm ± 945 nm appeared after t = 147 min with increasing intensity towards the end of the experiment. These data support a model in which protein aggregation occurs in a discrete form.

Similar DLS studies involving isolated wine proteins were previously published and focused on the impact of temperature, pH, ionic strength and sulfate on protein aggregation [40,42,64].

Comparing our results with those of [64], we can see a similar aggregation pattern occurring at 70 °C. These authors used real wine samples, without previous bentonite fining, containing 10 to 87 mg/L of SO_2. Among other factors which are inducing protein aggregation (pH, temperature, ionic strength) the presence of SO_2 may also be influencing their results, although this was not considered or stated by the authors in their published work. In accordance with our results, [64] also described that aggregation is strongly prevented during the heating treatments at 60 and 70 °C, but is triggered when temperatures are subsequently reduced. Some possible mechanisms of protein aggregation *in vitro* were described [157] and consist of (1) sequential particle–cluster aggregation, in which monomeric units add sequentially but individually to a growing aggregate; (2) multimeric cluster–cluster aggregation, characterized by the association of multimers of any size; and (3) nucleation-dependent aggregation, characterized by the slow formation of a critical size or nucleus followed by the rapid increase in size of the aggregate. These authors noted that a linear increase in light scattering during protein aggregation indicated a uniform multimeric polymerization reaction instead of nucleation-growth kinetics, which is characterized by a sigmoidal-shaped light-scattering curve. In our case, analysis of the light-scattering curve obtained for iTLP (illustrated by the Z-average curve and fitting in Figure 18) shows that it exhibits a sigmoidal-shape with a Boltzmann fitting ($R^2 = 0.95$), suggesting a nucleation-growth kinetics for wine protein aggregation.

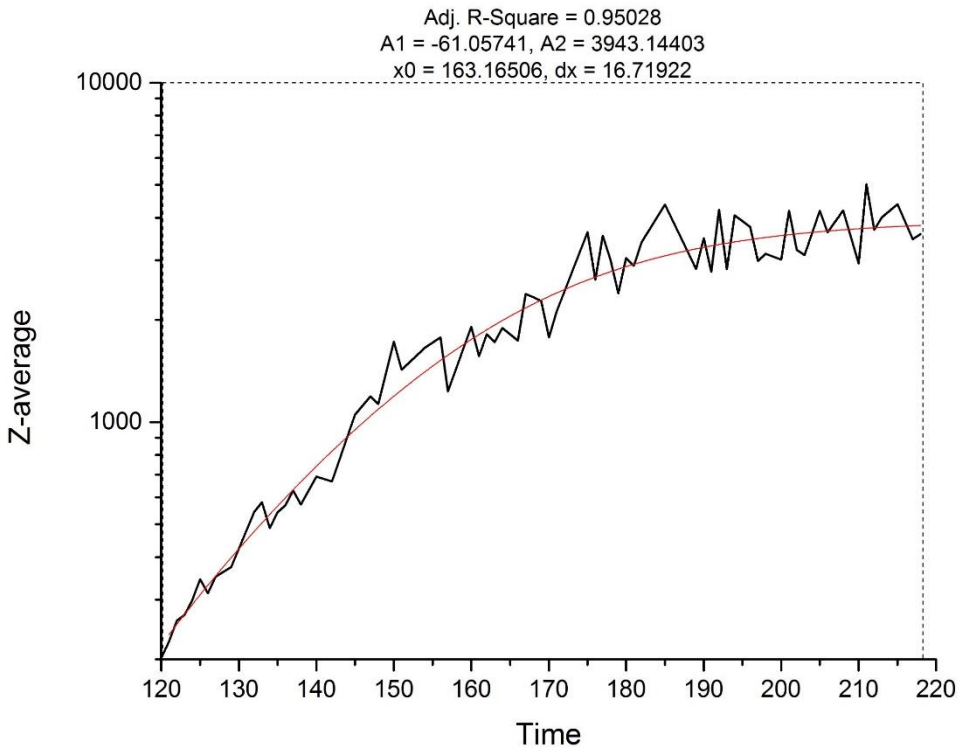

Figure 18 - Dependence of light scattering intensity on time for aggregation of iTLP with Boltzmann curve fitting.

Once the initial critical-sized multimeric nuclei are formed, supposedly by sequential association of individual protein molecules, a considerable number of potential sites become available for the addition of monomers or other small multimers, resulting in acceleration in the rate of polymerization. This hypothesis agrees with the observed appearance of a multimer with a hydrodynamic diameter of ca. 1008 nm (iTLP second species of aggregated form) while, at the same time, the first species of aggregate form starts to disappear (Figure 17B).

The amorphous aggregation process of TPLs was also described [158] with emphasis on the early-time aggregation. At early times, the aggregation process for thaumatins was well described by an isotropic tree-dimensional process whereas at late times aggregation displayed a two-dimensional cylindrical behaviour. Two hypotheses were proposed to explain the observed change in aggregation: 1) hydrophobic interactions between aggregate and monomer, with subsequent addition of monomers to the aggregate until stereochemical restrictions occurred due to a decrease in exposed hydrophobic areas available for the monomers to add; 2) large aggregates might clump together to form huge aggregates, decreasing the surface area available for monomer addition. Even though [158] used proteins and methods that differed from those reported in this work, a parallelism can be traced between both. Clumping of large aggregates can explain formation of larger size aggregates (in our case the third aggregated form; Figure 17B) without complete disappearance/interaction of the smaller ones (first aggregated form; Figure 17B). However, our

data focus more on late-time aggregation since it was not possible to acquire DLS data during the cooling step.

The DLS results in the presence of SO_2 show the influence of this compound on the protein refolding ability during the cooling step, leading to different conformation states that eventually give rise to rather large protein aggregates, which ultimately precipitate. We may infer that SO_2 interferes with the formation of disulfide bonds, but direct assessment of such reaction should be followed by other techniques, namely circular dichroism and tryptophan fluorescence spectroscopies.

The turbidity that develops upon cooling from 70 to 15 °C seems to be caused by the aggregation effect of SO_2 on iTLP, as revealed by following the temperature-induced changes in the UV absorption spectra. Using the molar absorption coefficient formula, we can estimate that the contribution to the absorbance at 280 nm is 56% related to the tryptophan content (3 residues), 40% to the tyrosine (8 residues) and 4% to the disulfide bonds (8 disulfide bonds). Figure 19 shows absorption spectra in the absence of SO_2, where the absorbance at 280 nm does not show any significant difference after decreasing the temperature from 70 to 15 °C. Conversely, in the presence of SO_2, turbidity appears followed by a decrease in the absorption at 280 nm when the sample is cooled to 15 ºC. This indicates protein aggregation (as seen in the DLS experiments) followed by partial precipitation (which decreases protein concentration in the bulk solution).

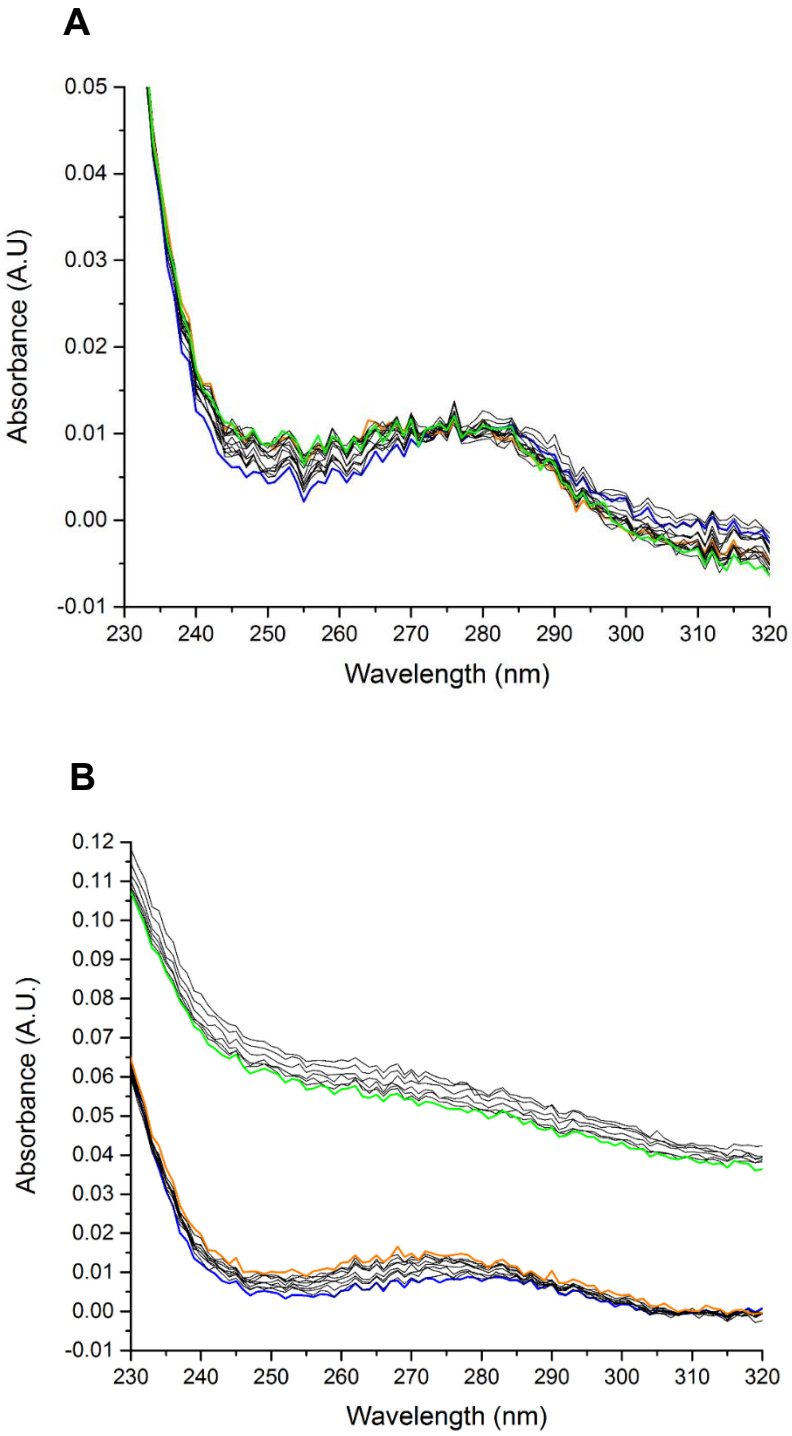

Figure 19 – Absorption spectra of iTLP during CD analysis. A) iTLP in model wine solution (absence of SO_2). B) iTLP in model wine solution in the presence of SO_2. Temperatures of 20 °C (prior to heat stress), 70 °C (after 120 min at 70 °C) and 15 °C (after 60 min at 15 °C following heat stress at 70 °C) are highlighted in blue, orange and green respectively. The remaining spectra gathered during the trial are represented as solid grey lines.

At the same time (UV spectra were acquired simultaneously to CD spectra in the same equipment), CD spectra were taken for both samples (Figure 20). The far-UV CD spectra of iTLP, at 20 ºC and in the absence of SO_2, showed two positive peaks at 194 and 231 nm and a negative peak at 212 nm. The CD spectra of iTLP in the presence of SO_2 presents a very similar spectrum either at 20 ºC and at 70 ºC. Thus, increasing the temperature from 20 to 70 ºC induced a severe change in the CD spectra regardless of the presence of SO_2. However, after decreasing the temperature to 15 ºC in the absence of SO_2, a regain of secondary structure was detected, characterized by the reappearance of the 230 nm band and a shift of the minimum ellipticity from 202 to 212 nm. When compared to the iTLP spectrum obtained after decreasing the temperature to 15 ºC in the presence of SO_2, the clear peak detected at 230 nm becomes reduced to a shoulder. This is a sign of recovery of secondary structure, although with a different conformation (Figure 20B).

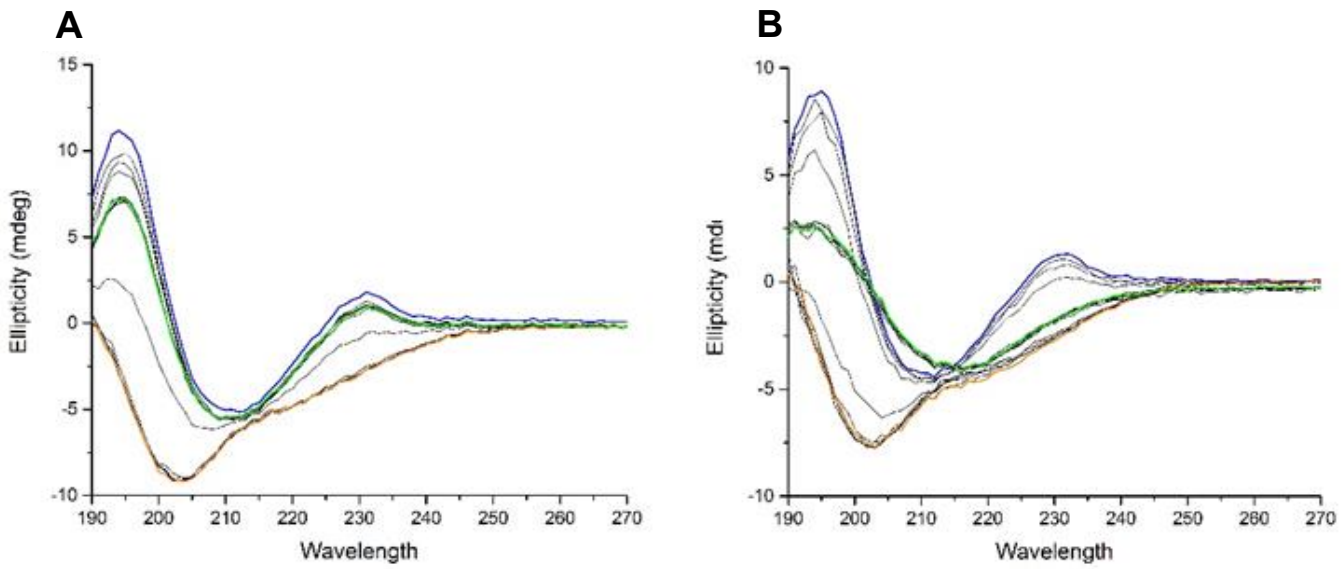

Figure 20 – A) CD spectra of iTLP (at 500 mg L^{-1}) in model wine solution (absence of SO_2). B) CD spectra of iTLP in model wine solution in the presence of SO_2 (at 600 mg L^{-1}). Spectra corresponding to temperatures of 20 °C, 70 °C and 15 °C are represented in blue, orange and green, respectively. The different spectra gathered during the time window of the trial are represented as solid grey lines.

To analyse the secondary structure of the proteins, the spectra were deconvoluted using the SELCON3, CONTIN and CDSSRT algorithms present in the Dichroweb portal [159,160]. The average results from these algorithms are presented in Table 6. The results from the individual algorithms are represented in Appendix A.

Table 6 - Secondary structure analysis of iTLP (with and without added SO_2) by the deconvolution of CD spectra with the algorithms SELCON3, CONTIN and CDSSTR. The values presented in this table

correspond to the averages of the results acquired by the different algorithms per each point represented as percentage. The dataset used in these analyses were the SP175 available in the Dichroweb portal. The individual values per each algorithm are available in Appendix A.

		Helix α	Sheet β	Turns	Random Coil
20 °C	**iTLP**	8.0	41.4	9.7	39.8
	iTLP + SO_2	8.4	42.1	9.6	39.4
70 °C	**iTLP**	11.6	30.3	14.9	42.2
	iTLP + SO_2	10.5	33.8	14.7	42.6
15 °C	**iTLP**	9.8	39.3	10.8	39.2
	iTLP + SO_2	21.2	28.3	11.7	38.5

The analysis of the results at 20 °C suggests that iTLP is characterized by a high content in β-sheets and a lower content in α-helices. Similar results for thaumatin-like proteins were reported previously [24,63]. Addition of SO_2 resulted in a slight decrease in the overall signal (Figure 20B). Nevertheless, no significant modification of the spectra was detected, meaning that the secondary structure of iTLP was practically unaffected by the presence of SO_2.

Analysing the secondary structure results for iTLP on the presence of SO_2, after heating and cooling, results in a decrease in the β-sheet content and an increase in the α-helix content when compared to iTLP in the absence of SO_2. This phenomenon can also be related with changes in disulfide bonds. In protein F2/4JRU, a thaumatin found in wine, it was shown that one of its domains comprising one loop and two β-strands, is stabilized by two disulfide bonds. The same authors also studied two isoforms of VVTL1 protein and showed that both β-strands and α-helices are stabilized by disulfide bonds. Based on our results and on previously published data, we can hypothesize that formation of both inter and intra molecular disulfide bonds by the action of SO_2 induces not only iTLP aggregation but also a decrease in its β-sheet content followed by an increase of the α-helix content. Thereby, the reaction between iTLP and SO_2 at high temperature induces formation of new configuration states of iTLP which will partially precipitate after decreasing the temperature of the solution, confirming previously DLS presented data.

The disappearance of the 230 nm band by the action of temperature or pH on proteins has already been reported by [161] when studying the conformation of α-neurotoxins of elapid venoms and neurohypophyseal hormones. These authors showed that closely related conformers of oxytocin differing in the chirality of their disulfide bridges presented different signals in the 220 – 230 nm

region. This is in accordance with previous observations showing that the 220 – 230 nm region is critically dependent on the disulfide torsion angles [162]. A change in disulfide bonds can induce a loss in signal in that region. Upon refolding, formation of a different pattern of disulfide bonds can change the torsion angles of these bonds (due to the non-native conformation of the protein), resulting in a significantly different signal on the 220 – 230 nm for iTLP in the presence of SO_2 after decreasing the temperature to 15 °C. In the absence of SO_2, a reappearance of this signal was noted for iTLP, most probably corresponding to reformation of the original disulfide bond pattern within the protein.

To analyse the thermal stability of iTLP in the presence of SO_2, we calculated the apparent melting temperature (T_m) based on the change of the molar ellipticity value at 222 nm. Since the unfold of the protein shows a sigmoid shape, fitting the values at 222 nm of the temperature gradient to a sigmoidal fit curve using the Boltzmann function allows to calculate the apparent melting temperature of the protein [163]. The molar ellipticity values at 222 nm during the temperature gradient for iTLP are represented in Figure 21.

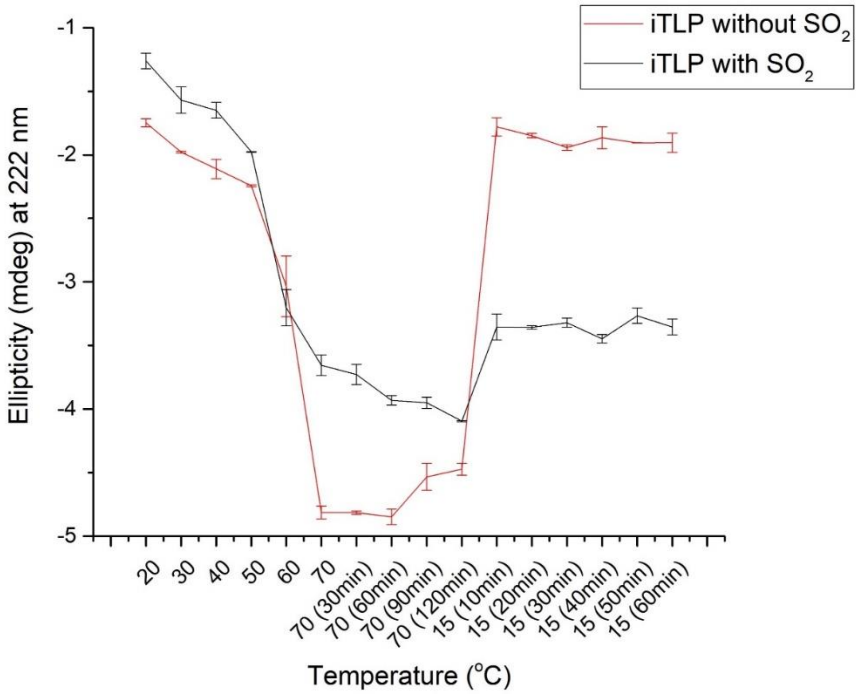

Figure 21 – Changes in molar ellipticity of iTLP at 222 nm. The temperature gradient consisted of 10 °C increments in the temperature range between 20 and 70 °C. Within parenthesis is represented the time at which the protein was at that temperature.

A T_m of 58.3 ± 2.4 °C and 57.3 ± 1.3 °C where calculated for iTLP without added SO_2 and iTLP with added SO_2 respectively. Although the fitting with the Boltzmann function was possible, a

more accurate calculation of the melting temperature would require gathering more points within the temperature window (between 20 °C and 70 °C). Nevertheless, based on the apparent melting temperature of iTLP in the two modalities, we can see that there is no noteworthy difference between samples. There is no apparent shift of the T_m in the iTLP with added SO_2, which indicates that this compound does not change the thermally induced unfolding rate of this protein. This result emphasizes that the reaction between iTLP and SO_2 occurs mainly during the heating step (2 hours at 70 °C) and after decreasing the temperature post heat stress.

Further evidence about the nature of disulfide bonds may be gathered from fluorescence measurements. Tryptophan fluorescence is known to be quenched by disulfide bonds through electron-transfer processes if tryptophan and disulfide are at a close distance [164]. A scrambling effect of disulfide bonds upon cooling in the presence of SO_2 would presumably lead to longer average distances which should stop this quenching effect. Under these conditions, fluorescence intensity should increase. This effect should not happen in the absence of SO_2 since the protein seems to refold to its original state. Fluorescence measurements confirmed this effect, as shown in Figure 22. During heating, in the sample without SO_2 (Figure 22A), fluorescence intensity increases slightly with a red shift, which reflects mainly the higher exposure of tryptophan residues.

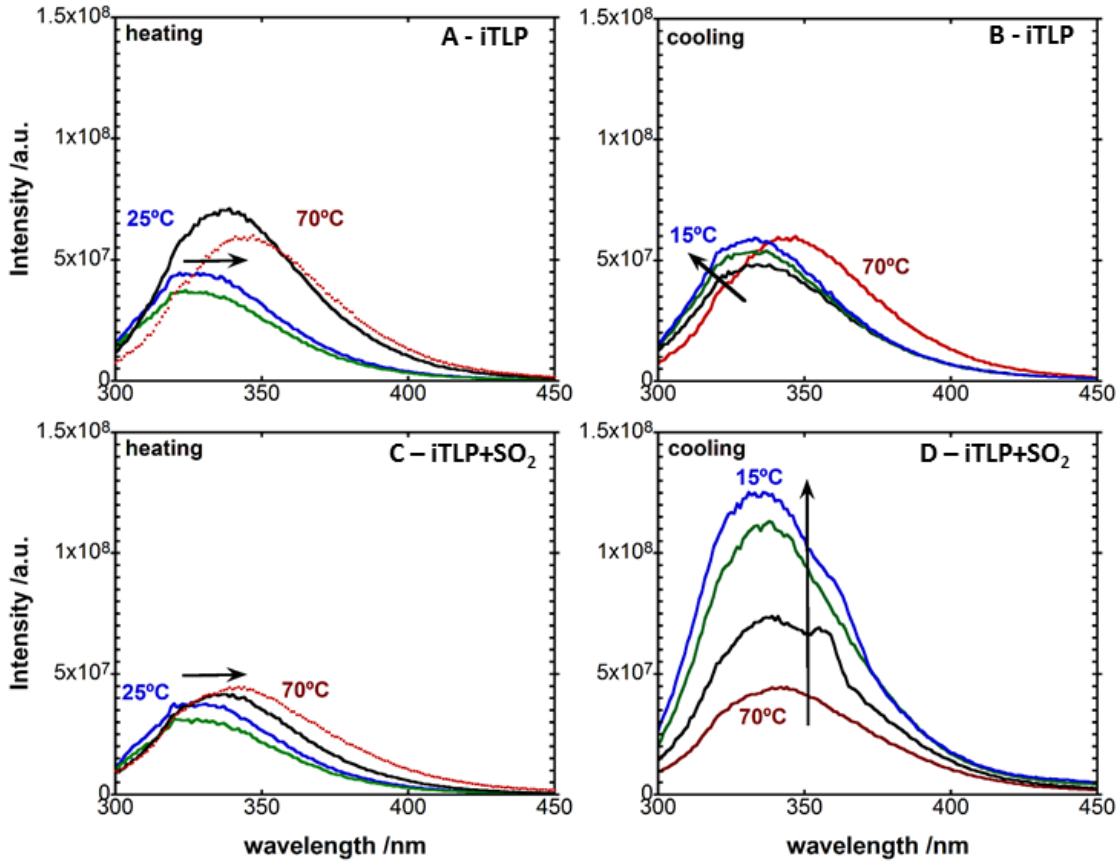

Figure 22 - Tryptophan emission intensity of A) and B) iTLP (100 mg L^{-1} in model wine solution in the absence of SO_2) and C) and D) iTLP (100 mg L^{-1} in model wine solution) in the presence of SO_2 (120 mg/L total SO_2). A) and C), heating: blue 25 °C, green 40 °C, black 60 °C and red 70 °C; B) and D), cooling (following heat stress represented in A) and C): red 70 °C, black 50 °C, green 25 °C and blue 15 °C). Black arrows represent the shift of the curves with time and temperature.

In the presence of SO_2 (Figure 22C) the observed result is the same. The cooling step performed after the heat stress, however, reveals a completely different behaviour between the samples. Without SO_2 (Figure 22B), the cooling follows the same trend backwards, so that at 15 °C the tryptophan fluorescence presents only a slight increase compared to the protein at 20 °C before heat stress. However, in the presence of SO_2 (Figure 22D), spectra shift again to the blue indicating refolding of the protein, but fluorescence intensity shows a 3-fold increase. This increase in Trp fluorescence is an indication that quenching by disulfide bonds is less effective. A similar phenomenon was reported for a cutinase reduced by the addition of DTT, confirming the proximity between Trp residues and the disulfide bridge observed in native cutinase [165]. This indicates that if a different pattern of S-S bonds is formed, it will be at longer distances from Trp residues, at positions which differ from those in native iTLP. This effect shows that SO_2 induces conformational changes also at the level of iTLP Trp residues, and this occurs as iTLP aggregates.

3.3.3.5 Structural studies on iTLP aggregates

To study iTLP aggregates formed after heat stress, their solubility was tested in a series of buffers with varying salt concentration, denaturant concentration and pH. The iTLP aggregate-containing protein pellet could be fully dissolved in two different buffers; buffer A (8 M urea, 200 mM NaCl, 30 mM sodium citrate, pH 3.0) and buffer B (4% w/v SDS, 200 mM NaCl, 200 mM Tris-HCl, pH 8.0). Based on our results, we hypothesized that SO_2 modulated aggregation of a major wine protein fraction, could be attributed to formation of new intra- and interprotein disulfide bonds, which could eventually evolve to protein aggregation. Solubilization of the protein pellet in buffer A or buffer B provided new insights about the nature of the aggregates, demonstrating full solubilization of iTLP aggregates in a denaturing, high ionic strength, non-reducing medium. Since the pellet is insoluble in 1 M NaCl (excluding ionic interactions) but soluble in buffer A or B, we may conclude that hydrophobic interactions also participate in the aggregation phenomena in addition to disulfide bond scrambling.

These buffers were chosen based on their action as described in the literature. Our main objective was to disrupt all non-covalent interactions on the protein aggregate to dissolve him. This way we could analyse the protein species within the aggregate. One way to disrupt non-covalent interactions would be to use a charged compound that disrupts hydrophobic interactions by providing a hydrophobic microenvironment [14].

Urea is one of the most versatile and commonly used denaturants for solubilizing proteins, including inclusion bodies. The most common work concentration range is between 6 and 9 M [166]. One of the mechanisms of protein denaturation by urea is due to weakening the hydrophobic interaction, as demonstrated for lysozyme in 8 M urea [167]. The buffer used in our trials was composed of 8 M urea, 200 mM NaCl and 30 mM citrate buffer pH 3. Our goal was to disrupt hydrophobic interactions with the urea and, at the same time, increasing the ionic strength of the medium with NaCl to avoid electrostatic interactions. The citrate buffer was chosen due to its similarity with wine pH but also due to its compatibility with the separation protocols.

A second strategy was to use a detergent to try to solubilize the protein aggregates. The most commonly used protein-denaturing detergent is sodium dodecyl sulfate (SDS), an anionic detergent. This is a very effective protein denaturant since it binds directly to the protein [168]. The second buffer consisted of 4% SDS, 200 mM NaCl, 200 mM Tris-HCL pH 8. This buffer was chosen to be compatible with the DTNB assay due to its pH requirements. Nevertheless, 4% SDS in citrate buffer at pH 3 also dissolved the aggregates formed after heat stress.

The solution used for DLS experiments was collected and centrifuged 10 min at 1,360 *g* to collect the aggregated protein. The pellet was solubilized in buffer A and a new analysis in the DLS was performed. The data collected after acquisition is represented in Figure 23.

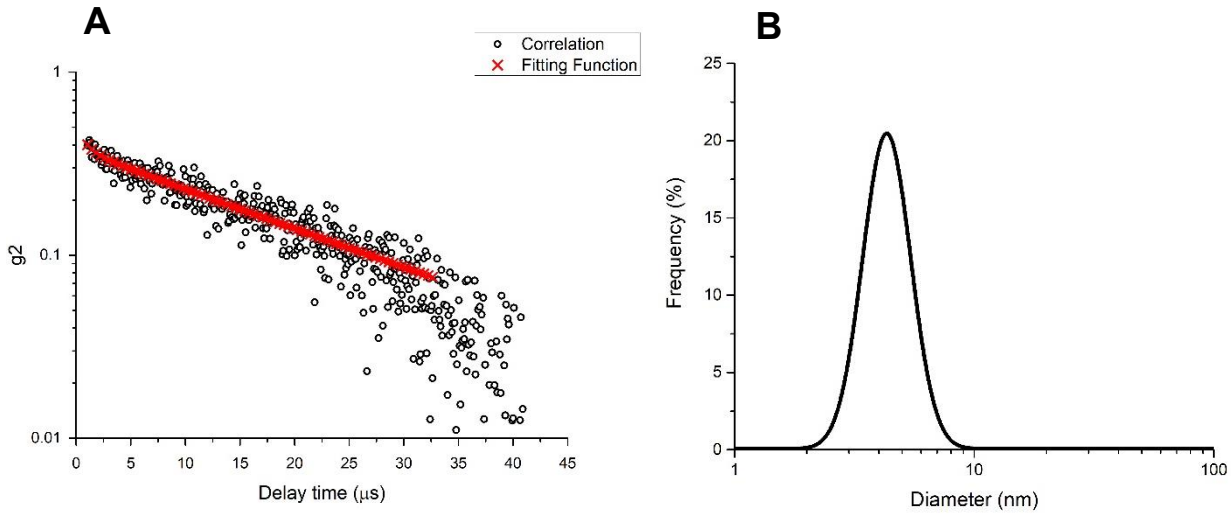

Figure 23 - A) Autocorrelation curve acquired by DLS nanoanalysis of the iTLP in wine model solution after heat stress. B) Size distribution frequency acquired by DLS nanoanalysis (represented as the protein diameter in nm) of the iTLP after heat stress dissolved in buffer A.

DLS analysis detected particles with an average diameter of 4.7 nm ± 1.14 nm. This value indicates that the particles in solution correspond mainly to monomeric iTLP. No other protein species were detected. This observation supports the view that iTLP 'monomers' are mainly associated by hydrophobic interactions in iTLP aggregates.

To identify other iTLP species not recognized by DLS, size-exclusion chromatography (SEC) of iTLP solubilized aggregates was performed. To achieve a good fractionation, buffer A was selected as mobile phase to ensure full solubilization of iTLP aggregates. A similar approach was reported [169] for characterizing apomyoglobin self-associated species in urea solutions. The chromatograms of iTLP dissolved in mobile phase and of iTLP after heat stability test in the absence or presence of SO_2 are represented in Figure 24.

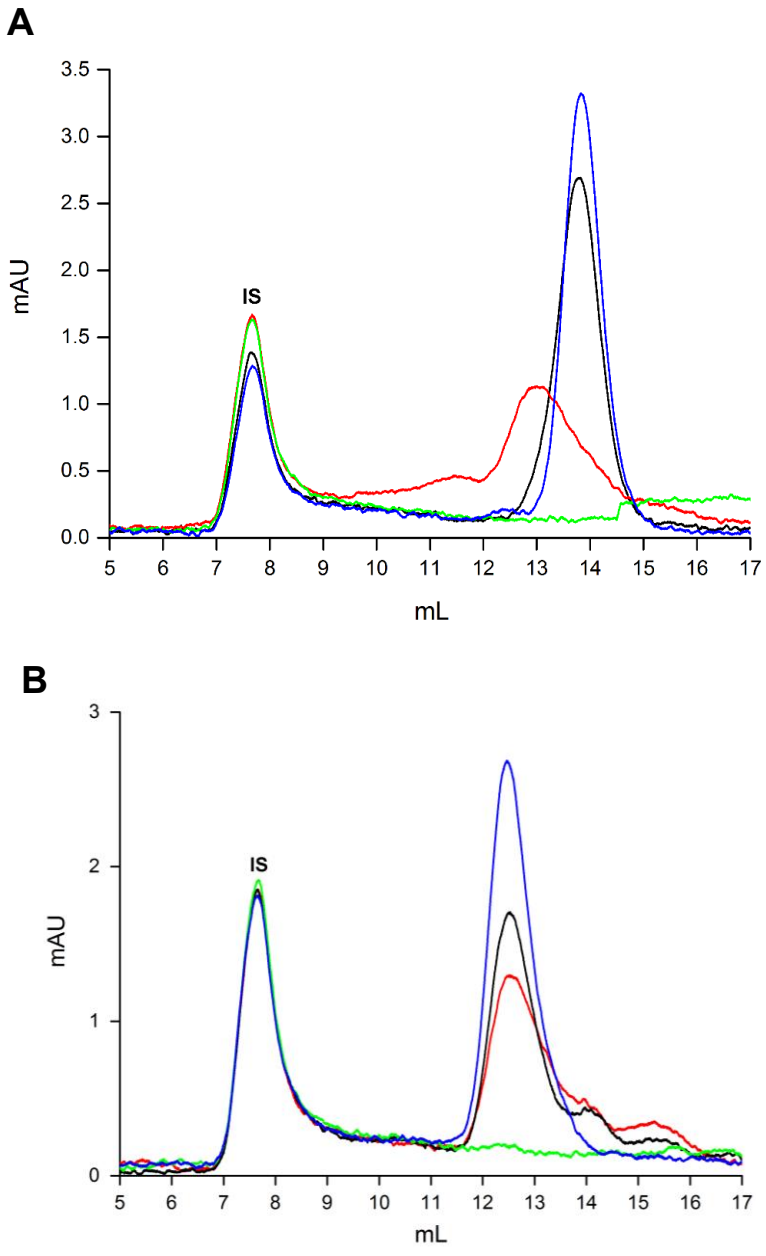

Figure 24 - Size-exclusion chromatogram of non-reduced (A) and reduced (B) iTLP dissolved in MWS (–), iTLP after heat stability test (absence of SO_2) (–), pellet (–) and supernatant (–) of iTLP after heat stability test (presence of SO_2) in buffer A. First peak at 7.9 min corresponds to blue dextran used as internal standard (IS).

The molecular weight of the different molecular species present in the non-reducing buffer (Figure 24A) was determined (Table 7). iTLP presented a single peak with a retention volume of 13.83 mL, corresponding to a calculated molecular weight of 21.1 kDa. Similarly, the same fraction after heat stress without addition of SO_2 presented a molecular weight of 21.4 kDa, showing that heat treatment has no impact on either iTLP size or in aggregation.

Table 7 - Molecular weight of the different molecular species present in the protein peaks depicted in Figure 24, calculated after their fractionation by non-reducing size exclusion chromatography.

Sample	Retention (mL)	Molecular weight (kDa)
iTLP in MWS	13.83	21.1
iTLP in MWS without SO_2	13.81	21.4
iTLP in MWS with SO_2	12.80	37.4
	11.44	79.4

The chromatographic profile of heat stressed iTLP with added SO_2 shows the presence of two major peaks, one with a retention of 11.44 mL, the other with 12.8 mL, corresponding to 37.4 and 79.4 kDa, respectively. This can be related to formation of dimeric and tetrameric molecular species when the protein is heat stressed in the presence of SO_2. The chromatographic profiles of the supernatants collected from the heat stressed samples (Figure 24) shows that there are no detectable protein peaks left in soluble form after iTLP heat stress.

To further analyse the chromatographic profile of iTLP aggregate units, statistical analysis was performed (Figure 25).

A

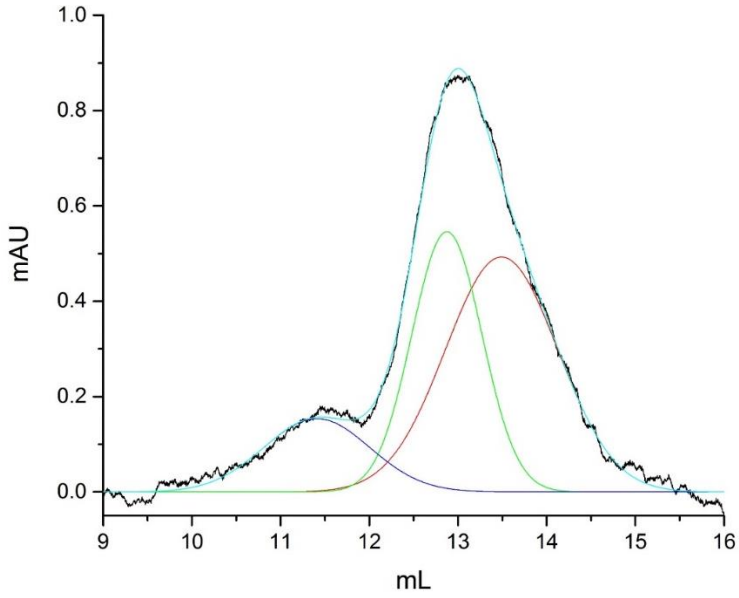

B

			Analysis by peak intensity		Analysis by number of molecules	
Peak	**Retention (mL)**	**Estimated MW**	**Integral**	**Quantity (%)**	**Corrected integral**	**Quantity (%)**
1	11.4	81	0.23	14.8	0.056	5.2
2	12.8	37	0.54	34.8	0.27	24.4
3	13.7	22.7	0.78	50.3	0.78	70.4

Figure 25 - A) Experimental data and corresponding fitting of the chromatographic profile of the heat stressed iTLP in the presence of SO_2 (baseline corrected). Multi-peak Gaussian analysis of the chromatogram is represented by the different Fit Peaks represented in the figure: iTLP after heat stability test (presence of SO_2) (–), fit peak 1 (–), fit peak 2 (–), fit peak 3 (–) and cumulative fit peak (–). B) The table describes the different protein species and discriminates their relative amounts based on the peaks integrals.

After fitting the chromatogram, it is possible to differentiate three different peaks corresponding to iTLP covalently linked tetrameric, dimeric and monomeric species. Considering that the number of Trp, Tyr and Phe residues remain constant during the experiment, we can calculate the number of molecules of the different species by dividing the integral for each species by the number of monomers present in the different species (division by two in the case of dimers, and by four in the case of tetramers). Analysing the number of molecules present in solution reveals that there are 70.4 % of iTLP monomers, 24.4 % of dimers and 5.2 % of tetramers. Thus, most of the molecules in solution are monomers that self-aggregated via hydrophobic and electrostatic interactions.

Samples identical to those used for Figure 24A were reduced using TCEP and subsequently analysed by SEC, as represented in Figure 24B. After reducing the samples and superimposing

the different chromatograms, a single major fraction is present in all samples that corresponds to monomeric iTLP (21.1 kDa). There is a shift in the retention time of all samples due to the complete unfold of the proteins present in solution which change the apparent measured molecular weight. The descrimination of the different molecular weights in the reduced samples was not possible since a calibration curve with reduced standard proteins was not performed. Nevertheless, considering that native iTLP in MWS is exclusively composed of monomers, we may infer the presence of monomeric species in the other samples by the values of peak retention. The presence of lower molecular weight polypeptides was also detected in the reduced heat stressed iTLP with or without SO_2 addition, possibly related to protein degradation during heat treatment.

The 'dimers' and 'tetramers' present in the nonreduced, heat stressed iTLP treated with SO_2 do not appear in the chromatogram of the same sample reduced with TCEP. This can lead to the conclusion that the 'dimers' and 'tetramers' can self-aggregat among themselves and/or with monomers, in a process involving not only hydrophobic and electrostatic interactions, but also scrambled intramolecular dissulfide bridges. Intermolecular dissulfide bridges do participate in the process of 'dimer' and 'tetramer' formation. Is is noteworthy to mention that we failed to detect the presence of iTLP 'trimers'. These results are in accordance with the hypothesis that the presence of HSO_3^- in solution and the high temperature-induced unfold of the proteins could cleave the wine intraprotein disulfide bonds followed by the formation of new intra- and interprotein disulfide bonds during the cooling step.

In several proteins, intramolecular disulfide bonds are required for folding into native structures and also contribute to increase protein thermal stability [8,169]. Reduction followed by aberrant scrambled disulfide bond formation results in protein misfolding [170]. The authors presented that thiol/disulfide exchange reactions lead to the formation of aggregates of disulfide-linked β-lactoglobulin monomers together with non-covalent interactions.

The chromatograms presented in Figure 24A and 24B are representative of a trial using iTLP at a concentration of 500 mg/L in wine model solution. This concentration does not mimic real wine conditions however, similar results were acquired when 100 mg/L of iTLP and different SO_2 concentrations were used (Figure 26). There is no apparent difference between the different concentrations of SO_2 except for 600 mg/L where a decrease in the signal was registered. Even with a possible significant difference, at this concentration range, it is difficult to get a worthwhile result due to the signal/noise ratio.

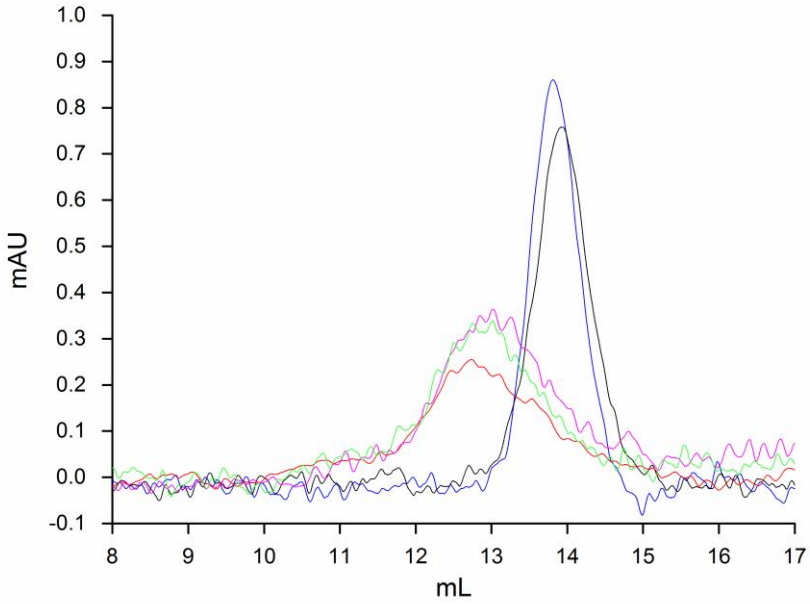

Figure 26 - Size-exclusion chromatogram of non-reduced iTLP dissolved in WMS (100 mg/L) (–), iTLP after heat stability test without SO_2 addition (–), pellet of iTLP after heat stability test with SO_2 (120 mg/L) dissolved in buffer A (–), pellet of iTLP after heat stability test with SO_2 (200 mg/L) dissolved in buffer A (–) and pellet of iTLP after heat stability test with SO_2 (600 mg/L) dissolved in buffer A (–).

Studying the reaction of DTNB with the sulfhydryl groups present in iTLP revealed the occurrence of free sulfhydryl groups after iTLP reduction and allowed studying the effect of high temperature. A specific protocol had to be optimized for the analysis of iTLP aggregates (further information in the Experimental section).

Since the aggregates are soluble in buffer A and buffer B, a new step was included in the standard DTNB protocol that allows analysing the free thiol groups of the solubilized aggregates.

All samples were treated equal except for the heat stressed samples that were subjected to a stress equal to the one induced during the heat stability test of wine proteins. To get information about the aggregated proteins, these were resuspended in buffer D (4% SDS, 200 mM NaCl, 200 mM Tris-HCL pH 8). iTLP does not have any of its 16 Cys residues with free sulfhydryl groups, since they all participate in eight disulfide bridges (based on available PDB data about VVTL1 protein). After statistical analysis, we can conclude that either iTLP (native), heat stressed iTLP and heat stressed iTLP in the presence of SO_2, do not present a significant difference in their number of free sulfhydryl groups (Figure 27). After statistical analysis, we can see that both iTLP (native), heat stressed iTLP and heat stressed iTLP in the presence of SO_2 do not present a significant difference in the content of free SH groups (Figure 27).

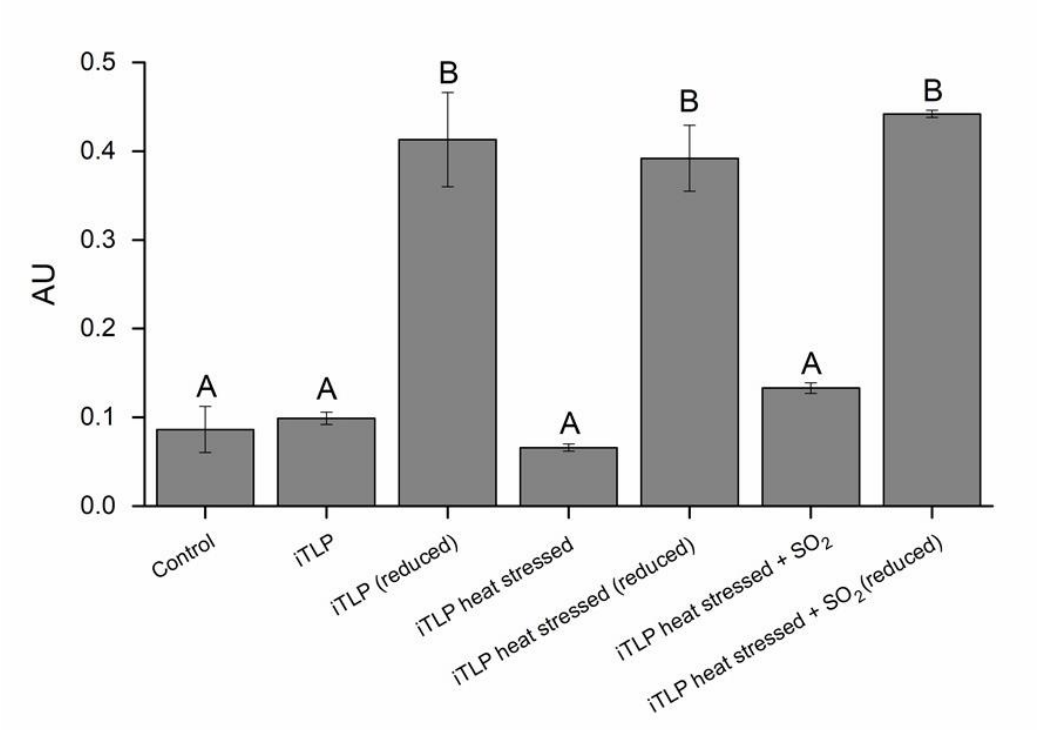

Figure 27 - Reaction of iTLP with DTNB reagent in buffer E containing 200 mM Tris-HCl, 8 M urea, pH 8.0. Control corresponds to the assay performed in the absence of protein. Mean values not sharing the same letter are significantly different (OneWay-ANOVA, Tukey HSD, $P < 0.05$).

If each one of the 16 iTLP Cys residues is bound to another Cys residue, we can say that there are no free sulphydryl groups in either native iTLP or heat stressed iTLP in the absence or presence of SO_2. In all cases the signal increases after reduction with TCEP due to the expected reduction of disulfide bounds. Similarly, under non-reducing conditions, no significant differences were observed among the three samples, showing all sulfhydryl groups are in free form in all samples. Overall, these results show formation of iTLP 'dimers' and 'tetramers' by intermolecular disulfide bridges, as well as the absence of free sulphydryl groups in the three samples examined. Furthermore, iTLP aggregates involve disulfide bridge scrambling among different iTLP molecules and consequent formation of new disulfide bridges leaving no free sulphydryl groups.

3.3.3.6 Effect of SO_2 addition on protein haze formation under real wine conditions

Following protein haze formation in a wine, the resulting precipitate contains not only proteins which "survived" the vinification process but also other compounds that potentially interacted with those proteins [11]. In fact, several studies published in the literature point to the participation of these non-proteinaceous compounds in the protein haze forming mechanism. [41] demonstrated

that protein haze formation in white wine shows an absolute requirement for one (or more) low molecular mass (<3 kDa) wine component which was termed the X-factor. Since this study, the <3 kDa wine fraction became generally accepted as containing a haze inducing group of unknown compounds.

To evaluate the interaction of SO_2 with wine proteins in real wine, we first assessed the SO_2 (free and total) content in wine (W), in the <3 kDa wine fraction (<3 kDa), and in the <3 kDa wine fraction after lyophilisation (<3 kDa AL) (Figure 28A). This assay was performed using a 2010 vintage Moscatel of Alexandria wine containing 80 mg/L of total protein. Following SO_2 quantification for all the samples, we observed that both <3 kDa wine fractions (before or after lyophilization) contained similar but slightly lower SO_2 concentrations when compared to the wine sample. These differences may be attributed to 1) residual sulfur dioxide remaining in the >3 kDa fraction after filtration and/or 2) the volatile nature of sulfur dioxide, which may be partially lost during lyophilization.

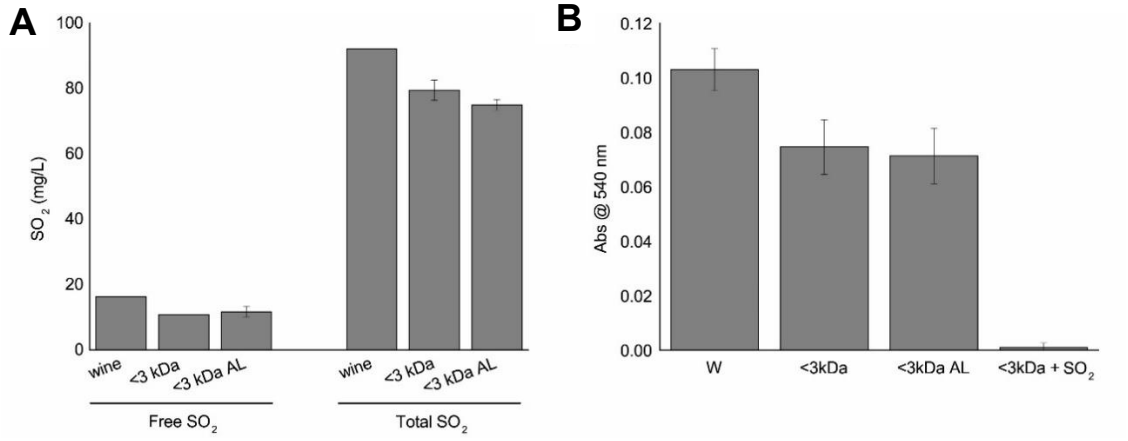

Figure 28 - A) Total and free SO_2 content of the sample wine (W), of the <3 kDa fraction (<3 kDa) and of the <3 kDa fraction after lyophilisation (<3 kDa AL). B) Haze development after heat stability test of sample wine (W; 80 mg/L protein), of the <3 kDa fraction added of total wine protein (<3 kDa; 80 mg/L protein), of the <3 kDa fraction after lyophilization added of total wine protein (<3 kDa AL; 80 mg/L protein), and of the <3 kDa fraction added of 120 mg/L total SO_2 without protein addition (<3 kDa + SO_2).

When identical fractions were subjected to heat stability test, a decrease of 27.6% and 30.8% in the formed haze was observed for both <3 kDa and <3 kDa AL fractions, respectively (Figure 28B). These values do not reflect the differences registered in SO_2 quantification (Figure 28A), but a tendency between the SO_2 content of a wine and its propensity to form haze after heat stress instead. As a control, the <3 kDa fraction was added of SO_2 (50 mg/L) in the absence of protein, revealing no haze formation upon heat stress, an expected result which confirms the strict necessity of protein for this type of haze to occur.

To provide further evidence that SO_2 induces protein haze formation, wines with and without added SO_2 were tested for their stability after heat stress. To achieve this, two single variety wines were produced in our lab, each one under two different conditions, with and without added SO_2. The summary analysis of the four resulting wines is represented in Table 8.

Total sulfur was quantified by Inductively Coupled Plasma - Atomic Emission Spectrometry (ICP-AES) and revealed significant differences within the samples. As expected, both wines with added SO_2 presented higher sulfur contents. Excluding sulfur added as SO_2, values of 68.4 and 7.1 mg/L for Moscatel Galego, and 94.1 and 4.7 mg/L for Moscatel of Alexandria, with and without added SO_2 respectively, were obtained. Sulfur speciation was not analysed but we may assume the SO_4 content of the samples to be reflected in the fraction of total sulfur that does not correspond to SO_2. If all non-SO_2 sulfur is present as SO_4; could it have any effect in protein haze? As referred above, the amount of sulphate required to induce protein haze was reported as 400 mg/L [43].

As expected, the wines added of SO_2 present a much higher content of both free and total SO_2 after vinification. Since there was no addition of SO_2 to the samples identified as 'without SO_2' it was expected the absence of the additive, which was not the case. In both cases the 'without SO_2' samples contained residual levels of SO_2, up to 16.2 ppm. These data are in accordance with previously reported data [171], who reported that natural SO_2 formation in wines (yeast by-product) may account for 15 to 125 ppm of residual SO_2 in the finished product.

Both wines with added SO_2 presented higher contents in total polyphenols and lower protein concentrations. Higher values of total polyphenols for samples with higher SO_2 content were reported when using the Folin Ciocalteau method, and attributed this effect to interference of sulfite with the method [172]. It was also reported that an increase of the metabisulphite concentration to 80 mg/L (i.e. approximately 51 mg/L SO_2) caused an increase of approximately 40 mg/L (expressed as caffeic acid equivalents) in the total phenolic content determined in model solutions [173]. Table 8 shows that an increase of 84 and 67.9 mg/L SO_2 originated an increment of 58.7 and 34.3 mg/L total polyphenols (expressed as tannic acid equivalents), respectively. To understand the impact of the addition of SO_2 on the wines under study, the four samples were subjected to heat stability test (Table 8).

Table 8 - Summary analysis of two varietal wines, each one produced with and without added SO_2. Means not sharing the same letter are significantly different (OneWay-ANOVA, Tukey HSD, $P < 0.05$).

Parameters	Moscatel Galego		Moscatel Alexandria	
	With SO_2	Without SO_2	With SO_2	Without SO_2
pH	3.12	3.11	3.19	3.25
Total protein (mg/L)	130.0^{a}	141.3^{a}	215.0^{b}	220.7^{b}
Free SO_2 (mg/L)	10.8^{b}	0.0^{c}	16.2^{a}	0.0^{c}
Total SO_2 (mg/L)	89.4^{a}	5.4^{d}	81.4^{b}	13.5^{c}
Total sulfur (mg/L) (determined by ICP-AES)	158.30	12.51	175.50	18.21
Alcohol content (% v/v)	11.9	12.0	12.5	12.5
Total polyphenol content (µg/mL eq. of tannic acid)	151.7^{a}	93.0^{c}	128.0^{b}	93.7^{c}
Haze formed after heat stability test (Abs. @ 540 nm)	0.075 ± 0.001^{c}	0.015 ± 0.003^{d}	0.206 ± 0.008^{a}	0.110 ± 0.001^{b}

The wines added of SO_2 originated a much higher haze level after heat stability test, with significant differences between with and without SO_2 samples for both wines. For Moscatel Galego, the sample without SO_2 was regarded as stable, since the resulting absorbance was lower than 0.02 AU, considered the threshold for wine protein instability after heat test. The same wine with SO_2 presented an absorbance of 0.075 AU ± 0.001 AU, which is considered as unstable to heat stress. These data are in good agreement with all results presented above.

The Moscatel of Alexandria varietal wine showed a similar behaviour when "with" and 'without SO_2' samples are compared, with the sample containing SO_2 presenting 87.8% higher turbidity when compared to the sample without SO_2. However, unlike Moscatel Galego, both samples were considered unstable after heat stress.

Despite the correlation of wine haze formation after heat stress with SO_2, significant differences between wine samples without SO_2 were observed. It is difficult to explain these differences at this stage, since no other assays were performed with these wines. However, such differences may be related to the differences in total SO_2 (2.5 fold higher in Moscatel of Alexandria) and protein content (1.6 fold higher in Moscatel of Alexandria). Nevertheless, it is evident that both SO_2 and protein content are strictly related to the potential of a wine to form haze after heat stress.

3.3.3.7 Updated mechanism for wine protein haze formation

Based on the recently revised unfolding and aggregation mechanisms of heat-unstable proteins in wine suggested by [5] and on our presented results, we propose an explanation for the full mechanism responsible for wine protein haze formation (Figure 29).

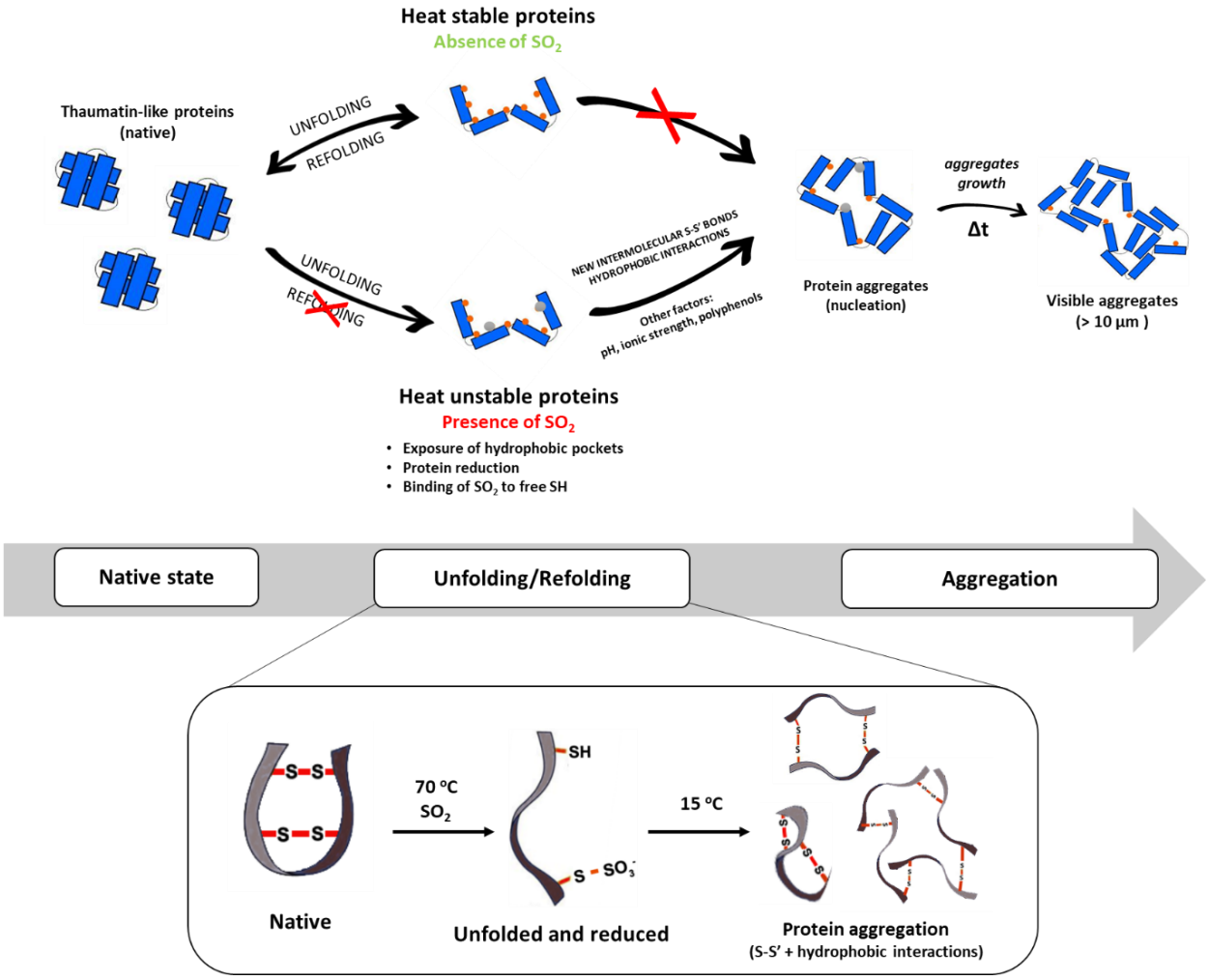

Figure 29 - Proposal of new mechanism for wine protein haze formation.

Vinification can be seen as a 'purification strategy' for grape pathogenesis-related proteins [174]. Following winemaking, the proteins that subsist are stable and folded. To trigger the aggregation and precipitation of these proteins, they must undergo an unfolding process in the presence of SO_2. The unfolding of these proteins can occur mainly due to exposure to high temperatures during storage or transportation of the wine. During this unfolding process, hydrophobic pockets of the proteins will be exposed to the surrounding aqueous environment and the SO_2 will reduce disulfide bonds and bind with part of TLP sulfhydryl groups [145]. Upon cooling, these unstable

proteins, mainly TLPs, will form a different pattern of S-S' bonds (resulting from the partial sulfonation of cysteines), which will result in altered protein configurations, inducing the formation of protein 'dimers' and 'tetramers', thus restraining TLP from refolding to its native state while leaving hydrophobic patches facing outwards. As a result, incorrectly folded TLP 'monomers', 'dimers' and 'tetramers' will aggregate during the refolding process. These aggregates are maintained mainly by hydrophobic interactions and may be modulated by other factors, including pH, ionic strength, organic acids or by other organic compounds that can bind/interact with the proteins [24,36,41]. This is translated by the crosslinking of different polypeptide species that will interact to form high molecular weight, insoluble protein aggregates, responsible for a visible haze in the wine following a nucleation growth kinetics (Figure 18).

3.3.4 Conclusions

Several decades of research have been dedicated to unravelling the chemical mechanism of white wine protein haze formation. Despite the very large number of important contributions made in this field, this mechanism remained to be elucidated. Also, many experiments were performed using potential haze forming effect of molecules at concentrations far greater than the range of values normally found in wines or those established by OIV. Successive attempts identified a multifactorial system with an absolute requirement for molecules other than the protein themselves. Thus, many researchers believed that complex chemistry was behind the precipitation of proteins in wines.

Here is presented a new mechanism, initially tested in model wine solution but later confirmed in real conditions, explaining protein aggregation in wines, which is essentially based on SO_2 and on the dynamic chemistry of Cys residues of wine proteins. Addition of HSO_3^- to must or wine (by the application of SO_2, $NaHSO_3$, $K_2S_2O_5$ or $KHSO_3$) induces cleavage of wine intraprotein disulfide bonds. This reaction is exacerbated by the high temperature-induced unfold of the proteins, whose exposed hydrophobic surfaces and buried cysteine/cystine residues further contribute to enhance interprotein interactions. After disulfide bond cleavage, HSO_3^- blocks transiently sulfhydryl groups in a process known as protein thiosulfonation or sulfitolysis, hindering thiol-disulfide exchange during protein interactions and allowing the interaction of the thiol-disulfide groups with other sulfhydryl groups present in the same or in a different protein molecule, leading to formation of new intra- and interprotein disulfide bonds. The latter are ultimately responsible for wine protein aggregation following a nucleation-growth kinetic model. We could detect that the major forces contributing for wine thaumatins aggregation in the presence of SO_2 are hydrophobic interactions mixed with covalent interaction by disulfide bridge scrambling between a fraction of the proteins. The analysis of the secondary structure of the

protein confirmed that the conformation of the unstable proteins with and without SO_2 is different after heat stress. It also allowed to detect severe changes in the disulfide bridges of the protein indicating a possible torsion of the angle of these bounds which can be related to the formation of wrong/different disulfide bridges not only inter but also intramolecular, confirming previous published results. The incorrect folding of the proteins will contribute to the exposure of protein hydrophobic pockets which can intensify the interaction with other molecules like polyphenols. This phenomenon can explain the binding of caffeic acid to the hydrophobic pockets of the protein after heat-unfolding and cooling in the presence of SO_2. Though we did not register any direct interaction between the protein and caffeic acid alone in model wine solution, this interaction can happen in real wine conditions, in the presence of SO_2, since it is one of the major compounds present in wine protein precipitate.

The chemical mechanism underlying the interaction of wine protein and sulfur dioxide was further explained and it can be the most common mechanism occurring in unstable commercial wines containing added SO_2. Although the high influence of SO_2 in the control of the protein aggregation in wine, this phenomenon continues to be likely wine-dependent and can be modulated by the wine matrix itself. The intricate and variable molecular complexity of wines certainly holds several effectors which act either positively or negatively on wine protein haze formation. Examples of both (isoelectric precipitation at high wine pH values and the stabilizing effect of organic acids commonly present in wines, respectively) have been previously published. Other significant factor influencing protein precipitation is the type of proteins present in a specific wine. Although there are several wine proteins from the same family or a similar one (e.g. thaumatins, osmotins, chitinases) their behaviour in the presence of SO_2 is not the same (Figure 12). In a specific wine, we found 46.6 % of the total protein (Figure 11) as highly reactive with SO_2 though, in other wine, this ratio can be completely different. With this in mind, there is the need to understand the behaviour of SO_2 with other varieties and evaluate its action when the ratio of available proteins is different from the one found in Moscatel (the variety used in our trials).

Since sulfur dioxide is almost ubiquitous in winemaking (due to lack of viable alternative), the problem cannot be resolved by removing or significantly decreasing the total sulfur dioxide content. The solution to this technological problem still resides in the removal of the unstable soluble proteins by bentonite or by other polymer avoiding their precipitation in the bottle.

The results achieved will certainly open the way to develop techniques which can find application in the wine industry all over the world.

4. Finding a bentonite alternative – Development of a new polymer to remove unstable proteins from white wines

4.1 Synthesis and structural characterization of dicarboxymethylcellulose

This work was developed in collaboration with Professor Thomas Heinze from the Center of Excellence for Polysaccharide Research, Friedrich Schiller University of Jena. I would like to thank Professor Thomas Heinze for the opportunity to work at his laboratory and for all the valuable inputs to my work. I would also like to thank Martin Gericke and Andreas Koschella for all the help during my stay at the group.

4.1.1 Introduction

Cellulose is considered the most abundant and renewable polymer resource available worldwide representing about 1.5 x 10^{12} tons of the total annual biomass production and is considered an almost inexhaustible source of raw material for the increasing demand for environmentally friendly and biocompatible products. This polymer is a versatile starting material for chemical conversions, aiming at the production of artificial, cellulose based threads and films as well as various stable cellulose derivatives used in many areas of industry and domestic life. It has many advantages, such as low cost, biocompatibility and biodegradability, which not only allow it to be used in furniture, clothing, packaging, paper and medical products in our daily life, but also has potential in numerous applications as bio-based materials, such as fibers, films, food casings and membranes. Therefore, effective utilization of cellulose will reduce the consumption of our limited fossil resources to protect the environment [175,176]. Nowadays, the pathways by which cellulose is accessed are mainly by biosynthesis (by plants, bacteria, algae and fungi) or by in-vitro synthesis (e.g. cellulases or ring-opening polymerization/deprotection) though the dominant is the production of cellulose from plants. As an example, in seed hairs of cotton, cellulose is available in almost pure form. In contrast, wood cellulose forms a native composite material with lignin and hemicelluloses from which it is isolated by large-scale chemical pulping, separation, and purification processes.

Cellulose is a linear and rigid homopolymer consisting of D-anhydroglucopyranose units. These units are linked together by β-(1→4) glycosidic bonds formed between C-1 and C-4 of adjacent glucose moieties (Figure 30). In the solid state, AGU units are rotated by 180° with respect to each other due to the constraints of β -linkage. In this manner, two adjacent structural units describe the disaccharide cellobiose. Each of the AGU units has three hydroxyl (OH) groups at C-2, C-3 and C-6 positions.

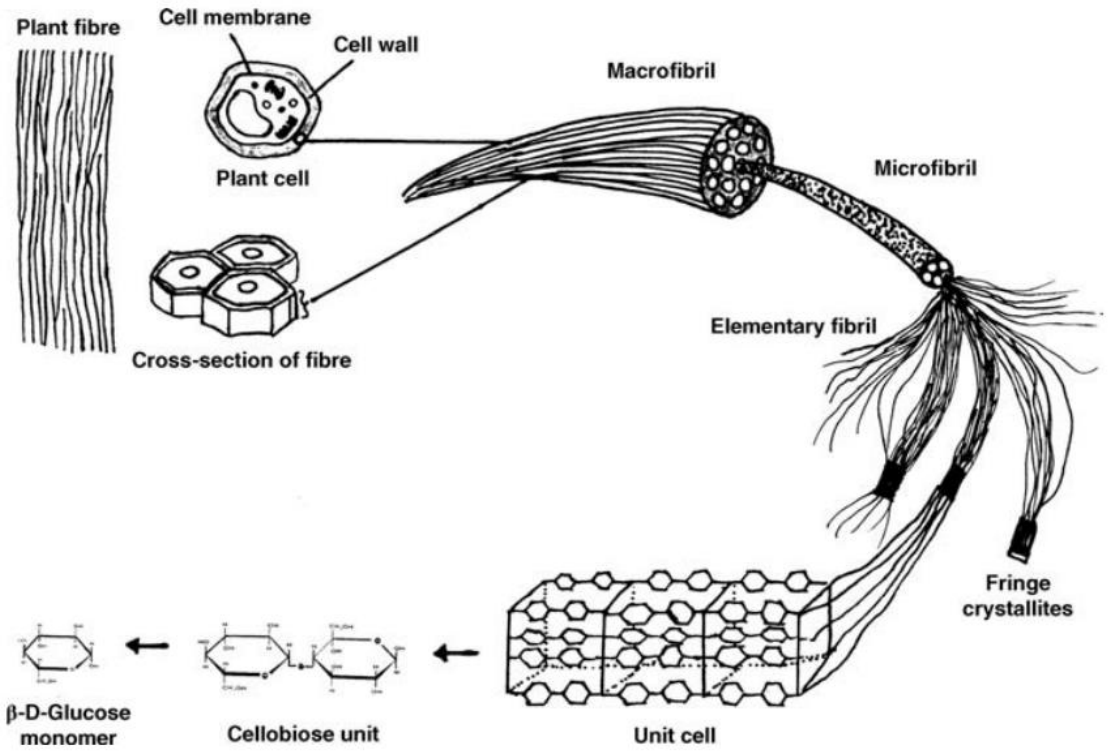

Figure 30 - Structural hierarchy of the cellulose fiber components from plant fiber to the glucose molecule [177].

As a result, cellulose is an extensive, linear-chain polymer with a considerable number of hydroxy groups (three per anhydroglucose unit (AGU)) present in the thermodynamically preferred $^4C_1$ conformation. Terminal groups at the either end of the cellulose molecule is quite different in nature from each other. The cellulose chain consists at one end of a D-glucose unit with an C4-OH group (the nonreducing end); the other end is terminated with an C1-OH group, which is in equilibrium with the aldehyde structure (the reducing end). Technical celluloses, such as bleached wood pulp, contain additional carbonyl and carboxy groups as a result of the isolation and purification processes that play a significant role in the processing of cellulose [178]. This molecular structure imparts cellulose with its characteristic properties: hydrophilicity, chirality, degradability, and broad chemical variability initiated by the high donor reactivity of the OH groups. It is also the basis for extensive hydrogen bond networks, which give cellulose a multitude of partially crystalline fiber structures and morphologies. The properties of cellulose are therefore determined by a defined hierarchical order in supramolecular structure and organization [176].

Understanding that cellulose is composed by glucose units that form long molecular chains covalently linked, opened the possibility of exploring polymer-analogous reactions. The hydroxyl groups of the AGU present in the cellulose skeleton can undergo the same kind of reactions as the corresponding low-molecular weight compounds (in this case glucose). The supramolecular

structure of the polymer and the distribution of the functional groups can play a key role in the rate and final degree of conversion. The discovery of the polymeric state of the cellulose molecule and the possible reactions that could be done with it was the origin of polymer science, which Staudinger expanded to other chain molecules and for which he was awarded the Nobel Prize in Chemistry in 1953 [176].

4.1.1.1 Synthesis of cellulose derivatives

Nowadays, several different cellulose derivatives are produced not only in laboratory but also industrially. Some examples of these derivatives comprise cellulose esters (e.g. cellulose acetate, cellulose sulfate), cellulose ethers (e.g. carboxymethylcellulose, silyl cellulose, aminocelluloses) and inorganic esters. The global production of these types of derivatives is represented in Figure 31.

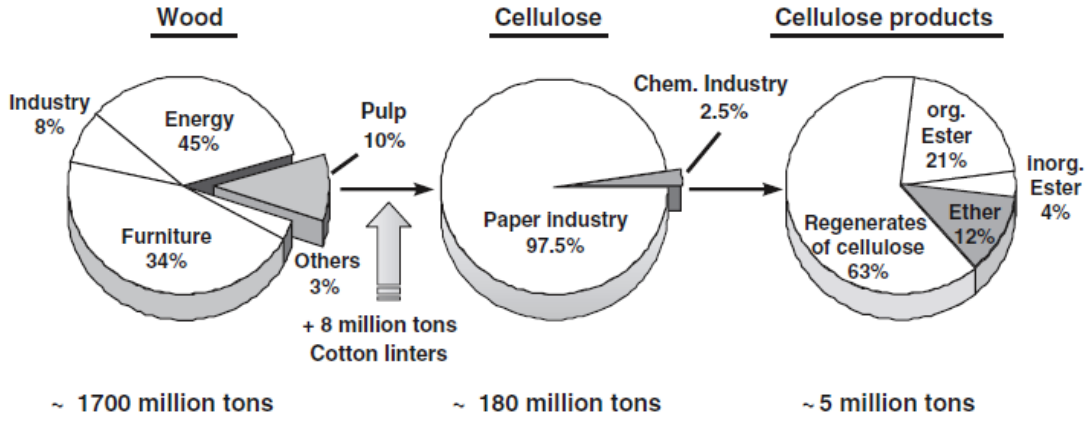

Figure 31 - Global use of wood for cellulose derivatives production in 2003 [179].

Approximately 2.5% of the cellulose pulp produced is used in the chemical industries with only 0.24% (4.8 million tons in 2003) being used for the synthesis of various esters and ethers of cellulose, producing cellulose fibers and films. The remaining majority of pulps produced (> 97%) are used in the manufacture of paper and paperboard [176,177].

Production of cellulose derivatives can be achieved both by heterogeneous and homogenous reactions. The insolubility of cellulose in water and in most organic solvents is the reason behind the fact that all commercially available products are currently produced through reactions of cellulose in the solid or in swollen state (heterogeneous reactions) [180]. Several questions emerge over substituent distribution in the product and over chain degradation during synthesis due to several variables: the repeating unit of cellulose has three hydroxyl groups available for reaction,

the stability of the chain forming acetal groups toward various reagents, the presence of oxygen, and mechanical and thermal load is limited.

In case of heterogeneous reactions, the accessibility and reactivity of the OH groups are clearly determined by hydrogen bond-breaking activation steps (through alkaline compounds such as NaOH) and by interaction with the reaction media (e.g. swelling) [180]. Thus, the direct transfer of the typical reactions of organic chemistry to cellulose is not easily done. Nevertheless, the control of cellulose activation and of the type of heterogeneous reaction permits effective synthesis of cellulose products with different degrees of substitution, reproducible substitution patterns and achieve desired properties at both the laboratory and production scales. Though, other important aspects of the synthesis procedures are understood only partially. Therefore, a lot of experience and the right "feeling" are still required in cellulose syntheses [176].

Cellulose has been used as raw material for different chemical reaction for about 150 years [176]. Cellulose as a precursor for chemical modifications was used even before its polymeric nature was known and well understood [175]. One of the milestones on this pathway was the discovery of cellulose nitrate (commonly misnamed 'nitrocellulose') by Schönbein in 1846. This was followed by the preparation of Schweizer's reagent (a cuprammonium hydroxide solution) as the first cellulose solvent, invented by Schweizer in 1857. Cellulose ethers were first reported in 1905 in a publication of W. Suida. This purely scientific work was followed in 1912 almost simultaneously – but independently – by the first patents for their production. Lilienfeld had already written down the reaction of cellulose with dimethyl sulfate to give water-soluble cellulose derivatives in 1912. It then took until 1927 before, based on the work by O. Ernst and K. Sponsel, the first industrial production of methylcellulose (MC) was taken up in Germany, where cellulose was reacted with gaseous methyl chloride in the presence of aqueous sodium hydroxide solution [6]. Technical production processes for cellulose ethers with, at first, only small alkyl groups (methylcellulose, ethylcellulose) were developed by IG. Farbenindustrie in 1919–1926 [177].

4.1.1.2 Cellulose ethers

Cellulose ethers produced nowadays are mainly used in the construction industry (90%). Only 10% of the produced cellulose ethers is used by the pharmaceutical industry, cosmetics and food industry[177]. One of the most produced cellulose ether is carboxymethylcellulose. Carboxymethylcellulose (CMC) was introduced in Germany shortly after World War I as a gelatin substitute. Though, the scale up to produce this derivative on an industrial scale was delayed due to high production costs and technical problems. The discovery, in 1935, that CMC improves the

quality of synthetic detergents and cleaning agents facilitated the large-scale production. Later, the economic importance of CMC increased strongly upon its use in oil drilling fluids (as borehole flushing additive) [181]. The oil soluble cellulose ether ethylcellulose (EC) has been produced industrially since 1930. Ever since, the production and application of cellulose ethers have developed strongly on a global scale. With the production of hydroxyethylcellulose (HEC) and hydroxypropylcellulose (HPC) (Figure 32) the range of types of water-soluble cellulose ethers was virtually brought to its present size [182].

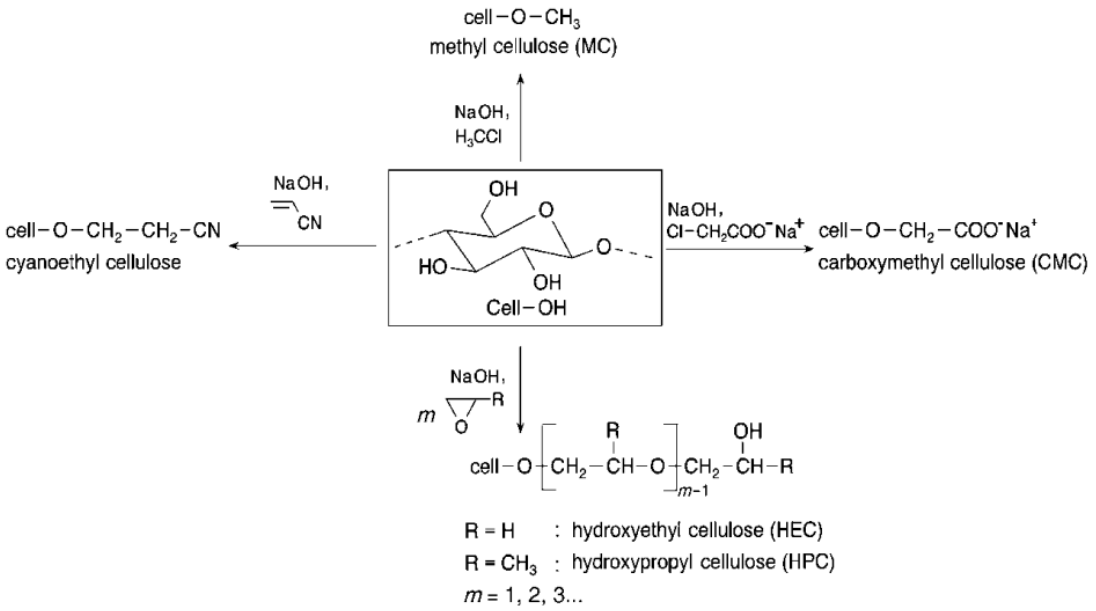

Figure 32 - Examples of commercial cellulose ethers (adapted) [176].

Cellulose ethers are known to present good solubility, have high chemical stability and are toxicologically innocuous. The especially relevant matter of water solubility (for example in polymers used in the food and pharmaceutical industry) can be controlled to a certain extent by the combination of ether groups, degree of substitution and the distribution of substituents. These ethers are used in a dissolved or highly swollen state and they are dominant polymers in numerous industrial applications where consistency in the quality of aqueous media and water-containing systems is required [183].

Etherification of cellulose on industrial scale is performed in aqueous alkaline or hydro-alcoholic alkaline media in which cellulose is present in a highly swollen state. Adding an alkaline solution to a non-ionic polymer such as cellulose can charge up the polymer and help with its solubility or swallowing. For cellulose this can be achieved either by association of an ionic charged specie (such as an ion or a surfactant) or via deprotonation or protonation of the hydroxyls groups [184].

The most common opinion about the action of alkaline solution in the dissolution of cellulose is that the deprotonated form hydrates with water capable to break the inter- and intramolecular hydrogen bonds between cellulose molecules [185] (Figure 33).

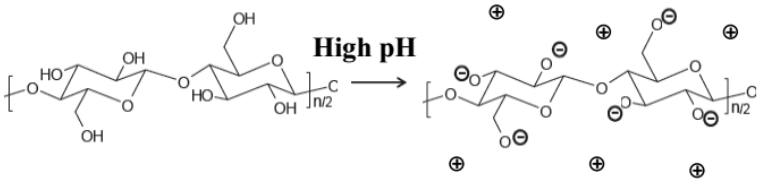

Figure 33 – Conversion of neutral cellulose into a polyelectrolyte by pH change: schematic representation of the ionization of the hydroxyls of cellulose in strong alkali medium (extremely high pH) [186].

Though, in normal industrial practices cellulose is activated with aqueous alkali hydroxide, mostly sodium hydroxide, but not at concentrations where it is soluble. Alkali treatment also results in the irreversible transformation of cellulose I (where the polymer chains have parallel conformation) into the less ordered cellulose II (antiparallel conformation) consequently causing a decrease in its crystallinity [187].

After activation of the cellulose, the most common approach for the etherification of cellulose is the O-alkylation with alkyl halides according to Williamson. Other approaches include epoxide addition and Michael addition of reagents with activated double bonds (Figure 32) [176,183].

4.1.1.3 Applications in Food Products

Native cellulose is used as raw material to produce partially depolymerized cellulose. The resulting products are microcrystalline cellulose (MCC) and powdered cellulose. Furthermore, highly purified cellulose in the form of pulps serves as basic material for producing functional cellulose ethers such as methylcellulose, cellulose gums (e.g. CMC), EC or HPC (Figure 32).

These partially or completely water-soluble cellulose derivatives are then incorporated as technological additives into various foods (e.g. wine, bread). Untreated native cellulose is used directly as additive in foods only very rarely – the ‘function’ is limited to the role of a filling substance (e.g. as support for yeasts in fermentation reactors). One field of indirect application is in the filtration of beverages, where cellulose acts as processing aid.

The application of CMC in wine is a widespread practice in the industry. CMC acts as a “protective colloid” due to its nature and is considered an alternative to the application of mannoproteins or metatartaric acid. Since this polymer can change the viscosity of the wine, it

will induce a stabilizing effect on the eventual precipitation of tartrate crystals with low temperatures [6]. Although it was described to promote solubilization and stabilization of proteins in solution [188], it is now known that application of CMC in protein unstable wines can induce their precipitation increasing the instability of that wine [121]. A negatively charged polymer such as CMC can behave quite differently to neutral polysaccharides with proteins and, consequently, with protein hazing. Conclusively, the negative-charged CMC might interact with positive-charged wine proteins or tannin/protein complexes. This impact was especially pronounced with intensively coloured red wines where besides soluble proteins, tannins, anthocyanins and derived pigments may represent the main targets for the polymer [121].

4.1.1.4 Cellulose derivatives as ion exchangers

The use of cellulose derivatives as ion exchangers is extensively described in the literature. Some of the most common cellulose derivatives used in chromatography to separate proteins are diethylaminoethyl cellulose (DEAE) (**7**), carboxymethyl cellulose (CMC) (**8**) and phosphate cellulose (PC)[189].

Some of commercially available cellulose based ion exchangers are represented in Figure 34. These are classified as weak ion exchange polymers (case of diethylaminoethyl cellulose (7) and carboxymethyl cellulose (8)) and strong ion exchange polymers (case of quaternary aminoethyl cellulose (9) and sulphopropyl cellulose (10)). What differentiates them is the pH range at which they can perform ion exchange. In strong ion exchange polymers, the working pH is 0 to 14 while in weak ion exchange polymers the pH working windows is around 5 to 9 [190]. This is strictly related to the polymer pKa and consequently the pH at which the polymer is electronically charged.

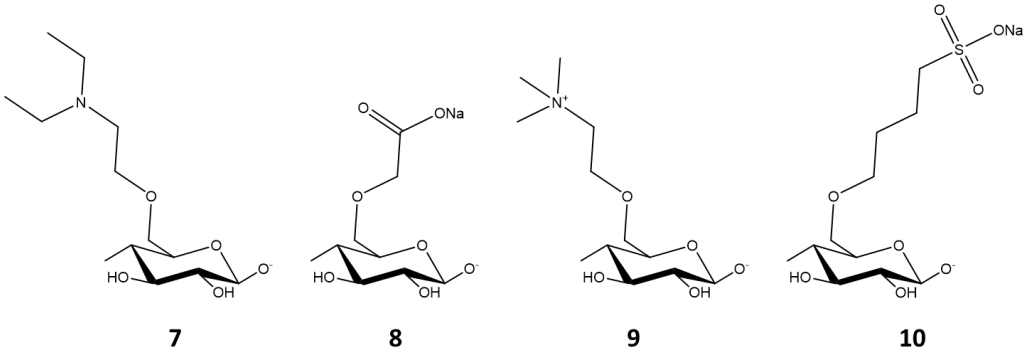

Figure 34 – Representation of diethylaminoethyl cellulose (7), carboxymethyl cellulose (8), quaternary aminoethyl cellulose (9) and sulphopropyl cellulose (10). In the figure cellulose is represented by an anhydroglucose unit.

Other cellulose ion exchangers also described in the literature but in less extent are oxycellulose [191] cellulose succinic half ester [189], cotton grafted co-polymers with acrylates, carbamoyethyl, carboxyethyl and poly(acrylamide) for dye removal [192,193] and niobium oxide coated cellulose fiber for the adsorption of phosphoric acid [194].

In terms of protein adsorption on modified cellulosic surfaces, some works have been published recently. The adsorption of anionic (carboxymethyl cellulose) and cationic (chitosan) polysaccharides on cellulose and subsequent adsorption of proteins having different charge densities was presented [195]. The authors demonstrate that unspecific protein adsorption on chitosan and on CMC is much higher than on neat cellulose, which is known for a rather low unspecific protein adsorption. As expected, the adsorption of protein (in this case BSA and IgG) on both chitosan and CMC modified cellulose is highly dependent on the system pH due not only to the protein charge but also to its isoelectric point. Following this work, [196] adapted this concept and showed that medical grade N,N,N-trimethyl chitosan can be immobilized on cellulose in a similar fashion and potentially used as matrices in order to produce patterned slides that are able to detect adsorption from 12 pM solutions of BSA on pads. With the same purpose, cellulose-4 [N,N,N-trimethylammonium]butyrate chlorides with different DS were adsorbed on cellulose thin films for BSA adsorption giving adsorption yields around 0.6 to 3.9 mg m $^{-2}$(dry mass) [197].

The use of ion exchange membranes for medium filtration is already described with some commercially available options. Some of this include the removal of nitrates from water with cationic cellulose membranes [198], ion exchange filter paper with crosslinked polystyrene with sulfonic acid groups (MN 616 LSB-50 from Macherey-Nagel) or polyethersulfone modified with sulfonic acid groups (Mustang S membranes from Pall).

4.1.1.5 Cellulose based ion exchangers in the wine industry

The OIV allows the use of cation exchange resins composed of sulfonated styrene-divinylbenzene copolymers or divinylbenzene-methacrylic acid copolymers for the tartaric stabilization of wines [199].

In the past, the most common way to use cation exchange resins in wines was the use of the cation resins in sodium form [6,200,201]. Nevertheless, their use has decreased greatly because the wine stayed much enriched in sodium content. If the cation resin is in hydrogen form, the exchange of cations of the wine by H^+ ions of the resin will originate a significant decrease in the wine pH. To avoid the considerable decrease in the wine pH after treatment, was suggested [202] treating only one fraction of the wine, or using a resin in the mixed forms. To avoid a large acidification or an excessive increase in sodium content, resins can also be used in the magnesium form.

Nowadays, the typical winery operation involves mixing a certain amount of wine treated by resins with the rest of the untreated wine. The amount of wine treated ranges usually from 10 to 20%, depending on the initial wine characteristics and must be evaluated in each case, to achieve the full potential of this technique [203]. Although the use of the cation and anion exchangers has been authorized in some countries as the United States and Australia, in Europe the use of the ion exchange resin is only accepted by the OIV for tartrate stabilization with cation exchangers in acid cycle [204].

The use of cellulose derivatives as an ion exchanger in wines is scarcely described in the literature. In fact, there is an insufficient amount of articles studying the impact of cation exchange in wines though its use can be beneficial to some wine characteristics from the chemical point of view [203]. The cellulose derivative most used in winemaking is CMC as started before. However, due to its pKa its capacity to perform ion exchange at the wine pH is very limited. Though there are some differences in the literature about the pKa of CMC, is was reported that at the wine pH only about 20% of the carboxymethyl groups carry negative charge in solution [205]. This can possibly explain the described reactivity of CMC with proteins, at the wine pH, which can induce their precipitation [121,206]. Since CMC will be partially deprotonated at the wine pH, this can perform cation exchange between its cation (normally sodium) and the wine proteins (that are mainly positively charged).

To produce an organic cellulose-based polymer (avoiding the use of inorganic substituents) with a pKa inferior to the wine normal pH (between 3.2 and 3.6), we searched for possible substituents based on organic acids with those characteristics. One organic acid that fitted in in this category was malonic acid. The modification of cellulose with malonic acid (reaction performed with sodium bromomalonate or sodium chloromalonate) was already described in the literature [207–209]. The final product, dicarboxymethyl cellulose (DCMC), showed to be water soluble and presented an average pKa of 2.1. Though the synthesis of this compound was already described, an in-depth structural characterization and data about its ability to perform cation exchange is scarce to none. Due to its inherent characteristics and similarity to other compounds already allowed to use in winemaking (i.e. CMC), we choose to study the synthesis, structural characterization and ability to remove wine proteins by cation exchange of DCMC.

4.1.2 Objective

The main objective of this work consisted in the production of cellulose polymers with a pKa lower than wine pH (3.2 – 3.5), capable of performing ion exchange in this acidic medium. These polymers will ultimately be used to remove positively charged unstable proteins from wine, stabilizing it. Different dicarboxymethylcellulose (DCMC) polymers were made from reactions with varying content of NaOH

4.1.3 Results and discussion

4.1.3.1 Synthesis of dicarboxymethyl cellulose

The synthesis of dicarboxymethylcellulose was already presented in the literature [209]. This reaction was later used [207], but with no detailed description. In both works, the cellulose was derivatized using 2-bromomalonic acid in isopropanol in a reactor at 130 °C. Though, the first reference for this reaction is described in a patent [208] where a reaction between cellulose and chloromalonic acid was performed in isopropanol at different temperatures in a reactor. Since we wanted to test a milder and less expensive condition, we opted to use a reaction based on the carboxymethylation of cellulose in a hydro-alcoholic media at lower temperatures.

In this work, the derivatization of the cellulose was carried out by a standard slurry method as previously described [210] for carboxymethylation of cellulose with some modifications. Since 2-bromomalonic acid is a very expensive reagent, malonic acid was brominated. This was achieved by the reaction of malonic acid with Br_2 in diethyl ether as described previously [211]. For the purification of 2-bromomalonic acid, a recrystallization using benzene was performed [212]. To avoid the use of benzene, this recrystallization was tested with other organic solvents including dichloromethane, chloroform and isopropanol although only with poor results. This method was previously published has a recrystallization although the method resulted more on a compound cleaning than a recrystallization per se. Since we synthesized 50 gr batches, it was necessary significant amounts of benzene for the purification of the product. NMR experiments revealed that after washing several times with benzene under agitation (normal protocol consisted of 5 x 100 mL benzene per 50 gr of product) we obtained a pure compound with a yield of around 80%. The 2-bromomalonic acid was then deprotonated with a 2 M NaOH solution yielding sodium 2-bromomalonate (BMA, **11**).

After synthesis and purification of sodium 2-bromomalonate, this will participate in a S_N2 reaction with the AGU of the cellulose under alkaline conditions to produce the cellulose derivative as represented in Figure 35. This is the most common approach for the etherification of cellulose

(e.g. for the production of CMC) where there is an *O*-alkylation with alkyl halides [175]. In our case, we used sodium 2-bromomalonate as the alkyl halide that will react with the free hydroxyls of the cellulose structure.

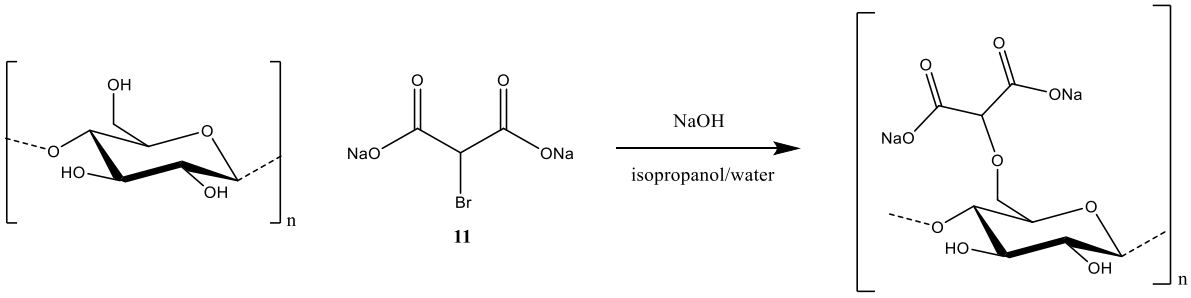

Figure 35 - Schematic representation of the reaction between the sodium bromomalonate (11) and the anhydroglucose unit of cellulose. In the figure, we can see a representation of a DS = 1 molecule substituted in the primary alcohol in C6.

In our experiments, cellulose (Macherey-Nigel Cellulose MN 400 Avicel with a mean DP of 40-200) was slurried in isopropanol, activated with NaOH and reacted with BMA at 60 °C. The summary of the conditions tested in this trial is represented in Table 9.

Table 9 - Summary of reaction conditions for DCMC1 to DCMC5.

sample identification	product mass	cellulose type	starting materials	ratio	NaOH in reaction (%)	H_2O in reaction (%)
DCMC1	2.39g	Avicel	cellulose: BMA: NaOH	1:2:0.54	5	8
DCMC2	3.03g	Avicel	cellulose: BMA: NaOH	1:2:1	10	8
DCMC3	3.67g	Avicel	cellulose: BMA: NaOH	1:2:1.6	15	8
DCMC4	4.84g	Avicel	cellulose: BMA: NaOH	1:2:2.2	20	8
DCMC5	5.41g	Avicel	cellulose: BMA: NaOH	1:2:3.2	30	8

During the reaction, some gelation occurred after increasing the temperature to 60 °C. Increasing gelation occurs with increasing quantity of NaOH. To aid the dispersion of the cellulose in

reaction, the gels were scraped from the glass with a metal rod. The gels disintegrate forming homogeneous suspensions about 2 hours after the beginning of the reaction. After five hours, the products were filtered and washed. Even with thorough washing steps of the final product with 70% methanol and pure methanol, the presence of residual starting material and/or reaction by-products could be possible. To analyse the final products, the crude had to be separated in soluble and insoluble fractions. To this, the samples were dissolved in MilliQ water, agitated for 2 hours and centrifuged to separate the supernatant from the precipitate. The soluble fractions were further analysed by NMR.

The contamination of the product was confirmed by NMR experiments of the soluble fractions of various products (Figure 36). In the ^{1}H NMR spectrum we can see the anomeric proton at 4.45 ppm and the protons from the anhydroglucose unit, between 4 and 3.1 ppm. There are also two signals at 4.15 and 4.28 ppm that would correspond to the substituent proton or to other contamination present in the reaction mixture.

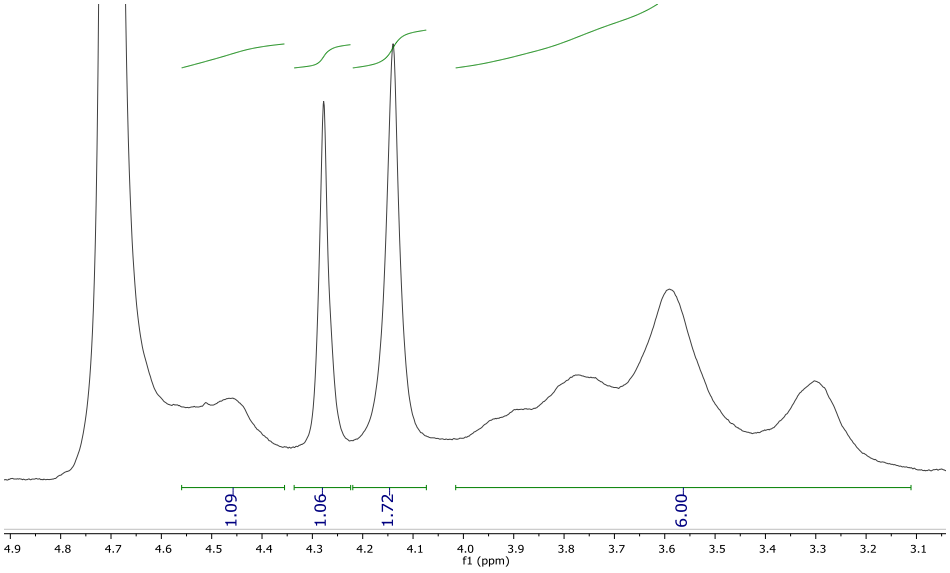

Figure 36 - ^{1}H NMR spectrum of sample DCMC3 in D_2O (water soluble fraction of the product).

By the analysis of the ^{13}C NMR spectra (Figure 37), we can see a spectrum like the one described by [207] with some differences. There are some intense signals in the carbonyls area and two very intense signals in the 83 and 75 ppm regions. This emphasized that the sample could be impure and residual starting material or reaction by-product could be present in the water-soluble fraction.

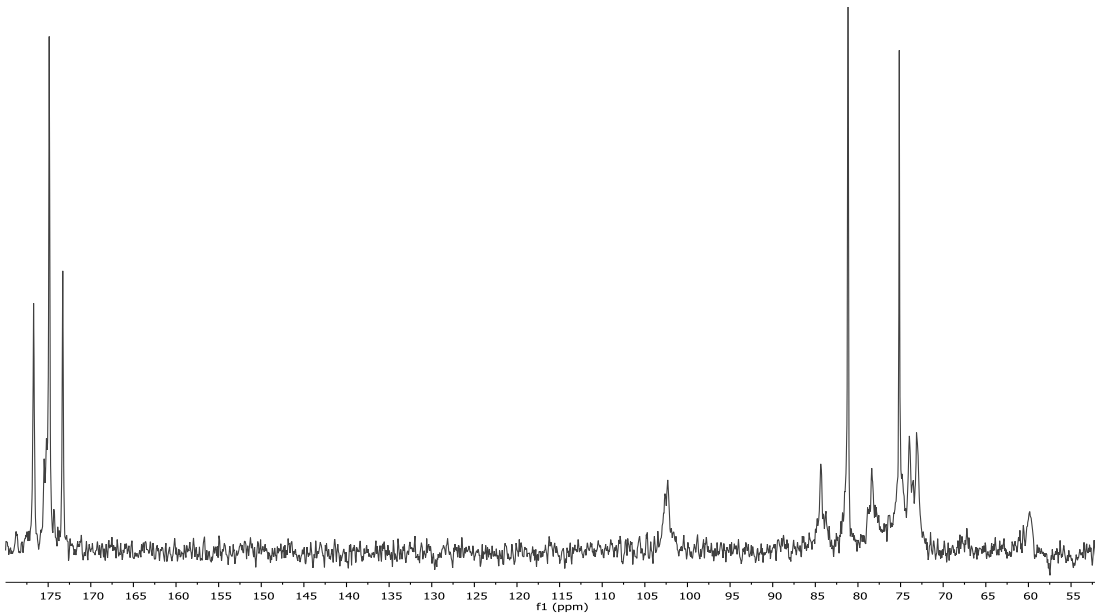

Figure 37 - ^{13}C NMR spectrum of sample DCMC3 in D_2O (water soluble fraction of the product).

Although the carbon spectrum presents an intense signal at 83 ppm similar the one presented by [207] for a higher DS cellulose derivative, the intense signal at 75 ppm mixed with the intense carbonyl signals lead us to confirm that the sample was impure. Though the contaminants were not isolated and identified, based on the possible reaction by-products, some of the possible contaminants are represented in Figure 38.

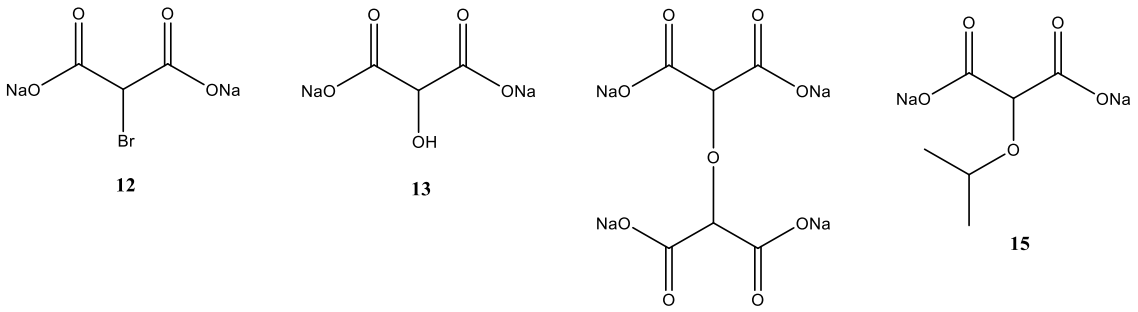

Figure 38 – Reaction by-products and starting materials possibly present in the crude of the cellulose derivatization.

Compound 12, the starting material, would present a carbon at around 44.6 ppm (excluding the carbonyls) and a proton signal at around 4.8 ppm (in D_2O) [213]. Compound 13, the possible degradation product known as tartronic acid (or hydroxymalonic acid), presents a tertiary carbon at 71 ppm and a proton signal at 4.9 ppm [214]. Compound 14, the ether resulting from the attack of the hydroxymalonic acid to the sodium bromomalonate also known as sodium 2,2'-oxydimalonate, would present a tertiary carbon signal at around 100 ppm, like the anomeric signal

of the cellulose, and a proton signal around 5 ppm (simulated). Finally, compound 15, the product of the attack of isopropanol to a molecule of sodium bromomalonate, would present not only the signals from the tertiary carbon of the malonic acid but also the very characteristic signals of the two methyl groups in the ^{1}H spectra at around 1.2 ppm and near 20 ppm in the ^{13}C spectra (simulated). Analysing our spectra and comparing with the ones already published [207], we can see that the contamination is particularly related to the signals at 4.28 ppm (^{1}H) and at 75 ppm (^{13}C). Due to that, we can infer that the possible contaminant is sodium hydroxymalonate resulting from the attack of the water present in the reaction media. The possible signal differences between our spectra and the literature [214] can be related to the deprotonation of our hydroxymalonic acid. Since the reaction is performed under basic conditions, it is to expect that the final product will be the sodium salt of the hydroxymalonic acid, which can result in the shift of the proton and carbon signals. Nevertheless, the peak at 83 ppm appears with an excessive intensity which can indicate that there can be another contamination not identifiable.

To further characterize these products, the samples (i.e. crude samples without separation between soluble and insoluble fractions) were further purified by dialysis in 6-8 KDa cellulosic membranes for 48 hours. After dialysis, the samples were separated between soluble and insoluble fractions by centrifugation and the soluble fraction was freeze dried.

4.1.3.2 Structure elucidation of DCMC

After dialysis and freeze drying, the percentage of water soluble materials was calculated, and elemental analysis was performed (Table 10).

Table 10 – Water soluble percentages and elemental analysis results for samples DCMC1 to DCMC5.

			Elemental analysis				
Sample identification	**Type of sample**	**% soluble (after dialysis)**	**C**	**H**	**N**	**S**	**Br**
DCMC1	Dial - Soluble	1.8	low mass available				
DCMC2	Dial - Soluble	37.3	35	4.73	0	0	0
DCMC3	Dial - Soluble	59.4	34.38	4.52	0	0	0
DCMC4	Dial - Soluble	67.9	34.51	4.59	0	0	0
DCMC5	Dial - Soluble	61	34.78	4.88	0	0	0

Except for sample DCMC5, we can see that the percentage of soluble material increase with increasing NaOH content. This can be related to the higher substitution of the AGU in the presence of higher NaOH concentration. With higher substitution patterns, it will have more carboxylic acid groups bond to the AGU which will consequently increase the water solubility of the polymer. Increasing degree of substitution in the presence of increasing quantities of NaOH was previously reported in the synthesis of carboxymethyl cellulose [210]. The lower percentage of soluble material in sample DCMC5, compared to DCMC4, can be related with technical problems during the purification of the sample (i.e. the dialysis membranes ruptured which implied a second purification step causing a possible loss in final product mass).

Based on the elemental analysis results, we can see that there is no bromine remaining in the dialyzed sample, indicating that we do not have starting material in the product. Also, the ration between carbon and hydrogen is within the expected quantity to a DCMC polymer with a DS between 0.5 and 1.

To elucidate the structure of the DCMC, the soluble purified samples were dissolved in D_2O for NMR experiments. We excluded sample DCMC1 from all NMR experiments since the final mass was too low to acquire good spectra. The ^1H spectra of the different samples are represented in Figure 39.

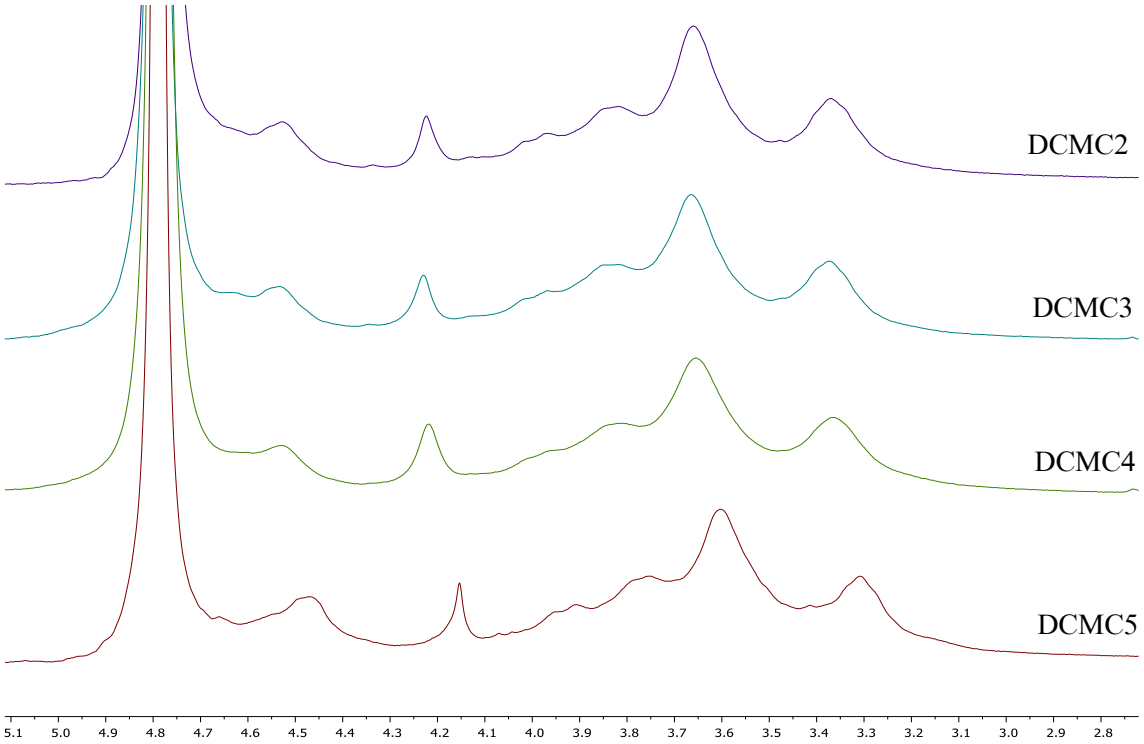

Figure 39 - Stacked ^{1}H NMR spectra of sample DCMC2 to DCMC5 in D_2O (water soluble fraction of the product).

Considering that the window between 4.05 and 3.1 ppm corresponds to 6 protons (anhydroglucose unit except the anomeric proton), we could integer the substituent proton (Hsub, between 4.18 (DCMC5) and 4.25 ppm (DCMC2 to 4)) and anomeric proton (between 4.45 and 4.53 ppm). The results from the integration are represented in Table 11.

Table 11 - Integrals of the different protons in samples DCMC2 to DCMC5. As reference, the area between 4.05 and 3.1 was adjusted to 6 protons.

Sample	H1 (anomeric)	H (sub)	H (2,3,4,5,6,6')
DCMC2	0.95	0.5	6
DCMC3	0.81	0.56	6
DCMC4	1.06	0.64	6
DCMC5	1.09	0.56	6

An approximation of the sample DS can be calculated based on the H(sub) integral, although the analysis of these results must be cautious since we do not have well resolved peaks nor a good baseline for a rigorous quantitative analysis. Since we are working with a polymer, the NMR signals will appear broad or poorly resolved due to the relaxation of these high molecular weight molecules. Nevertheless, we can see an increase in the DS from sample DCMC2 to DCMC4 and

a slight lower DS in sample DCMC5 when compared to sample 4. While showing some differences, the DS's of the different samples are very similar and its variances can be within the experimental error.

The ^{13}C NMR spectra of the same samples is represented in Figure 40. Although not quantitative, we can see a signal increment of the carbonyls comparing the samples 2, 3 and 4. The pattern and intensity of the carbonyls in sample 5 is significantly different. We can easily identify the anomeric carbon (C1) in all spectra at 102 ppm, as well as C6 at 60 ppm. Similarly to [207], we can see the appearance of a signal at around 67 ppm that is related to the substitution in position C6 with increasing quantities of NaOH. A signal increment is noticeable from sample 2 to 4, though sample 5 do not present any signal in this region. Due to the use of a higher concentration of NaOH in reaction DCMC5, this can occur in a different way increasing the substitution pattern in a free hydroxyl other than the one in C6.

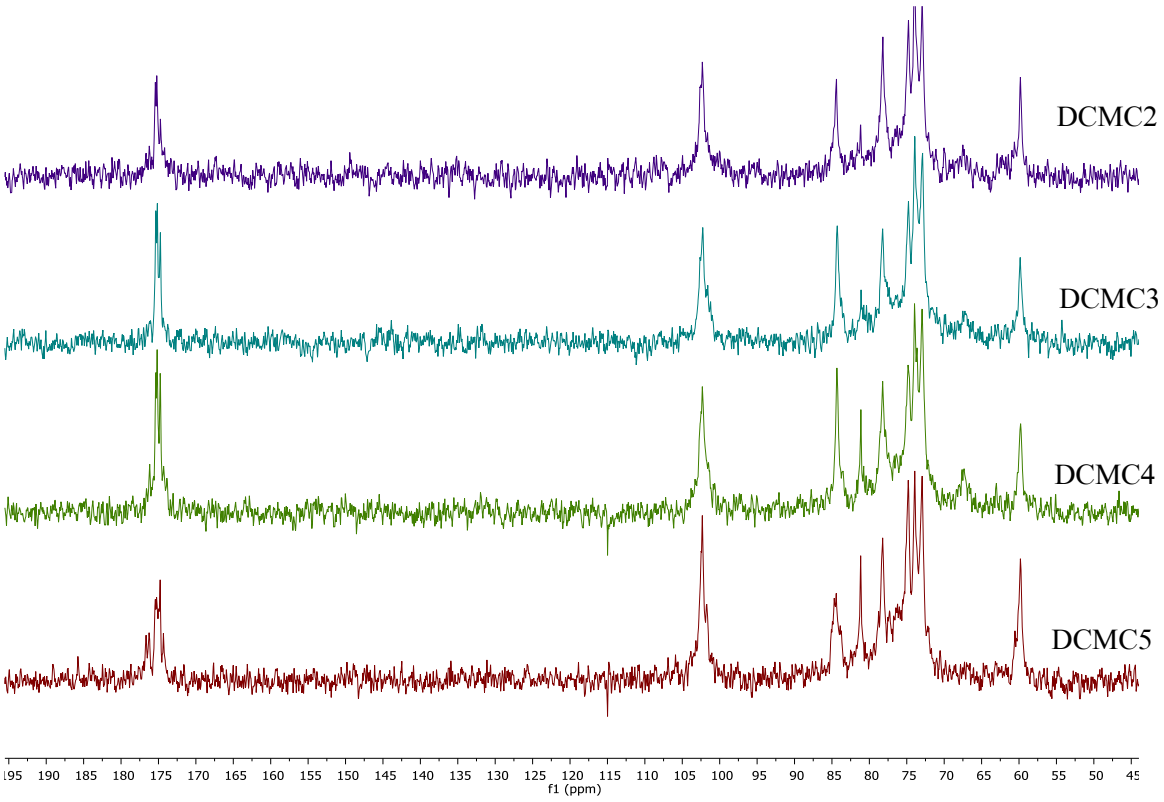

Figure 40 - Stacked ^{13}C NMR spectra of sample DCMC2 to DCMC5 in D_2O (water soluble fraction of the products).

An increase in the signal intensity of at 82 ppm is also noticeable comparing samples DCMC2 to DCMC4. In sample DCMC5 we can see a partial increase in the signal at 82 ppm but also a different pattern of the signal at 84.3 ppm when comparing with the remaining samples. This can be again related to a different substitution pattern of sample DCMC5.

To assign the remaining signals of the product, 2D NMR experiments were performed. The sample DCMC4 was chosen to assign the signals of the product since it appeared to have the highest DS. Although sample DCMC5 could have a higher DS, it had an atypical NMR pattern and we opted to use only sample 4 to the signal assignment.

In the COSY spectra, we can see correlation between the anomeric proton H1 and H2 and between H2 and H3 (Figure 41). The proton signals of H6 were identified as the signals at 3.72 and 3.9 ppm. The signals from H5 and H4 are probalby overlaping the signal of H3 at 3.55 ppm. Similar data has reported to cellulose in NaOD/D_2O [215]. As expected, it was not possible to identify any correlation between the proton from the substituent (4.15 ppm) and a proton from the AGU.

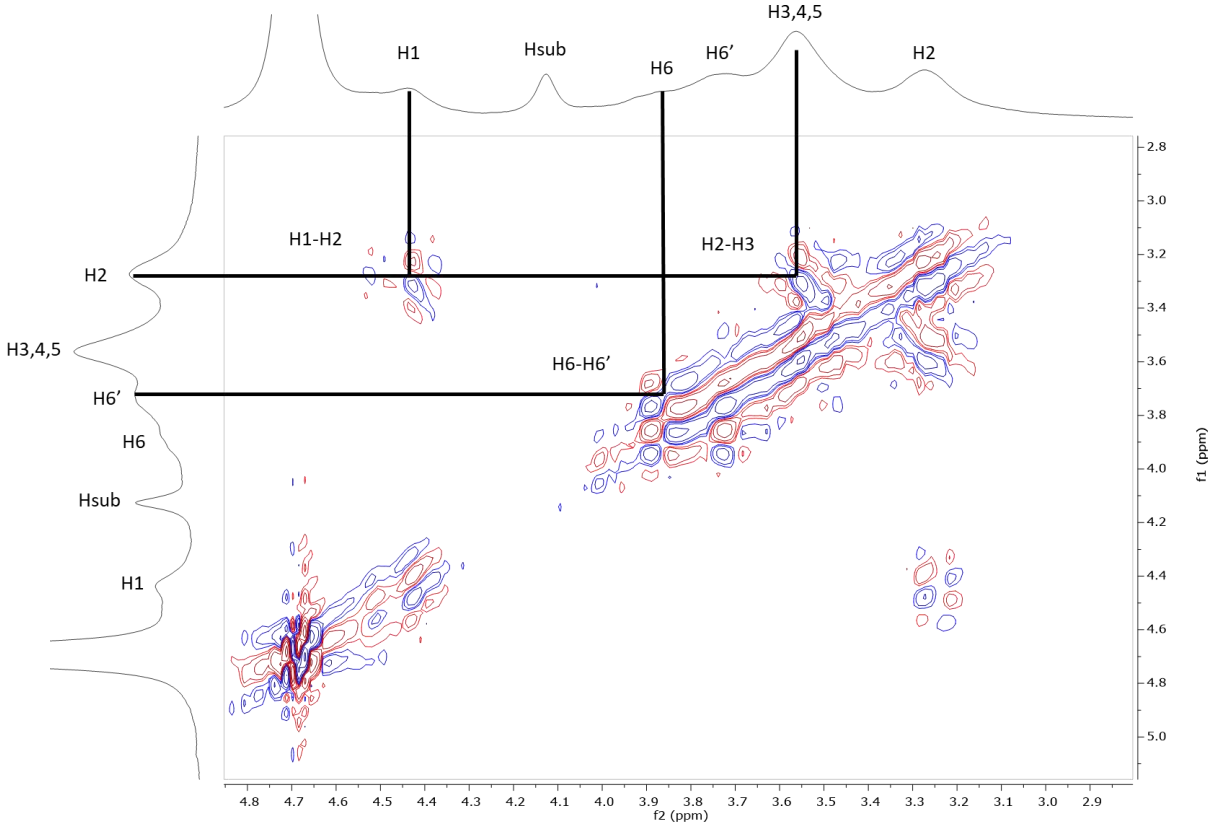

Figure 41 - COSY spectra of sample DCMC4 in D_2O.

The HSQC spectra (Figure 42) allowed to assign the remaining signals of the product. The signals corresponding to C4 and C5 were inferred by data from the literature when compared with carboxymethylcellulose HSQC spectra [216]. We cannot see any correlation between the protons H6 and C6', though in DEPT experiment (data not shown), C6' appears as a methylene group with a negative peak (as well as C6). The shift in the signal can be related to partial substitution of the AGU in position 6. We can also see two carbons correlating with the proton from the substituent.

Once more, this shift in the signal may be attributed to the derivatization of a different position of the AGU.

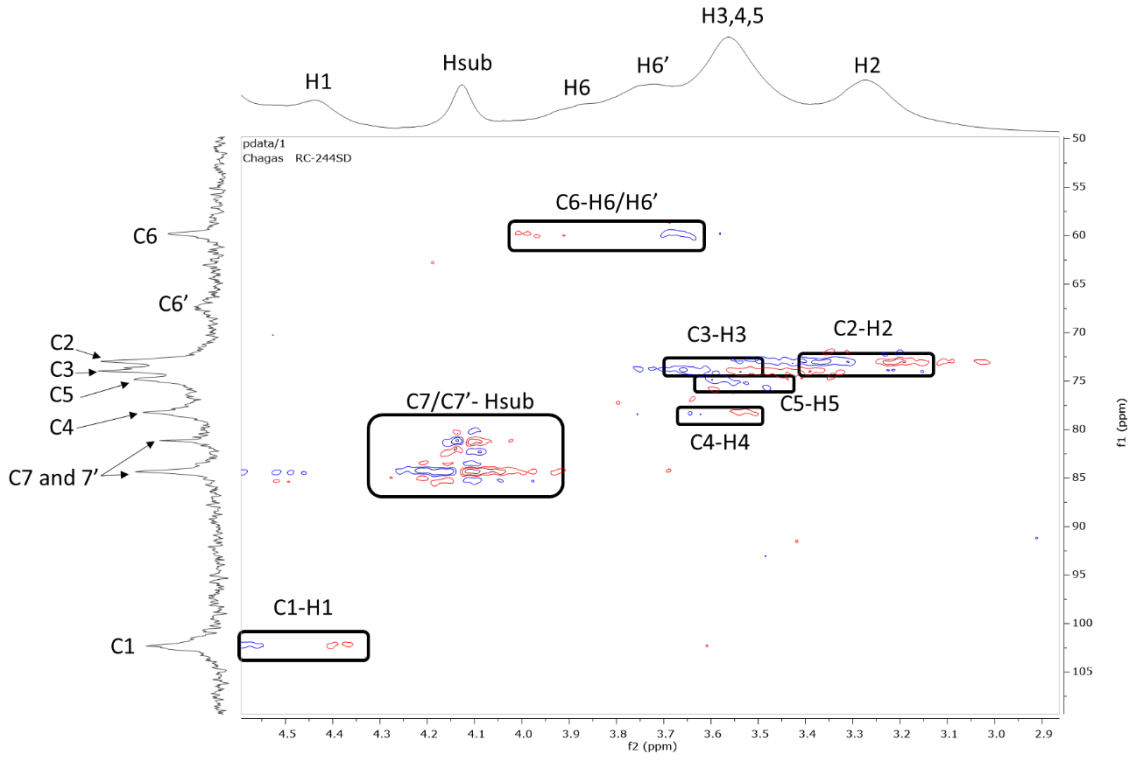

Figure 42 - HSQC spectra of sample DCMC4 in D_2O. Horizontal axis corresponds to the ^{1}H spectra, vertical axis corresponds to ^{13}C.

After performing INVERSE-GATED ^{13}C (data not shown), we registered a decrease in the signal intensity of the methylene group at C6 with increasing quantity of NaOH in the reaction. We registered no significant difference in the integrals of the normal ^{13}C NMR experiments and the INVERSE-GATED ^{13}C possibly due to the poorly resolved/noisy baseline of the latter. This signal loss was also described [207] for DCMC in particular when the DS is higher than 1 and for CMC where a decrease in the signal of C6 is noticeable in more substituted samples[216]. This is certainly related to the substitution of the AGU in C6 since this difference is followed by the appearance of the C6' signal at 67 ppm (Figure 42).

As a summary, the assignment of all signals is represented in Figure 43.

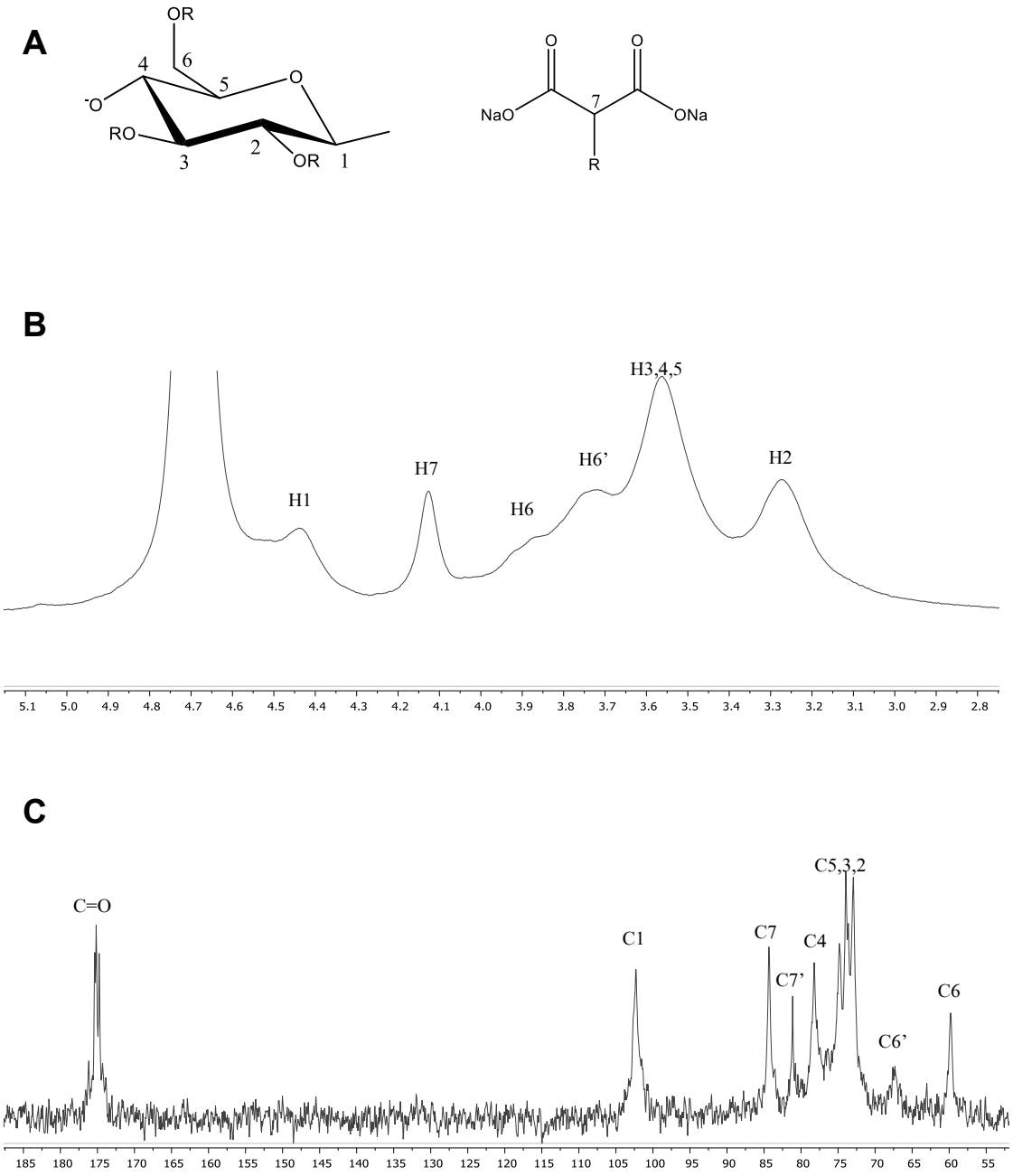

Figure 43 – Summary of the signals assignment of dicarboxymethylcellulose. A) schematic representation of the anhydroglucose unit and the substituent B) ^{1}H NMR spectra of DCMC4 C) ^{13}C NMR spectra of DCMC4.

To try to identify the positions where the substituent is linked to the AGU, HMBC analysis was performed (Figure 44).

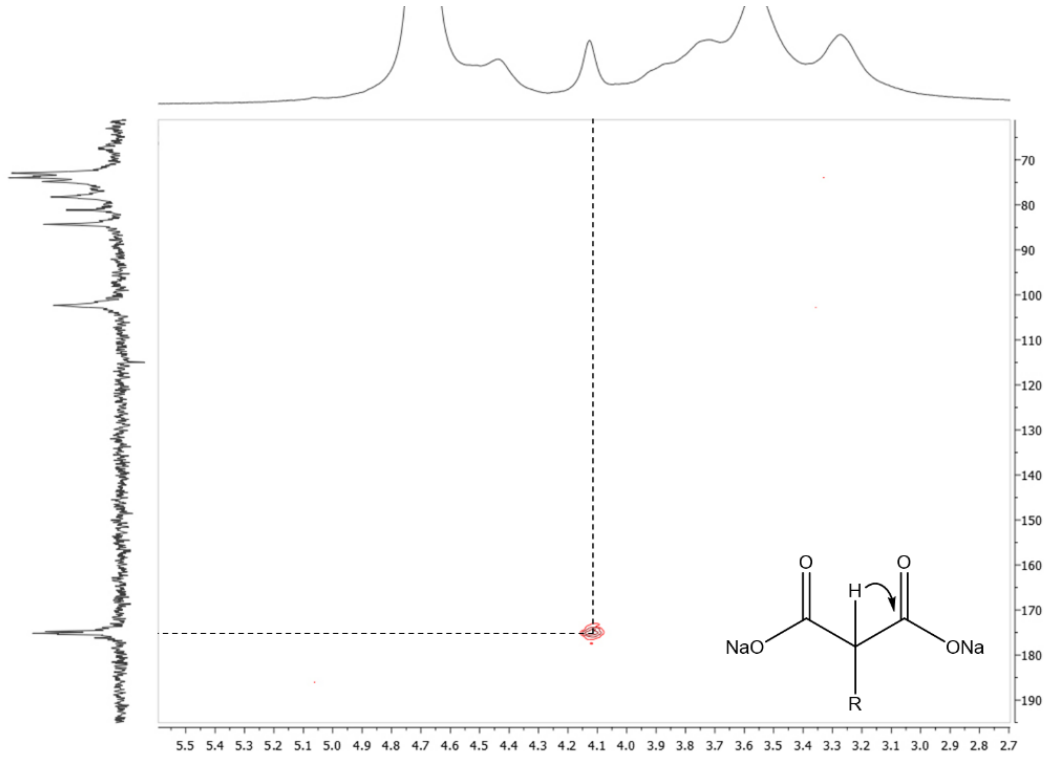

Figure 44 - HMBC spectra of sample DCMC4 in D_2O.

We can see the correlation between the carbonyl and the proton of the substituent in ^2J, confirming the position of the proton of the substituent. Reported data [207] described the signal at 84 ppm was C3' (AGU substituted in C3) though we do not have any data sustaining this result. Both signals at 81 and 84 ppm correspond to the substituent in two distinct positions. Based on the data presented above (Figure 43), C6 is one of the substituted position but, by the experiments performed, we do not have information about other substituted position.

The distribution of functional groups within the AGU was already evaluated for CMC revealing that the normal pattern of substitution is in the order C-2 ≥ C-6 > C-3 both for synthesis in totally heterogenous reaction (slurry process) and for homogeneous reaction in unconventional media [217–219]. For DCMC, there is no data available in the literature about its substitution pattern. Nevertheless, it is to expect a high substitution in C6, being a primary alcohol, and a partial substitution in position C2 or C3.

4.1.3.3 Acetylation of DCMC

To better understand the substitution pattern of DCMC, we acetylated a sample of DCMC4 to allow its solubilization in an organic solvent and a better resolution in the NMR experiments. Some methods were already described in the literature for the acetylation of CMC in acidic medium. Previous trials using basic conditions (i.e. pyridine) led to a non-derivatized DCMC sample. The methods already described in the literature are shown in Table 12. The method for the acetylation of DCMC was adapted from [220].

Table 12 - Literature where acetylation of CMC was performed and corresponding protocol.

Reference	Starting material	Protonation	Reaction conditions
[220]	CMC (DS 0.82)	2 h in 20% H_2SO_4	Acetic acid, acetic anhydride, sulphuric acid (3h at 50 °C)
[221]	CMC (DS 0.3 to 0.65)	10 to 120 min in 2-20% H_2SO_4	Acetic acid, acetic anhydride, sulphuric acid (4h at 50 °C)
[222]	CMC (DS 0.3)	30 min in 10% H_2SO_4	Acetic acid, acetic anhydride, sulphuric acid (30 min at 72 °C)
[223]	CMC (DS 0.63)	2 h in 20% H_2SO_4	Acetic acid, acetic anhydride, sulphuric acid (4h at 50 °C)

After workup, the sample was dissolved in DMSO to new NMR experiments. The ^1H spectrum of DCMC4Ac in DMSO is represented in Figure 45.

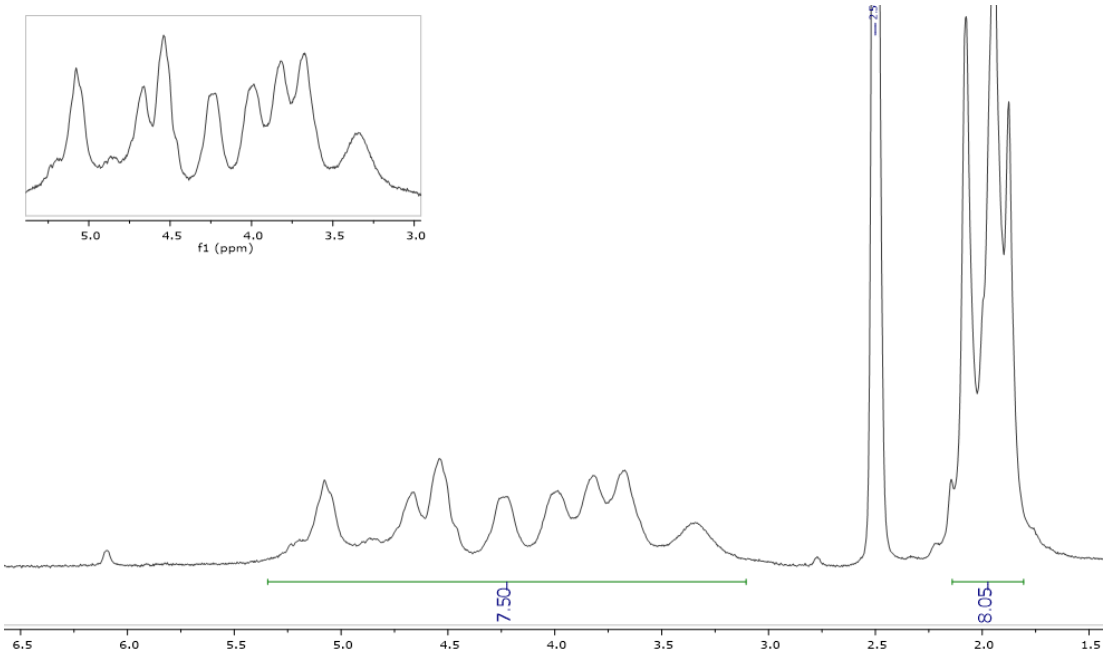

Figure 45 - ^{1}H NMR spectra of acetylated DCMC4 in DMSO.

We can see the backbone of DCMC as well as the acetyl groups resulting from the acetylation reaction. By the integral of the acetyl groups, we have at least two acetyl groups per anhydroglucose unit. Considering a DCMC DS of 0.5 for the product, is was to expect near 7.5 protons in the acetyl area. Though we have 8 protons in the -C*H*$_3$ area, it can be related to an integration error or to some acetic acid remaining in the matrix.

The ^{13}C NMR spectra of acetylated DCMC4 is represented in Figure 46. We can see a very similar carbon spectrum when compared to the non-acetylated sample although with lower resolution. This can be attributed to the fact that the non-acetylated sample spectrum was acquired with 70 mg of sample and the acetylated sample with just 20 mg. It is possible to see the appearance of a new carbonyl signal and other signal at 21 ppm corresponding to the -*C*H$_3$ of the acetyl groups. 2D NMR experiments of the acetylated sample were also performed but it was not possible to acquire additional information about the substituent positions.

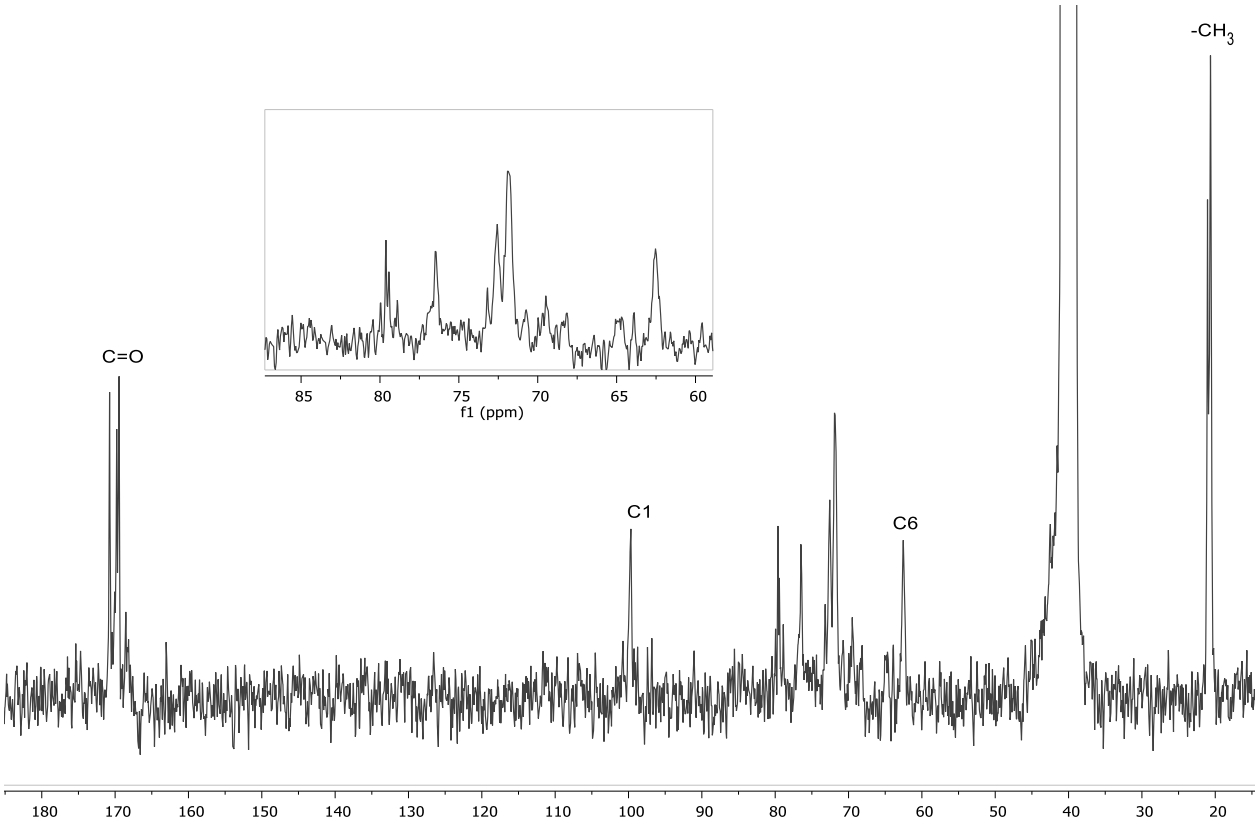

Figure 46 - ^{13}C NMR spectra of acetylated DCMC4 in DMSO.

The substitution pattern was also evaluated by ^{1}H NMR spectroscopy of the depolymerized samples heating in the presence of D_2SO_4 (acid hydrolysis). This technique is largely described in the literature and is a useful tool for the characterization of the partial DS at positions 2, 3 and 6 in carboxymethylcellulose [217,224,225]. Due to the cleavage of the glycosidic linkage, the α and β anomers of the glucose (of the different modified glucose units) are generated. In Figure 47 is represented the ^{1}H NMR spectra of the hydrolysed DCMC3 sample. We can see the characteristic signals of both anomeric protons (in α and β) and corresponding signal for substituted and unsubstituted O-2 position (O-2s and O-2u respectively). The triplet at 3.32 corresponds to the methylene group of O-6 and, together with the signals from O-2 and O-3, the partial DS of these positions in CMC can be calculated. The protons from the dicarboxymethyl group (in the different positions) are observed in the region between 3.4 and 4 ppm though no assignment was possible due to the complexity of the NMR spectra.

We were not able to calculate the partial DS of these positions in our polymer since, excluding the signal of O-2, we could not identify the signals of substituted and unsubstituted signals of O-6 and O-3. Although effective for the characterization of CMC, this method is not appropriate for the study of DCMC.

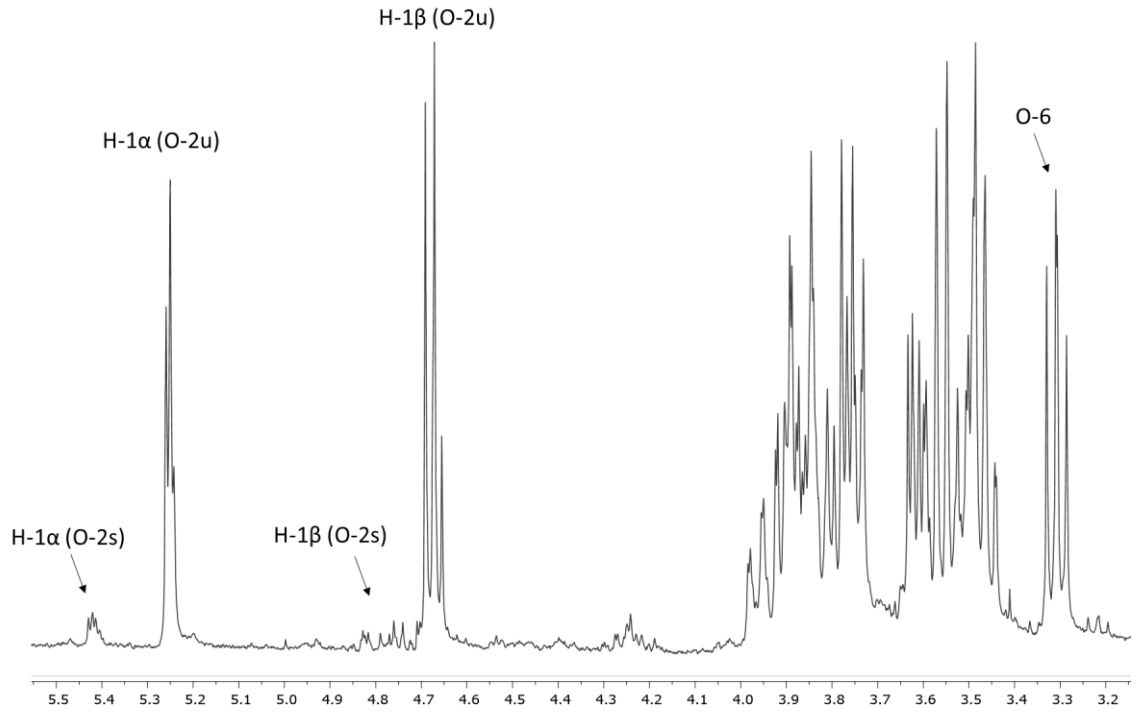

Figure 47 - ^{1}H NMR spectra of malonyl cellulose sample DCMC4 after hydrolytic chain degradation by D_2SO_4 during 5 hours at 90 °C. O represents the oxygen atom at position i (i=2,3 and 6), H-1 the proton at the anomeric carbon atom, α and β the configuration of glucose, s is used for substituted and u for unsubstituted positions.

Even with a significant amount of data regarding the structure of DCMC, we were not able to identify the partial DS at positions 2, 3 and 6 of our polymer. Another tested strategies passed through the derivatization of the polymer with formic acid (production of DCMC formate [226]) or the methylation of the polymer with dimethyl sulfate [227], though the assignment was also unsuccessful. Nevertheless, an average DS was possible to calculate based on the integration of the substituent in the ^{1}H NMR spectra of the water-soluble polymer (Table 11).

4.1.3.4 Infrared analysis of DCMC

The infrared spectra of all derivatized celluloses (in NaBr pellets) show the typical absorptions of cellulose as well as the appearance of new bands at 1625 cm $^{-1}$ (-COO^{-} asymmetric stretching), 1435 cm $^{-1}$ (-COO^{-} symmetric stretching) and 1340 cm $^{-1}$ (C-H bending) (Figure 48A and B). These bands correspond to the vibration of the carboxylate groups of the molecule confirming the presence of the substituent carboxylate group. All samples present a strong band in the region of 3400 cm^{-1} corresponding to the O-H stretching of the hydroxyls from the glucose repeating unit (Figure 48A). Since the DS of the samples is between 0.3 and 0.5 it was to expect a large quantity of free hydroxyl groups in the polymer.

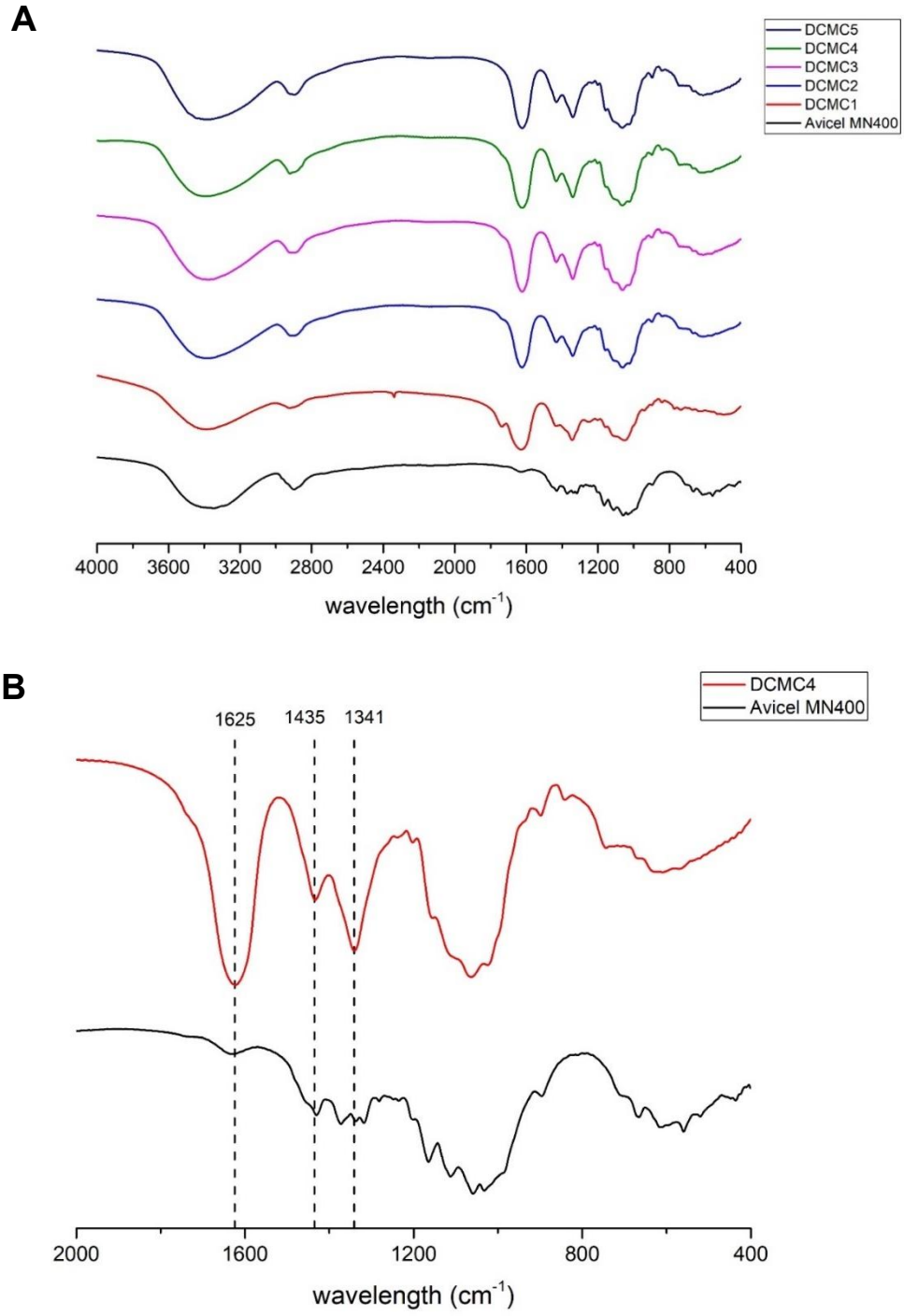

Figure 48 - A) Infrared spectra of the different synthesized samples B) expansion of the 2000 – 400 nm region in samples DCMC4 and underivatized cellulose (Avicel MN 400).

4.1.3.5 X-ray analysis of DCMC and Avicel

The X-ray patterns of Avicel cellulose and DCMC4 are shown in Figure 49 – Avicel and DCMC diffractograms. The diffraction peaks from Avicel cellulose at 2Θ angles of 14.86°, 16.68°, 22.66° and 34.53° for (101), (10ī), (002) and (040) planes are characteristic for cellulose I [228]. The

DCMC gave a diffractogram that clearly indicates an amorphous structure. This character is demonstrated by the absence of all peaks corresponding to planes (101), (10ī) and (002) of cellulose I. In fact, the DCMC diffractogram shows a major peak at 2Θ angles of 20.22° which is very similar to the diffractogram of regenerated amorphous cellulose [229].

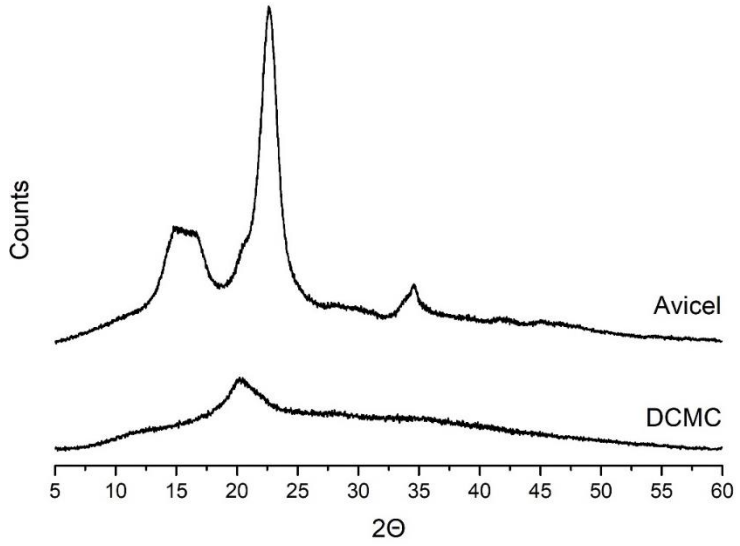

Figure 49 – Avicel and DCMC diffractograms

The crystallinity index (Ci) of both Avicel and DCMC was calculated based on following equation described by [230]:

$$Ci = \frac{(I002 - Iam)}{\mathrm{I002}}\ X\ 100$$

In this equation, where *Ci* expresses the relative degree of crystallinity, I_{002} is the maximum intensity (in arbitrary units) of the 002 lattice diffraction and *I*am is the intensity of diffraction in the same units at 2Θ angle of 18°. The calculated crystallinity index of Avicel cellulose was of 80.1%, which is a high value compared to the DCMC that presented no crystallinity. Although possible to use, this method was described to be very limitative (considers only the highest peak (002) in the formula) and to gives just a rough approximation of the contribution of amorphous cellulose [229]. Nevertheless, we could see that the resulting DCMC is amorphous.

4.1.3.6 DCMC degree of substitution (DS)

As presented before, the DS is defined as the number of substituent groups per anhydroglucose unit. The highest theoretical value of DS for cellulose is 3 (since there are only 3 hydroxyl groups to react). For commercially available CMC, the normal DS is within a range between 0.6 and 1 [231].

Several methods for the determination of CMC DS have been reported. Some of these methods include the quantitatively precipitation by multivalent metal ions [232], conductometric titration [207], colorimetry [233], HPLC [234] and NMR [235,236]. The American Society for Testing Materials (ASTM) also provides two different protocols for the DS calculation one based on a non-aqueous acid-base titration and other on the protonation of CMC followed by its dissolution in excess base and back-titration of the excess base [237]. We decided to quantify the sodium content of the polymer (which is directly related with its DS if the polymer is pure and in the sodium salt form) by ICP-AES. This technique was already described for carboxymethylstarch with good results [220].

Since our effort to determine DCMC DS by NMR resulted in inaccurate results, we opted to determine the DS by ICP after deprotonation and dialysis of the different polymers. This allowed to have the polymer in sodium salt form and to remove residual sodium from the base used to deprotonate the sample and/or sodium from the synthesis reaction. After determination of the sodium content by ICP-AES ($\%Na_{ICP}$), the DS was calculated based on the equation presented by [220] for carboxymethylstarch with some modifications. The DS was calculated from the following equation:

$$DS = \frac{162 \times (\%\frac{Na}{2}/23)}{100 - \left(147 \times \%\frac{Na}{2}/23\right)}$$

Where:

162 (g/mol) = molecular mass of an anhydroglucose unit of cellulose

147 (g/mol) = net increase in molecular mass of an anhydroglucose unit for each sodium malonate group added.

The Na quantification results by ICP-AES are represented in Table 13.

Table 13 – Sodium quantification by ICP-AES of deprotonated samples DCMC 2 to 5 (sodium salt form). The samples were hydrolyzed in nitric acid prior to ICP-AES analysis to protonate the samples.

Sample identification	% Na	DS (ICP_{calc})
DCMC2	6.67	0.32
DCMC3	8.97	0.44
DCMC4	9.27	0.46
DCMC5	9.9	0.51

We can see an increase in the DS with increasing NaOH quantity in the reactions. The calculated DS of the polymers show a maximum at 0.51 among the studied reactions. Compared to the less accurate NMR results (Table 11), we can see a more pronounced difference between samples. As stated before, being cellulose a polymer it will difficult the analysis of the NMR since we will have broader signals which can increase the noise of the spectra. With ICP we will not have that problem since we are only quantifying the total sodium present in the sample. Nevertheless, we registered a similar DS to the one calculated by NMR inside the experimental error, except for DCMC2 and DCMC4 that showed greater differences.

To calculate the DS by other technique and study the distribution pattern of the substituent in the AGU, the samples were analysed by anion exchange chromatography. The results of the different samples are represented in

Figure 50. Since we do not have standards for this compound (i.e. standards for the 2,3,6-tri-*O*-dicarboxymethylglucose, 2,3-,2,6-,3,6-di-*O*-dicarboxymethylglucose and 2-, 3- and 6-mono-*O*-dicarboxymethylglucose) we can only inference from the chromatogram the possible substitution pattern of the various products based on the published data for CMC using the same technique. The peak at 20.1 min was confirmed to be glucose by co-injection with the standard.

Comparing to already published chromatograms of CMC [238], we can see a similar chromatogram pattern of substitution but with significant differences in the retention times. The peak with a retention time of 18 min can correspond to the mono-substituted DCMC although it presents a retention time like the di-substituted CMC. Since DCMC has two carboxylic acid groups per substituent unit, it is possible that a mono-substitutes unit of DCMC presents a similar retention time as a di-substituted CMC. The peak at 16.7 min can be assigned to the di-substituted DCMC, which a similar retention time as the tri-substituted CMC (which presents a retention time of circa 17 min using the same system). The retention of the di-substituted polymer will be partially lower due to the number of carboxylic groups present in the DCMC polymer (4 in the di-substituted)

compared the ones in CMC (3 in the tri-substituted). Although it is possible to infer these peaks, posterior confirmation is needed (e.g. ion-exchange chromatography followed by MS). The integrals of the different peaks and DS calculated based on the peak areas are described in Table 14.

The third peak at 14.9 min could be assigned to the tri-substituted DCMC although there is no possible comparison with the CMC chromatograms due to the number of free carboxylic acids in the polymer. Although it is not impossible for this to happen, with a DS of around 0.5 (the average DS of our samples) it will be unlikely to have tri-substituted AGU. This peak shows a random difference between the four samples, with highest quantity in sample 3. Most probably, this peak corresponds to oligomers or high molecular weight fragments of the modified cellulose that were not completely hydrolysed during the first step of the method. Due to that, the calculated DS based on these chromatograms will not have into account the integral of the peak with a retention time of 14.9 min. Once more, we must emphasize that these results are merely indicative of a possible substitution pattern though, there is a high probability that the peaks at 18 and 16.7 min correspond to the mono and di-substituted AGU unit. More experiments to find the substitution pattern of these DCMC polymers is also being performed using capillary electrophoresis [239], though these data is not yet available.

Once again, the calculated DS by HPLC is within the values calculated both by NMR and by ICP-AES. All methods show some limitations for the calculation of the DCMC DS but we can have a relatively good estimation of the average DS with all methods.

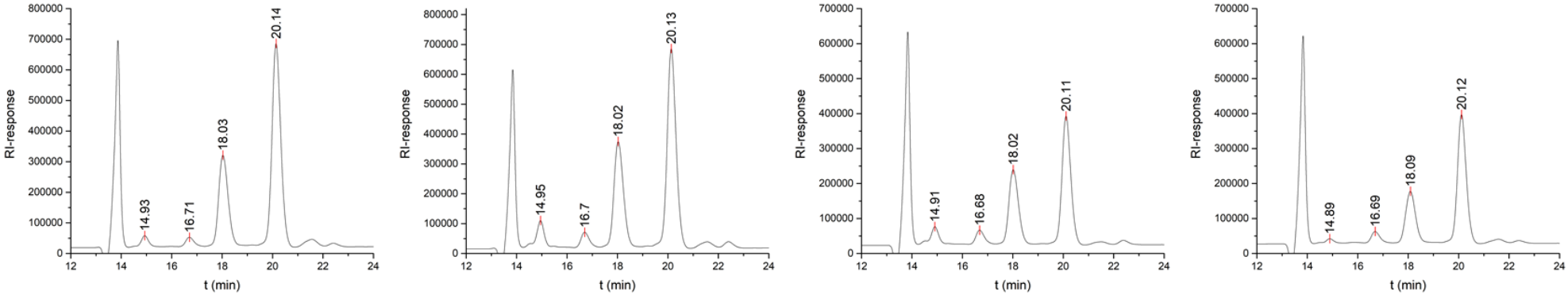

Figure 50 - Representative chromatograms of samples DCMC2 to DCMC5 hydrolytically depolymerized.

Table 14 - Areas and area percentage of the different substituted AGU units in samples DCMC2 to DCMC5

DCMC2				DCMC3				DCMC4				DCMC5			
	Index	**Area**	**AreaIntg (%)**		**Index**	**Area**	**AreaIntg (%)**		**Index**	**Area**	**AreaIntg (%)**		**Index**	**Area**	**AreaIntg (%)**
Unknown	1	16718.46	2.36	Unknown	1	40007.21	5.23	Unknown	1	24165.53	4.66	Unknown	1	8572.97	1.79
Di	2	16639.70	2.35	Di	2	24086.09	3.15	Di	2	20489.14	3.95	Di	2	17826.68	3.71
Mono	3	137668.90	19.48	Mono	3	162445.10	21.25	Mono	3	99251.82	19.12	Mono	3	72463.51	15.10
Glucose	4	277970.50	39.33	Glucose	4	282340.90	36.94	Glucose	4	154093.50	29.69	Glucose	4	154210.20	32.14
$DS_{(HPLC)}$	**0.39**			**$DS_{(HPLC)}$**	**0.45**			**$DS_{(HPLC)}$**	**0.51**			**$DS_{(HPLC)}$**	**0.44**		

4.1.3.7 DCMC degree of polymerization (DP) and intrinsic viscosity

4.1.3.7.1 Size exclusion chromatography (SEC)

For the characterization of the samples degree of polymerization (DP) the samples were further analysed by SEC in 0.1 M $NaNO_3$/0.05% NaN_3. SEC is the relative method; therefore, the determination of molar masses and molar mass distributions requires a calibration curve. The more expeditious way to perform a calibration curve is to calculate one using narrowly distributed standards with known molar masses having the same chemical nature as the sample to be investigated [240]. For NaDCMC there is a lack of suitable commercial standards and, for these reason, the calibration curve was performed using a pullulan standard set. The results are represented in Figure 51.

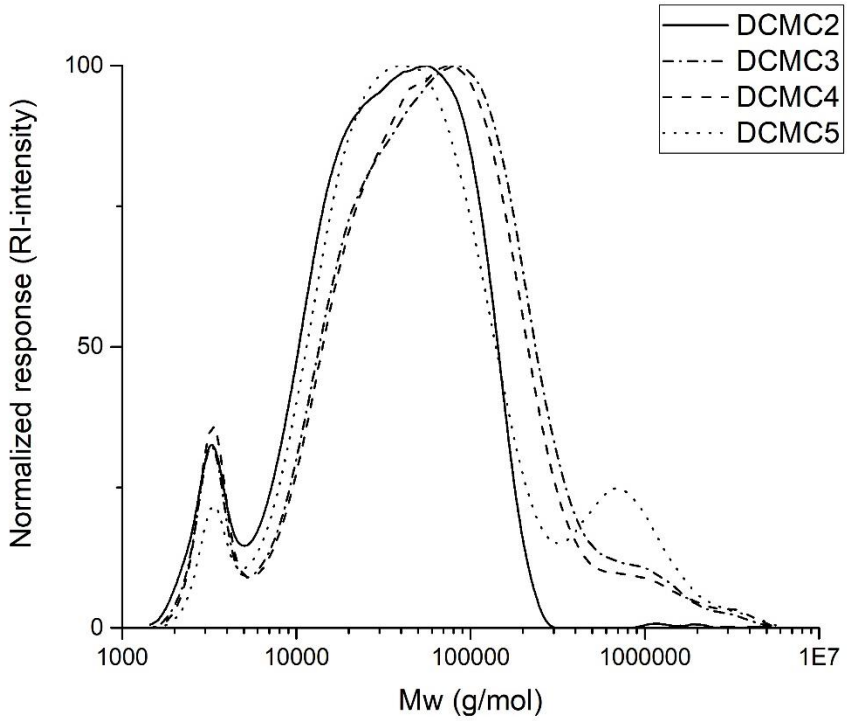

Figure 51 - Molecular weight distributions of samples DCMC2 to DCMC5 analyzed by size exclusion chromatography.

We can see a bimodal distribution in sample DCMC2 and a trimodal distribution in samples DCMC3, DCMC4 and DCMC5. All samples present a peak at around 3300 g/mol which corresponds to a very low DP species of cellulose or modified cellulose (DP of ± 15). The data related to the major peaks are summarized in Table 15.

Table 15 - Degree of polymerization of the different samples after treatment of the SEC results. The DS used to calculate the DP was calculated based on ICP-AES results.

Sample	DCMC2	DCMC3	DCMC4	DCMC5
MW (highest peak)	56153.1	84065.5	75031.2	39341.7
DS (ICP)	0.32	0.44	0.46	0.51
Mw (glu+sub)	208.4	227.1	230.2	237.0
DP (mw)	269.4	370.2	326.0	166.0

For the calculation of the DP, it was used the formula described in the literature [241] with some modifications. The adapted equation is as follows:

$$\text{Molecular weight (NaDCMC)} = DP \times (162 + (DS \times 147))$$

Where:

162 (g/mol) = molecular mass of an anhydroglucose unit of cellulose, 147 (g/mol) = net increase in molecular mass of an anhydroglucose unit for each sodium malonate group added, DS = DScalc by ICP-AES

We can see that the DP decreases in the order DCMC3 > DCMC4 > DCMC2 > DCMC5. Although there is an increase in the DP from sample DCMC2 to DCMC3, there is no direct correlation between the DP of the overall samples and the number of equivalents of base used in the different reactions. In fact, there is a significant decrease in the DP of sample DCMC5 which can be related to the degradation of the cellulose during the synthesis. Since we used Macherey-Nigel Cellulose MN 400 Avicel (with a mean DP of 40-200), it was to expect that the final DP of the derivatized samples was higher than 200 what happened to all samples besides for sample DCMC5.

4.1.3.7.2 Viscosity measurements

The reduced (η_{red}) and intrinsic ([η]) viscosity of the different DCMC samples are shown in Figure 52A. The reduced viscosity increased linearly with increasing DCMC concentrations in all samples. The results for the calculated intrinsic viscosity of the different samples are shown in Figure 22B. There is no significant difference in the intrinsic viscosity of samples DCMC2, DCMC3 and DCMC4 who presented values of 49.88 cm^3/g, 50.84 cm^3/g and 50.87 cm^3/g respectively. On the other hand, there is a significant difference between these samples and

sample DCMC5 which presented an intrinsic viscosity of 38.84 cm^3/g. Although presenting a DS similar to sample DCMC4, sample DCMC5 presents a much lower intrinsic viscosity.

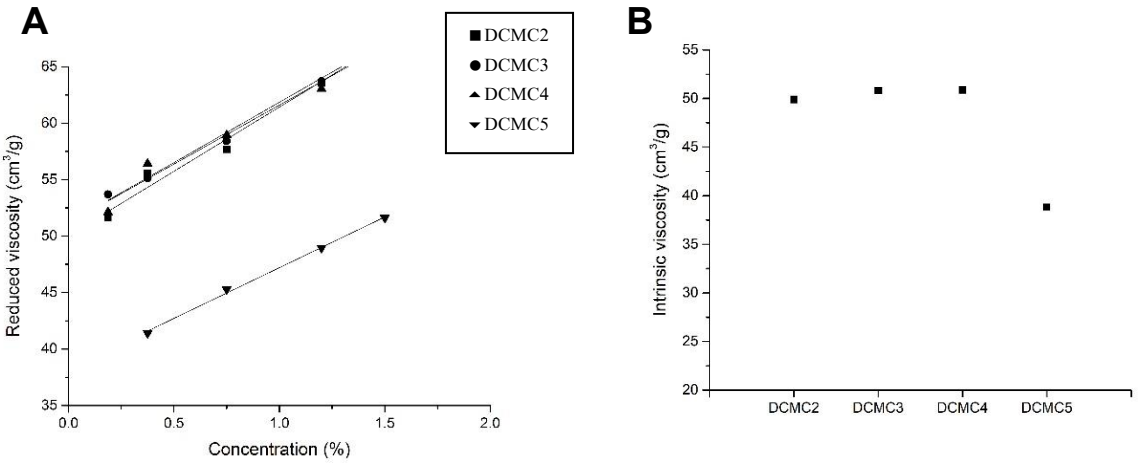

Figure 52 - A) Concentration dependence of reduced viscosity of samples DCMC2 to DCMC5 at 20 °C (samples were dissolved in 6% NaOH) B) Intrinsic viscosity of samples DCMC2 to DCMC5.

This phenomenon can be possibly related to lower DP of sample DCMC5 (Table 5) which can influence the overall characteristics of the polymer. Moreover, when comparing to the remaining samples, the lower DP value for DCMC5 together with the lower intrinsic viscosity value reveal the possible degradation of the polymer during reaction with high quantity of NaOH.

When compared to commercial CMC or CMC synthesized in homogenous media (NaOH/urea) [238], the DCMC shows a lower intrinsic viscosity for the same DP. As an example, CMC synthesized from Avicel in NaOH/urea medium showed a DS of 0.5, intrinsic viscosity of 86.2 cm^3/g and a DP of 131 [238]. Comparing with our samples, DCMC4 and 5 showed an intrinsic viscosity of 50.87 cm^3/g and 38.84 cm^3/g respectively with DP values of 326 and 166. This shows that DCMC showing a DS and DP similar to CMC presents lower intrinsic viscosity when compared in the same conditions (6 wt.% NaOH aqueous solution at 20 °C using an Ubbelohde viscometer). Although we can compare our results with available CMC data, the comparison is merely qualitative since we are comparing different polymers with different behaviours.

The molecular weight of the polymer can be estimated from the intrinsic viscosity [η] values. The Mark–Houwink equation, $[\eta]=KM^{\alpha}$, is generally employed to estimate the molecular weight of linear polymers, where K and α are constants for a given polymer/solvent/temperature system [242]. This was already employed to CMC [243,244]. Crössman et al. [245] showed that the DP of CMC can be calculated by the equation DP=[η]/0.0066. For DCMC none of these equations can be applied since the behaviour of this polymer regarding polyelectrolyte expansion in solution and the secondary polyelectrolyte effects such as ion exclusion by varying the ionic strength and/or pH

of the mobile phase and using different types of columns was not yet studied. Due to that, it is not yet possible to calculate the DP from the intrinsic viscosity of DCMC polymer.

4.1.4 Conclusions

We could synthesize different DCMC polymers using Avicel and sodium bromomalonate (11) as starting materials. In this work, we used heterogenous synthesis reaction in isopropanol/water, with NaOH as base, which resulted in polymers with a DS between 0.32 and 0.51. The pattern of substitution of the AGU was studied by NMR though further work should be performed in this area to acquire more reliable data. The DS of the different DCMC samples was calculated based on three different techniques (NMR, HPLC and ICP-AES) giving comparable results within the experimental error. The 2D NMR spectra as well as SEC and HPLC analysis was reported for the first time in this type of polymer. Future work on the structural analysis of this polymer will be focused on the better characterization of the AGU substitution pattern by NMR. This work also allowed to consolidate different methods for the characterization of DCMC, a valuable tool for the control of future reactions.

4.2 Production of a water-insoluble form of DCMC for the adsorption and removal of positive proteins from a solution

4.2.1 Introduction

Control over protein adsorption on surfaces is a key parameter in the design of advanced materials in a variety of technological fields. While in many areas protein adsorption is undesired (e.g. antifouling surfaces), in medical implants and tissue engineering a controlled deposition of proteins often allows for a faster healing process and recovery [196,246]. Cationic cellulose derivatives are an interesting class of compounds due to the availability of the raw material cellulose and the easy modification procedures to achieve cationization, which allows to tailor the material properties in order to realize the envisaged application, such as protein adsorption [196]. Both cationic cellulose (grafting the epoxide glycidyltrimethylammonium chloride (GTMAC) unto cellulose) and anionic cellulose (by the oxidation of the hydroxyl groups of the AGU by the radical 2,2,6,6-tetramethylpipiridine 1-oxyl (TEMPO)) were studied for cell attachment, though the negatively charged anionic cellulose films showed lack of cell attachment oppositely to positively charged ones. This phenomenon was explained by the possible ionic interactions between scaffold (anionic surface of cellulose) and the cells phospholipid bilayer [247].

The oxidation of cellulose by TEMPO will result in the production of a free carboxylic group in the AGU as shown in Figure 53.

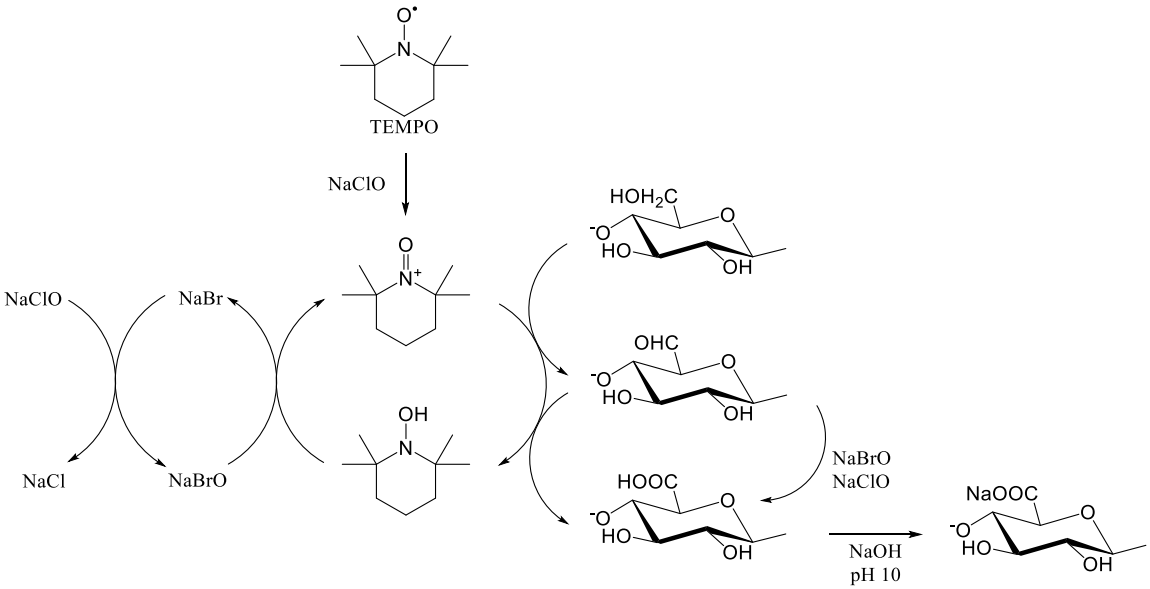

Figure 53 - Regioselective oxidation of C6 primary hydroxyls of cellulose to C6 carboxylate groups by TEMPO/NaBr/NaClO oxidation in water at pH 10–11 [248].

This cellulose derivative has a similar structure compared to CMC (8) (though it has one less oxygen and one methylene group) and its carboxylic group will probably present a similar pKa of the CMC one. As presented before, at the wine pH only about 20% of the carboxymethyl groups of CMC carry negative charge in solution [205]. Adsorption of ovalbumin was also evaluated in amphoteric chitosan/carboxymethylcellulose membranes with a maximum adsorption capacity

around pH 4.8 [249]. Due to that, CMC or the TEMPO-oxidized cellulose are not the most viable options for positively charged proteins adsorption at wine pH.

The synthesis and characterization of dicarboxymethylcellulose (DCMC) showed that this water-soluble polymer presents an average pKa of 2.1[207] without the introduction of any inorganic substituent (oppositely to sulfonic acid groups). We could synthesize this compound and perform its structural characterization using different techniques though its ability to perform cation exchange at low pH was not tested yet. To address this issue, we tested the crosslinked DCMC polymer with two different proteins to test its protein adsorption capacity in different buffers and evaluate its ability to remove these proteins from solution.

4.2.2 Objective

The objective of this work consisted in the production of a water-insoluble form of the dicarboxymethylcellulose polymer, capable of performing ion exchange at wine conditions to remove positive proteins from solution. Ultimately, these insoluble polymers can be adapted to a filtration apparatus to remove soluble proteins when a solution is passed through the polymer containing filter.

4.2.3 Results and discussion

4.2.3.1 First approach in the synthesis and production of DCMC films

Preceding note: The work described in the first approach to produce the cellulose films was performed prior to the work described in the synthesis second approach. With that in mind, some of the purification methods used in the second approach were not applied in this subchapter and therefore some values of DS may not correspond to the real DS values of these polymers.

4.2.3.1.1 Polymer preparation

In this work, of DCMC was carried out by a standard slurry method as previously described by [210] for carboxymethylation of cellulose though using sodium bromomalonate (11) and Avicel as starting material. The conditions used for the synthesis of these polymers are described in Table 16. After the synthesis of these polymers, they were thoroughly washed with 70% methanol prior to the drying process to remove possible by-products. After drying the products, these were further characterized.

Table 16 - Conditions used for the derivatization of cellulose with different quantities of sodium 2-bromomalonate (**11**).

Identifier	Ratio BMA: NaOH:AGU	Temp (ºC)	Reaction time (h)	BMA (g)	NaOH (40 %, mL)	Avicel (mg)	dH_2O	Isopropanol (mL)	Total H_2O (%)
DCMC6	2:3.5:1	60	3	1.1	0.85	400	0.43	15	8
DCMC7	1:3.5:1	60	3	0.6	0.85	400	0.43	15	8
DCMC8	0.7:3.5:1	60	3	0.4	0.85	400	0.43	15	8
DCMC9	0.5:3.5:1	60	3	0.3	0.85	400	0.43	15	8
DCMC10	0.2:3.5:1	60	3	0.1	0.85	400	0.43	15	8

Samples resulting from reactions with different amounts of NaBMA were analysed by ICP-AES (Table 177). The DS determination by this method is very accurate as shown before though it can be highly affected by the presence of NaOH, CH_3COONa, NaBMA or compound 13 resulting from the synthesis reaction. In this case, the products were only washed with methanol/water solutions to remove residual salts and filtered in a Büchner filter funnel with a sintered glass disc.

Conventionally prepared carboxymethyl cellulose (i.e. by slurry method) are water soluble at a DS as low as about 0.4 [250]. In our case, the DCMC is partially water-soluble at a DS of 0.6 and completely soluble at a DS of 1.53.

Table 17 -Degree of substitution calculated from the sodium content measured by ICP-AES and water solubility of the different samples.

Sample	% Na (ICP)	DS_{icp}	Water solubility
DCMC6	18.2	1.53	Soluble
DCMC7	13.6	0.85	Partially soluble
DCMC8	11	0.60	Partially soluble
DCMC9	9.41	0.47	Insoluble
DCMC10	6.69	0.30	Insoluble

4.2.3.1.2 Crosslinked sodium DCMC films preparation

Crosslinked sodium DCMC films were produced to determine the possibility of using this new type of polymer for the adsorption of positive proteins at acidic pH by ion exchange. Since DCMC6 showed to be highly soluble in water and presented the highest DS, we chose this sample to produce the films.

We adapted a crosslinking protocol normally applied in the production of crosslinked sodium CMC (also known as sodium croscarmellose) [251] to produce crosslinked sodium DCMC. The polymer was protonated by reacting it with 20% H_2SO_4 for 2 hours with constant agitation. After, the sample was washed with deionized water until pH 7, dried and crosslinked. The crosslinking reaction consisted of a heat treatment for 2 hours at 105 °C inside a Teflon petri dish. After crosslinking, the polymer was deprotonated by washing it in a saturated solution of sodium bicarbonate for 2 hours. This procedure allowed the production of a water insoluble, sodium form of polymer films (Figure 54) with the ability to perform ion exchange trails in aqueous buffers without dissolution of the polymer in the medium.

Figure 54 - DCMC6 film (150 mg of polymer) before crosslinking reaction.

4.2.3.1.3 Protein adsorption on the crosslinked NaDCMC films

Following synthesis of the DCMC films, the ability of these films to adsorb positive proteins at wine pH (pH 3 to 3.5) was evaluated. Prior to protein adsorption trials using isolated wine protein, we opted to perform these tests using a standard model protein. As model protein, cytochrome *c* (cytc) from horse heart was chosen. This soluble protein has around 12 kDa, presents positive net charge at acidic pH (pI of 10.5) and a strong resistance to acid since there is evidence that its conformation is stable at pH 1.5 [252].

To test the effect of increasing polymer dosages on the adsorption of cytc, an adsorption experiment was set up with different amounts of crosslinked sodium DCMC6 film using an initial cytc concentration of 0.5 mg/mL. The effect of polymer dosage on the removal of cytc from solution is shown in Figure 55.

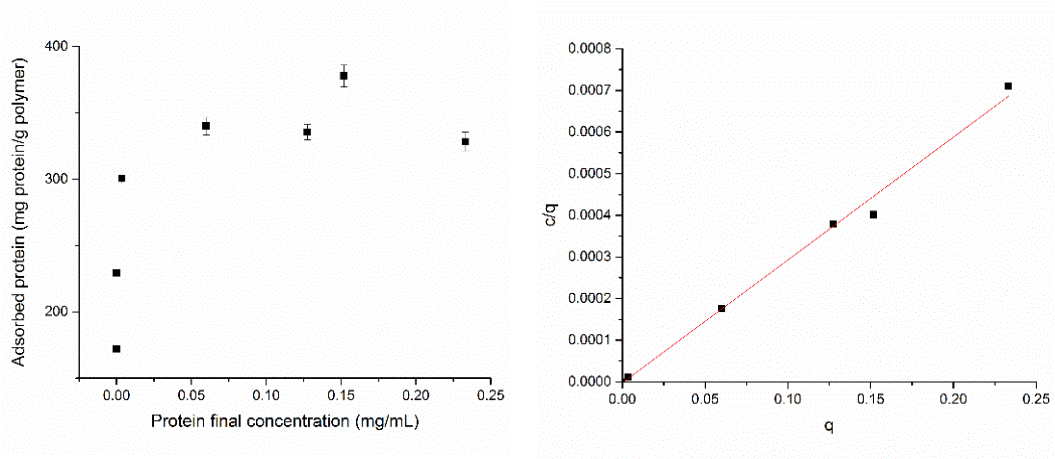

Figure 55 - A) Experimental adsorption isotherm for cytochrome *c* on a DCMC6 film in 25 mM citrate buffer, pH 3.2. B) Linear fitting of the experimental values presented in A based on the Langmuir isotherm model.

As expected, protein adsorption increases with increasing amounts of polymer until it reaches a saturation point at higher doses of polymer (also referred as plateau). This increasing adsorption results from the increasing binding sites availability because of higher polymer content. A representation of one adsorption trial using increasing quantities of polymer for the adsorption of cytc is shown in Figure 56.

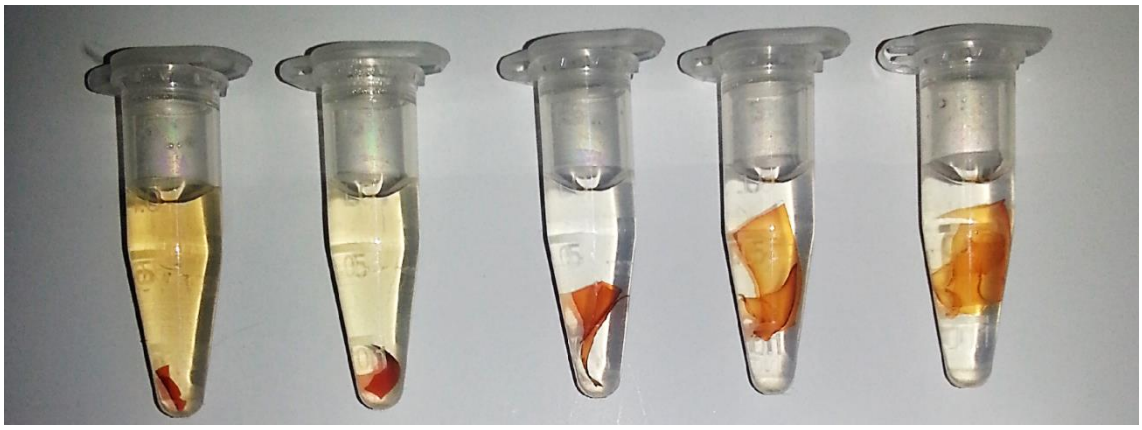

Figure 56 – Visualization of the increasing quantity of DCMC6 (from left to right) on the protein adsorption capacity. This image was gathered after 24 hours of contact between the polymer and the solution at 25 °C.

Since we performed this trial at constant temperature (25 °C), we could calculate the maximum amount of adsorbed protein and kinetic constant using an isotherm equation fitting. These parameters were estimated from the slope and intercept of the linearized form of the Langmuir equation showed in Equation 1 and represented in Figure 55B.

$$\frac{c}{q} = \frac{b}{a} * c + \frac{1}{a} \qquad \text{(Equation 1)}$$

In equation 1, c corresponds to the protein concentration in the buffer (mg/mL), q the protein concentration adsorbed in the polymer (mg/g), b is the kinetic constant (K_a) and a corresponds to (Q_{max} x K_a) where Q_{max} is the polymer maximum adsorption capacity (mg/g). By the linearization of the Langmuir equation we can extract 1/a as the intercept point and b/a as the slope of the linear adjustment. In our case, after linearization of the values represented in Figure 55B (R^2 = 0.994), we obtained values of 345 ± 15 mg/g and $4x10^{-7}$ for Q_{max} and K_a respectively.

It was described in the literature a maximum adsorption capacity of cytc (at 30 °C, pH 9.0) on PGMA-g-Cell-SO_3H of 157.13 mg/g [253]. Although this polymer presents a lower adsorption capacity compared to ours, we these comparison is merely qualitative since the temperature and pH of the experiment at which this polymer was tested are different.

4.2.3.2 Second approach in the synthesis and production of DCMC films

4.2.3.2.1 Polymer preparation

Similarly to the method described in the first approach, DCMC synthesis was carried out by a standard slurry method as previously described by [210] for carboxymethylation of cellulose though using sodium bromomalonate (11) and Avicel as starting material. The condition used for the synthesis of this polymer are represented in Table 18.

Table 18 - Conditions used for the synthesis of DCMC11.

Identifier	BMA: NaOH:AGU	Temp (°C)	Reaction time (h)	BMA (g)	NaOH (g)	Avicel (g)	dH_2O (mL)	Isopropanol (mL)
DCMC11	2.2:3.5:1	60	5	9.7	1.1	2	4.8	60

After synthesis of this polymer, it was thoroughly washed with 70% methanol followed by pure methanol. After drying in the vacuum, the product was dialyzed using 3.5 kDa cut-off cellulose acetate membranes against deionized water. The resulting dialyzed solution was freeze dried and store in a desiccator until used (Figure 57).

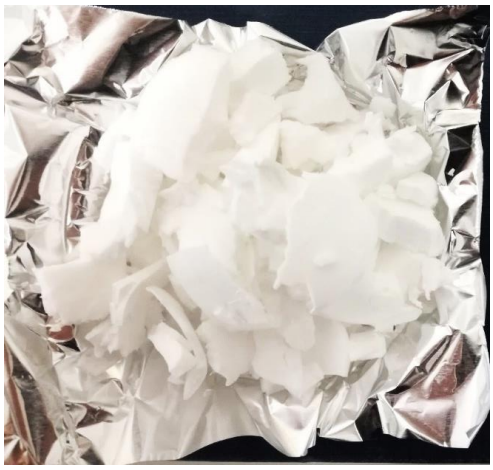

Figure 57 -Polymer (DCMC11) after dialysis and freeze drying.

The general aspect of the polymer changes drastically after dialysis compared to the polymer described in the first approach. After dialysis, the polymer is white with a foam/cotton-like structure. In the other hand, the polymer without dialysis (as in the first approach) is yellow/brown in colour and shows a stiffer foam-like structure possibly resulting from the presence of salts and other by-products.

4.2.3.2.2 Films preparation

Similarly to the first approach, a film of DCMC11 was casted in a Teflon plate. The polymer was dissolved in deionized water prior to the casting. After drying, the film was detached from the casting. The film contracted significantly compared to the less purified polymers produced in the first approach (Figure 58).

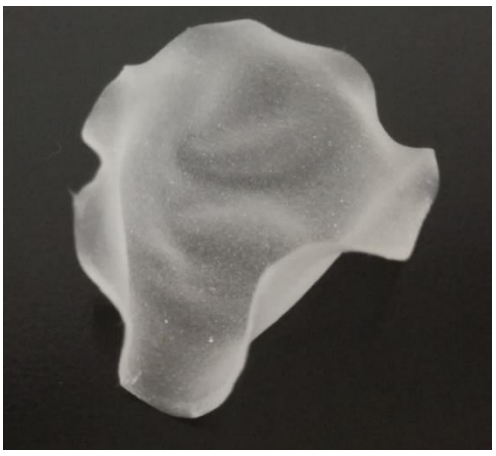

Figure 58 - Film of DCMC12 after drying and detaching from the Teflon casting.

The film was also much more brittle than the first ones which can be related to the lower content in contaminants and, consequently, a much higher content of pure polymer. The polymer was protonated in 20% H_2SO_4 for 2 hours followed by extensive washing with deionized water to neutral pH. After drying, the crosslinking process was performed by heating the dry sample at 105 °C for 2 hours.

Prior to this crosslinking process, we have tested different crosslinking temperatures as described in the original patent [251]. We registered that below 100 °C the crosslinking was ineffective resulting in a partially crosslinked polymer that would dissolve when washed with the basic solution for deprotonation. We opted to use the lower temperature to avoid decarboxylation of the malonate group. Decarboxylation of malonic acid in aqueous solution occurs at above 70 °C where it decomposes to acetic acid and carbon dioxide [254].

This type of crosslinking involving cellulose chains and heat results in the formation of new ester bonds between cellulose chains that will cause the crosslinking (Figure 59). Heating the dried protonated polymer will cause its dehydration and, consequently, the formation of new ester bonds between the acid groups of the substituent and free hydroxyl groups of near cellulose chains.

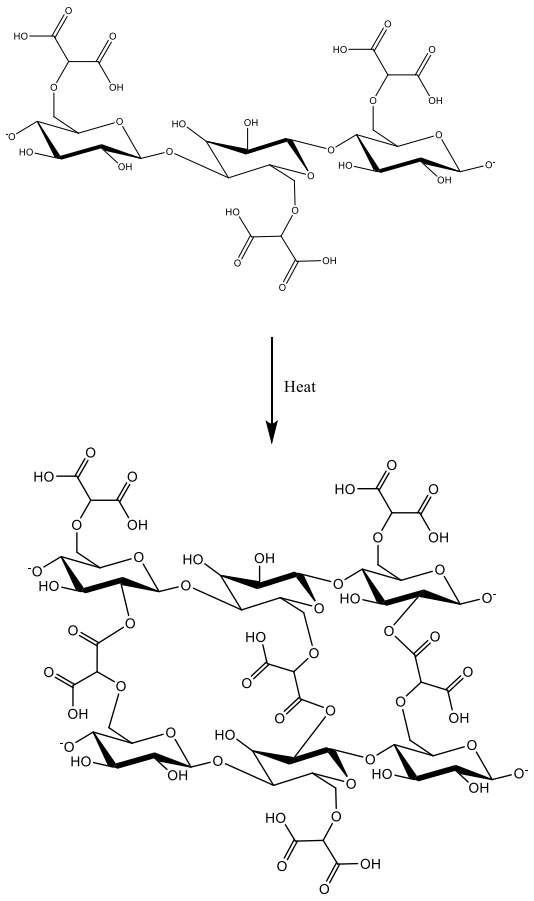

Figure 59 - Representation of the heat crosslinking reaction of DCMC.

Though effective, this reaction can have a major drawback due to the temperature treatment. As we increase the reaction temperature, the probability of decarboxylation of the substituent increases and, ultimately, we can convert the crosslinked DCMC to crosslinked CMC. Since the ion exchange of the polymer is dependent on the free carboxylic groups available, decarboxylation of the substituent will cause a decrease in the reactivity of the polymer and therefore a decrease in its maximum protein adsorption capacity. The pKa of DCMC has a value around 2.1 depending on the DS [207], whereas CMC have a pKa around 3.65 [255]. After crosslinking, the CMC will "lose" some of its free carboxylic acid groups in the formation of the ester but DCMC will be able to maintain one of its carboxylic acid groups "free" after crosslinking. At wine pH (between 3.1 and 3.6), CMC will be majorly protonated oppositely to DCMC that will be majorly in its deprotonated form. This phenomenon will cause DCMC to be able to perform ion exchange (oppositely to CMC). With that in mind and based on our results, crosslinking at 105 °C for 2 hours is a viable ratio time/temperature to produce water insoluble crosslinked DCMC.

After crosslinking, the polymer was washed and deprotonated in a saturated solution of $NaHCO_3$ for 2 hours. Next it was extensively washed with deionized water to remove residual salts and dried.

The degree of substitution of the polymer before and after crosslinking was evaluated by ICP-AES. Both samples were deprotonated, thoroughly washed with deionized water, and hydrolysed in concentrated nitric acid. The results of the ICP-AES are represented in Table 199.

Table 19 - Sodium quantification using ICP-AES and calculated degree of substitution (DS) of samples DCMC11 and DCMC11 crosslinked.

Sample	Integral (Na)	Na (mg/L)	Sample concentration (mg/mL)	Na (mg)	% Na	Calculated DS
DCMC11	16909261	147.1	1.30	0.147	11.32	0.62
DCMC11 crosslinked	8468834	66.2	2.52	0.066	2.63	0.1

We can see a significant difference in the Na content between the non-crosslinked and the crosslinked sample. This can be attributed to the "loss" of free carboxylic groups of the substituent that reacted with surrounding hydroxyls to form the crosslinked ester.

Future work will pass through the optimization of this reaction to produce an effective crosslinked polymer with higher free carboxylic groups available to react with soluble proteins. Use of heat as a crosslinking agent is very convenient when working with polymers to be used in the food industry since there is no addition of any other reagent. Nevertheless, OIV allows the use of some chemical crosslinking agents for the production of ion-exchange resins like formaldehyde [199]. Other crosslinking agents (already tested with CMC) and possible to be adapted to DCMC are 1,4-Butanediol diglycidyl ether [256], aluminium sulfate octadecahydrate [257] or epichlorohydrin [258].

4.2.3.2.3 Cytochrome *c* (cytc) adsorption on the crosslinked NaDCMC

To study the effect of increasing polymer dosages on the adsorption of cytc, an adsorption trial was set up with different amounts of crosslinked DCMC11 film using an initial cytc concentration of 0.5 mg/mL. Unexpectedly, the protein adsorption capacity of these highly purified films was very low compared to the impurified films shown in the first approach (Figure 55). Even after 96

hours of trial we have registered a maximum protein adsorption capacity of around 50 mg protein/g polymer.

Empirically, we saw that the films were much stiffer that the films of the first approach even after 96 hours in contact with the solution. In the first trial, the films hydrated and turn to a gel-like membrane in 1 to 2 hours contact with the solution. This can reflect a much more closed structure in the purified polymer which can be responsible for the low adsorption of proteins. Since the first polymers were not pure, there was the presence of salts within the structure of the films. In the protonation and deprotonation steps during the crosslinking process, the films were exposed to different buffers than could dissolve (and remove) part of this by-product salts from the film. The removal of these salts opened pores in the film structure which increased the specific area of the film and, therefore, its hydration capacity. With higher specific area, the impure films could remove more proteins from solution and presented a higher efficiency compared to the pure polymer films.

For a solid–liquid sorption process, the solute transfer is usually characterized by boundary layer diffusion, intraparticle diffusion or both. The steps that analyses the mechanisms of protein adsorption are as follows:

(1) Migration of the protein molecules from bulk of the solution to the surface of the adsorbent (external mass transfer resistance).

(2) Diffusion of the protein molecules through the boundary layer to the surface of the adsorbent (internal mass transfer resistance).

(3) Adsorption of the protein at an active site on the surface of the adsorbent.

(4) Intraparticle diffusion of protein into the interior pores of the adsorbent.

Generally, the last step is the equilibrium reaction and it is very rapid; the resistance is hence assumed to be negligible. The slowest step determines the rate-controlling parameter in the adsorption system. This rate-controlling parameter can be distributed between intraparticle and film diffusion mechanisms [259]. To decrease the resistance of the proteins to enter the film (film diffusion mechanism), we tried to disrupt the films structure to produce a powder to increase its specific area and decrease the resistance of the protein to diffuse in the polymer.

To partially disrupt the possible hydrogen bonds between the crosslinked DCMC chains, the films were washed with 100 mM NaOH for 30 minutes. After washing, the polymer lost its film structure and turned to a powder. After washing with deionized water until neutral pH, we registered that there was no significant loss of polymer weight. After drying, the polymer was applied in a cytc solution to test its ability to adsorb the protein present in the solution. Immediately after adding the polymer, the protein was totally adsorbed and the solution turn clear.

Based on these preliminary results, we have designed a new protein adsorption trial using cytc at a concentration of 1 mg/mL in a 30 minutes trial, at 25 °C, with constant agitation.

To study the effect of increasing polymer dosages on the adsorption of cytc, an adsorption trial was set up with different amounts of crosslinked DCMC11 (sodium form) powder using an initial cytc concentration of 1 mg/mL in 25 mM citrate buffer, pH 3.2. The effect of polymer dosage on the removal of cytc from solution is shown in Figure 60.

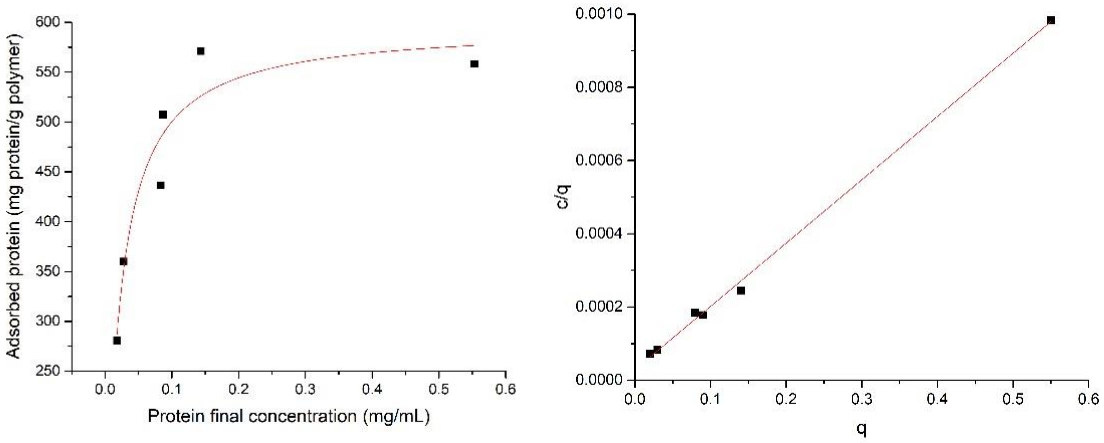

Figure 60 - A) Experimental adsorption isotherm for cytc (1mg/mL) on a NaDCMC11 powder in 25 mM citrate buffer, pH 3.2, for 30 minutes. In red is represented the nonlinear fitting using the Langmuir model equation B) Linear fitting of the experimental values presented in A based in the Langmuir model (R2 = 0.998).

By the linearization of the Langmuir equation (Figure 60 B, R^2 = 0.998), we obtained values of 588 ± 5 mg protein/g polymer and 56.67 for Q_{max} and Ka respectively. This polymer shows 1.7-fold more protein adsorption capacity than the polymer described in the first approach. Comparing with the polymer in the film form (after deprotonation with $NaHCO_3$), the powder presents a 29-fold higher protein adsorption capacity. The Langmuir model proposes that monolayer sorption occurs on the solid surface with identical homogeneous sites. It also suggests that no further adsorption takes place once the active sites are covered with target molecules [260]. Comparing the Ka values, we can see a significant difference between the polymer from the first approach (Ka = 4 x 10^{-7}) and the one from the second approach (Ka = 56.67). The representative appearance of the polymer powder added to the protein solution (after around 1 minute of contact) is shown in Figure 61.

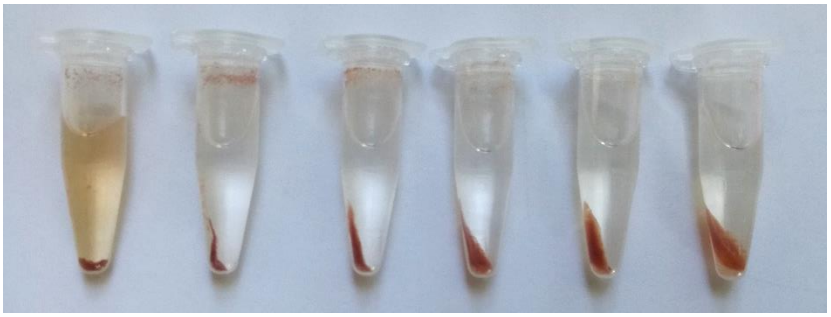

Figure 61 - Polymer DCMC11 crosslinked (powder form) added to a solution of Cytc (at 1 mg/mL). This image was taken after 1 minute contact between the polymer and protein solution. Vials were centrifuged prior to the photo to emphasize the difference between pellet and supernatant.

4.2.3.2.4 Isolated wine protein adsorption on crosslinked NaDCMC

Since the protein adsorption capacity of the polymer was validated at pH 3.2, we performed a new trial with isolated wine protein in model wine solution (5 g/L tartaric acid, 12% EtOH, pH 3.2). Similarly to the later trial with cytc, we used the polymer in powder form after deprotonation and disintegration using 100 mM NaOH.

To study the effect of increasing polymer dosages on the adsorption of isolated wine protein, an adsorption trial was set up with different amounts of crosslinked DCMC11 (sodium form) powder using an initial isolated wine protein concentration of 1 mg/mL in model wine solution pH 3.2. The effect of polymer dosage on the removal of isolated wine protein from solution is shown in Figure 62.

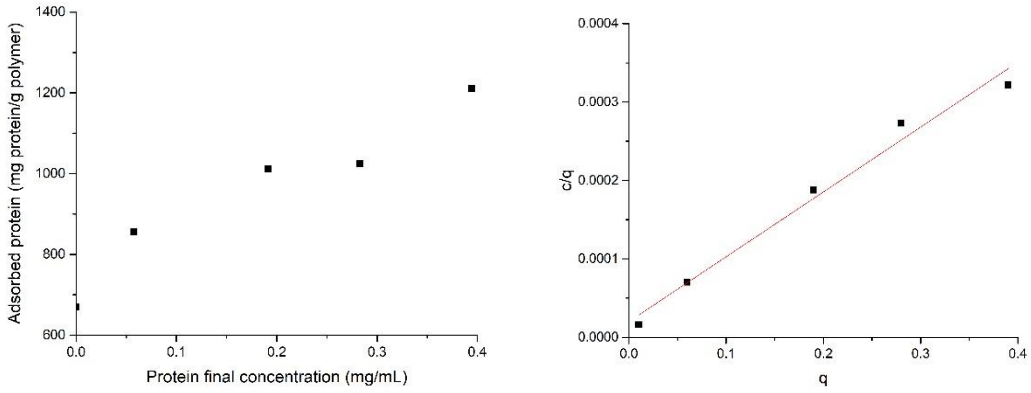

Figure 62 - A) Experimental adsorption isotherm for isolated wine protein (IWP) at 1 mg/mL, for 30 minutes, on NaDCMC6 in model wine solution (5 g/L tartaric acid, 12% ethanol, pH 3.2). B) Linear fitting of the experimental values presented in A based on the Langmuir model (R^2 = 0.982).

Although the results using isolated wine protein do not form a plateau (which is directly related with the saturation point of the polymer and therefore with the maximum adsorption capacity, Figure 62A), we were able to linearize the results using the Langmuir model (Figure 62B, R^2 = 0.982). Analysing the results of the linearization, we obtained values of 1250 ± 10 mg protein/g polymer and 26.7 for Q_{max} and Ka respectively. To have a more accurate fitting, it would be necessary to perform a new trial using lower amounts of polymer although that was not possible due to protein availability.

Comparing the maximum adsorption capacity between proteins, the DCMC11 powder can remove 2 times more wine protein from model wine solution than cytc from citrate buffer. Although valid, this observation is merely qualitative since we are comparing proteins of different sizes (cytc with 12 kDa and total wine proteins with sizes around 21 kDa) in different buffers (25 mM citrate buffer vs model wine solution). Nevertheless, it was validated that the DCMC11 polymer can remove positively charged wine proteins from solution at a pH like the one found in commercial wines (pH 3.2).

4.2.3.2.5 Removal of soluble proteins from wine with DCMC11 powder

As proof of concept, and since the wine matrix is much more complex than the model wine solution used in this type of trials, we have used our polymer directly in an unstable wine. Two milligrams of polymer were added to 2 mL of centrifuged Moscatel of Alexandria wine (final concentration of 1 g polymer/L). This was a Moscatel produced in our laboratory from the 2010 vintage with grape originated from the Instituto Superior de Agronomia vineyard. After 30 minutes of contact, the wine was centrifuged and the protein present in the supernatant quantified. The control wine presented a total protein concentration of 324 mg/L ± 3 mg, oppositely to the wine reacted with the polymer for 30 minutes than showed a protein concentration of 56 mg/L ± 17 mg. These results show that the DCMC11 polymer in wine conditions can remove around 270 mg protein /g polymer. This is a much lower adsorption capacity than the one showed for the isolated wine protein in model wine solution (Q_{max} = 1250 mg/g) although many other factors are interfering in the ion exchange capacity of the polymer.

Further work must be performed to optimize the use of the DCMC powder in wine to increase its adsorption capacity in winery conditions. In a recent study, the correlation between bentonite requirement and the concentration different wine protein fractions was presented. The authors showed that for wines containing around 300 mg/L of PR proteins, it was necessary around 700 mg/L of bentonite to remove these unstable proteins [261]. Overall, the maximum adsorption capacity of bentonite was around 428 mg protein / g bentonite. The value described in the literature is superior to the one acquired using DCMC in real wine condition, though this was just a preliminary trial using one polymer in non-optimized conditions and this value can be much higher after optimization.

4.2.3.2.6 Synthesis cost analysis

Considering the synthesis of polymer 6.26.6 that resulted in 1.02g of final product, a cost analysis regarding commercial reagents prices. A summary of the synthesis cost is represented in Table 20.

Table 20 - DCMC production cost analysis (1.02 g of polymer DCMC11). The prices described in the table are based on commercially available reagents except for 2-bromomalonic acid.

Reagent	Quantity	Price (€)
2-bromomalonic acid	10 g	1.69
Sodium hydroxide	1 g	0.02
Avicel	2 g	0.32
Isopropanol PA	60 mL	0.3
Methanol PA	100 mL	0.33
	Total (€)	2.66

To produce DCMC we had to synthesize the starting material 2-bromomalonic acid (or 2-bromopropanedioic acid) as described earlier. Some companies have 2-bromomalonic acid available like Gentaur (250 mg vials, 253 € each) or Stratech (250 mg vials, 369 € each) though the reagents were excessively expensive.

One malonic acid esters, diethyl bromomalonate, is commercialized at 23 € for 25 mL (ACROS, 90 – 95% solution) which is a much lower price compared to the pure acid. Using this ester could be a good option (e.g. increase the solubility of the starting material in the reaction media) and its deprotection, although not described, might be achievable in basic conditions like the ones used in our synthesis. This would require using a higher number of base equivalents in the reaction to deprotonate the acid resulting from the deprotection and the resulting product can be different from the ones synthesized previously. Other possible deprotection methods could involve salts as LiCl though this could lead to the decarboxylation of the molecule by the Krapcho reaction (Figure 63) [262].

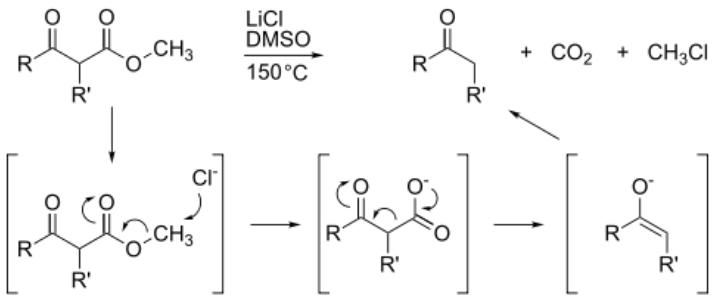

Figure 63 - Diagram showing mechanism of the Krapcho reaction.

We have synthesized this starting material as described in the Methods section using malonic acid and bromine as starting materials. The calculation of the product cost in Table 20 comprises the synthesis of 2-bromomalonic acid using the method performed in our laboratory.

Using extra pure laboratory reagents, we managed to produce our DCMC polymer at a cost of 2.66 €/g including only the costs of the starting materials. Analysing the polymer total cost, we can see that around 64% of it relies on the production of 2-bromomalonic acid. Bentonite, the most used wine additive for protein removal as a commercial cost between 0.7 and 2.5 €/kg [69]. Without further optimization, our polymer as a cost much higher than bentonite though it is currently being synthesize in small scale using laboratory/research grade reagents.

Future optimization/scale up procedures will pass in the decrease and recycling of the solvents used in the reaction and workup. The two main solvents used in this reaction (isopropanol and methanol) can be distilled to remove salts and by-products and reused in further synthesis.

4.2.4 Conclusion

After synthesis and purification of the DCMC polymer we could produce both polymer films and powders with ion exchange ability. Increasing the specific area of the polymer (e.g. by using porous films or powders) we could increase the ion exchange rate. We have registered an increase in the maximum adsorption capacity in the polymer with higher specific area (powder form) which can be directly related with the availability of the substituent groups to react with the proteins in solution.

The Langmuir adsorption model was found to fit the experimental data for both proteins (cytc and isolated wine protein) satisfactorily in accordance with the liner correlation coefficients of the linearized data. The hypothesis that the DCMC polymer could remove positively charged proteins at pH 3.2 was validated for the two proteins in two different buffers at 25 °C. A preliminary trial using the polymer in real wine conditions showed that, although with a lower protein removal

yield compared to bentonite, this polymer can be a valid alternative to the conventional method of removing proteins from wines.

Further work must be performed to optimize the application/use of the polymer directly in wine or to use the polymer in different formats (e.g. filter membrane) increasing its contact with the proteins and, therefore, increasing its adsorption capacity.

4.3 Production of a cellulose membrane filter containing DCMC polymer for in-line filtration and removal of soluble proteins.

This work was developed in collaboration with RAIZ (Instituto de Investigação da Floresta e Papel) who provided not only paper pulp for the synthesis but also the opportunity to work at their research laboratory. I would like to acknowledge Paula Pinto (RAIZ R&D Director) for the opportunity and José Carlos for all the help producing the cellulose membranes.

I would also like to thank José Caninhas and Filipe Cardoso from Quinta do Piloto for giving the Moscatel Grapes to produce the wine used in this experiment.

4.3.1 Objective

The main objective of this work was to produce a cellulose membrane filter containing DCMC that could perform ion-exchange during a filtration process. With that in mind, the main goals are:

1) synthesize DCMC polymer staring from industrial paper pulp to reduce production cost

2) incorporate the resulting DCMC polymer in cellulose filter membranes

3) test the new cellulose/DCMC membranes in a filtration apparatus and test its ion-exchange capacity with proteins

4.3.2 Results and discussion

4.3.2.1 Polymer synthesis

To produce new DCMC polymers, paper pulp was used as starting material. Though less expensive that Avicel (microcrystalline cellulose), working with paper pulp for synthesis raises new technological challenges. Paper pulp, oppositely to pure crystalline cellulose, is composed by other components such as hemicellulose, lignin and extractives. As an example, the content of these components in bleached kraft pulps are represented in Table 21.

Table 21 - Natural composition of pine and birch wood and corresponding kraft pulps derived from them (adapted from [263])

Component	Wood component		Kraft pulp component	
	Pine (%)	Birch (%)	Pine (%)	Birch (%)
Cellulose	39	40	73	64
Hemicellulose	30	37	19	32
Lignin	27	20	6	4
Extractives	4	3	1	1

Although the carboxymethylation of hemicelluloses was already described [264], a reaction comparable to one using microcrystalline cellulose as starting material should not be expected. Other challenge of using paper pulp as starting materials relies on the physical aspect of the reaction. Paper pulp presents longer fibers with a more rigid structure and higher DP. Paper pulps can present a DP between 1590 and 4500 [265] oppositely to the cellulose used in previous chapters

which had a DP of around 400. This can induce significant differences in the rheological behaviour of the resulting polymers.

Synthesis was carried out by a standard slurry method as previously described by [210] for carboxymethylation of cellulose though using sodium bromomalonate (11) and bleached kraft paper pulp as starting materials. The condition used for the synthesis of this polymer are represented in Table 22.

Table 22 - Conditions used for the derivatization of cellulose with sodium 2-bromomalonate (**11**).

Sample	BMA: NaOH:AGU	Temp (*°C*)	Reaction time (h)	BMA (g)	NaOH (g)	Paper pulp (g)	Isopropanol (mL)	Total H_2O (%)
DCMC 12	2:1:1	60	5	5.56	0.53	2	60	8
DCMC 13	2:1.6:1	60	5	5.56	0.80	2	60	8
DCMC 14	2:2.2:1	60	5	5.56	1.06	2	60	8
DCMC 15	2:3.2:1	60	5	5.56	1.59	2	60	8

Paper pulp is also much more challenging to work at heterogenous conditions than microcrystalline cellulose since the pulp tend to clump from the beginning of the reaction which will difficult the contact of the starting materials. This is even more exacerbated if the agitation is ineffective (e.g. magnetic steerer). The final products presented a yellow to brown colour. After synthesis, the polymers were thoroughly washed with 70% methanol followed by pure methanol. After dialysis against deionized water, the polymers were freeze dried and store in a desiccator until used.

Similarly to the method described in the latter subchapter, after dialysis the DCMC polymers are white with a foam/cotton-like structure. To maintain this foam-like structure, we opted not to deprotonate the sample in the 20% H_2SO_4 solution. Instead, we opted to deprotonate the sample using HCl gas generated by the method described in literature [266]. The apparatus used to protonate the samples is represented in Figure 64.

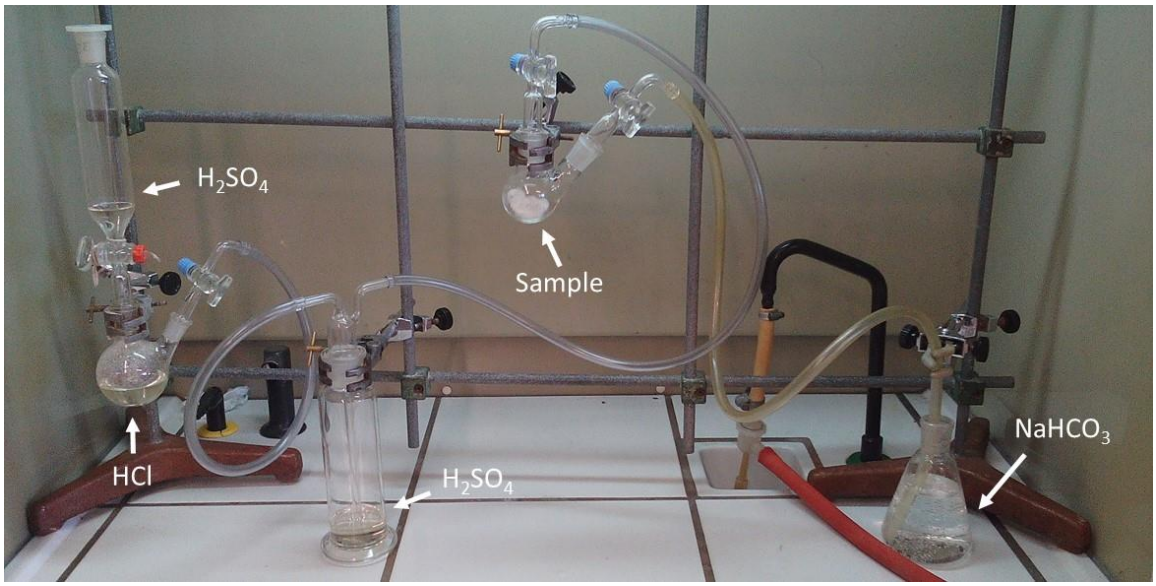

Figure 64 - Apparatus used to generate HCl gas. The dry cellulose samples were exposed to HCl gas for 30 minutes to guarantee their protonation.

A stream of HCl was passed through the sample for 30 minutes and then the sample was placed under vacuum to remove residual HCl gas. After protonation, the samples were heat crosslinked as previously described. After crosslinking, the samples were deprotonated using a saturated solution of $NaHCO_3$ for 2 hours followed by washing with deionized water to remove residual salts. A summary of the weight loss (starting from 2 g of each sample) during all synthesis steps is described in Table 23.

Table 23 - A summary of the weight loss (starting from 2 g of each sample) during the purification and crosslinking steps of DCMC polymers 12 to 15.

Sample	Mass before dialysis (g)	Mass after dialysis (g)	Mass after deprotonation with $NaHCO_3$ (g)
DCMC12	2.03	0.48	0.30
DCMC13	2.06	0.36	0.33
DCMC14	2.04	0.68	0.48
DCMC15	2.02	0.56	0.35

The DS of the different polymers (before and after crosslinking) was evaluated by ICP-AES. All samples were protonated and hydrolysed in concentrated nitric acid before analysis. The results of the ICP-AES are represented in Table 24.

Table 24 - Sodium quantification using ICP-AES and calculated degree of substitution (DS) of samples DCMC 12 to 15.

Sample	Na (mg/L)	Sample concentration (mg/mL)	Na (mg)	Na (%)	DS (calculated)
DCMC 12	121.8	2.82	0.122	4.32	0.18
DCMC 13	145.5	2.5	0.146	5.82	0.25
DCMC 14	15932	2.56	0.159	6.22	0.27
DCMC 15	76.6	2.2	0.077	3.48	0.14
DCMC 12 CL	44.6	3.74	0.045	1.19	0.04
DCMC 13 CL	55.1	3.34	0.055	1.65	0.06
DCMC 14 CL	7.49	3.44	0.007	0.22	0.01
DCMC 15 CL	108.9	3.22	0.109	3.38	0.13

Analysing the ICP results, we can see an increase in the DS with increasing NaOH concentration except for sample DCMC 15. This can be attributed to partial degradation of the polymer with high content of NaOH in the reaction mixture. A similar phenomenon was already described in a previous subchapter when producing DCMC using Avicel. After crosslinking, we can see a drastic decrease of the measured Na content and consequently in the samples DS. Once more, this can be related to a high degree of crosslinking and, therefore, a decrease in the free carboxylic groups available for ion exchange. Although there is an increase in the DS from samples 12 to 15 (except for sample 14), we cannot establish a good correlation due to the small number of samples synthesized.

All samples were analysed by FTIR-ATR after drying (Figure 65). The starting material does not present any carbonyl band as expected since there was no prior chemical modification of the cellulose. Both dialyzed and crosslinked samples show the carbonyl band resulting from the derivatization (i.e. presence of carboxylic acid groups). After deprotonation of the sample, we can see a shift of the carbonyl band result of the formation of the salt. We can see some residual signal of the carbonyl of the protonated form of the polymer that can be the result of insufficient deprotonation by the $NaHCO_3$. This can also explain some discrepancies in calculated DS of these polymers since some polymers could be partially protonated and therefore the measured Na content do not correspond to the real carboxylate groups available.

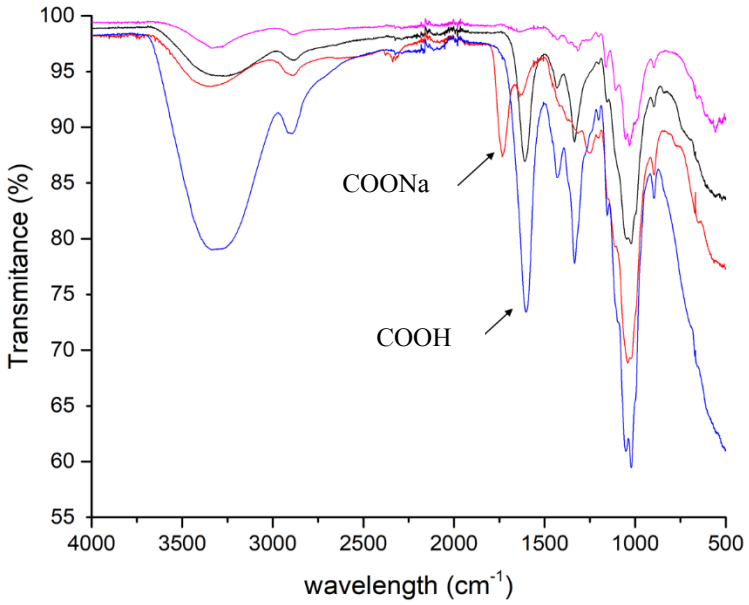

Figure 65 - FTIR-ATR spectra of Kraft pulp (-), dialyzed DCMC 13 (-), crosslinked protonated DCMC 13 (-) and crosslinked deprotonated (sodium salt) DCMC 13 (-).

4.3.2.2 Production of cellulose sheets with added DCMC

Our first objective in the production of cellulose sheets was to test the ability of these to act as filter membranes. To that, different cellulose sheets with varying paper weight were produced. These sheets were tested in a Buchner funnel do determine their resistance on water filtration. We registered that paper sheets had to have a minimum of 1 g paper/sheet to guarantee their structure after filtration of water.

To produce the filter sheets, the same kraft paper used in the synthesis of polymers DCMC 12 to 15 was used as supporting material. The polymers were added to the paper slurry (i.e. kraft pulp disintegrated in deionized water) prior to sheet making and homogenized with a propeller homogenizer. The paper pulp slurry was then processed in a pulp evaluation apparatus (Mavis Engineering LTD) to form the paper sheets. The sheets presented a diameter of 16 cm with a variable weight between 1.2 and 1.4 g depending on the quantity of paper pulp and polymer added to the slurry. An example of a sheet after drying is represented in Figure 66.

Figure 66 - Paper sheet with DCMC added at a concentration of 18% (w/w). The spots scattered along the sheet correspond to the added DCMC.

4.3.2.3 Evaluation of the ion exchange capacity of the filter sheets containing DCMC

To evaluate the ion exchange capacity of the paper sheets, the sheets were tested in a 10 mL Amicon ultrafiltration cell with a cytc solution. To fit in the cell apparatus, the filter sheets were cut to circumferences with 2.6 cm diameter. To guarantee the physical structure of the membranes, a non-modified paper filter with the same diameter was placed under the modified paper sheet. A schematic representation of the apparatus is represented in Figure 67.

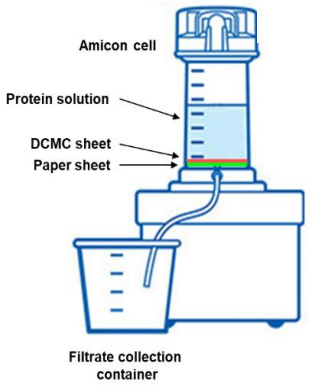

Figure 67 - Filtration apparatus used to test the DCMC sheets.

The DCMC sheets chosen to test were DCMC 12CL, 13CL and 15CL. We opted to discard DCMC 14CL due to its low DS. After assembly of the filtration apparatus with the corresponding membrane, a sequence of buffers was applied to the membrane. A summary of the several steps is described above:

5 mL H_2O

5 mL 10 mM NaOH (deprotonation of the membrane)

10 mL H_2O (or until neutral)

5 mL 25 mM citrate, pH 3.2

5 mL protein solution (Cytc at 0.4 mg/mL, 25 mM citrate pH 3.2) *

5 mL H_2O

5 mL 1M NaCl *

20 mL H_2O

5 mL 25 mM citrate, pH 3.2

5 mL protein solution (Cytc at 0.4 mg/mL, 25 mM citrate pH 3.2) *

5 mL H_2O

5 mL 1M NaCl *

** Samples gathered for posterior protein quantification.*

We must emphasize that this was a one-time trial and the quantities used of each buffer were not optimized.

Previous results showed that we could regenerate DCMC polymers using a 1M solutions of NaCl. We included two NaCl washes in the protocol to remove the adsorbed proteins for further quantification. After adding the protein solution and prior to adding NaCl we performed a washing step with deionized water to guarantee that the protein eluted with the NaCl was specifically adsorbed to the membrane.

The visual aspect of the membranes after filtration of the protein solution and washing with deionized water is represented in Figure 68. Since cytc is a heme protein it presents a distinctive red colour which helps to see if the protein is reacting with the membrane.

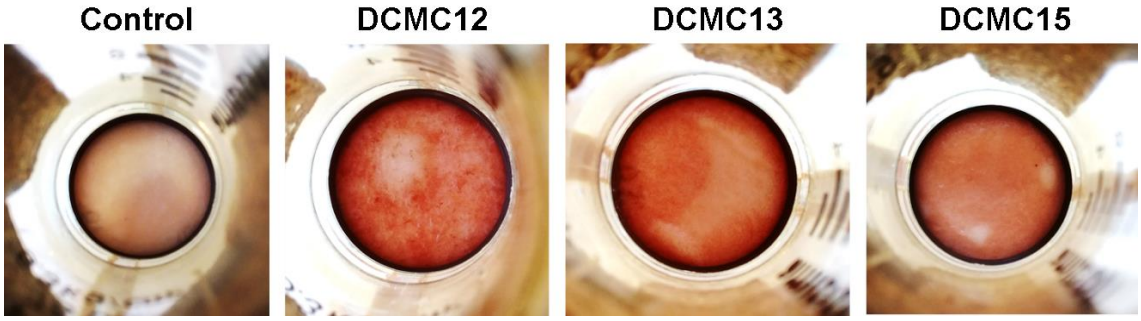

Figure 68 - Representation of the DCMC membranes after filtration of Cytc solution and washing with deionized water.

The results for the protein adsorption assay are represented in Table 25. Oppositely to the action of 100 mM NaOH on the films described in a previous sub-chapter, using 10 mM of NaOH does not disrupt the physical structure of the polymer and therefore the membranes remained intact. To evaluate the regeneration capability of the polymer, we perform two consecutive passages of protein solution in the same membranes with elution and washing steps between them.

After passing 5 mL of protein solution, the first flow-through (1st FT) was collected for protein quantification. All elutions (between membranes DCMC 12CL to 15CL) were timed giving a value of 26 s ± 2 s (for 5 mL of protein solution). This allowed to calculate an average flowrate of 11.1 ± 0.4 mL/min. Since we did not apply any pressure on the filtration apparatus we could not control the flow rate of the trial. Nevertheless, based on the times gathered during the assay, the flow rate was fairly constant.

As shown in Table 25, there are significant differences between samples. As expected, the control membrane did not adsorb any quantifiable protein. Membrane 12CL and 15CL showed 57.6 and 90.6 mg protein/g cellulose of protein adsorption capacity. Based on the calculated DS of the crosslinked polymers, it was to except a higher adsorption capacity on polymer 15 since it has a higher number of free carboxylate groups available to react with the protein. Polymer 13CL showed a very low adsorption capacity compared to the other two in the 1st FT.

Table 25 – Protein adsorption capacity calculations for polymers DCMC 12CL, 13CL and 15CL. Each membrane was tested in duplicate.

Membrane	**Control**	**DCMC 12CL**	**DCMC 13CL**	**DCMC 15CL**
Mass of membrane (g)	1.455	1.5522	1.4332	1.5289
Mass of polymer (g)	0	0.265	0.185	0.262
% polymer in membrane	0	17.1	12.9	17.1
Average mass of filters (mg)	44.55	41.95	39.95	42.8
Total area in cm^2 (2.6 cm ⦸)	5.31	5.31	5.31	5.31
Paper weight (mg/cm^2)	8.4	7.9	7.5	8.1
Usable area in cm^2 (2.2 cm ⦸)	3.79	3.79	3.79	3.79
Mass of filter (2.2 cm ⦸, mg)	31.8	30	28.5	30.6
mass of polymer in filter (mg)	0	5.1	3.7	5.2
Starting protein mass (mg)	2	2	2	2
Protein mass 1st FT (mg)	1.953	1.706	1.991	1.526
Adsorbed protein (mg)	0.047 ± 0.01	0.294 ± 0.05	0.009 ± 0.1	0.474 ± 0.03
Adsorption capacity (mg protein/g polymer)	**0**	**57.6 ± 10.0**	**2.5 ± 0.4**	**90.6 ± 6.9**
Starting protein mass (mg)	2	2	2	2
Protein mass 2nd FT (mg)	1.901	1.535	1.756	1.454
Adsorbed protein (mg)	0.10 ± 0.02	0.465 ± 0.04	0.244 ± 0.05	0.546 ± 0.04
Adsorption capacity (mg protein/g polymer)	**0**	**90.9 ± 9.8**	**66.2 ± 13.2**	**104.2 ± 8.4**

In Figure 68 we can see that there are white spots in scattered in the membranes. For DCMC 12CL and 15CL these spots were probably caused by the heterogeneous distribution of the polymer along the membrane. In DCMC 13CL we can see a significant white marc in the middle of the membrane that was caused by the presence of air between the membrane and the paper filter. When using a multi-layer system, air must be removed from the middle of the membranes to avoid channelling of the liquid between the membranes. This can justify the very low protein adsorption of this membrane in the 1st FT. Before filtering more protein stock solution, the membranes were washed and negative pressure was applied by pulling the liquid with a syringe. This way the two layers of filter membranes stuck together avoiding the formation of preferential channels in the second filtration.

After elution and washing of the membranes, new protein stock solution was filtered. The second flow-through (2nd FT) was collected for protein quantification similarly to 1st FT. We registered the values of 90.9 mg/g, 66.2 mg/g and 104.2 mg/g of protein adsorption capacity for polymers

12CL to 15CL respectively. We can see an increment of protein adsorption capacity of 33.3 mg/g in DCMC 12CL, 63.7 mg/g in DCMC 13CL and 13.64 mg/g in DCMC 15CL. Due to channelling in DCMC 13CL this data is not relevant. However, for polymer 12CL and 15CL, we can not only validate the regeneration of the polymer by washing with NaCl but also register an increase of the polymer protein adsorption capacity. This phenomenon can be related to several factors like: 1) decrease in the channelling by the action of negative pressure applied during the washing steps, 2) better hydration of the membranes which will cause the swelling of the membrane and consequently increase of the specific area, 3) higher deprotonation of the polymer by washing with a concentrated NaCl solution. All calculations of the final protein adsorption capacity were performed considering a membrane internal diameter of 2.2 cm instead of 2.6 cm since the O-ring of the apparatus partially blocked the membrane availability to filter.

4.3.2.4 Removal of soluble proteins from wine with cellulose/DCMC membrane

As a preliminary trial, 10 mL of a Moscatel of Alexandria from Quinta do Piloto (2016 vintage) was filtered in the same Amicon apparatus using two 2.6 cm of diameter consecutive sheets of DCMC 15CL. The protein was quantified previous to filtration and after filtration to access the protein removed by this operation. The results from the filtration operation are described in Table 26. Though the resulting wine after filtration was not protein stable (measured by a heat stability test), the removal of proteins from wine in a condition like the ones found winery (direct filtration of the wine with just one flow-though, no buffers, no pH adjustment) showed that this technology can be used to remove soluble proteins from wine and consequently stabilize it. In this case, the wine was not completely stable though this was caused by the high protein content of the wine even after filtration.

Optimization of this technology can lead to the production of membrane filters containing DCMC for the removal of soluble protein from wines in an in-line system like the ones already used in a normal winery. Other technology that uses this single-step stabilization and clarification goal is Oenofine XL filtration system (PALL). Bentonite is dosed upstream of the hollow fibers polyvinylidene difluoride (PVDF) membranes which allows to clarify and stabilize the wine at the same time. Though, the inconvenient of using bentonite continues present. If optimized, our technology will allow the clarification and stabilization of wines in a single-step without using any bentonite or other additive.

Table 26 – Protein adsorption capacity calculation of polymer DCMC15CL (incorporated in cellulose sheets) after filtering 10 mL of Moscatel of Alexandria wine. In this trial, two sheets of 2.6 cm of diameter

were used. Both starting and final protein concentration were measured directly in the wine prior and after filtration by the Bradford method.

Membrane	**DCMC 15CL**
% polymer in membrane	17.1
Mass of filters (mg)	90.1
Total area in cm^2 (2 x 2.6 cm ⦸)	10.6
Paper weight (mg/cm^2)	8.1
Usable area in cm^2 (2 x 2.2 cm ⦸)	7.6
Mass of filter (2 x 2.2 cm ⦸, mg)	61
Mass of polymer in filter (mg)	10.4
Starting protein concentration (mg/L)	186
Final protein concentration (mg/L)	86
Adsorbed protein (mg)	1
Adsorption capacity (mg protein/g polymer)	**96.15**

4.3.3 Conclusions

We have produced cellulose sheets with dicarboxymethylcellulose polymers presenting different degree of substitution added to its structure. The resulting sheets were structurally resistant to water passage and filtration trials were performed. After adaptation of the cellulose sheets to a filtration apparatus, we could quantify the adsorption of cytc model solutions at pH 3.2 after filtration. These sheets contained between 12.9 and 17.1% of DCMC polymer and showed maximum adsorption capacities between 2.5 and 104.2 mg protein per g of polymer.

Direct filtration of wine using cellulose sheets added of DCMC polymer allowed to remove soluble wine proteins from solution and partially stabilize the resulting wine. After protein quantification on the original and filtered wine, we were able to calculate a maximum adsorption capacity of 96.2 mg wine protein/ g polymer on sheets with DCMC15 polymer.

These trials validated that DCMC can be used in a filter/membrane form to remove soluble, positive proteins at pH 3.2. The scale-up of this technology can be the first step to produce a new generation of plate filters for the in-line clarification and protein stabilization of wines. Using our polymer as an in-line filter, producers could skip the application of a stabilizing additive (i.e. bentonite), do less wine manipulations (e.g. less wine passage and consequently less opportunity

for oxidation), produce less lees and stabilize the wine at the same time as solids in suspension are removed.

5. General conclusions

The work presented in this thesis is based on the necessity to understand two different phenomena: 1) how do proteins aggregate in a wine after heat exposure, and 2) how can we avoid these proteins to aggregate and produce haze without significant intervention in the wine. Based on these broad queries, we went farther and attempted to answer several related but more specific questions:

Which wine compounds (either from grapes or artificially added) can induce or modulate protein aggregation upon heat stress?

How do these compounds interact with wine proteins upon heat stress?

Are we able to remove these compounds from the wine, thus avoiding the removal of protein using bentonite?

If we cannot remove the compounds that interact with wine proteins, can we remove the proteins using a lower impact alternative methodology?

Different works available in the literature identified a multifactorial system with an absolute requirement for some molecules, other than the protein themselves, which induce wine proteins to aggregate upon heat stress. We started by assessing which compounds were bound to proteins after these aggregation and precipitation processes. We found that the major compound present in the precipitate other that aggregated protein was caffeic acid. This compound occurs normally in wine both in free form (i.e. caffeic acid) or as an ester of tartaric acid (i.e. caftaric acid). Caftaric acid was therefore synthesized in our laboratories. After testing both species with isolated wine protein in wine model solution, we registered that none of these compounds no induced haze after a heat stress. Based on the possible redox reactions involving this type of compounds (ortodiphenols) and proteins, we changed the standard, extensively described in the literature model wine solution (5 g/L tartaric acid, 12% v/v ethanol and pH adjusted to 3.2) for another wine model, closer to what happens under real wine conditions. The new proposed model wine solution comprises the same components of the standard model wine solution, plus the addition of sulfur dioxide (SO_2), an almost ubiquitous additive used in winemaking. This compound is not only an antiseptic, but also antioxidant and a well-known reducer compound.

After adding SO_2 to wine proteins, we could register that this induces cleavage of wine intraprotein disulfide bonds and promotes protein aggregation. This reaction is greatly exacerbated by the high temperature-induced unfold of the proteins, whose exposed hydrophobic surfaces and buried cysteine residues further contribute to enhance subsequent interprotein

interactions. After disulfide bond cleavage, HSO_3^- blocks transiently sulfhydryl groups in a process known as protein sulfitolysis, which will allow the interaction of the thiol-disulfide groups with other sulfhydryl groups present in the same or in a different protein molecule, leading to formation of novel intra- and interprotein disulfide bonds. The latter are ultimately responsible for wine protein aggregation following a nucleation-growth kinetic model. The action of SO_2 in wine proteins was tested in different isolated protein fractions and thaumatin-like proteins were identified not only as the major protein fraction in Moscatel wine but also the most susceptible to aggregate after heat exposure in the presence of SO_2.

We could detect that the major forces contributing for wine thaumatin aggregation in the presence of SO_2 result from a combination of hydrophobic interactions with covalent interactions by 'disulfide bridge scrambling' among protein molecules. These proteins (TLPs) are known to have a high content of cysteines and disulfide bonds (e.g. some wine thaumatins have 16 Cys and 8 disulfide bonds) which is crucial aspect on this particular mechanism. The analysis of the secondary structure of the protein confirmed that the conformation of the unstable proteins with and without SO_2 is different after heat stress. It also allowed to detect severe changes in the disulfide bridges of the protein, indicating the formation of wrong/different pattern of disulfide bridges not only inter but also intramolecular. Upon cooling, the incorrect refolding of the proteins will then contribute to exposure of protein hydrophobic pockets, which can intensify the interaction with other 'improperly refolded proteins', as well as with other wine constituents, such as polyphenols. This phenomenon could explain the binding of caffeic acid to the hydrophobic pockets of the protein after heat-unfolding and cooling in the presence of SO_2.

The chemical mechanism underlying the interaction of wine proteins with sulfur dioxide was further studied and it may constitute the most common mechanism occurring in protein-unstable commercial wines containing added sulfur dioxide. Albeit the supposedly essential participation of SO_2 in wine protein aggregation, this phenomenon continues to be likely wine-dependent and may be modulated by the wine matrix itself. The intricate and variable molecular complexity of wines certainly holds several effectors which act either positively or negatively on wine protein haze formation. There is still the need to understand the behaviour of sulfur dioxide (in its different forms, i.e. free SO_2 and combined SO_2) with other grape varieties (other than Moscatel), and evaluate its action when the composition of the wine in proteins is different. Other parameters like vinification type and conditions (e.g. more of less extraction of grape skin compounds, fermentation temperature, wood maturation, lees contact time during maturation) can also have noticeable influence in the resulting stability of a white wine. Understand the impact of these diverse factors on protein stability can be a great tool for a winemaker.

Besides the great effort of several research teams to find a viable alternative to sulfur dioxide, this additive is almost ubiquitous in winemaking. Protein haze formation cannot be resolved by

removing or significantly decreasing the total sulfur dioxide content unless a different preservative/antioxidant is introduced in the market. The solution to this technological problem still resides in the removal of the unstable soluble proteins by bentonite or by other substance to avoid their undesirable precipitation in the bottle.

With the aim of obtaining a new processing aid for the removal of soluble proteins from wine, we design a new polymer capable of being used by the food industry. Our goal to use sustainable and renewable materials was achieved using cellulose as starting material.

We synthesized a new cross-linked dicarboxymethylcellulose polymer capable of performing cation exchange at the pH normally found in wines (i.e. between 3.2 and 3.6). The dicarboxymethylcellulose (DCMC) molecule has already been synthesized and described in the literature though is structural analysis and performance as an ion exchanger were not investigated in-depth.

After synthesizing dicarboxymethylcellulose using Avicel as starting material, this was structurally studied using different techniques including NMR, HPLC, FTIR, XRD, among others. After optimization of the synthesis reaction and purification of the resulting polymers, we could achieve polymers with different degrees of substitution (i.e. between 0.18 and 0.62), different degree of polymerization (dependent of the base concentration in the reaction) and different rheological behaviour (viscosity). These polymers were cross-linked, and its ion exchange capacity tested both with cytc and isolated wine protein in mode wine solution. Using the polymer in powder form, we achieve a maximum adsorption capacity of 1250 mg protein/g polymer for isolated wine protein and 588 mg protein /g polymer for cytc. Using real wine with the DCMC powder, we could achieve a maximum adsorption capacity of 270 mg protein /g polymer.

Since our main objective was to use this polymer as a processing aid and not as an, we developed cellulose membranes added of DCMC that could filter wine and simultaneously remove positively charged proteins. DCMC synthesized from paper pulp was added to cellulose pulp and new composite cross-linked DCMC-cellulose filter membranes (comprising between 12 and 17% w/w of cross-linked DCMC) were casted. These membranes were tested in a filtration apparatus and cation exchange capacity was evaluated using cytc in a buffer solution. The membrane maximum adsorption capacity was around 104 mg protein /g polymer using direct filtration without added pressure. Filtration of real wine using the same membranes revealed a maximum adsorption capacity of 96.1 mg proteins / g polymer.

This preliminary study showed that cross-linked DCMC can be an effective polymer for the adsorption and removal of soluble wine proteins and can be adapted to an in-line technology turn in a possible processing aid usable in winemaking. Further work should be performed to optimize

reaction conditions for posterior scaling-up. Other relevant future work perspectives include increasing the polymer content in the composite membranes, using alternative starting materials to increase reaction yield and the production of plate filters capable of being adapted onto already available industrial filtration apparatus. If possible to adapt these membranes to an industrial environment, these have great characteristics like: 1) they use a sustainable and renewable starting material, cellulose; 2) the membranes are reusable after regeneration using mild conditions (such as, for example, high ionic strength or weak base solutions); 3) the polymer is recyclable and possibly biodegradable; 4) the polymer can be used as a processing aid (filter, film or powder); 5) the polymer has an "all-organic" structure (based on the introduction of carboxylic acids in the cellulose AGU) oppositely to other OIV allowed ion exchange resins. With further research, the cross-linked DCMC filters can be a viable bentonite alternative in a short to medium term.

6. Experimental

6.1 Reagents and standards

Caffeic acid (HPLC standard), trifluoroacetic acid (TFA; HPLC grade), polyvinylpolypyrrolidone (PVPP), methanol, benzene and sulfuric acid (96%) were purchased from Sigma-Aldrich (USA). Sodium hydroxide, hydrochloric acid and sodium chloride were obtained from Panreac (Spain). L-Ascorbic acid, ethylenediaminetetraacetic acid (disodium salt; EDTA), sodium citrate and citric acid were obtained from Merck (EMD Millipore Corporation, USA). Acetonitrile (HPLC grade) was obtained from JTBaker (USA). Ethyl acetate was obtained from BDH Chemicals (VWR international, USA). Sodium hydrogen sulfite, sodium citrate, citric acid, ammonium sulfate and potassium phosphate were acquired from Merck (EMD Millipore Corporation, USA). Poly(vinylpolypyrrolidone) (PVPP) was purchased from Sigma-Aldrich.

6.2 Equipment

Fluorescence spectra were recorded on a SPEX Fluorolog-3 Model FL3-22 spectrofluorimeter, with an excitation wavelength of 290 nm. Dynamic light scattering experiments were conducted on a Horiba SZ-100 Nanoparticle analyzer. Chromatographic analyses were carried out using a Waters Alliance HPLC (Waters Corp., Milford, MA, USA) equipped with an auto-injector (Waters 717plus), a column thermo-regulator and a photodiode array detector (Waters 2996). NMR experiments were recorded on a Bruker AMX400 and a Bruker Avance 400 MHz spectrometer in the adequate deuterated solvent. The acquired spectra were treated in MestreNova. Protein purification was performed in a ÄKTA Pure system (GE Healthcare). Circular dichroism analysis was performed in a Chirascan qCD (Applied Photophysics Ltd., Surrey, UK). ICP-AES (inductively coupled plasma-atomic emission spectrometer) was performed using a Horiba Jobin-Yvon Ultima model equipped with a 40.68 MHz RF generator, a Czerny–Turner monochromator with 1.00 m (sequential) and an autosampler AS500. Intrinsic viscosity was measured in a Micro Ostwald viscometer (Type I). SEC measurements of the DCMC polymers were carried out with a JASCO equipment (RI 930 detector, PU 980 pump, SUPREMA 1000 column). Infrared spectra were recorded on a Perkin-Elmer Spectrum One 1600 FT-IR spectrometer or a Perkin-Elmer Spectrum Two FT-IR spectrometer, equipped with a Perkin-Elmer Universal ATR Sampler Accessory.

6.3 Biological materials

The wine used in the experiments described in Section 3.1 was a varietal Moscatel of Alexandria white wine, 2009 vintage, from Instituto Superior de Agronomia, Portugal. The grapes were hand harvested in September 2009, pressed and the free running juice fermented in stainless steel tanks. No malolactic fermentation took place. The resulting wine had an alcohol content of 14.3% (v/v), 5.6 g/L total acidity (expressed as tartaric acid), 0.33 g/L of volatile acidity (expressed as acetic acid), pH 3.2, 25 mg/L free SO_2, 140 mg/L total SO_2 and 190 mg/L total protein (measured by a modification of the Lowry method described by [267]). The wine was divided into 100 mL aliquots and stored frozen at -20 ºC until used.

The wine used in the experiment described in Section 3.3 (first protein isolation) was a varietal Moscatel of Alexandria white wine, 2010 vintage, from Instituto Superior de Agronomia, Lisbon, Portugal. The grapes were hand harvested in September 2010, pressed and the free running juice fermented in inox tanks at controlled temperature. No malolactic fermentation took place. The resulting wine had an alcohol content of 13% (v/v), pH 3.2 and 80 mg/L total protein. The wine was divided into 100 mL aliquots and stored frozen at -20 ºC until used.

The wines used in the experiment described in Section 3.3 (second protein isolation) were from the varieties Moscatel of Alexandria and Moscatel Galego, 2014 vintage, from Instituto Superior de Agronomia, Lisbon, Portugal. The grapes were hand harvested in August 2014, pressed by hand and the free running juice fermented in 2.5 L vats at 25 ºC. Where appropriate, SO_2 was applied during pressing (47 mg/L $NaHSO_3$) and at the end of fermentation (140 mg/L $NaHSO_3$). After fermentation, all wines were divided into 100 mL aliquots and stored frozen at -20 ºC until used. No malolactic fermentation took place.

The used model wine solution (MWS) consist of 12% (v/v) ethanol, 5 g/L tartaric acid and pH adjusted to 3.2. We have considered a ratio of 100 mg L^{-1} of protein for 120 mg L^{-1} of total SO_2 has a concentration like what is found in some wines. This ratio was used in the spectrofluorimeter trial though for the remaining trails we had to increase the protein concentration to increase its signal. For that, we increased both protein and SO_2 by 5-fold to a protein final concentration of 500 mg L^{-1} and a total SO_2 final concentration of 600 mg L^{-1}. In all trials SO_2 was added as $NaHSO_3$ which yields SO_2 at a percentage of 64% (Merck).

For the synthesis of the DCMC membranes with paper pulp, we used bleached kraft paper pulp from *Eucalyptus globulus* from RAIZ.

The wine used for the protein adsorption trials using the DCMC membranes was done from Moscatel of Alexandria grapes from Quinta do Piloto, vintage 2016, in our laboratory.

6.4 Dynamic Light Scattering (DLS)

The DLS equipment determines the size of colloidal particles in the range between 0.8 nm and 8 μm. A diode-pumped solid-state laser (DPSS) 532 nm, 10 mW Class I laser was used as the light source. Autocorrelation curves were acquired with low 'noise' and were analysed by the equipment software, which enables retrieval of the particle average hydrodynamic diameter (Z) and polydispersity assuming the Stokes-Einstein equation is followed. All samples were filtered prior to preparation and all glassware used was washed with filtered Millipore water to avoid any type of dust contamination. Experimental autocorrelation curves could be obtained acquiring the signal for 15 s. In this work, in the time-dependent DLS experiment, 30 s of acquisition time was selected, rendering 'noiseless' autocorrelation curves. The geometry applied was 90º and a Peltier system was employed for temperature control. Size distribution analysis was carried out with the software provided by the equipment manufacturer. To avoid unnecessary data interpretation, the intensity frequency of the size distributions was selected.

6.5 Sulfur dioxide quantification

Free and total sulfur dioxide were quantified using the method OIV-MA-AS323-04B described in the "Compendium of international methods of analysis", published in 2009 by the International Organization of Vine and Wine (OIV). Briefly, free sulfur dioxide was determined by direct titration with iodine. Combined sulfur dioxide was subsequently determined by iodometric titration after alkaline hydrolysis. The sum of free and combined SO_2 values gave the total sulfur dioxide content of the sample.

Sulfite corrections were performed by addition of $NaHSO_3$, which yields SO_2 at a percentage of 64% (Merck).

6.6 Protein instability test

Evaluation of the wine susceptibility to form protein haze was performed according to a published protein instability test [268] with minor modifications. Five mL samples were sealed in test tubes with screw caps and heated at 80 °C for 2 h in a water bath, followed by cooling in ice for 2 h. After allowing the samples to warm to 25 °C, the increase in turbidity was detected spectrophotometrically at 540 nm in 1 mL plastic cuvettes. Differences in wine turbidity (before and after the heat treatment) have been shown to correlate directly to wine protein instability [85].

All measurements were performed in triplicate for posterior statistical analysis. In practical terms, a wine is considered unstable when the difference in absorbance between heated and unheated controls is greater than 0.02 absorbance units [269].

6.7 Protein haze sediment isolation

The sediment was isolated from 5 L of wine since previous studies involving lower volumes revealed to be insufficient due to the small quantity of the extracted compounds, which is incompatible with the minimum quantity required for NMR analysis.

Following heat induction of protein haze formation in 5 L of experimental white wine, the sample was centrifuged, and the supernatant discarded. The sediment was washed thoroughly with Milli-Q water to eliminate unbound compounds, frozen at -80 ºC and freeze-dried. This precipitate consisted in tiny granulated pale-yellow to brown particles. The dried sediment had a mass of 419 mg, which accounts for approximately 0.008% (w/w) of the starting wine.

6.8 Alkaline hydrolysis of wine protein sediments

The method described by [270] was followed with some modifications. The dried residue obtained after inducing protein haze in 5 L of the experimental wine was dissolved in 5 mL of distilled water and mixed in a vortex for 5 min. The sample was then submitted to alkaline hydrolysis in a dry bath at 50 °C for 30 min in 2 M NaOH, 10 mM EDTA, and 1% (w/v) L-ascorbic acid in a final volume of 15 mL. At the end of the incubation period, the pH was brought at 3.0 with 2 M HCl. Sodium chloride was added to the solution until saturation and the sample was extracted four times with ethyl acetate (4 volumes). After each extraction, the sample was centrifuged (3,000 *g*, 5 min), and the supernatants were collected. The organic phase was dried in a rotary evaporator at 40 ºC. The resulting residue was dissolved in a final volume of 1 mL methanol; then, 1 mL of MilliQ water was added, followed by 5 min mixing in the vortex. The sample was filtered through a 0.22 µm nylon filter prior to RP-HPLC-DAD analysis.

6.9 RP-HPLC-DAD instrumentation

The chromatographic separation was carried out in an analytical pentafluorophenyl (PFP) column (Luna PFP (2), 4.6 id x 250 mm, 5 µm, Phenomenex) at 35 ºC. The mobile phases were (A) 0.1% (w/v) TFA and (B) acetonitrile. The gradient was linear at a flow rate of 1 mL/min from 0 - 30% B for 40 min, 30 – 70% B for 20 min, 70 – 100% B for 5 min, and 100% B for 10 min, followed by re-equilibration of the column in A for 5 min. Diode array detection was performed from 190

to 400 nm. For the separation of compounds for subsequent structure identification, a semi-preparative PFP column (Luna PFP (2), 10 id x 250 mm, 5 µm, Phenomenex) at 35 ºC was used. The compounds were identified by comparing their UV-vis spectra with published data (Pereira et al. 2010) and by ^{1}H NMR.

Protein isolation by cation exchange chromatography (SCX)

For the isolation of the wine total protein, the method described by [14] was used with some modifications. The wine sample was adjusted to pH 3.0 with HCl and treated with 30 g/L PVPP overnight at 4 ºC. The wine was vacuum filtered through three layers of Miracloth (Merck) and then through 0.45 µm and 0.2 µm polyethersulfone (PES) filter. All chromatographic steps were executed at room temperature. Using an AKTA Pure pump (Amersham Biosciences), filtered wine was loaded at 6 mL/min on a cation exchange column (RESOURCE S, 6 mL bed volume, Amersham Biosciences) previously equilibrated with 30 mM sodium citrate, pH 3.0. The column was then connected to an AKTA Pure chromatography system with UV detector (Amersham Biosciences) and washed at 6 mL/min with 100 mL of 30 mM sodium citrate, pH 3.0. Bound proteins were eluted at 6 mL/min with 30 mM sodium citrate containing 1 M NaCl, pH 3.0 (buffer B) using the following gradient: 0 min, 0% B; 25 min, 100% B and held. The protein fraction was collected and desalted into water twice on gel filtration columns (PD-10, GE Healthcare), lyophilized and stored at -20 ºC.

6.10 Separation of isolated wine proteins by hydrophobic interaction chromatography (HIC)

The proteins isolated by SCX were further separated by HIC. Before use, the sample was thawed and dissolved in 50 mM sodium citrate containing 1.25 M ammonium sulfate, pH 3.0, and loaded on a Phenyl Superose HR 5/5 HIC column (GE Healthcare). After each injection, the column was washed with 6 mL of 50 mM sodium citrate, pH 3.0, containing 1.7 M ammonium sulfate and bound proteins were eluted at 0.5 mL/min with a 30 mL gradient to 50 mM sodium citrate, pH 3.0. Fractions were pooled based on absorption profiles at 280 nm, desalted in PD-10 columns, lyophilized and stored at -20 °C until use.

6.11 Size Exclusion Chromatography (SEC)

The size exclusion chromatography (SEC) protocol was as follows. Fifty µg of protein (with or without heat stress; Table 1) was fractionated using a Superose 12 10/300 GL column (GE Healthcare) at 25 °C. The mobile phase consisted of 8 M urea, 150 mM NaCl, 50 mM sodium citrate, pH 3 at a flow rate of 0.5 mL/min. Running time was 40 min and UV detection at 280 nm

was used to monitor the elution profile. The calibration curve was performed using blue dextran, ferritin type 1, bovine serum albumin and cytc as standards (all from Sigma Aldrich).

6.12 Synthetic route for caftaric acid (6)

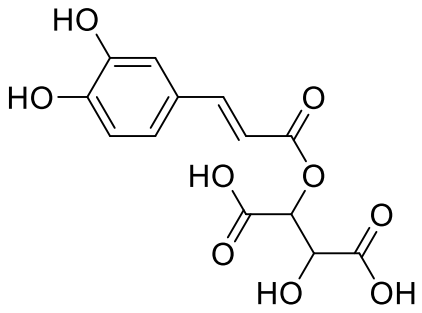

6

Caftaric acid was synthesised by the route described in Figure 7. The di-TBDMS ether of caffeic acid was prepared by the methods of [136] and [271] with some modifications. Briefly, caffeic acid (300 mg, 1.67 mmol) in dry CH_2Cl_2 (8 mL) at room temperature under N_2 was reacted with TBDMSCl (878 mg, 5.83 mmol), Et_3N (1.5 mL, 10.76 mmol) and DMAP (20.34 mg, 166 μmol) overnight. The crude product (870 mg) was obtained as a white precipitate which was dried in a rotary evaporator. The crude trisilyl ether (870 mg, 1.66 mmol) was dissolved in 1:1 MeOH/H_2O (14 mL) and treated with K_2CO_3 (230 mg, 1.66 mmol) at room temperature for 3 h. The resulting product was used crude (one spot by TLC) in the following step. Compound 5 was prepared based on the method of Capone et al. (2012) using dimethyl L-tartrate (4) instead of diethyl L-tartrate. Crude disilyl ether (227 mg, 557 μmol), dimethyl tartrate (268 mg, 1.5 mmol), *N,N*-dicyclohexylcarbodiimide (DCC; 138 mg, 668 μmol) and 4-dimethylaminopyridine (DMAP; 34 mg, 278 μmol) in CH_2Cl_2 (8 mL) were stirred overnight at room temperature. Caftaric acid was obtained after cleaving the silyl ethers and hydrolysing the methyl esters. Compound 5 (214 mg, 0.3 mmol) was dissolved in dry THF under N_2 and the flask was cooled in ice prior to the next step. TBAF (294 mg, 1.1 mL of 1M TBAF in dry THF) was added to the solution and after 5 min the reaction was raised to room temperature. The resulting solution was dried by evaporation in a rotary evaporator and the crude was dissolved in EtOAc and washed with saturated NaCl solution (3 x 10 mL). The organic phase was dried (Na_2SO_4) and concentrated in vacuum. LiOH (44 mg, 1.0 mmol) and 3:1 MeOH/H_2O (1.9 mL) were added to the residue, and the solution was stirred at room temperature for 3 h. The methanol was removed in vacuum, and water (2 mL) was added. The solution was acidified with HCl 1 M to pH 1, saturated with NaCl and extracted with EtOAc (6 × 5 mL). The combined organic extracts were dried ($MgSO_4$) and concentrated under vacuum to give an orange-brown gum. The extract was further fractionated by HPLC and the resulting

fractions analysed by NMR. The fraction containing pure caftaric acid presented the following spectra: ^{1}H NMR (400 MHz, methanol-d4) δ 7.68 (d, *J* = 16.0 Hz, 1H), 7.08 (d, *J* = 2.1 Hz, 1H), 6.99 (dd, *J* = 8.2, 2.1 Hz, 1H), 6.80 (d, *J* = 8.2 Hz, 1H), 6.34 (d, *J* = 15.9 Hz, 1H), 5.56 (d, *J* = 2.4 Hz, 1H), 4.77 (d, *J* = 2.4 Hz, 1H). This characterization is in accordance with previously published data [272].

6.13 Analysis of the protein secondary structure by Circular Dichroism (CD)

Circular dichroism (CD) spectra were recorded in the far UV region between 190 and 320 nm, bandwidth of 1 nm, three scans per temperature point with a 0.02 cm path-length quartz cylindrical cell (Helma UK Ltd) using protein concentrations of 0.5 mg/mL. The temperature was adjusted by a TC 125 temperature controller (Quantum Northwest) coupled to the CD equipment. To minimize the interference of tartaric acid in CD spectra, the optically inactive *meso* form of tartaric acid was used. The model solution used in CD trials presented the following composition: 5 g/L *meso*-tartaric acid, 12% (v/v) ethanol, pH 3.2 adjusted with NaOH.

6.14 Fluorescence spectroscopy

All spectra were corrected with correction functions provided by the supplier following standard procedures. To allow reproducibility, all measurements were performed in the same experimental session. Emission spectra of tryptophan in 0.1 M phosphate buffer pH 7 was also recorded as a function of temperature to ensure correct experimental conditions. To guarantee reproducibility, measurements were performed in triplicate with different protein samples.

6.15 Statistical analysis

All data are expressed as mean ± standard deviation (n = 3). Statistical comparisons between values were established with univariate analysis and Tukey's post-hoc test (p = 0.05) using SPSS software (IBM SPSS Statistics Version 20).

6.16 DTNB assay

Since there was the need to solubilize the protein aggregates to perform the DTNB assay, the buffers used in the standard method were adapted. Based on the ability of buffer A and B to dissolve the protein aggregates, Buffer D and E that consist in two denaturant buffers with pH 8

to be compatible with the DTNB assay were included. All samples were treated equal except the heat stressed samples that were subjected to a heat test prior to the DTNB assay.

A summary of the modification of the DTNB trial is further described:

6.16.1 DTBN assay of protein without heat stress

Isolated wine protein (H4 from HIC, Figure 1B) was dissolved in water at a concentration of 50 µM. To 250 µL of protein solution, 250 µL of Buffer D (Tris-HCl 200 mM, SDS 4% w/v, pH 8) were added, for a protein final concentration of 25 µM. Samples to be reduced were added of 0.88 µL of 2-mercaptoethanol. After equilibration for 1 h at 25 °C, proteins were precipitated by adding trichloroacetic acid (TCA) to a final concentration of 10% (w/v). The sample was incubated on ice for 30 min, followed by centrifugation for 2 min at 6700 *g* and the pellet washed twice with cold acetone to remove traces of TCA. The pellet was suspended in 350 µL of Buffer E (Tris-HCl 200 mM, urea 8 M, pH 8) and equilibrated at 25 °C for 5 min. To each reduced sample, 0.88 µL of 2-mercaptoethanol were added.

6.16.2 DTNB assay of heat stressed protein

Isolated wine protein (H4 from HIC, Figure S1B) was dissolved in water at a concentration of 50 µM. To 250 µL of protein solution, 250 µL of Buffer C (tartaric acid 10 g/L, ethanol 24%, pH 3.2) were added, for a protein final concentration of 25 µM and a concentration of tartaric acid and ethanol equivalent to a wine model solution (tartaric acid 5 g/L ethanol 12% (w/v)). To samples 'with SO_2', 2.34 µL of a $NaHSO_3$ 100 mg/mL solution were added, for a final concentration of 300 mg/L total SO_2). The samples were then subjected to a heat stability test followed by dilution with 500 µL of Buffer D. 0.88 µL of 2-mercaptoethanol were added to samples to be reduced. After equilibration for 1 h at 25 °C, proteins were precipitated by adding TCA to a final concentration of 10% (w/v). The sample was incubated on ice for 30 min, centrifuged 2 minutes at 6700 *g* and the pellet washed twice with cold acetone to remove traces of TCA. The pellet was suspended in 350 µL of Buffer E (Tris-HCl 200 mM, urea 8 M, pH 8) and equilibrated at 25 °C for 5 min.

The DTNB assay was performed applying 100 µL of sample per well in a 96 well microplate followed by 100 µL of Buffer E and 1.33 µL of DTNB solution (3.96 mg/mL). The plate was shaken, and after 10 min incubation at 25 °C, absorbance at 412 nm was read. A summary of the trial is represented in Table 27.

Table 27 - Detailed description of the DTNB method used for the quantification of the free thiol groups in the different protein species.

Native	Native reduced	HST	HST reduced	HST SO_2	HST SO_2 reduced
250 µL Protein (50 uM) 250 µL Buffer D	250 µL Protein (50 uM) 250 µL Buffer D 0.88 µL 2ME solution	250 µL Protein (50 uM) 250 µL Buffer C	250 µL Protein (50 uM) 250 µL Buffer C	250 µL Protein (50 uM) 250 µL Buffer C 2.34 µL $NaHSO_3$ (100 mg/mL)	250 µL Protein (50 uM) 250 µL Buffer C 2.34 µL $NaHSO_3$ (100 mg/mL)
		↓ HST	↓ HST	↓ HST	↓ HST
		Add 500 µL Buffer A	Add 500 µL Buffer D Add 1.76 µL 2 ME (final concentration 25 mM)	Add 500 µL Buffer D	Add 500 µL Buffer D Add 1.76 µL 2ME (Final concentration 25 mM)
wait 1 hour					
Add TCA (final concentration 10%) 60 µL 100% (w/v) TCA + 40 µL Buffer D	Add TCA (final concentration 10%) 60 µL 100% (w/v) TCA + 40 µL Buffer D	Add TCA (final concentration 10%) 130 µL 100% (w/v) TCA + 170 µL Buffer D	Add TCA (final concentration 10%) 130 µL 100% (w/v) TCA + 170 µL Buffer D	Add TCA (final concentration 10%) 130 µL 100% (w/v) TCA + 170 µL Buffer D	Add TCA (final concentration 10%) 130 µL 100% (w/v) TCA + 170 µL Buffer D
30 min on ice					
Centrifuge 2 min at 6700 *g* Wash with cold acetone 2x	Centrifuge 2 min a t 6700 g Wash with cold acetone 2x	Centrifuge 2 min at 6700 *g* Wash with cold acetone 2x	Centrifuge 2 min at 6700 *g* Wash with cold acetone 2x	Centrifuge 2 min at 6700 *g* Wash with cold acetone 2x	Centrifuge 2 min at 6700 *g* Wash with cold acetone 2x
Dry the pellet					
Add 350 µL de Buffer E Wait 5 min	Add 350 µL de Buffer E Wait 5 min	Add 350 µL de Buffer E Wait 5 min	Add 350 µL de Buffer E Wait 5 min	Add 350 µL de Buffer E Wait 5 min	Add 350 µL de Buffer E Wait 5 min
Dissolve the pellet					
DTNB assay in 96 well microplate					
			100 µL sample per well 100 µL Buffer E per well 1.33 µL DTNB solution per well		

6.17 Synthesis of 2-bromomalonic acid (BMA) and sodium 2-bromomalonate (11)

The synthesis of 2-bromomalonic acid was carried out by the methods previously described by [211]. Bromine (15.5 g, 5 mL, 0.097 mol) was added dropwise to a well stirred and ice cooled mixture of malonic acid (10 g, 0.097 mol) in diethyl ether (100 mL). After the reaction of bromine, the solid malonic acid promptly dissolves. The reaction mixture was left at room temperature for 1 hour after complete dissolution of the solid malonic acid. The diethyl ether was distilled off under reduced pressure and the residue kept over potassium hydroxide in a vacuum desiccator until hydrogen bromide was completely absorbed. The product was further dried under a vacuum line at room temperature. The resulting material was hygroscopic with a strong orange color. For further purification, the product was washed with benzene [213] resulting in hygroscopic pale orange powder (yield: 80%). ^{1}H NMR (400 MHz, DMSO-d_6) δ 5.18 (-CBr*H*-) ^{13}C NMR (100 MHz, DMSO-d_6) δ 166.39 (-*C*OOH), 44.91 (-*C*BrH-). IR (FTIR-ATR) 3470, 1586, 1414, 1335, 1193, 1175, 938, 793, 726 cm^{-1}.

After confirmation of the product purity, this was dissolved in water and the pH adjusted to 7 with NaOH to produce sodium 2-bromomalonate (11). After drying under vacuum, this salt was stored at -20 °C until needed.

6.18 Synthesis of dicarboxymethylcellulose in isopropanol/aqueous NaOH

Derivatization of the cellulose was carried out by a standard slurry method as previously described [210] for carboxymethylation with sodium monochloroacetate with some modifications.

General method

400 mg of air-dry cellulose (Avicel) in 15 mL isopropanol was stirred vigorously, while the appropriate quantity of 40% (w/v) aqueous NaOH was added dropwise during 10 min at room temperature. Stirring with a magnetic stirrer was continued for 1 h and the desired quantity of sodium 2-bromomalonate (**11**) was added. After complete homogenization, the mixture was placed on a water bath at 60 °C for 3 to 5 h with vigorous stirring. If the mixture clump during the reaction, this was detached from the glass with a metal spatula. When finished, the reaction mixture was filtrated, suspended in 100 mL of 70% (v/v) methanol and neutralized with acetic acid. The product was washed three times with 20 mL of 80% (v/v) aqueous methanol and subsequently with 20 mL methanol. The product was dried under vacuum at room temperature until constant weight.

sample identification	cellulose type	Ratio (Cellulose:BMA:NaOH)	% NaOH solution	% H_2O in reaction	$DS_{icp-aes}$	DS_{NMR}	DS_{HPLC}	DP	Elemental analysis			
									C	H	N	Br
DCMC1	Avicel	1:2:0.54	5	8	0.05	-	-	-	-			
DCMC2	Avicel	1:2:1	10	8	0.32	0.50	0.39	269.4	35.0	4.73	0	0
DCMC3	Avicel	1:2:1.6	15	8	0.44	0.56	0.45	370.7	34.4	4.52	0	0
DCMC4	Avicel	1:2:2.2	20	8	0.46	0.64	0.51	326.0	34.5	4.59	0	0
DCMC5	Avicel	1:2:3.2	30	8	0.51	0.56	0.44	166.0	34.8	4.88	0	0
DCMC6	Avicel	1:2:3.5	40	8	1.53	-	-	-	-			
DCMC7	Avicel	1:1:3.5	40	8	0.85	-	-	-	-			
DCMC8	Avicel	1:0.7:3.5	40	8	0.60	-	-	-	-			
DCMC9	Avicel	1:0.5:3.5	40	8	0.47	-	-	-	-			
DCMC10	Avicel	1:0.2:3.5	40	8	0.30	-	-	-	-			
DCMC11	Avicel	1:2.2:3.5	40	8	0.62	-	-	-	-			
DCMC12	Kraft pulp	1:2:1	40	8	0.18	-	-	-	-			
DCMC13	Kraft pulp	1:2:1.6	40	8	0.25	-	-	-	-			
DCMC14	Kraft pulp	1:2:2.2	40	8	0.27	-	-	-	-			
DCMC15	Kraft pulp	1:2:3.2	40	8	0.14	-	-	-	-			

6.19 Acetylation of DCMC

The method for acetylation of dicarboxymethylcellulose was adapted from a described method [220] (Figure 69). In a round-bottom flask, sodium dicarboxymethylcellulose (NaDCMC, 50 mg) was suspended in 20% sulfuric acid (2 mL) with vigorous stirring at room temperature for 2 h. The slurry of protonated DCMC (H-DCMC) was washed with MilliQ until the water tested neutral, and then washed with 3 × 5 mL glacial acetic acid volumes to remove the residual water. Centrifugation of the sample between each washing allowed to change the acid without significant loss of the sample. The H-DCMC was transferred to a round-bottom flask placed in an ice bath, and suspended in glacial acetic acid (250 uL). Acetic anhydride (150 uL) and sulfuric acid (6 uL) were added to the chilled slurry, the temperature was raised to 50 °C and the solution was vigorously stirred for 3 h or until the solution clarified.

The reaction solution was concentrated by evaporation (45 °C) and the product precipitated with deionized water. The water was extracted by centrifuging the suspension. The pellet was resuspended in deionized water and the process was repeated until reaching a neutral pH. The acetylated DCMC (Ac-DCMC) powder was dried to remove residual water. The resulting polymer was analysed by ^{1}H and ^{13}C NMR in deuterated chloroform. ^{1}H NMR (250 MHz, DMSO) δ 5.25 – 3.20 (m, AGU) 2.25 – 1.75 (m, CH_3). ^{13}C NMR (63 MHz, DMSO) δ 170.21, 169.76, 169.31, 100.51, 79,23, 76.52, 73.79, 72.52, 71.80, 65.05, 20.81, 20.57. IR (FTIR-ATR) 3462, 2965, 1749, 1433, 1375, 1232 and 1050 cm^{-1}.

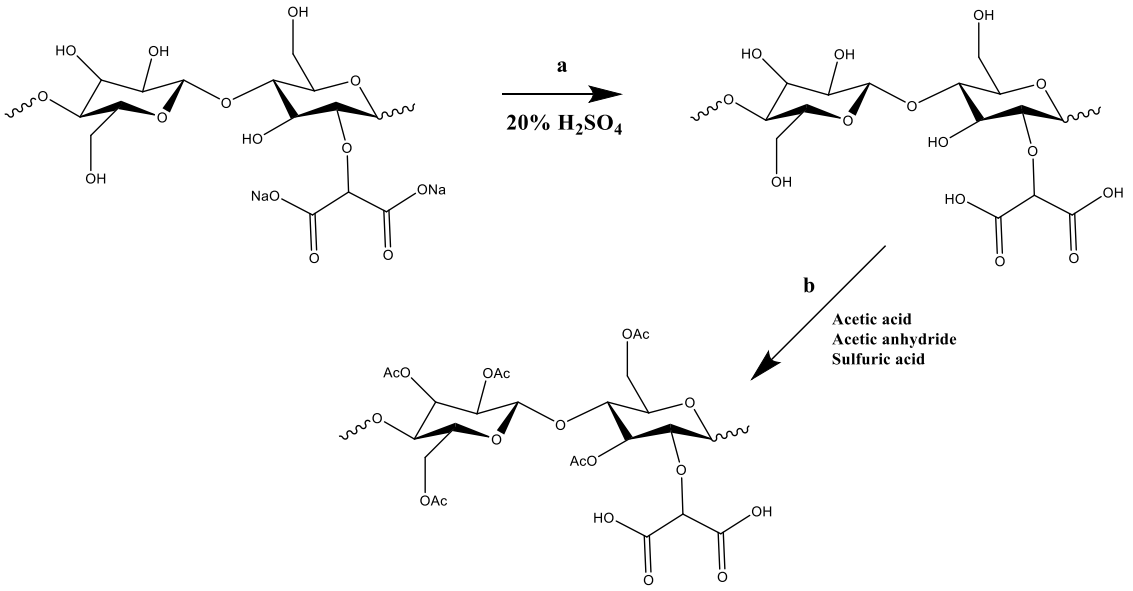

Figure 69 - DCMC acetylation reaction scheme.

6.20 Formylation of DCMC

The Method B for the acetylation of CMC was adapted from the method described by [226] with some modifications. Briefly, 200 mg of dry Na-CMC (1 eq) were added to 4 mL of formic acid. After agitation of the mixture, 370 µL of acetic anhydride (5 eq) were added to the slurry. The reaction occurred during 24 hours at room temperature. The product was precipitated by pouring the solution in ten-fold amount of diethyl ether. The precipitate was isolated by filtration and washed with acetone. The precipitate was further dried in under vacuum at room temperature.

For the NMR experiments, the 60 mg of product was suspended in DMSO with vigorous agitation for 24 hours. A small portion of LiCl was added to the mixture to increase the solubility of the polymer in the DMSO. The mixture was centrifuged for 15 minutes at 6700 g to remove particles in suspension prior to NMR experiments.

6.21 Sodium content determination by ICP-AES

A known amount (approx. 5 mg per sample) of sodium dicarboxymethylcellulose was weighted in new vials and suspended in pure nitric acid. The samples were incubated at 60 °C for 1 hour prior to analysis. Sodium was quantified by ICP-AES. After determination of the sodium content by ICP-AES ($\%Na_{ICP}$), the DS was calculated based on the equation presented by Stojanovic, et al. [5] for carboxymethyl starch with the corrected mass of the substituent. The DS was calculated from the following equation:

$$DS = \frac{162 \times (\%\frac{Na}{2}/23)}{100 - \left(147 \times \%\frac{Na}{2}/23\right)}$$

Where:

162 (g/mol) = molecular mass of an anhydroglucose unit of cellulose

147 (g/mol) = net increase in molecular mass of an anhydroglucose unit for each sodium dicoarboxymethyl group added.

6.22 Intrinsic viscosity

Intrinsic viscosities ([g]) of DCMC were determined in 6 % (w/v) NaOH aqueous solution at 20 °C as proposed [238,241] with some modifications. The original concentration of DCMC in 6% (w/v) NaOH was 20 g/L and remaining dilutions were performed using the same stock solution.

6.23 Size exclusion chromatography (SEC) of DCMC

The eluent used for SEC analysis was an aqueous solution of 0.1 M $NaNO_3$/0.05% NaN_3. The concentration of the polymer solution was in the range 1.1 - 1.9 g/l and the flow rate was 1 ml/min. Calibration was carried out with pullulan standard and PSS (Mainz) software was used for data evaluation.

6.24 Anion exchange chromatography (AE-HPLC)

The AE-HPLC analysis of the DCMC samples was carried out as described by [210,238]. In brief, hydrolysis of 100 mg of DCMC was dispersed in 2 mL $HClO_4$ (70%) and after 10 min at room temperature diluted with 18 mL of distilled water. This mixture was kept at 100 °C for 16 h. The solution obtained was carefully neutralized with 2 M KOH and kept at 4 °C for 1 h to guarantee a complete precipitation of the $KClO_4$. The precipitate was filtered off and washed three times with distilled water. The obtained solution was reduced to approximately 3 mL and diluted with distilled water to give exactly 5 mL sample. Chromatographic experiments were carried out at 65 ^{o}C with 50 mM H_2SO_4 as eluent with a flow rate of 0.5 mL/min in a Bio-Rad Aminex HPX-87 H column.

6.25 X-ray Diffraction (XRD)

X-ray diffraction patterns of Avicel cellulose and malonyl cellulose was recorded with a MiniFlex II (RIGAKU), using CuKa radiation at 30 kV and 15 mA in the 2θ range of 5^{o} – 60^{o} at a speed of 2^{o} min^{-1}.

6.26 DCMC Film preparation

Film preparation was performed as described by Ferreira, et al. [6] with some modifications. Malonylcellulose solutions were prepared by dissolving freeze dried sodium malonylcellulose in distilled water (15 mg/mL) under stirring, at room temperature, until complete dissolution. Air bubbles were removed under vacuum, and the solution was transferred to Teflon petri dishes and left to dry at 30 ◦ C during 48 h.

6.27 DCMC film crosslinking

The production of crosslinked sodium DCMC was performed based on the method for the production of crosslinked sodium carboxymethyl cellulose already described [251] with some modifications. After casting procedure, the dry films of sodium DCMC were placed in 50 mL of 20% H_2SO_4. This will cause the protonation of the cellulose derivative to allow its crosslinking reaction. The protonated film is removed of the acid solution and washed in MilliQ water until neutral pH. The films were placed in the Teflon petri dishes and the crosslinking reaction was performed in an oven at 105 °C for 1 to 2 h (depending on the trial described in the text). The wrinkled films were removed from the petri dishes and allowed to cool at room temperature. After cooling, the films were placed in a saturated $NaHCO_3$ to form the sodium salt of the remaining acid groups that do not react during the crosslinking reaction. After washing with MilliQ water until neutral pH, we dried the crosslinked sodium DCMC films in an oven at 50 °C. The resultant films were stored in a desiccator until needed.

7. References

(1) OIV. (2016) OIV 2016 Statistical Report on Global Vitiviniculture.

(2) FAO. (2016) FAOSTAT.

(3) MaketLine, and MarketLine. (2012) Wine: Global Industry Almanac.

(4) Butzke, C. E., Vogt, E. E., and Chacón-Rodríguez, L. (2012) Effects of heat exposure on wine quality during transport and storage. *J. Wine Res. 23*, 15–25.

(5) Van Sluyter, S. C., McRae, J. M., Falconer, R. J., Smith, P. A., Bacic, A., Waters, E. J., and Marangon, M. (2015) Wine protein haze: Mechanisms of formation and advances in prevention. *J. Agric. Food Chem. 63*, 4020–4030.

(6) Ribéreau-Gayon, P., Glories, Y., Maujean, A., and Dubourdieu, D. (2006) Handbook of Enology, The Chemistry of Wine: Stabilization and Treatments: Second Edition. *Handb. Enol. Chem. Wine Stab. Treat. Second Ed.* 2nd ed. Willey & Sons, Chichester, UK.

(7) Ciaccio, N. A., and Laurence, J. S. (2009) Effects of disulfide bond formation and protein helicity on the aggregation of activating transcription factor 5. *Mol. Pharm. 6*, 1205–1215.

(8) Trivedi, M., Laurence, J., and Siahaan, T. (2009) The Role of Thiols and Disulfides on Protein Stability. *Curr. Protein Pept. Sci. 10*, 614–625.

(9) Rombouts, I., Lagrain, B., Scherf, K. A., Lambrecht, M. A., Koehler, P., and Delcour, J. A. (2015) Formation and reshuffling of disulfide bonds in bovine serum albumin demonstrated using tandem mass spectrometry with collision-induced and electron-transfer dissociation. *Sci. Rep. 5*, 12210.

(10) Sauvage, F. X., Bach, B., Moutounet, M., and Vernhet, A. (2010) Proteins in white wines: Thermo-sensitivity and differential adsorbtion by bentonite. *Food Chem. 118*, 26–34.

(11) Esteruelas, M., Kontoudakis, N., Gil, M., Fort, M. F., Canals, J. M., and Zamora, F. (2011) Phenolic compounds present in natural haze protein of Sauvignon white wine. *Food Res. Int. 44*, 77–83.

(12) Hsu, J.-C., and Heatherbell, D. A. (1987) Isolation and Characterization of Soluble Proteins in Grapes, Grape Juice, and Wine. *Am. J. Enol. Vitic. 38*, 6–10.

(13) Ferreira, R. B., Piçarra-Pereira, M. A., Monteiro, S., Loureiro, V. B., and Teixeira, A. R. (2001) The wine proteins. *Trends Food Sci. Technol. 12*, 230–239.

(14) Van Sluyter, S. C., Marangon, M., Stranks, S. D., Neilson, K. A., Hayasaka, Y., Haynes, P. A., Ian Menz, R., and Waters, E. J. (2009) Two-Step purification of pathogenesis-related proteins from grape juice and crystallization of thaumatin-like proteins. *J. Agric. Food Chem. 57*, 11376–11380.

(15) Waters, E. J., Shirley, N. J., and Williams, P. J. (1996) Nuisance Proteins of Wine Are Grape Pathogenesis-Related Proteins. *J. Agric. Food Chem. 44*, 3–5.

(16) Waters, E. J., Wallace, W., and Williams, P. J. (1992) Identification of Heat-Unstable Wine Proteins and Their Resistance to Peptidases. *J. Agric. Food Chem. 40*, 1514–1519.

(17) Tabilo-Munizaga, G., Gordon, T. A., Villalobos-Carvajal, R., Moreno-Osorio, L., Salazar, F. N., Pérez-Won, M., and Acuña, S. (2014) Effects of high hydrostatic pressure (HHP) on the protein structure and thermal stability of Sauvignon blanc wine. *Food Chem. 155*, 214–220.

(18) Marangon, M., Van Sluyter, S. C., Robinson, E. M. C., Muhlack, R. A., Holt, H. E., Haynes, P. A., Godden, P. W., Smith, P. A., and Waters, E. J. (2012) Degradation of white wine haze proteins by Aspergillopepsin i and II during juice flash pasteurization. *Food Chem. 135*, 1157–1165.

(19) Monteiro, S., Piçarra-Pereira, M. A., Mesquita, P. R., Loureiro, V. B., Teixeira, A., and Ferreira, R. B. (2001) The wide diversity of structurally similar wine proteins. *J. Agric. Food Chem. 49*, 3999–4010.

(20) Pocock, K. F., Hayasaka, Y., McCarthy, M. G., and Waters, E. J. (2000) Thaumatin-like proteins and chitinases, the haze-forming proteins of wine, accumulate during ripening of grape (Vitis vinifera) berries and drought stress does not affect the final levels per berry at maturity. *J. Agric. Food Chem. 48*, 1637–1643.

(21) Somssich, I. E., and Hahlbrock, K. (1998) Pathogen defence in plants—a paradigm of biological complexity. *Trends Plant Sci. 3*, 86–90.

(22) van Loon, L. C. (1985) Pathogenesis-related proteins. *Plant Mol. Biol. 4*, 111–116.

(23) Monteiro, S., Piçarra-Pereira, M. A., Teixeira, A. R., Loureiro, V. B., and Ferreira, R. B. (2003) Environmental conditions during vegetative growth determine the major proteins that accumulate in mature grapes. *J. Agric. Food Chem. 51*, 4046–4053.

(24) Marangon, M., Van Sluyter, S. C., Waters, E. J., and Menz, R. I. (2014) Structure of haze forming proteins in white wines: Vitis vinifera thaumatin-like proteins. *PLoS One 9*, e113757.

(25) Linthorst, H. J. M., and Van Loon, L. C. (1991) Pathogenesis- related proteins of plants. *CRC. Crit. Rev. Plant Sci. 10*, 123–150.

(26) Waters, E., and Høj, P. (1999) Grape proteins involved in white wine heat instability: a short review of current knowledge and future perspectives., in *Colloids and Mouthfeel in Wines*, pp 41–49.

(27) Moretti, R., and Berg, H. (1965) Variability among wine to protein clouding. *Am. J. Enol. Vitic. 16*, 69–78.

(28) Bayly, F. C., and Berg, H. W. (1967) Grape and Wine Proteins of White Wine Varietals. *Am. J. Enol. Vitic. 18*, 18–32.

(29) Pueyo, E., Dizy, M., and Polo, M. C. (1993) Varietal differentiation of must and wines by means of protein fraction. *Am. J. Enol. Vitic. 44*, 255–260.

(30) Waters, E. J., Wallace, W., Tate, M. E., and Williams, P. J. (1993) Isolation and Partial Characterization of a Natural Haze Protective Factor from Wine. *J. Agric. Food Chem. 41*, 724–730.

(31) Dawes, H., Boyes, S., Keene, J., and Heatherbell, D. (1994) Protein Instability of Wines: Influence of Protein Isolelectric Point. *Am. J. Enol. Vitic. 45*, 319–326.

(32) Pellerin, P., Waters, E., and Brillouet, J. M. (1993) Characterization of two arabinogalactan-proteins from red wine. *Carbohydr. Polym. 22*, 187–192.

(33) Dizy, M., Bisson, L. F., Page, S. D. S., Vineyards, D., and Vineyard, D. (1999) White Wine Protein Analysis by Capillary Zone Electrophoresis. *Am. J. Enol. Vitic. 50*, 120–127.

(34) Tyson, P. J., Luis, E. S., Day, R. W., Walker, B., and Lee, T. H. (1981) Research note on estimation of soluble protein in must and wine by high performance liquid chromatography. *Am. J. Enol. Vitic.* 241–243.

(35) Santoro, M. (1995) Fractionation and Characterization of must and wine proteins. *Am. J. Enol. Vitic. 46*, 250–254.

(36) Marangon, M., Vincenzi, S., Lucchetta, M., and Curioni, A. (2010) Heating and reduction affect the reaction with tannins of wine protein fractions differing in hydrophobicity. *Anal. Chim. Acta 660*, 110–118.

(37) Marangon, M., Van Sluyter, S. C., Haynes, P. A., and Waters, E. J. (2009) Grape and wine proteins: Their fractionation by hydrophobic interaction chromatography and identification by chromatographic and proteomic analysis. *J. Agric. Food Chem. 57*, 4415–4425.

(38) D'Amato, A., Fasoli, E., Kravchuk, A. V., and Righetti, P. G. (2011) Mehercules, adhuc Bacchus ! the debate on wine proteomics continues. *J. Proteome Res. 10*, 3789–3801.

(39) Falconer, R. J., Marangon, M., Van Sluyter, S. C., Neilson, K. A., Chan, C., and Waters, E. J. (2010) Thermal stability of thaumatin-like protein, chitinase, and invertse isolated from sauvignon blanc and semillon juice and their role in haze formation in wine. *J. Agric. Food Chem. 58*, 975–980.

(40) Marangon, M., Sauvage, F. X., Waters, E. J., and Vernhet, A. (2011) Effects of ionic strength and sulfate upon thermal aggregation of grape chitinases and thaumatin-like proteins in a model system. *J. Agric. Food Chem. 59*, 2652–2662.

(41) Batista, L., Monteiro, S., Loureiro, V. B., Teixeira, A. R., and Ferreira, R. B. (2010) Protein haze formation in wines revisited. The stabilising effect of organic acids. *Food Chem. 122*, 1067–1075.

(42) Dufrechou, M., Poncet-Legrand, C., Sauvage, F. X., and Vernhet, A. (2012) Stability of white wine proteins: Combined effect of pH, ionic strength, and temperature on their aggregation. *J. Agric. Food Chem. 60*, 1308–1319.

(43) Pocock, K. F., Alexander, G. M., Hayasaka, Y., Jones, P. R., and Waters, E. J. (2007)

Sulfate - A candidate for the missing essential factor that is required for the formation of protein haze in white wine. *J. Agric. Food Chem. 55*, 1799–1807.

(44) Waters, E. J., Alexandre, G., Muhlack, R., Pocock, K. F., Colby, C., O'neill, B. K., Hoj, P. B., and Jones, P. (2005) Preventing protein haze in bottled white wine. *Aust. J. Grape Wine Res. 11*, 215–225.

(45) Koch, J., and Sajak, E. (1959) A review and some studies on grape protein. *Am. J. Enol. Vitic. 10*, 114–123.

(46) Siebert, K. J., and Lynn, P. Y. (1997) Mechanisms of Adsorbent Action in Beverage Stabilization. *J. Agric. Food Chem. 45*, 4275–4280.

(47) Yokotsuka, K., Nozaki, K., and Kushida, T. (1983) Turbidity formation caused by interaction of must proteins with wine tannins. *J. Ferment. Technol. 61*, 413–416.

(48) Waters, E. J., Peng, Z., Pocock, K. F., and Williams, P. J. (1995) Proteins in white wine, I: Procyanidin occurrence in soluble proteins and insoluble protein hazes and its relationship to protein instability. *Aust. J. Grape Wine Res. 1*, 86–93.

(49) Mesquita, P. R., Piçarra-Pereira, M. A., Monteiro, S., Loureiro, V. B., Teixeira, A. R., and Ferreira, R. B. (2001) Effect of Wine Composition on Protein Stability. *Am. J. Enol. Vitic. 52*, 324–330.

(50) Fenchak, S. F., Keirr, W. L., and Corredig, M. (2002) Multifactorial Study of Haze Formation in Model Wine Systems. *J. Food Qual. 25*, 91–105.

(51) Quirós, M., Gonzalez-Ramos, D., Tabera, L., and Gonzalez, R. (2010) A new methodology to obtain wine yeast strains overproducing mannoproteins. *Int. J. Food Microbiol. 139*, 9–14.

(52) Waters, E. J., Pellerin, P., and Brillouet, J. M. (1994) A Saccharomyces mannoprotein that protects wine from protein haze. *Carbohydr. Polym. 23*, 185–191.

(53) Dambrouck, T., Marchal, R., Cilindre, C., Parmentier, M., and Jeandet, P. (2005) Determination of the grape invertase content (Using PTA-ELISA) following various fining treatments versus changes in the total protein content of wine. Relationships with wine foamability. *J. Agric. Food Chem. 53*, 8782–8789.

(54) Brown, S. L., Stockdale, V. J., Pettolino, F., Pocock, K. F., De Barros Lopes, M., Williams, P. J., Bacic, A., Fincher, G. B., Høj, P. B., and Waters, E. J. (2007) Reducing haziness in white wine by overexpression of Saccharomyces cerevisiae genes YOL155c and YDR055w. *Appl. Microbiol. Biotechnol. 73*, 1363–1376.

(55) Schmidt, S. A., Tan, E. L., Brown, S., Nasution, U. J., Pettolino, F., Macintyre, O. J., De Barros Lopes, M., Waters, E. J., and Anderson, P. A. (2009) Hpf2 glycan structure is critical for protection against protein haze formation in white wine. *J. Agric. Food Chem. 57*, 3308–3315.

(56) Vincenzi, S., Crapisi, A., and Curioni, A. (2014) Foamability of Prosecco wine: Cooperative effects of high molecular weight glycocompounds and wine PR-proteins. *Food Hydrocoll. 34*, 202–207.

(57) Gazzola, D., Van Sluyter, S. C., Curioni, A., Waters, E. J., and Marangon, M. (2012) Roles of proteins, polysaccharides, and phenolics in haze formation in white wine via reconstitution experiments. *J. Agric. Food Chem. 60*, 10666–10673.

(58) Besse, C., Clark, A., Scollary, G. (2000) Investigation of the role of total and free copper in protein in haze formation. *Aust. Grapegrow. Winemak.*

(59) Siebert, K. J., Carrasco, A., and Lynn, P. Y. (1996) Formation of Protein−Polyphenol Haze in Beverages. *J. Agric. Food Chem. 44*, 1997–2005.

(60) Dufrechou, M., Vernhet, A., Roblin, P., Sauvage, F. X., and Poncet-Legrand, C. (2013) White wine proteins: How does the pH affect their conformation at room temperature? *Langmuir 29*, 10475–10482.

(61) Mira de Orduña, R. (2010) Climate change associated effects on grape and wine quality and production. *Food Res. Int. 43*, 1844–1855.

(62) Siebert, K. J., and Lynn, P. Y. (2003) Effects of alcohol and pH on protein-polyphenol haze intensity and particle size. *J. Am. Soc. Brew. Chem 61*, 88–98.

(63) Di Gaspero, M., Ruzza, P., Hussain, R., Vincenzi, S., Biondi, B., Gazzola, D., Siligardi, G., and Curioni, A. (2017) Spectroscopy reveals that ethyl esters interact with proteins in wine. *Food Chem. 217*, 373–378.

(64) Dufrechou, M., Sauvage, F. X., Bach, B., and Vernhet, A. (2010) Protein

Aggregation in White Wines: Influence of the Temperature on Aggregation Kinetics and Mechanisms. *J. Agric. Food Chem. 58*, 10209–10218.

(65) Florin, T. H. J., Neale, G., Goretski, S., and Cummings, J. H. (1993) The Sulfate Content of Foods and Beverages. *J. Food Compos. Anal. 6*, 140–151.

(66) OIV. (2017) Compendium of international methods of analysis of wines and musts.

(67) Jakob, L. (1962) Bentotest. *Das Weinblatt*.

(68) P. Hoj, D. Tattersall, K. Adams, K. Pocock, Y. Hayasaka, van Heeswijck, R. W. (2000) The ´haze proteins´of wine -a summary of properties, factors affecting their accumulation in grapes, and the amount of bentonite required for their removal from wine., in *Proceedings of ASEV 50th Anniversary Meeting, Seatttle, Whashington, USA.*, pp 149–154. American Society for Enology and Viticulture: Davis, CA, Seattle, WA.

(69) Majewski, P., Barbalet, A., and Waters, E. J. (2011) $1 Billion Hidden Cost of Bentonite Fining. *Aust. New Zeal. Grapegrow. Winemak. 1307*, 58–62.

(70) Plançon, A. (2001) Order-disorder in clay mineral structures. *Clay Miner. 36*, 1–14.

(71) Miller, G. C., Amon, J. M., Gibson, R. L., and Simpson, R. F. (1985) Loss of wine aroma attributable to protein stabilization with bentonite or ultrafiltration. *Aust. Grapegrow. Winemak.*

(72) Voilley, A., Lamer, C., Dubois, P., and Feuillat, M. (1990) Influence of Macromolecules and Treatments on the Behavior of Aroma Compounds in a Model Wine. *J. Agric. Food Chem. 38*, 248–251.

(73) Lubbers, S., Charpentier, C., and Feuillat, M. (1996) Etude de la retention de composes d'arome par les bentonites en mout, vin et milieux modeles. *Vitis 35*, 59–62.

(74) Lambri, M., Dordoni, R., Silva, A., and de Faveri, D. M. (2010) Effect of bentonite fining on odor-active compounds in two different white wine styles. *Am. J. Enol. Vitic. 61*, 225–233.

(75) Vela, E., Hernández-Orte, P., Castro, E., Ferreira, V., and Lopez, R. (2017) Effect of bentonite fining on polyfunctional mercaptans and other volatile compounds in Sauvignon blanc wines. *Am. J. Enol. Vitic. 68*, 30–38.

(76) Guillou, C., Aleixandre, J. L., García, M. J., and Lizama, V. (1998) Clarification influence upon sensorial and analytical characteristics of Muscat dry wine. *OENO One 32*, 111.

(77) Lagace, L. S., and Bisson, L. F. (1990) Survey of yeast acid proteases for effectiveness of wine haze reduction. *Am. J. Enol. Vitic. 41*, 147–155.

(78) Tattersall, D. B., Pocock, K. F., Hayasaka, Y., Adams, K., van Heeswijck, R., Waters, E. J., and Høj, P. B. (2001) Pathogenesis Related Proteins — Their Accumulation in Grapes during Berry Growth and Their Involvement in White Wine Heat Instability. Current Knowledge and Future Perspectives in Relation to Winemaking Practices, in *Molecular Biology & Biotechnology of the Grapevine*, pp 183–201. Springer Netherlands, Dordrecht.

(79) Musee, N., Lorenzen, L., and Aldrich, C. (2006) Decision support for waste minimization in wine-making processes. *Environ. Prog. 25*, 56–63.

(80) Chagas, R., Monteiro, S., and Boavida Ferreira, R. (2012) Assessment of Potential Effects of Common Fining Agents Used for White Wine Protein Stabilization. *Am. J. Enol. Vitic. 63*, 574–578.

(81) Chibata, R., Weetall, H. H., Zelko, J. T., and Bailey, L. F. (1984) A New Method for the Stabilization of White Wine. *Am. J. Enol. Vitic. 35*, 212–215.

(82) Sarmento, M. R., Oliveira, J. C., and Boulton, R. B. (2000) Selection of low swelling materials for protein adsorption from white wines. *Int. J. Food Sci. Technol. 35*, 41–47.

(83) Sarmento, M. R., Oliveiraz, J. C., Slatner, M., and Boulton, R. B. (2001) Effect of Ion-Exchange Adsorption on the Protein Profiles of White Wines. *Rev. Agaroquimica y Tecnol. Aliment. 7*, 217–224.

(84) Fukuzaki, S., Urano, H., and Nagata, K. (1996) Adsorption of bovine serum albumin onto metal oxide surfaces. *J. Ferment. Bioeng. 81*, 163–167.

(85) Pachova, V., Ferrando, M., Guell, C., and Loapez, F. (2002) Protein Adsorption onto Metal Oxide Materials in White Wine Model Systems. *J. Food Sci. 67*, 2118–2121.

(86) Pashova, V., Güell, C., and López, F. (2004) White Wine Continuous Protein Stabilization by Packed Column. *J. Agric. Food Chem. 52*, 1558–1563.

(87) Marangon, M., Lucchetta, M., and Waters, E. J. (2011) Protein stabilisation of white wines using zirconium dioxide enclosed in a metallic cage. *Aust. J. Grape Wine Res. 17*, 28–35.

(88) Lucchetta, M., Pocock, K. F., Waters, E. J., and Marangon, M. (2013) Use of zirconium dioxide during fermentation as an alternative to protein fining with bentonite for white wines. *Am. J. Enol. Vitic. 64*, 400–404.

(89) Dey, P. M. (1990) Carbohydrates. Academic Press.

(90) Grassin.C. (1992) Pressing enzymes in the apple industry.Fruit Processing. *Fruit Process.* 7.

(91) Feuillat, M. et al. (1988) Production de colloides par les levures dans les vins mousseux élaborés selon la méthode champenoise. *Rev. Française d'Oenologie 111*, 36–45.

(92) Lao, C., Lopez-Tamames, E., Buxaderas, S., and Torre-BoronatT, M. C. (1996) Grape Pectic Enzyme Treatment Effect on White Musts & Wines Composition. *J. Food Sci. 61*, 553–556.

(93) Aleixandre, J. L., Padilla, A. I., Navarro, L. L., Suria, A., García, M. J., and Álvarez, I. (2003) Optimization of making barrel-fermented dry muscatel wines. *J. Agric. Food Chem. 51*, 1889–1893.

(94) Pocock, K. F., Hoj, P. B., Adams, K. S., Kwiatkowski, M. J., and Waters, E. J. (2003) Combined heat and proteolytic enzyme treatment of white wines reduces haze forming protein content without detrimental effect. *Aust. J. Grape Wine Res. 9*, 56–63.

(95) Cordonnier, R., and Dugal, A. (1968) Les activites proteolytiques du raisin. *Annu. Technol. Agric.* 189–206.

(96) Charoenchai, C., Fleet, G. H., Henschke, P. A., and Todd, B. E. N. . (1997) Screening of non- Saccharomyces wine yeasts for the presence of extracellular hydrolytic enzymes. *Aust. J. Grape Wine Res. 3*, 2–8.

(97) Maturano, Y. P., Assof, M., Fabani, M. P., Nally, M. C., Jofré, V., Rodríguez Assaf, L. A., Toro, M. E., Castellanos de Figueroa, L. I., and Vazquez, F. (2015) Enzymatic activities produced by mixed Saccharomyces and non-Saccharomyces cultures:

relationship with wine volatile composition. *Antonie van Leeuwenhoek, Int. J. Gen. Mol. Microbiol. 108*, 1239–1256.

(98) Leitão, M. C., Teixeira, H. C., Barreto Crespo, M. T., and San Romão, M. V. (2000) Biogenic amines occurrence in wine. Amino acid decarboxylase and proteolytic activities expression by Oenococcus oeni. *J. Agric. Food Chem. 48*, 2780–2784.

(99) Klar, A. J. S., and Halvorson, H. O. (1975) Proteinase activities of Saccharomyces cerevisiae during sporulation. *J. Bacteriol. 124*, 863–869.

(100) Rawlings, N. D., and Barrett, A. (2013) Introduction: Peptidases of Unknown Catalytic Type, in *Handbook of Proteolytic Enzymes*, pp 3747–3749.

(101) Bilinski, C. A., Russell, I., and Stewart, G. G. (1987) Applicability of yeast extracellular proteinases in brewing: Physiological and biochemical aspects. *Appl. Environ. Microbiol. 53*, 495–499.

(102) Rosi, I., Costamagna, L., and Birtuccion, M. (1987) Screening for Extracellular Acid Protease(S) Production By Wine Yeasts. *J. Inst. Brew. 93*, 322–324.

(103) Ubeda Iranzo, J. ., Briones Pérez, A. ., and Izquierdo Cañas, P. . (1998) Study of the oenological characteristicsand enzymatic activities of wine yeasts. *Food Microbiol. 15*, 399–406.

(104) Conterno, L., and Delfini, C. (1994) Peptidase activity and the ability of wine yeasts to utilise grape must proteins as sole nitrogen source. *J. Wine Res. 5*.

(105) Moreno-Arribas, V., Pueyo, E., and Polo, M. C. (1996) Peptides in Musts and Wines. Changes during the Manufacture of Cavas (Sparkling Wines). *J. Agric. Food Chem. 44*, 3783–3788.

(106) Fleet, G. H. (2003) Yeast interactions and wine flavour. *Int. J. Food Microbiol. 86*, 11–22.

(107) Carnevillier, V., Charpentier, C., and Feuillat, M. (2000) Production de peptides par Saccharomyces cerevisiae au fours de la fermentation er de l'autolyse sur moût Chardonnay., in *6 Symposium Internation d'Oenologie*, pp 287–289.

(108) Esti, M., Benucci, I., Lombardelli, C., Liburdi, K., and Garzillo, A. M. V. (2013)

Papain from papaya (Carica papaya L.) fruit and latex: Preliminary characterization in alcoholic-acidic buffer for wine application. *Food Bioprod. Process. 91*, 595–598.

(109) Benucci, I., Esti, M., and Liburdi, K. (2015) Effect of wine inhibitors on the proteolytic activity of papain from Carica papaya L. latex. *Biotechnol. Prog. 31*, 48–54.

(110) Benucci, I., Esti, M., and Liburdi, K. (2014) Effect of free and immobilised stem bromelain on protein haze in white wine. *Aust. J. Grape Wine Res. 20*, 347–352.

(111) Benucci, I., Lombardelli, C., Cacciotti, I., Liburdi, K., Nanni, F., and Esti, M. (2016) Chitosan beads from microbial and animal sources as enzyme supports for wine application. *Food Hydrocoll. 61*, 191–200.

(112) Benucci, I., Lombardelli, C., Liburdi, K., Acciaro, G., Zappino, M., and Esti, M. (2016) Immobilised native plant cysteine proteases: packed-bed reactor for white wine protein stabilisation. *J. Food Sci. Technol. 53*, 1130–1139.

(113) Waters, E. J., Wallace, W., and Williams, P. J. (1991) Heat Haze Characteristics of Fractionated Wine Proteins. *Am. J. Enol. … 42*, 123–127.

(114) Dupin, I. V. S., Stockdale, V. J., Williams, P. J., Jones, G. P., Markides, A. J., and Waters, E. J. (2000) Saccharomyces cerevisiae mannoproteins that protect wine from protein haze: Evaluation of extraction methods and immunolocalization. *J. Agric. Food Chem. 48*, 1086–1095.

(115) Dupin, I. V. S., McKinnon, B. M., Ryan, C., Boulay, M., Markides, A. J., Jones, G. P., Williams, P. J., and Waters, E. J. (2000) Saccharomyces cerevisiae mannoproteins that protect wine from protein haze: Their release during fermentation and lees contact and a proposal for their mechanism of action. *J. Agric. Food Chem. 48*, 3098–3105.

(116) Dubourdieu, D., and Moine-Ledoux, V. (1994) No Title. *Brev. d'Invention Fr. 2*, 726–284.

(117) Cabello-Pasini, A., Victoria-Cota, N., Macias-Carranza, V., Hernandez-Garibay, E., and Muñiz-Salazar, R. (2005) Clarification of wines using polysaccharides extracted from seaweeds. *Am. J. Enol. Vitic. 56*, 52–59.

(118) Marangon, M., Stockdale, V. J., Munro, P., Trethewey, T., Schulkin, A., Holt, H. E., and Smith, P. A. (2013) Addition of carrageenan at different stages of winemaking for

white wine protein stabilization. *J. Agric. Food Chem. 61*, 6516–6524.

(119) Cottereau, P., Trotta, F., and Lopez, R. (2014) Using reticulate biopolymers for protein stabilisation of wine. *Proc. 37th World Congr. Vine Wine*.

(120) Mierczynska-Vasilev, A., Boyer, P., Vasilev, K., and Smith, P. A. (2017) A novel technology for the rapid, selective, magnetic removal of pathogenesis-related proteins from wines. *Food Chem. 232*, 508–514.

(121) Claus, H., Tenzer, S., Sobe, M., Schlander, M., König, H., and Fröhlich, J. (2014) Effect of carboxymethyl cellulose on tartrate salt, protein and colour stability of red wine. *Aust. J. Grape Wine Res. 20*, 186–193.

(122) Heinze, T., and Koschella, A. (2005) Carboxymethyl ethers of cellulose and starch - A review, in *Macromolecular Symposia*, pp 13–39.

(123) Lee, J. H., and Talcott, S. T. (2002) Ellagic acid and ellagitannins affect on sedimentation in muscadine juice and wine. *J. Agric. Food Chem. 50*, 3971–3976.

(124) Siriwoharn, T., Wrolstad, R. E., and Durst, R. W. (2006) Identification of Ellagic Acid in Blackberry Juice Sediment. *J. Food Sci. 70*, C189–C197.

(125) Moussa-ayoub, T. E., El-samahy, S. K., and Rohn, S. (2011) Flavonols , betacyanins content and antioxidant activity of cactus Opuntia macrorhiza fruits Identification and quantification of flavonol aglycons in cactus pear (Opuntia ficus indica) fruit using a commercial pectinase and cellulase preparation. *Food Chem. 2011*, 2010–2011.

(126) Kim, K. H., Tsao, R., Yang, R., and Cui, S. W. (2006) Phenolic acid profiles and antioxidant activities of wheat bran extracts and the effect of hydrolysis conditions. *Food Chem. 95*, 466–473.

(127) Krygier, K., Sosulski, F., and Hogge, L. (1982) Free, Esterified, and Insoluble-Bound Phenolic-Acids .2. Composition of Phenolic-Acids in Rapeseed Flour and Hulls. *J. Agric. Food Chem. 30*, 334–336.

(128) Jeong, C.-H., Jeong, H. R., Choi, G. N., Kim, D.-O., Lee, U., and Heo, H. J. (2011) Neuroprotective and anti-oxidant effects of caffeic acid isolated from Erigeron annuus leaf. *Chin. Med. 6*, 25.

(129) Cornard, J.-P., and Lapouge, C. (2006) Absorption spectra of caffeic acid, caffeate and their 1:1 complex with Al(III): density functional theory and time-dependent density functional theory investigations. *J. Phys. Chem. A 110*, 7159–7166.

(130) Connell, J. E. O., and Fox, P. F. (2000) Proposed mechanism for the e ! ect of polyphenols on the heat stability of milk. *Int. Dairy J. 9*, 523–536.

(131) Nuthong, P., Benjakul, S., and Prodpran, T. (2009) Effect of some factors and pretreatment on the properties of porcine plasma protein-based films. *LWT - Food Sci. Technol. 42*, 1545–1552.

(132) Rawel, H. M., and Rohn, S. (2002) Interactions of different phenolic acids and fla v onoids with soy proteins. *Int. J. Biol. Macromol. 30*, 137–150.

(133) Suryaprakash, P., Kumar, R. P., and Prakash, V. (2000) Thermodynamics of interaction of caffeic acid and quinic acid with multisubunit proteins. *Int. J. Biol. Macromol. 27*, 219–228.

(134) Pérez-Magariño, S., Ortega-Heras, M., and Cano-Mozo, E. (2008) Optimization of a solid-phase extraction method using copolymer sorbents for isolation of phenolic compounds in red wines and quantification by HPLC. *J. Agric. Food Chem. 56*, 11560–11570.

(135) Tian, R. R., Pan, Q. H., Zhan, J. C., Li, J. M., Wan, S. B., Zhang, Q. H., and Huang, W. D. (2009) Comparison of phenolic acids and flavan-3-ols during wine fermentation of grapes with different harvest times. *Molecules 14*, 827–838.

(136) Capone, D. L., Black, C. A., and Jeffery, D. W. (2012) Effects on 3-Mercaptohexan-1-ol precursor concentrations from prolonged storage of sauvignon blanc grapes prior to crushing and pressing. *J. Agric. Food Chem. 60*, 3515–3523.

(137) Pereira, V., Câmara, J. S., Cacho, J., and Marques, J. C. (2010) HPLC-DAD methodology for the quantification of organic acids, furans and polyphenols by direct injection of wine samples. *J. Sep. Sci. 33*, 1204–1215.

(138) Danilewicz, J. C. (2007) Interaction of sulfur dioxide, polyphenols, and oxygen in a wine-model system: Central role of iron and copper. *Am. J. Enol. Vitic. 58*, 53–60.

(139) Marangon, M., Van Sluyter, S. C., Neilson, K. A., Chan, C., Haynes, P. A., Waters,

E. J., and Falconer, R. J. (2011) Roles of grape thaumatin-like protein and chitinase in white wine haze formation. *J. Agric. Food Chem. 59*, 733–740.

(140) Esti, M., Benucci, I., Liburdi, K., and Garzillo, A. M. V. (2015) Immobilized pineapple stem bromelain activity in a wine-like medium: Effect of inhibitors. *Food Bioprod. Process. 93*, 84–89.

(141) Prigent, S. V. E., Voragen, A. G. J., Visser, A. J. W. G., Van Koningsveld, G. A., and Gruppen, H. (2007) Covalent interactions between proteins and oxidation products of caffeoylquinic acid (chlorogenic acid). *J. Sci. Food Agric. 87*, 2502–2510.

(142) Budryn, G., and Rachwal-Rosiak, D. (2013) Interactions of Hydroxycinnamic Acids with Proteins and Their Technological and Nutritional Implications. *Food Rev. Int. 29*, 217–230.

(143) Prigent, S. V. E., Voragen, A. G. J., Li, F., Visser, A. J. W. G., Van Koningsveld, G. A., and Gruppen, H. (2008) Covalent interactions between amino acid side chains and oxidation products of caffeoylquinic acid (chlorogenic acid). *J. Sci. Food Agric. 88*, 1748–1754.

(144) Oliveira, C. M., Ferreira, A. C. S., De Freitas, V., and Silva, A. M. S. (2011) Oxidation mechanisms occurring in wines. *Food Res. Int. 44*, 1115–1126.

(145) Lundblad, R. (2014) Chemical Reagents for Protein Modification, Fourth Edition. CRC Press.

(146) Garde-Cerdán, T., López, R., Garijo, P., González-Arenzana, L., Gutiérrez, A. R., López-Alfaro, I., and Santamaría, P. (2014) Application of colloidal silver versus sulfur dioxide during vinification and storage of Tempranillo red wines. *Aust. J. Grape Wine Res. 20*, 51–61.

(147) Elias, R. J., and Waterhouse, A. L. (2010) Controlling the fenton reaction in wine. *J. Agric. Food Chem. 58*, 1699–1707.

(148) McArdle, J. V., and Hoffmann, M. R. (1983) Kinetics and mechanism of the oxidation of aquated sulfur dioxide by hydrogen peroxide at low pH. *J. Phys. Chem. 87*, 5425–5429.

(149) Li, N., Qi, G., Sun, X. S., and Wang, D. (2012) Effects of Sodium Bisulfite on the

Physicochemical and Adhesion Properties of Canola Protein Fractions. *J. Polym. Environ. 20*, 905–915.

(150) Zhang, L., and Sun, X. S. (2008) Effect of sodium bisulfite on properties of soybean glycinin. *J. Agric. Food Chem. 56*, 11192–11197.

(151) Erickson, H. P. (2009) Size and shape of protein molecules at the nanometer level determined by sedimentation, gel filtration, and electron microscopy. *Biol. Proced. Online 11*, 32–51.

(152) Han, J. C., and Han, G. Y. (1994) A Procedure for Quantitative Determination of Tris(2-Carboxyethyl)phosphine, an Odorless Reducing Agent More Stable and Effective Than Dithiothreitol. *Anal. Biochem. 220*, 5–10.

(153) Singh, R. (1995) Rapid Reduction Reagents for Bonds in Proteins of Disulfide. *Immuno Gen. Inc 22*, 259–266.

(154) Getz, E. B., Xiao, M., Chakrabarty, T., Cooke, R., and Selvin, P. R. (1999) A Comparison between the Sulfhydryl Reductants Tris(2-carboxyethyl)phosphine and Dithiothreitol for Use in Protein Biochemistry. *Anal. Biochem. 273*, 73–80.

(155) Waters, E. J., Hayasaka, Y., Tattersall, D. B., Adams, K. S., and Williams, P. J. (1998) Sequence Analysis of Grape (*Vitis vinifera*) Berry Chitinases That Cause Haze Formation in Wines. *J. Agric. Food Chem. 46*, 4950–4957.

(156) Catsimpoolas, N., and Meyer, E. W. (1970) Gelation phenomena of soybean globulins (I): Protein-protein interactions. *Cereal Chem. 47*, 559–570.

(157) Speed, M. A., King, J., and Wang, D. I. C. (1997) Polymerization mechanism of polypeptide chain aggregation. *Biotechnol. Bioeng. 54*, 333–343.

(158) Stranks, S. D., Ecroyd, H., Van Sluyter, S., Waters, E. J., Carver, J. A., and Von Smekal, L. (2009) Model for amorphous aggregation processes. *Phys. Rev. E - Stat. Nonlinear, Soft Matter Phys. 80*.

(159) Whitmore, L., and Wallace, B. A. (2004) Analysis of peptaibol sequence composition: implications for in vivo synthesis and channel formation. *Eur. Biophys. J. 33*, 233–237.

(160) Whitmore, L., and Wallace, B. A. (2008) Protein secondary structure analyses from circular dichroism spectroscopy: Methods and reference databases. *Biopolymers 89*, 392–400.

(161) Hider, R. C., Kupryszewski, G., Rekowski, P., and Lammek, B. (1988) Origin of the positive 225-230 nm circular dichroism band in proteins. Its application to conformational analysis. *Biophys. Chem. 31*, 45–51.

(162) Kahn, P. C. (1979) The interpretation of near-ultraviolet circular dichroism. *Methods Enzymol. 61*, 339–378.

(163) Sengottaiyan, P., Petrlova, J., Lagerstedt, J. O., Ruiz-Pavon, L., Budamagunta, M. S., Voss, J. C., and Persson, B. L. (2013) Characterization of the biochemical and biophysical properties of the Saccharomyces cerevisiae phosphate transporter Pho89. *Biochem. Biophys. Res. Commun.*

(164) Cowgill, R. W. (1967) Fluorescence and protein structure XI. fluorescence quenching by disulfide and sulfhydryl groups. *Biochim. Biophys. Acta 140*, 37–44.

(165) Neves-Petersen, M. T., Gryczynski, Z., Lakowicz, J., Fojan, P., Pedersen, S., Petersen, E., and Bjørn Petersen, S. (2009) High probability of disrupting a disulphide bridge mediated by an endogenous excited tryptophan residue. *Protein Sci. 11*, 588–600.

(166) Rabilloud, T. (2000) Proteome Research: Two-Dimensional Gel Electrophoresis and Identification Methods. *Princ. Pract.*

(167) Palmer, I., and Wingfield, P. T. (2012) Preparation and extraction of insoluble (Inclusion-body) proteins from Escherichia coli, in *Current Protocols in Protein Science*, p 6.3.1-6.3.18. John Wiley & Sons, Inc., Hoboken, NJ, USA.

(168) Reynolds, J. A., and Tanford, C. (1970) Binding of Dodecyl Sulfate to Proteins at High Binding Ratios. Possible Implications for the State of Proteins in Biological Membranes. *Proc. Natl. Acad. Sci. 66*, 1002–1007.

(169) Chow, C., Kurt, N., Murphy, R. M., and Cavagnero, S. (2006) Structural Characterization of Apomyoglobin Self-Associated Species in Aqueous Buffer and Urea Solution. *Biophys. J. 90*, 298–309.

(170) Toichi, K., Yamanaka, K., and Furukawa, Y. (2013) Disulfide scrambling describes

the oligomer formation of superoxide dismutase (SOD1) proteins in the familial form of amyotrophic lateral sclerosis. *J. Biol. Chem. 288*, 4970–4980.

(171) Taylor, S. L., Higley, N. A., and Bush, R. K. (1986) Sulfites in foods: Uses, analytical methods, residues, fate, exposure assessment, metabolism, toxicity, and hypersensitivity. *Adv. Food Res. 30*, 1–76.

(172) Abramovi??, H., Ko??merl, T., Poklar Ulrih, N., and Cigi??, B. (2015) Contribution of SO2 to antioxidant potential of white wine. *Food Chem. 174*, 147–153.

(173) Gil, D. M. de A., and Rebelo, M. J. F. (2009) Metabisulfite interference in biosensing and Folin-Ciocalteu analysis of polyphenols. *Microchim. Acta 167*, 253–258.

(174) Ferreira, R. B., Monteiro, S. S., Piçarra-Pereira, M. A., and Teixeira, A. R. (2004) Engineering grapevine for increased resistance to fungal pathogens without compromising wine stability. *Trends Biotechnol.*

(175) Klemm, D., Schmauder, H.-P., and Heinze, T. (2005) Cellulose, in *Biopolymers Online*. Wiley-VCH Verlag GmbH & Co. KGaA, Weinheim, Germany.

(176) Klemm, D., Heublein, B., Fink, H. P., and Bohn, A. (2005) Cellulose: Fascinating biopolymer and sustainable raw material. *Angew. Chemie - Int. Ed. 44*, 3358–3393.

(177) Wüstenberg, T. (2015) Cellulose and cellulose derivatives in the food industry : fundamentals and applications.

(178) Röhrling, J., Potthast, A., Rosenau, T., Sixta, H., and Kosma, P. (2002) Determination of carbonyl functions in cellulosic substrates. *Lenzinger Berichte*.

(179) (2005) Anon. *Eur. Coatings J.* 36–41.

(180) Klemm, D., Philipp, B., Heinze, T., Heinze, U., and Wagenknecht, W. (1998) Comprehensive Cellulose Chemistry. *New York Wiley-VCH 2*, 389.

(181) Whistler, R. L., and BeMiller, J. N. (2012) Industrial Gums: Polysaccharides and Their Derivatives: Third Edition. *Ind. Gums Polysaccharides Their Deriv. Third Ed.*

(182) Chemischen, D. (1999) des Fonds der Chemischen Industrie.

(183) Poersch-Parcke, H. G., and Kirchner, R. (2003) Solutions (Wolff Cellulosics

GmbH, Ed.) 2nd ed. Walsrode.

(184) Pinkert, A., Marsh, K. N., and Pang, S. (2010) Reflections on the solubility of cellulose. *Ind. Eng. Chem. Res. 49*, 11121–11130.

(185) Cai, J., Zhang, L., Liu, S., Liu, Y., Xu, X., Chen, X., Chu, B., Guo, X., Xu, J., Cheng, H., Han, C. C., and Kuga, S. (2008) Dynamic self-assembly induced rapid dissolution of cellulose at low temperatures. *Macromolecules 41*, 9345–9351.

(186) Medronho, B., Duarte, H., Alves, L., Antunes, F., Romano, A., and Lindman, B. (2015) Probing cellulose amphiphilicity. *Nord. Pulp Pap. Res. J. 30*, 58–66.

(187) Heinze, T. (2005) Polysaccharides I structure, characterisation and use. *Adv. Polym. Sci.* Springer.

(188) Feddersen, R. L., and Thorp, S. N. (1993) Chapter 20 – Sodium Carboxymethylcellulose, in *Industrial Gums*, pp 537–578.

(189) Peterson, E. A., and Sober, H. A. (1956) Chromatography of Proteins. I. Cellulose Ion-Exchange Adsorbents. *J. Am. Chem. Soc. 78*, 751–755.

(190) Roos, P. H. (1999) Ion Exchange Chromatography. *Protein Liq. Chromatogr.*

(191) Yackel, E. C., and Kenyon, W. O. (1942) The Oxidation of Cellulose by Nitrogen Dioxide. *J. Am. Chem. Soc. 64*, 121–127.

(192) El-Hilw, Z. H. (1999) Synthesis of cotton-bearing DEAE, carbamoyethyl, carboxyethyl, and poly(acrylamide) graft for utilization in dye removal. *J. Appl. Polym. Sci. 73*, 1007–1014.

(193) Waly, A., Abdel-Mohdy, F. A., Aly, A. S., and Hebeish, A. (1998) Synthesis and characterization of cellulose ion exchanger. II. Pilot scale and utilization in dye heavy metal removal. *J. Appl. Polym. Sci. 68*, 2151–2157.

(194) Pavan, F. A., Francisco, M. S. P., Landers, R., and Gushikem, Y. (2005) Adsorption of phosphoric acid on niobium oxide coated cellulose fiber: Preparation, characterization and ion exchange property. *J. Braz. Chem. Soc. 16*, 815–820.

(195) Orelma, H., Filpponen, I., Johansson, L. S., Laine, J., and Rojas, O. J. (2011) Modification of cellulose films by adsorption of cmc and chitosan for controlled

attachment of biomolecules. *Biomacromolecules 12*, 4311–4318.

(196) Mohan, T., Ristić , T., Kargl, R., Doliska, A., Köstler, S., Ribitsch, V., Marn, J., Spirk, S., and Stana-Kleinschek, K. (2013) Cationically rendered biopolymer surfaces for high protein affinity support matrices. *Chem. Commun. 49*, 11530.

(197) Mohan, T., Niegelhell, K., Zarth, C. S. P., Kargl, R., Köstler, S., Ribitsch, V., Heinze, T., Spirk, S., and Stana-Kleinschek, K. (2014) Triggering protein adsorption on tailored cationic cellulose surfaces. *Biomacromolecules 15*, 3931–3941.

(198) Mautner, A., Kobkeatthawin, T., and Bismarck, A. (2017) Efficient continuous removal of nitrates from water with cationic cellulose nanopaper membranes. *Resour. Technol. 3*, 22–28.

(199) OIV. (2017) International Œnological CODEX. *OIV.int*.

(200) Tamborini, A., and Magro, A. (1970) Il trattamento dei vini con resine scambiatrici e il rapporto potassio: sodio. *Riv. di Viticiltura e di Enol.* 89–94.

(201) Rankine, B. C. (1985) Using ion exchange for prevention of tartrate precipitation in wine. *Aust. Grapegrow. Winemak. 263*.

(202) Mourgues, J. (1993) Utilisation des résines échangeuses d'ions. *Rev OEnol. 69*, 51–54.

(203) Cabrita, M. J., Garcia, R., and Catarino, S. (2016) Recent developments in wine tartaric stabilization, in *Recent advances in wine stabilization and conservation technologies*, pp 49–63.

(204) Mira, H., Leite, P., Ricardo-Da-Silva, J. M., and Curvelo-Garcia, A. S. (2006) Use of ion exchange resins for tartrate wine stabilization. *J. Int. des Sci. la Vigne du Vin 40*, 223–246.

(205) Gerbaud, V., Gabas, N., Blouin, J., and Crachereau, J. C. (2010) Study of wine tartaric acid salt stabilization by addition of carboxymethylcellulose (CMC): Comparison with the « protective colloids » effect. *J. Int. des Sci. la Vigne du Vin 44*, 231–242.

(206) Sommer, S., Dickescheid, C., Harbertson, J. F., Fischer, U., and Cohen, S. D. (2016) Rationale for Haze Formation after Carboxymethyl Cellulose (CMC) Addition to Red

Wine. *J. Agric. Food Chem. 64*, 6879–6887.

(207) Kötz, J., Nehls, I., Philipp, B., and Diamantoglou, M. (1991) Zum polyelektrolytverhalten von dicarboxymethylcellulose. *Das Pap. 45*, 226–231.

(208) Diamantoglou, M., and Cornelissens, E. (1974) Dicarboxymethyläther von poly- und oligosacchariden als waschkratverstärkende zusatzimittel für waschmittel. DE2410560A1.

(209) Diamantoglou, M., Mägerlein, H., Zielke, R., Maegerlein, H., and Zielke, R. (1977) Polycarboxylate aus polysacchariden, holz und holzähnlich zusammengesetzten stoffen als neuartige sequestriermittel. *Tenside Deterg. 14*, 250–256.

(210) Heinze, T., and Pfeiffer, K. (1999) Studies on the synthesis and characterization of carboxymethylcellulose. *Die Angew. Makromol. Chemie 266*, 37–45.

(211) Barbucci, R., Casolaro, M., and Fini, A. (1990) Thermodynamics of Protonation and Copper(11) Complex Formation of a-Aminomalonic Acid t. *J. Chem. Soc. Dalt. Trans*.

(212) Yanchishin, V. A., Karlivan, G. A., and Valter, R. É. (1998) Synthesis and properties of dipyridinium betaines of derivatives of 1,4-benzoquinone and tetracyanoquinodimethane. *Chem. Heterocycl. Compd. 34*, 312–315.

(213) Yamaguchi, T., Yoshimoto, M., Ohmori, T., Nakaiwa, M., and Akiya, T. (1996) Bromomalonic acid as a source of photochemically produced Br - ion in the Ru(bpy) 32+-catalyzed Belousov-Zhabotinsky reaction. *Chem. Phys. Lett. 2614*, 0–5.

(214) Furrow, S. D., and Aurentz, D. J. (2010) Reactions of iodomalonic acid, diiodomalonic acid, and other organics in the briggs-rauscher oscillating system. *J. Phys. Chem. A 114*, 2526–2533.

(215) Kamide, K. (2005) 2 - Characterization of Molecular Structure of Cellulose Derivatives, in *Cellulose and Cellulose Derivatives*, pp 25–188. Elsevier, Amsterdam.

(216) Kono, H., Oshima, K., Hashimoto, H., Shimizu, Y., and Tajima, K. (2016) NMR characterization of sodium carboxymethyl cellulose: Substituent distribution and mole fraction of monomers in the polymer chains. *Carbohydr. Polym. 146*, 1–9.

(217) Heinze, T., and Liebert, T. I. M. (1999) Carboxymethylation of cellulose in unconventional media. *Cellulose 6*, 153–165.

(218) Bryjak, M. (1998) Modification of porous polyacrylonitrile membrane. *Angew. Makromol. Chemie 260*, 53–63.

(219) Baar, A., Kulicke, W.-M., Szablikowski, K., and Kiesewetter, R. (1994) Nuclear magnetic resonance spectroscopic characterization of carboxymethylcellulose. *Macromol. Chem. Phys. 195*, 1483–1492.

(220) Ernsting, M. J., Tang, W. L., Maccallum, N., and Li, S. D. (2011) Synthetic modification of carboxymethylcellulose and use thereof to prepare a nanoparticle forming conjugate of docetaxel for enhanced cytotoxicity against cancer cells. *Bioconjug. Chem. 22*, 2474–2486.

(221) El-Sakhawy, M., Kamel, S., Salama, A., and Sarhan, H.-A. (2014) Carboxymethyl Cellulose Acetate Butyrate: A Review of the Preparations, Properties, and Applications. *J. Drug Deliv. 2014*, 1–6.

(222) Han, B., Zhang, D., Shao, Z., Kong, L., and Lv, S. (2013) Preparation and characterization of cellulose acetate/carboxymethyl cellulose acetate blend ultrafiltration membranes. *Desalination 311*, 80–89.

(223) Nakimoshi, H. (1985) Carboxyalkyl acetyl celluloses, their salts and a process for the preparation of them (Daicel Chemical Industries Ltd. Japan, O., Ed.).

(224) Liebert, T. F., and Heinze, T. J. (2001) Exploitation of reactivity and selectivity in cellulose functionalization using unconventional media for the design of products showing new superstructures. *Biomacromolecules 2*, 1124–1132.

(225) Gu, H., He, J., Huang, Y., and Guo, Z. (2012) Water soluble carboxymethylcellulose fibers derived from alkalization-etherification of viscose fibers. *Fibers Polym. 13*, 748–753.

(226) Heinze, T., and Heinze, U. (1997) The first approach to non-aqueous solutions of carboxymethylcellulose. *Macromol. Rapid Commun. 18*, 1033–1040.

(227) Tezuka, Y., Tsuchiya, Y., and Shiomi, T. (1996) 13C NMR determination of substituent distribution in carboxymethylcellulose by use of its peresterified derivatives.

Carbohydr. Res. 291, 99–108.

(228) Tingaut, P., Zimmermann, T., and Lopez-Suevos, F. (2010) Synthesis and characterization of bionanocomposites with tunable properties from poly(lactic acid) and acetylated microfibrillated cellulose. *Biomacromolecules 11*, 454–464.

(229) Park, S., Baker, J. O., Himmel, M. E., Parilla, P. A., and Johnson, D. K. (2010) Cellulose crystallinity index: measurement techniques and their impact on interpreting cellulase performance. *Biotechnol. Biofuels 3*, 10.

(230) Segal, L., Creely, J. J., Martin, A. E., and Conrad, C. M. (1959) An Empirical Method for Estimating the Degree of Crystallinity of Native Cellulose Using the X-Ray Diffractometer. *Text. Res. J. 29*, 786–794.

(231) Aggeryd, I., and Olin, Å. (1985) Determination of the degree of substitution of sodium carboxymethylcellulose by potentiometric titration and use of the extended henderson-hasselbalch equation and the simplex method for the evaluation. *Talanta 32*, 645–649.

(232) Conner, A. Z., and Eyler, R. W. (1950) Analysis of Sodium Carboxymethylcellulose. *Anal. Chem. 22*, 1129–1132.

(233) Eyler, R. W., Klug, E. D., and Diephuis, F. (1947) Determination of Degree of Substitution of Sodium Carboxymethylcellulose. *Anal. Chem. 19*, 24–27.

(234) Heinze, T., Erler, U., Nehls, I., and Klemm, D. (1994) Determination of the substituent pattern of heterogeneously and homogeneously synthesized carboxymethyl cellulose by using high- performance liquid chromatography. *Die Angew. Makromol. Chemie 215*, 93–106.

(235) Nehls, I., Wagenknecht, W., Philipp, B., and Stscherbina, D. (1994) Characterization of cellulose and cellulose derivatives in solution by high resolution 13C-NMR spectroscopy. *Prog. Polym. Sci. 19*, 29–78.

(236) Kowsaka, K., Okajima, K., and Kamide, K. (1991) Determination of the Distribution of Substituent Groups in Sodium Cellulose Sulfate: Assignment of 1H and 13C NMR Peaks by Two-Dimensional COSY and CH-COSY Methods. *Polym. J. 23*, 823–836.

(237) ASTM. (2015) Standard D1439 - 15.

(238) Qi, H., Liebert, T., Meister, F., and Heinze, T. (2009) Homogenous carboxymethylation of cellulose in the NaOH/urea aqueous solution. *React. Funct. Polym. 69*, 779–784.

(239) Harnisch, H., Hühner, J., Neusüß, C., Koschella, A., Heinze, T., and Scriba, G. K. E. (2016) Development and validation of a capillary electrophoresis method for the characterization of sulfoethyl cellulose. *J. Sep. Sci. 39*, 4645–4652.

(240) Shakun, M., Maier, H., Heinze, T., Kilz, P., and Radke, W. (2013) Molar mass characterization of sodium carboxymethyl cellulose by SEC-MALLS. *Carbohydr. Polym. 95*, 550–559.

(241) Crössmann, F., Klaus, W., Mergenthaler, F., and Souci, S. W. (1964) Zur physikalischen und chemischen charakterisierung der als lebensmittel-zusatzstoffe verwendeten celluloseäther. *Z. Lebensm. Unters. Forsch.* Springer-Verlag.

(242) Yang, F., Li, G., He, Y. G., Ren, F. X., and Wang, G. xiang. (2009) Synthesis, characterization, and applied properties of carboxymethyl cellulose and polyacrylamide graft copolymer. *Carbohydr. Polym. 78*, 95–99.

(243) Eremeeva, T. E., and Bykova, T. O. (1998) SEC of mono-carboxymethyl cellulose (CMC) in a wide range of pH; Mark-Houwink constants. *Carbohydr. Polym. 36*, 319–326.

(244) Rinaudo, M., Danhelka, J., and Milas, M. (1993) A new approach to characterising carboxymethylcelluloses by size exclusion chromatography. *Carbohydr. Polym. 21*, 1–5.

(245) Souci, S. W., Crössmann, F., and Mergenthaler, E. (1964) Zur physikalischen und chemischen charakterisierung der als lebensmittel-zusatzstoffe verwendeten celluloseäther. *Z. Lebensm. Unters. Forsch.*

(246) Tateishi, T., Chen, G., and Ushida, T. (2002) Biodegradable porous scaffolds for tissue engineering. *J. Artif. Organs 5*, 77–83.

(247) Courtenay, J. C., Johns, M. A., Galembeck, F., Deneke, C., Lanzoni, E. M., Costa, C. A., Scott, J. L., and Sharma, R. I. (2017) Surface modified cellulose scaffolds for tissue engineering. *Cellulose 24*, 253–267.

(248) Isogai, A., Saito, T., and Fukuzumi, H. (2011) TEMPO-oxidized cellulose nanofibers. *Nanoscale 3*, 71–85.

(249) Feng, Z., Shao, Z., Yao, J., and Chen, X. (2008) Protein adsorption and separation on amphoteric chitosan/ carboxymethylcellulose membranes. *J. Biomed. Mater. Res. - Part A 86*, 694–700.

(250) Heinze, T., Haack, V., and Rensing, S. (2004) Starch derivatives of high degree of functionalization. 7. Preparation of cationic 2-hydroxypropyltrimethylammonium chloride starches. *Starch/Staerke 56*, 288–296.

(251) Marder, H., Field, N., and Shinohara, M. (1980) Preparation of water-insoluble carboxymethyl cellulose absorbents. Google Patents.

(252) Coletta, M., Costa, H., De Sanctis, G., Neri, F., Smulevich, G., Turner, D. L., and Santos, H. (1997) pH dependence of structural and functional properties of oxidized cytochrome c'' from Methylophilus methylotrophus. *J. Biol. Chem. 272*, 24800–24804.

(253) Anirudhan, T. S., and Senan, P. (2011) Adsorptive characteristics of Bovine Serum Albumin onto cationic langmuir monolayers of sulfonated poly (glycidylmethacrylate)-grafted cellulose: Mass transfer analysis, isotherm modeling and thermodynamics. *Langmuir Monolayers Thin Film Technol. 168*, 678–690.

(254) Strittmatter, H., Hildbrand, S., and Pollak, P. (2000) Malonic Acid and Derivatives, in *Ullmann's Encyclopedia of Industrial Chemistry*. John Wiley & Sons, Inc., Hoboken, NJ, USA.

(255) Dogsa, I., Tomšič , M., Orehek, J., Benigar, E., Jamnik, A., and Stopar, D. (2014) Amorphous supramolecular structure of carboxymethyl cellulose in aqueous solution at different pH values as determined by rheology, small angle X-ray and light scattering. *Carbohydr. Polym. 111*, 492–504.

(256) Leonardis, M., Palange, A., Dornelles, R. F. V, and Hund, F. (2010) Use of cross-linked carboxymethyl cellulose for soft-tissue augmentation: preliminary clinical studies. *Clin. Interv. Aging 5*, 317–322.

(257) Braihi, A. J. (2014) Proposed Cross-Linking Model for Carboxymethyl Cellulose /Starch Superabsorbent Polymer Blend. *Int. J. Mater. Sci. Appl. 3*, 363.

(258) Hasanah, A. N., Elyani, I., Sriwidodo, Muchtaridi, Muhtadi, A., and Musfiroh, I. (2015) Epichlorohydrin as crosslinking agent for synthesis of carboxymethyl cellulose sodium (Na-CMC) as pharmaceutical excipient from water hyacinth (Eichorrnia Crassipes L.). *Int. J. Chem. Sci. 13*, 1227–1237.

(259) Kast, W. (1985) Principles of adsorption and adsorption processes, in *Chemical Engineering and Processing: Process Intensification*, p 118.

(260) Langmuir, I. (1918) The adsorption of gases on plane surfaces of glass, mica and platinum. *J. Am. Chem. Soc. 40*, 1361–1403.

(261) Tian, B., Harrison, R., Morton, J., Jaspers, M., Hodge, S., Grose, C., and Trought, M. (2017) Extraction of Pathogenesis-Related Proteins and Phenolics in Sauvignon Blanc as Affected by Grape Harvesting and Processing Conditions. *Molecules 22*, 1164.

(262) Krapcho, A. P., Glynn, G. A., and Grenon, B. J. (1967) The decarbethoxylation of geminal dicarbethoxy compounds. *Tetrahedron Lett. 3*, 215–217.

(263) Roberts, J. (1996) The Chemistry of Paper. Royal Society of Chemistry, Cambridge.

(264) Ren, J. L., Sun, R. C., and Peng, F. (2008) Carboxymethylation of hemicelluloses isolated from sugarcane bagasse. *Polym. Degrad. Stab. 93*, 786–793.

(265) Hallac, B. B., and Ragauskas, A. J. (2011) Analyzing cellulose degree of polymerization and its relevancy to cellulosic ethanol. *Biofuels, Bioprod. Biorefining 5*, 215–225.

(266) Morgan, E. . (1990) Vogel's textbook of practical organic chemistry. 5th edn. *Endeavour 14*, 148.

(267) Bensadoun, A., and Weinstein, D. (1976) Assay of proteins in the presence of interfering materials. *Anal. Biochem. 70*, 241–250.

(268) de Bruijn, J., Valdebenito, A., Loyola, C., Serra, I., Salazar, F., and López, F. (2009) Continuous Stabilization of Chardonnay with Ion-Exchage Resin: Influence on Protein and Phenolic Profile of Wine. *Chil. J. Agric. Res. 69*, 54–59.

(269) Pocock, K. F., and Waters, E. J. (2006) Protein haze in bottled white wines: How

well do stability tests and bentonite fining trials predict haze formation during storage and transport? *Aust. J. Grape Wine Res. 12*, 212–220.

(270) Nardini, M., Cirillo, E., Natella, F., and Scaccini, C. (2002) Absorption of Phenolic Acids in Humans aft er Coffee Consumption. *J Agric Food Chem 50*, 5735–5741.

(271) Bogucki, D. E., and Charlton, J. L. (1997) A non-enzymatic synthesis of (*S*)-(−)-rosmarinic acid and a study of a biomimetic route to (+)-rabdosiin. *Can. J. Chem. 75*, 1783–1794.

(272) Fontanel, D., Galtier, C., Viel, C., and Gueiffier, A. (1998) Caffeoyl quinic and tartaric acids and flavonoids from Lapsana communis L. subsp. communis (Asteraceae). *Zeitschrift fur Naturforsch. - Sect. C J. Biosci. 53*, 1090–1092.

8. Appendix A

Table 28 - Results from the different algorithms used in the analysis of the circular dichroism results.

iTLP in wine model solution

		Helix1	Helix2	Strand1	Strand2	Turns	Unordered	Total	NRMSD
20 °C	SELCON3	0.028	0.078	0.287	0.126	0.094	0.375	0.988	0.322
	CONTIN	0	0.073	0.278	0.132	0.097	0.418	0.998	0.163
	CDSSTR	0	0.06	0.28	0.14	0.1	0.4	0.98	0.025
	Average	0.01	0.07	0.28	0.13	0.10	0.40	0.99	
	STDEV	0.013	0.008	0.004	0.006	0.002	0.018	0.007	
	Total %	α-helix	8.0	β-sheet	41.4	Turns	9.7	Random Coil	39.8
70 °C	SELCON3	0.052	0.088	0.171	0.114	0.153	0.41	0.987	0.156
	CONTIN	0.046	0.082	0.19	0.114	0.153	0.415	1	0.084
	CDSSTR	0.01	0.07	0.2	0.12	0.14	0.44	0.98	0.029
	Average	0.036	0.080	0.187	0.116	0.149	0.422	0.989	
	STDEV	0.019	0.007	0.012	0.003	0.006	0.013	0.008	
	Total %	α-helix	11.6	β-sheet	30.3	Turns	14.9	Random Coil	42.2
15 °C	SELCON3	0.035	0.081	0.257	0.122	0.105	0.38	0.979	0.299
	CONTIN	0.035	0.084	0.257	0.132	0.108	0.385	1.001	0.071
	CDSSTR	0	0.06	0.27	0.14	0.11	0.41	0.99	0.029
	Average	0.02	0.08	0.26	0.13	0.11	0.39	0.99	
	STDEV	0.016	0.011	0.006	0.007	0.002	0.013	0.009	
	Total %	α-helix	9.8	β-sheet	39.3	Turns	10.8	Random Coil	39.2

iTLP in model wine solution added of SO_2

		Helix1	Helix2	Strand1	Strand2	Turns	Unordered	Total	NRMSD
20 °C	SELCON3	0.029	0.077	0.293	0.129	0.088	0.376	0.992	0.205
	CONTIN	0	0.085	0.274	0.136	0.089	0.416	1	0.126
	CDSSTR	0	0.06	0.28	0.15	0.11	0.39	0.98	0.028
	Average	0.01	0.07	0.28	0.14	0.10	0.39	0.99	
	STDEV	0.014	0.010	0.008	0.009	0.010	0.017	0.008	
	Total %	α-helix	8.4	β-sheet	42.1	Turns	9.6	Random Coil	39.4

70 °C	SELCON3	0.058	0.085	0.223	0.118	0.162	0.424	1.071	0.185
	CONTIN	0.029	0.084	0.197	0.126	0.14	0.423	0.999	0.14
	CDSSTR	0	0.06	0.22	0.13	0.14	0.43	0.98	0.031
	Average	0.03	0.08	0.21	0.12	0.15	0.43	1.02	
	STDEV	0.024	0.012	0.012	0.005	0.010	0.003	0.039	
	Total %	α-helix	10.5	β-sheet	33.8	Turns	14.7	Random Coil	42.6

15 °C	SELCON3	0.119	0.111	0.179	0.093	0.119	0.379	1	0.269
	CONTIN	0.086	0.099	0.191	0.105	0.112	0.406	0.999	0.126
	CDSSTR	0.11	0.11	0.18	0.1	0.12	0.37	0.99	0.054
	Average	0.11	0.11	0.18	0.10	0.12	0.39	1.00	
	STDEV	0.014	0.005	0.005	0.005	0.004	0.015	0.004	
	Total %	α-helix	21.2	β-sheet	28.3	Turns	11.7	Random Coil	38.5